Identification of Intracellular Protein Binding Partners of Cisplatin and Their Role in Acquired and Intrinsic Resistance

Dissertation

zur

Erlangung des Doktorgrades (Dr. rer. nat.)

der

Mathematisch-Naturwissenschaftlichen Fakultät

der

Rheinischen Friedrich-Wilhelms-Universität Bonn

vorgelegt von

SOPHIE MÖLTGEN

aus

Bergisch Gladbach

Bonn 2020

Angefertigt mit der Genehmigung der Mathematisch-Naturwissenschaftlichen Fakultät der Rheinischen Friedrich-Wilhelms-Universität Bonn.

Meiner Familie

"Data! Data! Data!" he cried impatiently. "I can't make bricks without clay."

Sherlock Holmes, The Adventure of the Copper Beeches

Table of Contents

Abbreviations

A	Adenine
A2780/A2780cis	Human Ovarian Carcinoma Cell Lines; cisplatin-sensitive and -resistant, respectively
ACN	Acetonitrile
ADPR	ADP-ribose
Akt	protein kinase B
ALDH1 A1	Aldehyde Dehydrogenase 1 family, member A1
ANOVA	One-way Analysis of Variance
Apaf1	Apoptotic Protease Activating Factor 1
APS	Ammoniumperoxodisulfate
ASK1	Apoptosis Signal-regulating Kinase 1
ATM	Ataxia Telangiectasia Mutated Protein
ATP7A/B	ATPase Copper Transporting Alpha and Beta
ATR	RAD3-related Protein
Axl	Axl receptor tyrosine kinase
Bax	Bcl-2-associated X Protein
BCA	Bicinchoninic Acid
Bcl-2	B-cell Lymphoma 2
BMI	Body Mass Index
BODIPY	Boron-dipyrromethene
BPB	Bromphenol Blue
BRCA1/2	Breast Cancer 1 and 2, early onset
BS^3	Bis(sulfosuccinimidyl)suberate
BSA	Bovine Serum Albumin
c-Abl	Cellular Abelson Murine Leukemia Viral Oncogene Homologue 1
CBB	Coomassie Brilliant Blue
CASY	Cell Analysis System
CETN2	Centrin-2
CFDA	Carboxyfluorescein Diacetate

CHAPS	3-[(3-Cholamidopropyl)dimethylammonio]-1-propanesulfonate
CHK1/2	Checkpoint Kinases 1/2
CI	Combination Index
Cisplatin	Cis-Diamminedichloridoplatinum(II)
CLB	Cell Lysis Buffer
COP9	Constitutive Photomorphogenesis 9
CSA/CSB	Cockayne syndrome proteins type A and B
CTR1/2	Copper Transporter Protein 1/2
CuAAC	Copper-Catalyzed Azide-Alkyne Cycloaddition
CYT C	Cytochrome c
DACH	1,2-Diaminocyclohexane
DAPI	4′,6-Diamidino-2-phenylindole-dihydrochloride
DISC	Death-inducing Signaling Complex
DJ-1	Protein/Nucleic Acid Degylcase DJ-1
DMF	Dimethylformamide
DMP	Dimethylpimelimidate
DMSO	Dimethylsulfoxide
DNA	Deoxyribonucleic Acid
dsRNA	double-stranded RNA
DSS	Disuccinimidylsuberate
DTT	Dithiothreitol, (2S,3S)-1,4-Bis(sulfanyl)butane-2,3-diol
EC_{50}	Half maximal effective concentration; refers to the concentration of a compound where 50% of its maximal effect is observed
ECACC	European Collection of Authenticated Cell Cultures
ECL	Enhanced Chemiluminescence
EDTA	Ethylenediaminetetraacetic Acid
EF1A1	Elongation Factor 1 alpha-1

EGFR	Epidermal Growth Factor Receptor
EMT	Epithelial-mesenchymal Transition
ERBB2	V-erb-b2 Avian Erythroblastic Leukemia Viral Oncogene Homolog 2
ERK	Extracellular Signal-regulated Kinase
ESI	Electrospray Ionization
ESI-MS/MS	ESI-coupled Tandem Mass Spectrometry
FA	Formic Acid
FADD	Fas-associated Death Domain Protein
FAK	Focal Adhesion Kinase
FCS	Fetal Calf Serum
FDA	Food and Drug Administration
F-DDP	Fluorescein-cisplatin
FGFR2	Fibroblast Growth Factor Receptor 2
FITC	Fluorescein Isothiocyanate
FiVe1	FOXC2-inhibiting Vimentin effector 1
FOLFOX	Chemotherapy Regimen: Folinic Acid, 5-FU and Oxaliplatin
G	Guanine
Gadd45a	DNA-damage-inducible Protein Alpha
GAPDH	Glyceraldehyde 3-phosphate Dehydrogenase
GDP	Guanosine Diphosphate
GG-NER	Global Genome NER
Grb2	Growth Factor Receptor Bound Protein 2
GRP78	Glucose-regulated Protein 78 kDa
GSH	Glutathione
GSTP1	Glutathione-S-Transferase π 1
GTP	Guanosine Triphosphate
HCT-8/HCT-8ox	Human Ileocecal Colorectal Adenocarcinoma Cell Lines; oxaliplatin-sensitive and -resistant, respectively
HDI	The Human Development Index
HED	Hydroxyethyldisulfide

HEPES	4-(2-Hydroxyethyl)-1-piperazineethanesulfonic Acid
Her2	Human Epidermal Growth Factor Receptor 2
HMGB1/4	High Mobility Group Box 1/4
HPLC	High-performance Liquid Chromatography
HRP	Horseradish Peroxidase
HSA	Human Serum Albumin
IAA	Iodoacetamide
IC_{50}	Half maximal inhibitory concentration; refers to the concentration of a compound where the response is reduced by half
IEF	Isoelectric Focusing
IP	Immunoprecipitation
IPG	Immobilized pH Gradient
JNK	c-Jun N-terminal Kinase
Keap1	Kelch-like ECH-associated Protein 1
LA-ICP-MS	Laser Ablation Inductively Coupled MS
LC-MS	Liquid Chromatography–Mass Spectrometry
LLOQ	Lower Limit of Quantification
MAPK	Mitogen-activated Protein Kinase
MATE2	Multidrug and Toxin Extrusion 2
MDR1	Multidrug Resistance Protein 1
MET	Mesenchymal–epithelial Transition
MKK3/4/6	Mitogen-activated Protein Kinase Kinase 3/4/6
MLH1	*mutL* homolog 1
MMR	Mismatch Repair
mRNA	messenger RNA
MRP2	Multidrug Resistance Protein 2
MS	Mass Spectrometry
MT	Metallothioneins

MTT	3-(4,5-Dimethylthiazol-2-yl)-2,5-diphenyltetrazolium Bromide or Thiazolyl Blue Tetrazolium Bromide
MYO	Myoglobin
m/z	mass-to-charge ratio
nanoHPLC	Nano High-performance Liquid Chromatography
NC	Negative Control
NCD	Noncommunicable Diseases (predominantly cardiovascular diseases, cancer, diabetes, or chronic respiratory diseases)
NER	Nucleotide Excision Repair
NF-kB	Nuclear Factor-kB
NHS	N-hydroxysuccinimidyl
NL	Nonlinear
NP-40	Nonylphenoxypolyethoxylethanol-40
NRF2	Nuclear Factor E2-related Factor 2
NSCLC	Non-small Cell Lung Cancer
OCT1/2/3	Organic Cation Transporter 1/2/3
Oxaliplatin	[(1R,2R)-cyclohexane-1,2-diamine](ethanedioato-O,O')platinum(II)
PARP	Poly(ADP-ribose)polymerase
PBS	Phosphate-buffered Saline
PBS-T	Phosphate-buffered Saline with Tween®-20
PCNA	Proliferating Cell Nuclear Antigen
PDIA1/3/6	Protein Disulfide Isomerase Alpha 1/3/6
P-gp	P-glycoprotein
PI	Propidium Iodide
PI3K	Phosphoinositide 3-kinase
PLCγ1	Phospholipase C, Gamma 1
P/S	Penicillin/Streptomycin
PSM	Peptide Spectrum Matches
PTEN	Phosphatase and Tensin Homolog

PVDF	Polyvinylidene Fluoride
RACK1	Receptor for Activated Protein C Kinase 1
RAD23B	UV Excision Repair Protein RAD23 Homolog B
RIPA	Radioimmunoprecipitation Assay
RISC	RNA-induced Silencing Complex
RF	Resistance Factor
RNA	Ribonucleic Acid
RNAi	RNA Interference
RNAse	Ribonuclease
ROS	Reactive Oxygen Species
RPA	Replication Protein A
rpm	Revolutions per minute
RPMI	Roswell Park Memorial Institute
RSR	Relative Survival Rate
RT	Room Temperature
SCLC	Small-cell Lung Cancer
SDS	Sodium Dodecyl Sulfate
SDS-PAGE	Sodium Dodecyl Sulfate Polyacrylamide Gel Electrophoresis
SEM	Standard Error of the Mean
SH2/3	Src Homology 2/3
SH3C	C-terminal of SH3
SHC	SHC-transforming Protein 1
SHI	Statutory Health Insurance
siRNA	Small Interfering RNA
Sos	Son of sevenless
TBS	Tris-buffered Saline
TBS-T	Tris-buffered Saline with Tween®-20
TCA	Trichloroacetic Acid
TCGA	The Cancer Genome Atlas
TC-NER	Transcription-coupled NER
TEMED	N,N,N',N'-Tetramethylethylenediamine
TFIIH	Transcription Factor II Human

TGF-ß1	Transforming Growth Factor ß1
THPTA	Tris(3-hydroxypropyltriazolylmethyl)amine
TLK199	Ezatiostat-HCl
TNF	Tumor Necrosis Factor
TRAF2	TNF Receptor-associated Factor 2
Tris Base	Tris(hydroxymethyl)aminomethane
Tris HCl	Tris(hydroxymethyl)aminomethane Hydrochloride
TrxR	Thioredoxin Reductase
ULOQ	Upper Limit of Quantification
VEGF	Vascular Endothelial Growth Factor
VRAC	Volume-regulated Anion Channels
WHO	World Health Organization
XELOX	Chemotherapy Regimen: Capecitabine and Oxaliplatin
XIAP	X-linked Inhibitor of Apoptosis
XPA, XPB, XPD, XPF, XPG	Xeroderma Pigmentosum Type A, B, D, F and G
XPC	Xeroderma Pigmentosum, Complementation Group C
XPF-ERCC1	Xeroderma Pigmentosum Type F-Excision Repair Cross-complementation Group 1
1D	One-dimensional
2D	Two-dimensional
2D-DIGE	Two-dimensional Differential In-gel Electrophoresis
5-FU	5-Fluorouracil

1   Introduction

Once considered to be a disease of the rich, cancer nowadays poses a global threat and challenges all countries worldwide. While cardiovascular diseases cause more deaths globally, cancer is the leading cause of death in high or very high Human Development Index (HDI) countries, such as Canada, USA, most countries in Europe, Japan, Singapore [1,2]. In 2012, approximately 14 million new cases were recorded and 8 million patients fell victim to their illness [3]. Only 3 years later, an incidence of about 18 million cases was determined and about 9.5 million cancer-related deaths affected patients worldwide (Figure 1.1) [2]. In this regard, men and women are concerned relatively equally.
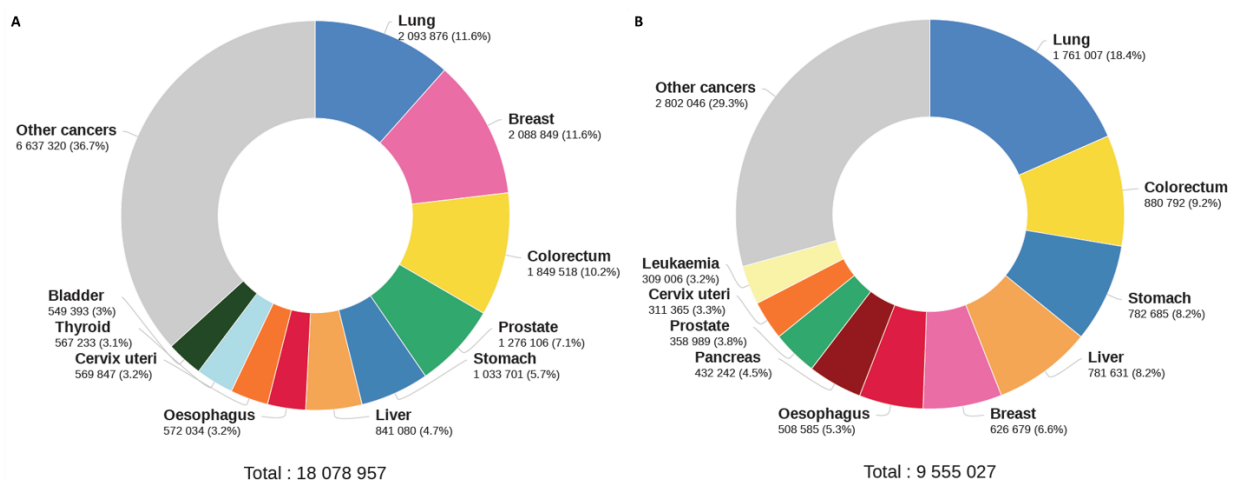
Figure 1.1 Estimated number of new cases (A) and deaths (B), respectively, in 2018, worldwide, both sexes, all ages [4].

Amongst other factors, the steadily increasing incidence rate can be explained by a constantly ageing population and changing reproductive behavior due to urbanization and economic development [2,5]. Additionally, prevailing lifestyles, especially in industrialized countries with high HDI, including dietary habits and the level of physical activity, favor the emergence of diverse entities [2]. In particular, the consumption of red meat or highly processed food and the consumption of excessive amounts of alcohol or smoking should be mentioned here. This is consistent with a strong association of obesity and lack of exercise with the development of a variety of cancers, such as colorectal, ovarian, kidney, pancreas and many more [2]. The occurrence of infections and a lack of countermeasures, especially in low- and middle-income countries, are also a considerable factor in the development of certain cancers [2]. Interestingly, the incidence rate in low-HDI countries, such as India and many African

countries, appears to be less pronounced than in the industrialized world (Figure 1.2). Although for many entities, incidence rates in developed countries are 2- to 3-fold higher than in non-developed or transitioning countries, it is noticeable that the differences in mortality rates are only slightly higher [6]. Nevertheless, as a result of globalization, changes in lifestyle naturally also have an impact on previously rather low-HDI countries being in transition now and especially in these countries predicted increases in cancer burden are proportionally the greatest [2].

ASR (World) per 100 000

≥ 253.9
183.8–253.9
138.3–183.8
106.5–138.3
< 106.5

Not applicable
No data
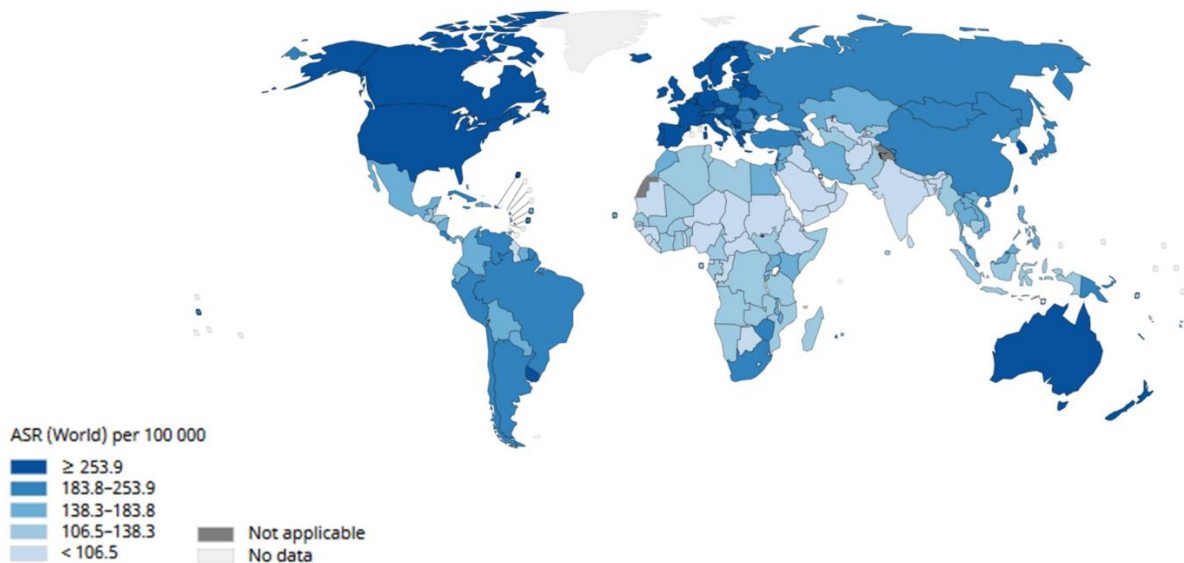
Figure 1.2 Estimated age-standardized incidence rates (World) in 2018, all cancers, both sexes, all ages [4].

Although global cancer-related mortality is rising from year to year [2,3], a more detailed examination reveals that an increase in mortality rates especially for breast cancer, prostate cancer and colorectal cancer, can be seen predominantly in transitioning countries, while in high-HDI countries rates tend to stagnate or even decline [2]. Above all, this can be attributed to socioeconomic differences, which result in insufficient prevention, diagnosis and treatment measures. This goes along with the opportunity and feasibility of intervening early in the cancer development process and preventing advanced stages and thus reducing the risk of mortality. Access to effective but affordable medication is also crucial in this respect. Particularly with regard to the earliest possible detection of the disease through frequent prophylactic examinations and financial security in the event of treatment, major differences between countries can be registered. It is not without reason that in its *Global Action Plan for the Prevention and Control of Noncommunicable Diseases* (NCD) the World Health Organization (WHO) has described the introduction of universal health coverage and

easy access to essential health services and medicines as indispensable for combating mortality from NCD worldwide [7].

If several decades ago the common goal was to eradicate cancer [8], it has since become clear that malignant neoplasms are incredibly diverse and that the definition of curability applying to most other diseases does not hold true in oncology. Due to high relapse rates in many types of cancers, oncologists usually speak of a cure if complete remission can be maintained for 5 years [9]. Even though the overall 5-year relative survival rate (RSR) for cancer patients could be increased about 20% from the 1970s to almost 70% in the 2010s, this still leaves about 30% of patients uncured. In addition, survival rates vary greatly between different entities, lung and pancreatic cancer being amongst the most lethal ones [2,10,11]. As mentioned above, the chance of curability of cancer is often dependent on the progress of the disease at the time of detection and the extent, to which certain cancers lead to death, correlates greatly with the social and economic status of the country [6]. Success in the fight against cancer is considered conversion of a rather acute disease into a chronic disease, amongst other factors due to the shift from conventional chemotherapies to targeted therapies directed at certain biomarkers present, and the application of immunotherapies [9]. However, these drugs often have a noticeably disadvantage of high costs and raise the associated question of financial feasibility. In 2018, oncological drugs accounted for merely 1.1% of all prescriptions in the German statutory health insurance (SHI) drug market. On the other hand, though, they caused the highest costs at approximately €7 billion [12].

With regard to health-economical aspects and ever-increasing health care costs associated with innovative cancer therapies in conjunction with a frequent failure of both novel and well-established therapies due to the development of resistance or discontinuation of therapy due to intolerable side effects, the elucidation of intracellular interactions of the antitumor drugs in as much detail as possible is essential. Only then it will be possible to improve understanding of efficacy and toxicity as well as to unravel yet unknown details about resistance development.

1.1   Ovarian Cancer

1.1.1   Classification, Incidence, and Mortality

Ovarian cancer is the 8th most common malignant disease in women and by far the most common cause of gynecological cancer deaths (Figure 1.3) [2,6]. Amongst other factors, this poor outcome can be attributed to the fact that this disease itself is more or less asymptomatic and if symptoms occur, these are very unspecific. Moreover, there are only few certain and modifiable risk factors and, above all, no reliable screening methods [2,13–15]. As a result, at the time of most diagnoses, tumors are often already in far advanced stages, where they usually have metastasized and the 5-year RSR is only about 30% [2]. To make it worse, it has been found that patients who present at late stages will suffer from disease recurrence within 18 months [14].

Figure 1.3 Estimated number of new cases (A) and deaths (B), respectively, in 2018, worldwide, females, all ages [4].

Furthermore, the histological diversity of ovarian cancer complicates the correct treatment algorithm. Roughly speaking, ovarian cancer can be classified into 5 histopathological subtypes, the recognition of which is extraordinarily complex and imperatively requires evaluation by specialists. The subtypes high-grade serous, endometrioid, clear cell, mucinous, and low-grade serous ovarian cancer, differ not only in their genetic mutation profile but also in their response to chemotherapy and thus their prognosis [14]. While poorly differentiated high-grade serous ovarian cancer responds very well to chemotherapy, survival is still low. In contrast, generally well-differentiated endometrioid, low-grade serous and mucinous carcinomas, for one thing, respond less to chemotherapy but have a better prognosis [2]. In addition, the few known risk factors also have an impact on each subtype. As an example, the use of

oral contraceptives has been associated with a low risk of serous, endometrioid and clear cell carcinomas, but not for mucinous carcinomas [2]. The variability of the characteristics is apparently so great that ovarian cancer is more and more seen not as one disease with different epithelial subtypes, but rather as several distinct diseases [14]. It is therefore important that the existing tumor is very well characterized and that reliable biomarkers are found, which allow diagnosis at an early stage and development of appropriate personalized therapies [13].

1.1.2 Treatment

Depending on the stage of the tumor at diagnosis, treatment of ovarian cancer varies. In general, in both early and advanced ovarian cancer, therapy is usually initiated surgically with the aim of removing the entire tumor. Undetected tumor remnants not only have a negative prognostic impact, they also often lead to inadequate subsequent adjuvant therapy as a monotherapy would be given priority over combination therapy because the tumor would be classified as an early stage (see paragraph below) [15]. However, especially in advanced ovarian carcinomas, the radicality of tissue removal always includes the possibility of increased morbidity and in particularly distinctive cases, tumor freedom cannot be achieved [15].

Surgery is then succeeded by systemic platinum-based primary therapy (mainly carboplatin, but also cisplatin, especially at advanced stages) [13,15]. In the case of early ovarian carcinomas, monotherapy is preferable to combination therapy due to the lack of evidence of better effectiveness of the latter [15]. In contrast to this, first-line chemotherapy for advanced ovarian cancer consists of a combination of platinum-based chemotherapy with paclitaxel [15,16]. Furthermore, an additional treatment with the vascular endothelial growth factor (VEGF) inhibitor bevacizumab can be considered [15,16]. In the case of a breast cancer gene (BRCA1/2, early onset) mutation and initial response to platinum-containing first-line therapy, maintenance therapy with a poly(ADP-ribose)polymerase (PARP) inhibitor, such as olaparib, should be administered beyond complete remission [15].

Although surgery and first-line chemotherapy result in a high number of complete remissions, the count of recurrences is not negligible either [13]. Surgical treatment of patients suffering from relapses is rather rare and no data regarding possible improvement of prognosis is available [15]. Systemic therapies are much more relevant

in these cases and it is noteworthy that the course of action is mainly directed by the interval from the last platinum-containing treatment to the point of progression in addition to factors such as patient preferences, age, endurance and genetic factors. Here, a distinction is made between platinum-sensitive and platinum-resistant recurrent ovarian cancer. The former is characterized by a progression-free period after primary therapy of at least 6 months, while platinum resistance is manifested by progression within the first 6 months after primary treatment [15]. In case of platinum-sensitive tumors, a platinum-containing combination therapy is used, which consists of carboplatin or cisplatin combined with either pegylated liposomal doxorubicin, paclitaxel or gemcitabine. Further addition of bevacizumab to the platinum/paclitaxel and platinum/gemcitabine schemes results in significant improvement of progression-free survival [13,15]. In the case of a positive BRCA1/2 mutation, maintenance therapy with a PARP inhibitor can be considered [15]. Often, however, platinum resistance occurs after primary therapy. In this case, platinum-containing regimens are avoided and pegylated liposomal doxorubicin, gemcitabine, paclitaxel or topotecan are taken into consideration as monotherapy [15].

It may be noted that recurrent disease is not curable per se but proportionately very well treatable. The median survival with recurrent platinum-sensitive ovarian cancer is roughly 3 years. Nevertheless, from the time of onset of platinum resistance, median survival is only about 1 year [14]. This vividly illustrates the urgent need in new anti-tumor drugs for treatment of ovarian cancer and the great potential that lies in the clarification of the mechanisms of platinum resistance development. In particular, the combination of platinum compounds with novel agents holds great opportunities.

1.2   Colorectal Cancer

1.2.1   Classification, Incidence, and Mortality

Globally, colorectal cancer is the second most common cancer in women and third most common cancer in men (Figure 1.3, Figure 1.4) [2,6]. When looking at the incidences of colorectal cancer, however, it can be noticed that this seems to be a disease occurring mainly in more advanced countries. This is illustrated by the estimated age-standardized incidence rates in high-HDI countries, such as Australia and many European countries, which are about 5 times higher as in low-HDI countries, such as many African countries [2]. Nevertheless, incidence rates of colorectal cancer

have increased in countries in transition, whereas in high-income countries, rates have either stabilized or decreased [17]. Additionally, incidence has been increasing in younger age groups in a diverse set of countries [18].

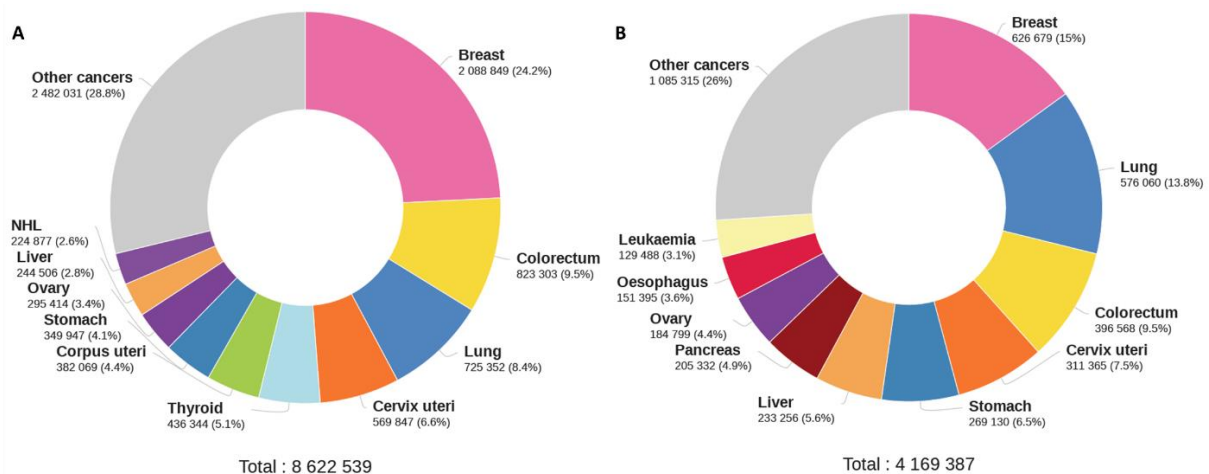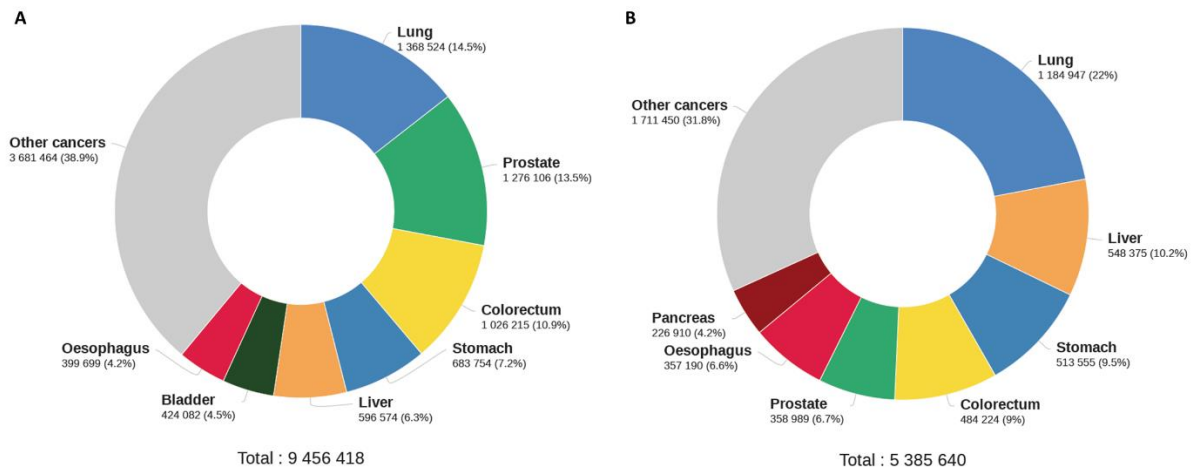**Figure 1.4 Estimated number of new cases (A) and deaths (B), respectively, in 2018, worldwide, males, all ages [4].**

This can be explained by changes in behavior patterns in developing countries and adoption of lifestyles more typical of industrialized countries, which are risk factors for the development of colorectal cancer [2]. Amongst others, this includes the shift of dietary patterns from high intake of fruits, vegetables, whole grains, nuts and seafood to the consumption of red meat, sugar-sweetened beverages, refined grains and candy in developing countries, especially in combination with decreased physical exercise and increasing body mass indices (BMI) [2,6]. According to this, colorectal cancer is a highly preventable disease. On the other hand, screening methods are routinely offered primarily in high-HDI countries, allowing early detection and early intervention before cancer has manifested itself [2,6].

Correspondingly, mortality rates have decreased in countries with high HDI, and increased in many low- and middle-income countries. As in the case of ovarian cancer, the stage at diagnosis has a significant influence on the outcome [2]. Furthermore, financial and cultural barriers cause a delay or restrictions in access to innovative therapies and use of high-quality treatment guidelines in low-income countries [2]. For this reason, colorectal cancer still causes the second most cancer-related deaths worldwide (Figure 1.1) [6].

Like ovarian cancer, colorectal cancer is histopathologically extremely diverse and can roughly be categorized into the more common sporadic carcinomas and hereditary

forms (only about 3-5%). Depending on the molecular pathogenesis mutation profile, treatment response and, thus, prognosis may differ [17].

1.2.2 Treatment

Comparable to the initial approach with ovarian cancer, surgical intervention with a curative aim is the first step in the treatment of colorectal cancer. This is done either openly or laparoscopically, which has some advantages like faster return of bowel movement and the need for less blood transfusions during surgery, but also takes longer and is associated with higher costs [17,19]. After surgery, an adjuvant therapy depending on the stage and exact location of the carcinoma is initiated. While at stage I neither colon nor rectal carcinomas benefit from adjuvant chemotherapy, at stages II and III therapy should be commenced within 8 weeks after surgery, if possible [19]. Especially at more advanced stages of colon carcinomas, chemotherapy is usually based on oxaliplatin in combination with folinic acid and 5-fluorouracil (5-FU) (FOLFOX regimen) or capecitabin (XELOX regimen) [19]. The therapy of rectal cancer differs: Tumors of the lower and middle third of the rectum should first be treated with neoadjuvant radiochemotherapy, which includes oral capecitabine or infusional 5-FU [19]. In the adjuvant setting, radiochemotherapy can be considered as an alternative to the already mentioned regimens [19].

In contrast to the above case, treatment of metastatic colorectal cancer is a lot more complex and highly variable. In general, choice and intensity of chemotherapy are based on the following criteria: Depending on the general condition of the patient, it is determined whether he or she seems suitable for intensive therapy. The extent of the disease often determines whether a curative option is applicable or whether therapy should be palliative. Furthermore, molecular biological and pharmacogenetic diagnosis of the tumor always precedes treatment initiation [17]. This includes mutation status, which may indicate additional treatment with anti-epidermal growth factor receptor (EGFR) or anti-VEGF antibodies [17,19]. Nowadays, tyrosine kinase inhibitors and anti-PD1 immunotherapies are also frequently used, especially at more advanced stages [20]. It should be added that if the option exists, the primary aim here is surgical resection of all metastases, too [17,19].

Even though there have been real advances in classical and targeted therapy regimens, resistance to treatment remains a considerable challenge, especially in long-term management of incurable metastatic colorectal cancer [21].

1.3 Antitumor Platinum Complexes

Although first synthesized by Michel Peyrone in 1845 [22], it was only in 1965 that Rosenberg et al. accidentally discovered the extraordinary antiproliferative properties of cisplatin (Figure 1.5) in an experiment conducted to study the effects of an electric field on the growth of *Escherichia coli* [23]. Cisplatin has since come a long way. After initial in vitro experiments, it was shown that cisplatin had antitumor effects on sarcoma 180, leukemia L1210 and Ehrlich ascites tumors in mice. First efforts to elucidate the mechanism of action demonstrated the interaction of cisplatin with deoxyribonucleic acid (DNA), ribonucleic acid (RNA), and proteins [24–27]. After positive results of clinical trials in human cancer patients initiated in the early 1970s, cisplatin was approved for therapy of testicular, ovarian and bladder cancer in 1978 by the Food and Drug Administration (FDA) [28] and has been implemented in several tumor entities thus far [29]. Cisplatin, as the oldest platinum drug approved, is very effective in many tumor entities and especially in testicular cancer it leads to extremely high cure rates of up to 95% [30]. However, the use of cisplatin is limited by severe side effects such as nephropathy and emesis, often leading to the termination of treatment [31,32]. Apart from this, it soon became apparent that the initial response to treatment with cisplatin was lost over time and ultimately culminated in resistance [29].

For these reasons, the search for alternative platinum-based compounds that are just as efficient but feature more favorable adverse effect profiles has been going on. With carboplatin (Figure 1.5), one of these candidates was finally approved for the treatment of ovarian cancer in 1989 and even though it is less potent than cisplatin, it is much better tolerated [29]. Due to the existing cross-resistance with cisplatin, however, carboplatin could only be used in cisplatin-sensitive tumors and did not extend the therapeutic profile, e.g. being active against resistant tumors [29]. Nevertheless, carboplatin has replaced cisplatin as the platinum drug of choice in many treatment regimens nowadays, in order for patients to receive the least aggressive therapy as possible [32,33].

The development and approval of a third-generation platinum drug oxaliplatin in 2002 (Figure 1.5) was considered another monumental achievement [33], as the compound differs from its predecessors for its unique spectrum of activity and distinctive side effects [34,35]. It was found that oxaliplatin expressed cytotoxic activity in cancers that were believed to be insensitive towards platinum drugs up to that point, such as colorectal cancer [33], and contrary to cisplatin and carboplatin, its side effects constitute primarily neuropathies [36]. Today nearly 50% of all cancer treatments are platinum-based [37], showing their importance in cancer therapy.
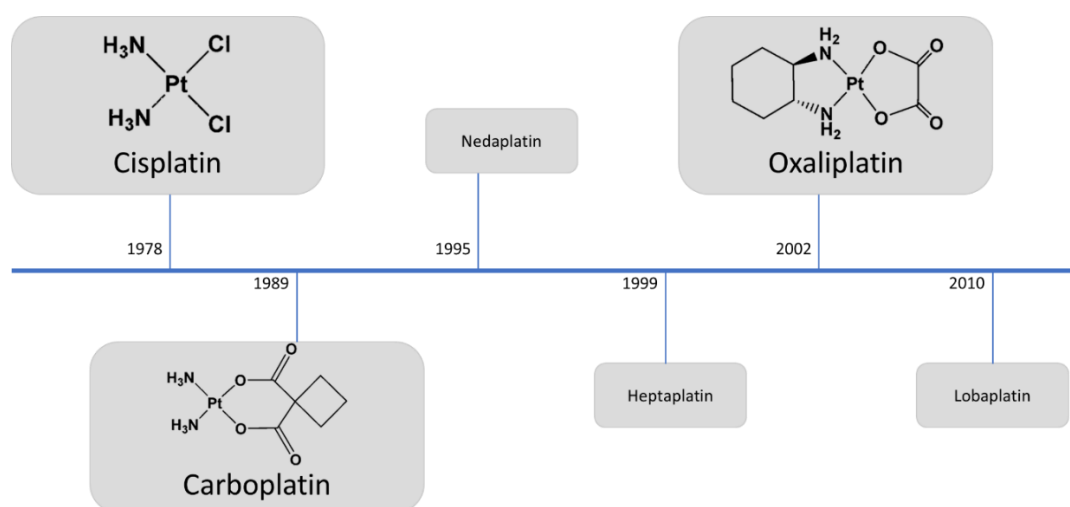
Figure 1.5 Timeline illustrating regulatory approval of Pt-based drugs in clinical use. Modified from Kenny et al. [37].

Despite extensive efforts, most compounds did not show significant advantages over cisplatin [29], and only three more platinum drugs have found limited access into the clinic. Yet, all of them were only approved in individual countries in Asia and are therefore of rather minor importance. Namely they are nedaplatin, heptaplatin and lobaplatin [37,38].

1.3.1 Cellular Uptake and Bioactivation

After intravenous application, cisplatin and carboplatin remain unchanged and uncharged extracellularly, due to a high chloride concentration of approximately 100 mM, which suppresses the cleavage of the leaving groups [39]. While a great amount of the applied cisplatin is readily bound to serum proteins and is therefore inactivated, binding affinity of carboplatin seems to be lower [40,41]. Exclusively unbound cisplatin and carboplatin enter the cell, primarily via passive diffusion but also actively via transporters [39]. The latter are likely to be copper transporters 1 and 2 (CTR1 and CTR2). Additionally, organic cation transporter 2 (OCT2) has been

implicated to take part in active uptake of platinum into kidney and cochlea cells, thus causing nephro- and ototoxicity [42]. Moreover, Planells-Cases and colleagues claimed that heteromeric LRRC8 volume-regulated anion channels (VRAC) have a significant impact on cisplatin uptake [43]. However, despite strong evidence, data regarding active transport mechanisms is sometimes controversial and the relevance of these transporters has not been clarified conclusively [42,44].

Triggered by the significantly lower chloride concentration within the cell (2-10 mM), one or both chloride leaving groups are then replaced (Figure 1.6) [45]. Above all, this leads to formation of monoaqua complexes and diaqua complexes. The latter being highly reactive, though, will then interact with nucleophilic structures, such as DNA, RNA, glutathione (GSH), metallothioneins (MT) or proteins [46]. As mentioned above, carboplatin's reaction rate is lower than that of cisplatin [47]. Taken together, merely about 1% of all intracellular platinum reaches nuclear DNA [48,49]. Interestingly, bioactivation of cisplatin is much faster than of carboplatin and adduct formation of carboplatin is about 10 times slower. For this reason, carboplatin has to be applied in about 20-40-fold higher concentrations to achieve the same effect. The active species, however, are the same [33].

Oxaliplatin also binds to plasma proteins to a high extent after intravenous application [50]. The free, unbound fraction, however, is likely to exchange its oxalate groups for chlorides extracellularly [51]. Yet, this mechanism is not undisputed, as $Pt(DACH)Cl_2$ could not be detected in vivo [52]. Oxaliplatin and its potentially formed subspecies are then also transported into the cell via passive diffusion or active uptake [39]. Apart from CTR1, but not CTR2, mainly OCTs are assumed to be involved. Beside OCT1 and OCT2, OCT3 seems to take part in active influx of oxaliplatin. This is of notice, since organic transporters are probably not relevant in the uptake of cisplatin and carboplatin by tumor cells [42,53]. On the other hand, there is a contradictory evidence showing that OCT3 does not take on a role in oxaliplatin uptake as well [54]. Once inside the cell, chloride ligands of $Pt(DACH)Cl_2$ are also ultimately exchanged for water due to the lower chloride concentrations (Figure 1.6) and after formation of aqua complexes, the latter react with intracellular nucleophiles [42]. The reactivity of the aquated oxaliplatin species, at least towards GSH, seems to be similar to that of cisplatin [47]. Yet, the bulky 1,2-diaminocyclohexane (DACH) ligand ultimately results in structural

differences of the evolving aqua complexes from the ones of the previous generations of platinum drugs [55].
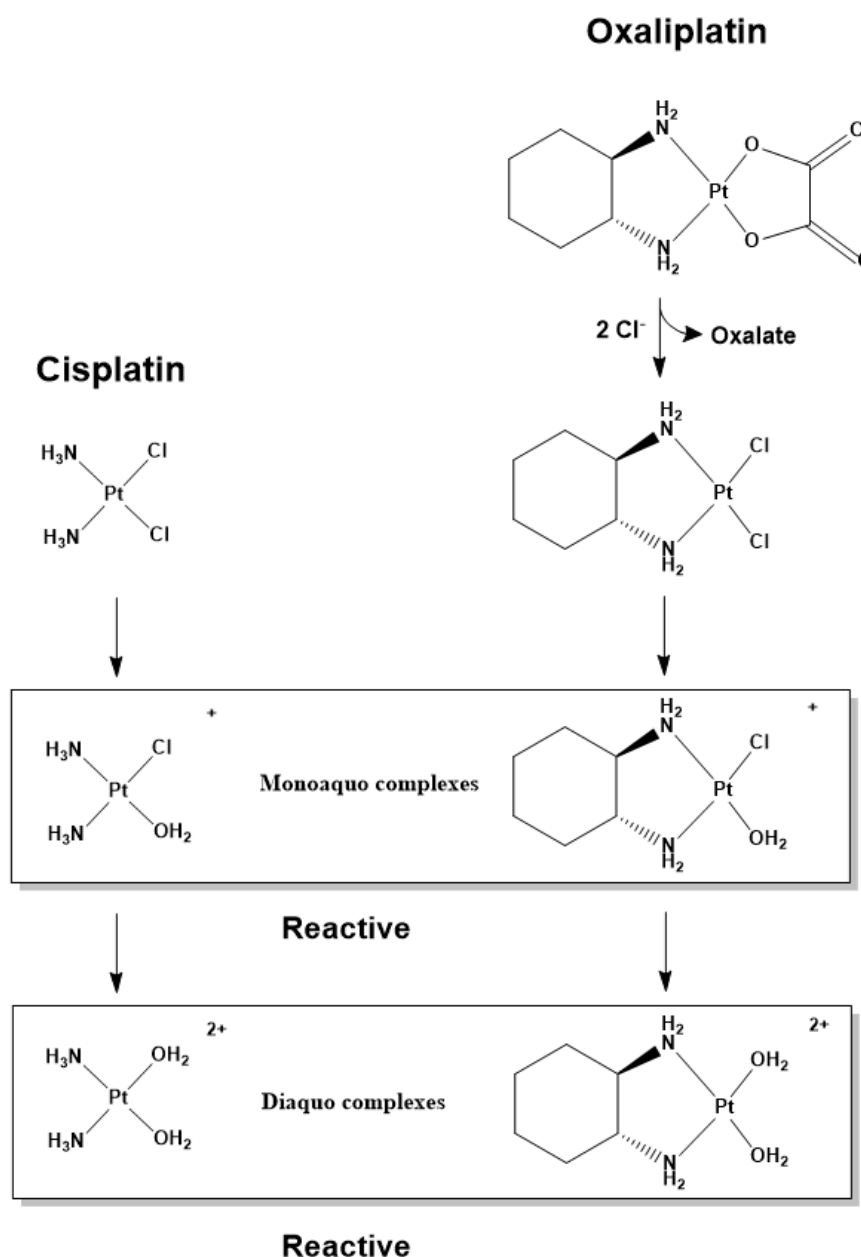
Figure 1.6 Major oxaliplatin and cisplatin metabolites upon bioactivation. Modified from Di Francesco et al. [56].

1.3.2 Mode of Action

Following the formation of reactive aqua complexes, platinum compounds can unfold their cytotoxic properties. Even though only small fractions of intracellular platinum can be detected in the nucleus, as mentioned before, the general assumption is that the antitumor effects of both cisplatin and carboplatin as well as oxaliplatin are mainly due to the generation of DNA adducts [29]. First and foremost, platinum hereby binds to

the N7 of the purine bases guanine (G) and adenine (A) and therefore leads to mono-
and bifunctional adducts (Figure 1.7). When considering bifunctional adducts,
intrastrand (~60-65% adjacent 1,2-GG-intrastrand, ~25-30% adjacent 1,2-AG-
intrastrand and ~5-10% 1,3-GNG-intrastrand adducts, where bound guanines are
separated by an unmodified nucleotide, Figure 1.7) and interstrand (1-3% GG-
interstrand adducts, Figure 1.7) crosslinks have been reported [42]. The proportional
distribution of adducts is comparable for cisplatin, carboplatin and oxaliplatin and
differs only slightly [42]. Additionally, the formation of platinum-DNA-protein bonds has
been described [50]. The most frequently formed 1,2-GG-intrastrand crosslink leads to
DNA strand breaks, triggered by a spatial distortion of the DNA helices [42,57]. Due to
the structural differences of the reactive aqua complexes, as mentioned above, Pt-
DNA adducts of cisplatin and carboplatin can be distinguished from the adducts
generated by oxaliplatin [57]. While binding sites are the same for all three platinum
compounds, the bulky hydrophobic DACH ligand of oxaliplatin induces a more
pronounced change in the DNA structure [57]. Triggered by DNA strand breaks,
various processes are subsequently activated ultimately leading to cell death.
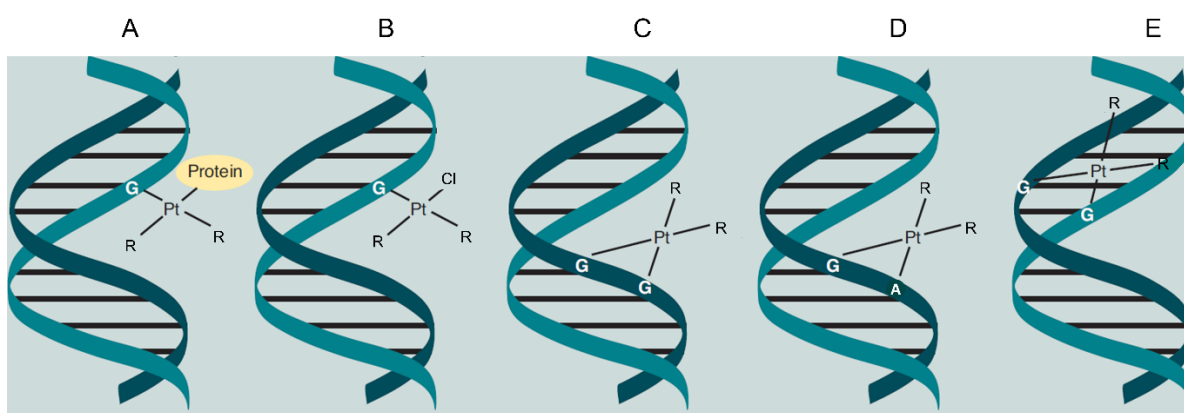
Figure 1.7 Binding of platinum drugs to its target DNA resulting in platinum-protein-DNA adducts (A), platinum-DNA monoadducts (B), 1,2-GG-intrastrand platinum-DNA adducts (C), 1,2-AG-intrastrand platinum DNA-adducts (D) and GG-interstrand platinum-DNA adducts (E). Modified from Ott et al. [50].

Interestingly, oxaliplatin shows lower reactivity towards DNA and the extent to which
oxaliplatin binds to DNA is lower compared to cisplatin [56,58]. It was previously
assumed that cisplatin, carboplatin and oxaliplatin have only slightly different
mechanisms of action. However, recent conclusions have revealed significant
disparities. It has been shown that oxaliplatin does not induce certain DNA damage
responses and instead triggers ribosomal biogenesis stress, which then leads to cell
death [35]. All in all, though, the differences in activity between the first- and second-

generation compounds in comparison to third-generation compounds have not been resolved in detail to date and further elucidating studies are needed.

It is also interesting that DNA binding does not seem to correlate with cytotoxicity [59] and that cytotoxicity could even be detected in enucleated cells [60,61]. This suggests that other mechanisms, transmitted by intracellular proteins and associated with nuclear and cytoplasmic signaling pathways, potentially play an important role [45].

Finally, the mechanism of action of platinum compounds is frequently linked to occurring adverse effects of the therapy. Induced by interaction with DNA of fast-dividing cells, the effect of platinum drugs is not limited to tumors but also impacts fast-dividing healthy tissue cells. This is why side effects, such as emesis, mucosis, and hair loss are very common in chemotherapy [36]. However, it is the distinctive adverse effect profiles of cisplatin, carboplatin and oxaliplatin that have been associated with differential protein binding and specific uptake into or efflux out of certain tissues. Exemplarily, a possible efflux of oxaliplatin from renal proximal tubular epithelial cells by multidrug and toxin extrusion 2 (MATE2) transporter may prevent its accumulation and, consequently, nephrotoxicity [53]. Likewise, inhibition of CTR1 by pre-treatment with copper sulfate was suggested to prevent cisplatin-induced ototoxicity in mice [62].

1.3.3   Cellular Response

The binding of platinum complexes to DNA induces various cellular processes (Figure 1.8), the most important of which are described in more detail below. It is worth noting that not all proteins involved actively pursue the task of detecting DNA damage and some of them are activated only upon recognition of such damages.
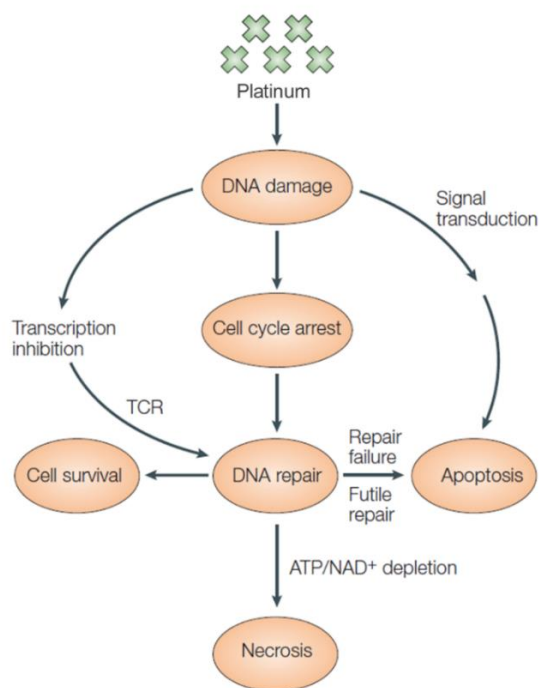
Figure 1.8 Schematic overview of platinum-DNA adduct-induced cellular responses. Modified from Wang et al. [31].

1.3.3.1   Inhibition of DNA Synthesis

First and foremost, after the formation of both intra- and interstrand crosslinks, DNA polymerases lose the ability to attach due to the structural changes of the helices. However, this only applies to about 90% of cases [42], as the cell is able to bypass platinum-DNA lesions by a mechanism called translesion synthesis (replicative bypass), which enables the DNA synthesis to continue at least for the time being (Chapter 1.3.3.2) [42].

1.3.3.2   Recognition of DNA Damage, Cell Cycle Arrest and DNA Repair Mechanisms

As a result of DNA damage, the cell cycle is halted through activation of checkpoint kinases 1 and 2 (CHK1, CHK2) in order for the cell to assess the damage and to initiate repair mechanisms [42]. It has been shown that cisplatin probably induces primarily G2/M phase arrest, which prevents the transfer of damaged DNA to daughter cells during mitosis [31]. Next, either DNA repair or apoptosis is initiated [63]. Considering the path the cell choses, data is inconclusive. Some studies found that cell cycle arrest can be regarded as inhibitory to the cytotoxic processes associated with cisplatin as cell cycle arrest is imperative for the induction of the nucleotide excision repair (NER)

[46]. It appears, therefore, that DNA damage has to be extensive for the cell to undergo apoptosis [46].

The NER pathway is the major DNA repair mechanism. It acts non-specifically regarding the recognition of platinum-DNA adducts and repairs all cisplatin-, carboplatin- and oxaliplatin-induced lesions alike [42,64]. Briefly, NER can be distinguished into two different sub-pathways: The global genome NER (GG-NER) and the transcription-coupled NER (TC-NER) (Figure 1.9). While GG-NER is responsible for the repair of helix-distorting lesions, TC-NER removes transcription-blocking lesions [65]. These two differentiate solely between the damage recognition processes. GG-NER comes into place when damage to nucleotides results in structural changes of the DNA helices, whereas TC-NER is activated when RNA polymerase II comes to a halt during transcript elongation [65]. Briefly, xeroderma pigmentosum, complementation group C (XPC), associated with UV excision repair protein RAD23 homolog B (RAD23B) and centrin-2 (CETN2), is the main damage recognition protein in GG-NER. Upon binding of XPC, RAD23B is cleaved from the complex. In TC-NER, on the other hand, the Cockayne syndrome proteins type A and B (CSA, CSB) form a complex at the site of a lesion in the template strand, which leads to reverse translocation (backtracking) of the RNA polymerase II [31,65]. After successful detection of the DNA lesion, Transcription factor II Human (TFIIH; consisting of 7 subunits, including xeroderma pigmentosum type B and D (XPB, XPD), xeroderma pigmentosum type G (XPG), xeroderma pigmentosum complementation group A (XPA) and replication protein A (RPA)) is recruited to the lesion in subsequent steps and simultaneous dissociation of XPC results in the unwinding of the damaged DNA strand. Next, the nuclease xeroderma pigmentosum type F-excision repair cross-complementation group 1 (XPF-ERCC1) binds to DNA, induces dual incisions around the damaged nucleotides, and leads to excision of an about 30 nucleotide-long single strand DNA fragment. Finally, proliferating cell nuclear antigen (PCNA) recruits several DNA polymerases for DNA re-synthesis and NER is terminated by ligation of the new strand [31,65]. It is believed that NER preferentially repairs 1,3-intrastrand over 1,2-intrastrand crosslinks, thus supporting the hypothesis that especially the latter contribute to cytotoxicity [57]. Interestingly, tumor suppressor p53 seems to interact with several crucial components of NER machinery, such as XPC, TFIIH and RPA [31,46].
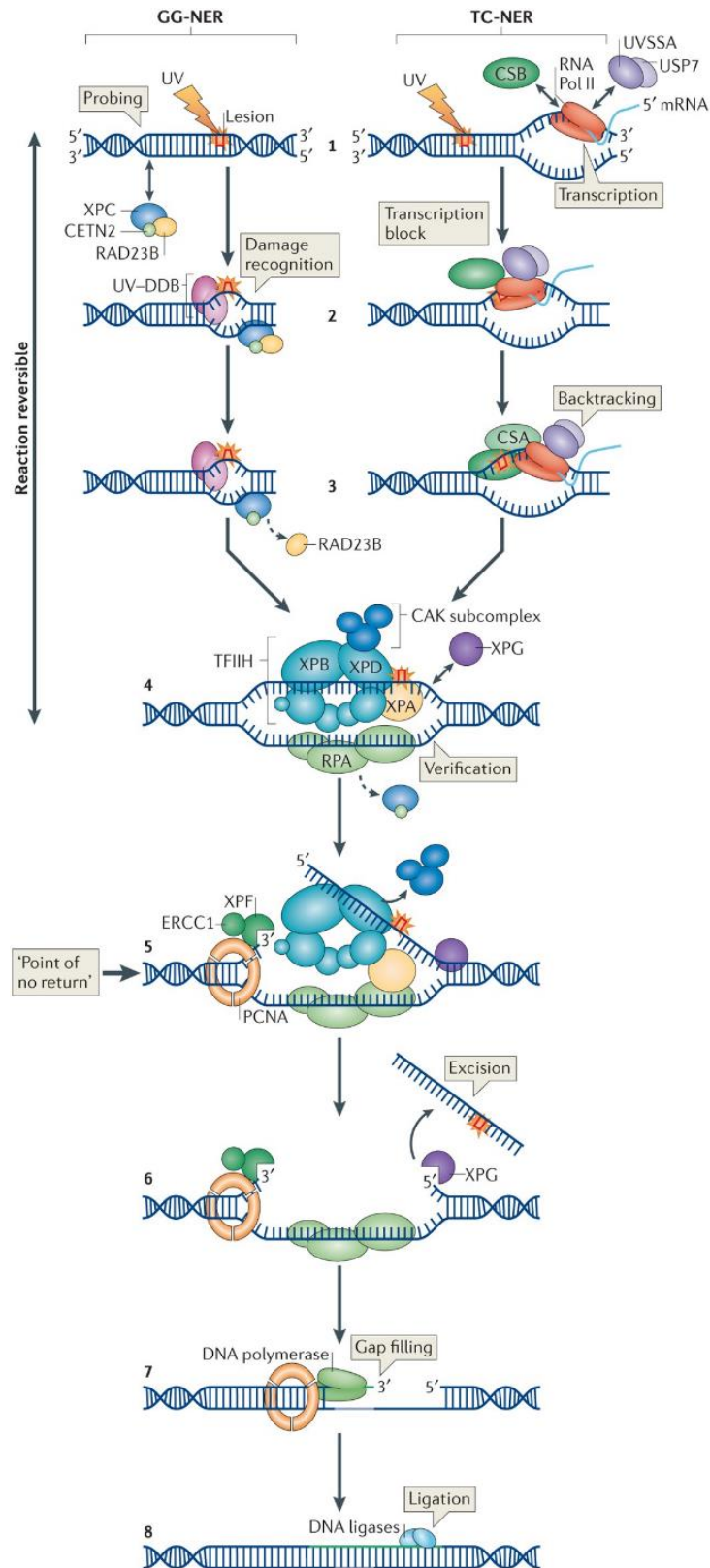
Figure 1.9 Process of the nucleotide excision repair mechanism [65].

Although DNA synthesis is basically blocked due to structural changes of the helices, the cell is still able to maintain limited synthesis via special DNA polymerases, so-called translesion synthesis polymerases in a mechanism called replication bypass or

translesional DNA synthesis. These polymerases are able to circumvent platinum-DNA adducts on the DNA template and perform DNA replication without leaving a gap in the new strand by incorporating random nucleotides opposite of the platinated ones [42]. Consequently, this leads to mismatches of base pairs in the new DNA strand, which are then recognized by the mismatch repair (MMR) system. Next, the complement bases to the platinum-DNA adducts are removed and resynthesized in the newly synthesized strand instead of removal of the lesion itself [31]. The DNA adduct is then bypassed repeatedly in futile cycles of repair, ultimately resulting in apoptosis caused by emerging DNA gaps [66]. Additionally, the MMR system can also detect other DNA damage and triggers the activation of various signaling pathway regulators, such as p53, p73 and cellular Abelson murine leukemia viral oncogene homologue 1 (c-Abl), which also results in an initiation of apoptosis [31].

MMR seems to be essential for the efficacy of cisplatin and carboplatin, whereas recognition of oxaliplatin-DNA adducts is lower to negligible [42]. Fundamentally, this also applies to the detection of oxaliplatin-DNA lesions by enzymes involved in the replication bypass, for which oxaliplatin adducts are poor substrates [56]. Due to steric reasons, replication bypass is significantly limited and MMR enzymes cannot bind to DACH-containing adducts [55]. This leads to the conclusion that MMR plays only a minor, if any, role in the mechanism of action of oxaliplatin. In this context, Nehmé et al. found that MMR led to different signaling when comparing cisplatin and oxaliplatin treatment. In MMR-proficient cells both c-Jun N-terminal kinase (JNK) as well as c-Abl were activated upon treatment with cisplatin, whereas in MMR-deficient cells activation of JNK was reduced and c-Abl response was completely absent. In the case of oxaliplatin treatment, on the other hand, neither in MMR-deficient nor MMR-proficient cells activation of JNK or c-Abl could be detected [67]. Amongst other factors, the shortage of recognition by enzymes involved in replication bypass or MMR is considered one of the main reasons for the lack of cross-resistance and the deviating spectrum of activity of oxaliplatin in comparison to cisplatin and carboplatin [31].

1.3.3.3 Interaction with DNA-binding Proteins

Various DNA-binding proteins are affected by cisplatin, carboplatin and oxaliplatin adducts. This includes, most notably, DNA-damage repair proteins, transcription factors activated by platinum-induced signaling cascades and DNA polymerases, such as the previously described translesion synthesis polymerases [53].

Besides the already addressed proteins, the high mobility group box 1 (HMGB1) protein is worth mentioning. This DNA chaperone protein comprises two HMG domains capable of recognizing and binding with high affinity to bent DNA, more precisely, to 1,2-intrastrand-GG crosslinks [42,57]. It has been implicated in promoting cytotoxicity of all platinum drugs by first interacting with damaged DNA and then shielding it from repair by NER [42,46] and preventing replicate bypass [57]. Yet, affinity for oxaliplatin adducts seems to be lower than for cisplatin and carboplatin adducts [57]. Moreover, the platinum-DNA-HMGB1 complex is able to block transcription factors. However, formation of disulfide bond between two cysteines in the second HMG domain must be prevented in order for the protein to be able to achieve sensitization to cisplatin. Interestingly, high expression of high mobility group box 4 (HMGB4), a variant of the protein where one of the cysteines is replaced by a tyrosine, as is the case in testicular cancer, positively correlated with cisplatin sensitivity [42].

1.3.3.4   Apoptosis and Necrosis

When DNA damage surpasses a critical threshold, cellular repair mechanisms are superseded by cell death activation [46]. However, the nature of cell death initiated by cisplatin is concentration-dependent and is determined by the level of cellular damage [48]. Apoptosis is the main cell death mode and can be distinguished into the intrinsic and the extrinsic pathway [68]. The intrinsic form is commenced by translocation of platinum-induced Bcl-2-associated X protein (Bax) from the cytosol to the mitochondria, triggered by an increase in the ratio between Bax and its anti-apoptotic counterpart B-cell lymphoma 2 (Bcl-2). Next, a release of pro-apoptotic factors such as cytochrome c leads to activation of the caspase-9/caspase-3 cascade through apoptotic protease activating factor 1 (Apaf1, Figure 1.10) [31,46]. Alternatively, the extrinsic pathway proceeds without participation of the mitochondria and operates, amongst others, via activation of death receptor Fas by ligand FasL [46]. Through binding of FasL, adaptor protein Fas-associated death domain protein (FADD) is recruited and binds to the receptor, and hence, via interacting with initiator caspase 8, forms the death-inducing signaling complex (DISC) [69]. Following this, upstream caspase 8 activates downstream caspase 3. In both cases, activation of caspase 3 is responsible for direct activation of deoxynucleases and, consequently, apoptosis [48].
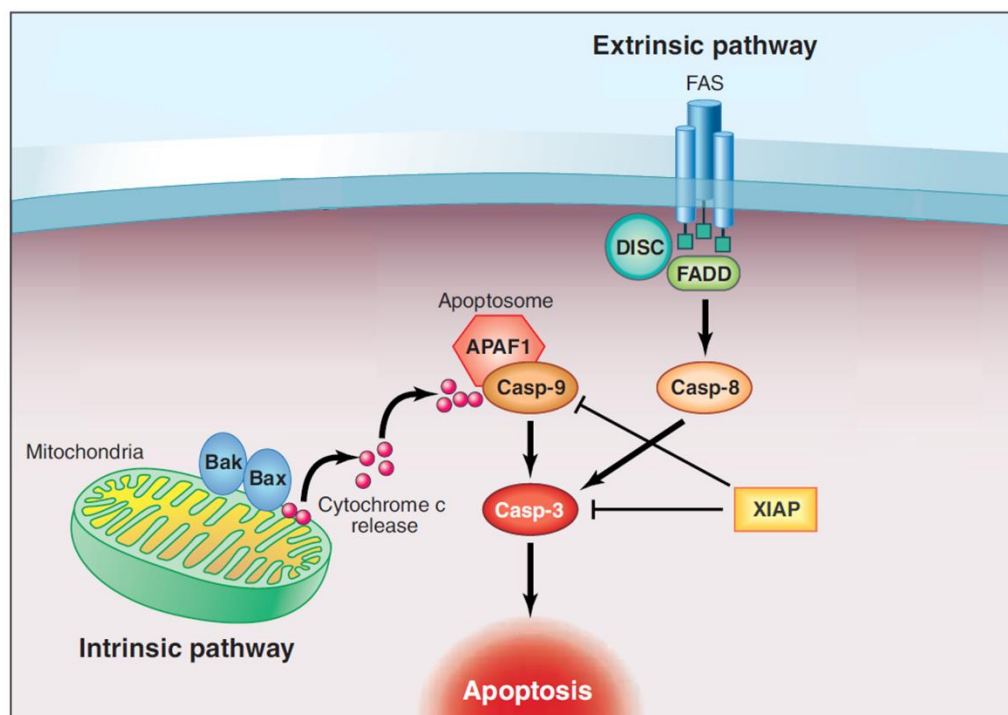
Figure 1.10 Intrinsic and extrinsic apoptosis pathways. Modified from Denicourt et al. [69].

In the event of exorbitant DNA damage, on the other hand, PARP is hyperactivated, which will lead to cleavage of NAD^+ and transfer of ADP-ribose (ADPR) moieties to carboxyl groups of nuclear proteins. The ultimate consequence of the resulting deficiency of NAD^+ and, due to the inhibition of its production by missing NAD^+, deficiency of ATP is necrosis [31,70]. Hereby, ATP levels are the critical factor. In case of sufficient amounts of ATP intracellularly, caspase activity can be maintained, PARP can be cleaved and apoptosis is the cell death mechanism induced. However, if ATP levels are too low, cells die via necrosis [70].

1.3.3.5   Signaling Pathways after Recognition of Platinum-DNA Adducts

Upon DNA-damage-recognition, various signaling cascades are activated. These pathways are highly complex and intertwined in many ways (Figure 1.11). There is evidence for different signaling activated by cisplatin and carboplatin in comparison to oxaliplatin [57]. Interestingly, even though the exact mechanisms and interconnections are not fully elucidated to date, not all of the involved pathways enhance platinum cytotoxicity and some are even associated with the development of resistance. The relative intensity of the signals and the crosstalk between the pathways seems to determine whether it comes to cell death or cell survival [46].
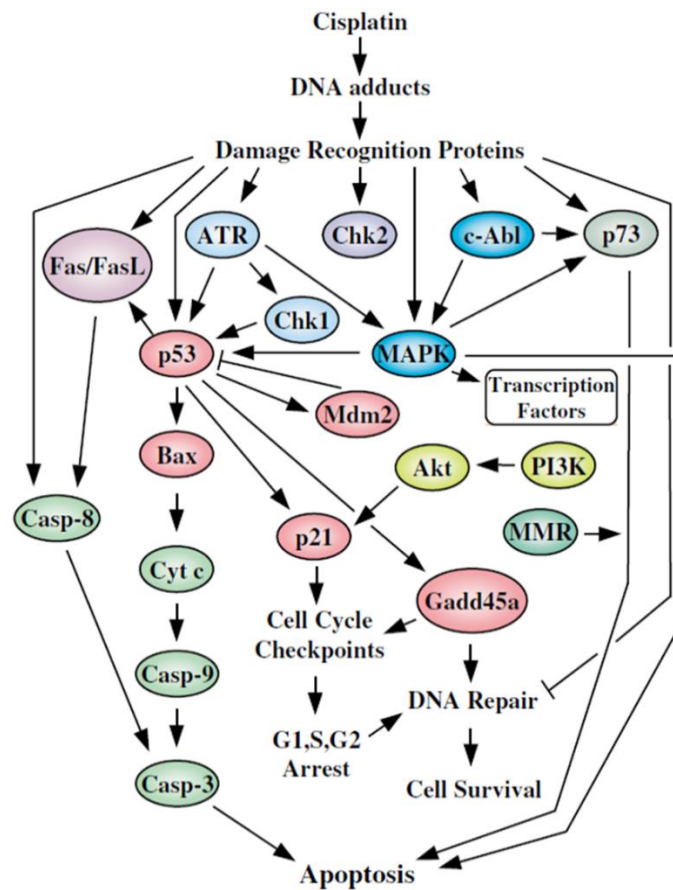
Figure 1.11 Simplified schematic overview of pathways involved in mediating cisplatin-induced cellular effects. Modified from Siddik et al. [46].

One of the proteins affected by cisplatin-induced DNA lesions is c-Abl. Once activated by DNA damages, c-Abl is transmitting DNA-damage signals from the nucleus into the cytoplasm. Possible downstream effectors of the tyrosine kinase c-Abl include p73, mitogen-activated protein kinase (MAPK) and tumor suppressor protein p53 [31]. Phosphorylated p73 is known to induce apoptosis [46]. As addressed before, c-Abl signaling seems to be relevant only in the context of cisplatin treatment and does not appear to be activated upon oxaliplatin exposure [67].

Phosphorylation of tumor suppressor protein p53 by MAPK upon exposure to stress stimuli leads to inhibited cell proliferation by inducing either cell cycle arrest or apoptosis [31,71]. Additionally, p53 activation can also be induced via prior activation of ataxia telangiectasia mutated protein (ATM) or, preferably, RAD3-related protein (ATR). ATR further mediates the activation of CHK1 [46]. Yet, while some studies prove a positive correlation between cisplatin cytotoxicity and p53 activity, other results question these conclusions [31]. In this context, p53 seems to be involved in DNA repair processes by activation of p21 and growth arrest and DNA-damage-inducible

protein alpha (Gadd45a). Hereby, Gadd45a associates with PCNA, amplifies NER activity and, therefore, protects cells from platinum-induced cytotoxicity [46].

The MAPK pathway is composed of three major sub-families, namely extracellular signal-regulated kinase (ERK), JNK and p38. MAPKs are responsible for controlling cell proliferation, cell differentiation and cell death [42]. Besides being activated equally by cisplatin, endogenous trigger of these cascades differ slightly: While the ERK pathway is primarily induced by growth factors and cytokines, JNK and p38 are initiated by various stress signals [31,42]. However, especially considering both ERK and JNK pathways, evidence of involvement in cisplatin-induced cytotoxicity has not been resolved entirely and seems to be dependent on the cellular context and the degree of DNA damage, at least to some extent [31,42,46].

In contrast, the phosphoinositide 3-kinase (PI3K)/protein kinase B (Akt) pathway undisputedly serves an anti-apoptotic purpose. This is carried out by phosphorylation and modulation of several downstream target proteins and, subsequently, downregulation of pro-apoptotic signaling cascades, which are stimulated by platinum treatment [31,72]. Amongst others, Akt phosphorylates X-linked inhibitor of apoptosis (XIAP) and thereby prevents its ubiquitination. Increased levels of XIAP, in turn, have been associated with a reduction of cisplatin-induced caspase 3 activity and apoptosis [31]. Furthermore, the activation of nuclear factor-kB (NF-kB) and following diminished apoptosis are also conveyed by Akt [31].

1.4   Platinum Resistance

The major drawback of platinum-based chemotherapy is inherent (primary) and acquired (secondary) resistance [33,45]. Its development is a phenomenon that not only leads to the absence of a positive risk-benefit ratio and to dominance of unwanted adverse reactions but also hinders the total eradication of the tumor in many cases and subsequently results in increasing mortality rates [3,6,73]. It has been shown that only a small proportion of the intracellular platinum reaches the nucleus and can thus interact with DNA leading to apoptosis [48]. As mentioned above, most of the cellular processes that are induced after DNA damage are not only relevant for the cytotoxicity of cisplatin but are also involved in the development of resistance. Amongst the most prominent reasons for the occurrence of reduced susceptibility towards platinum drugs are reduced accumulation, increased inactivation, enhanced repair or tolerance of

DNA lesions and modifications of pro- and anti-apoptotic signaling pathways. Some of these mechanisms have been thoroughly investigated [33,45,74]. On the contrary, the fate of the platinum in the cytosol and the relevance of alternative binding partners for tumor cell sensitivity and resistance are largely unelucidated. In principle, these mechanisms can be classified according to functional and hierarchical parameters: pre-, on-, post- and off-target mechanisms (Figure 1.12) [45].
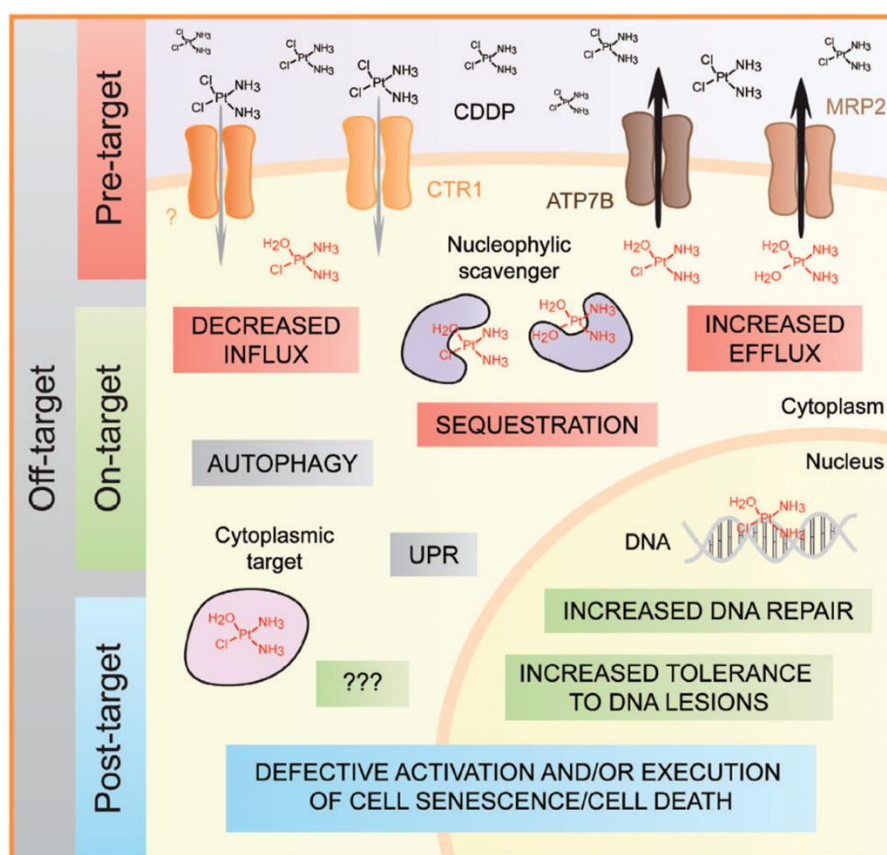
Figure 1.12 Molecular mechanisms of cisplatin resistance [45].

In part, these processes apply equally to all platinum drugs, but then again, differences in the development of resistance between cisplatin and carboplatin vs. oxaliplatin have also been observed [42,75]. The formation of divergent DNA adducts due to conformational differences between cisplatin and oxaliplatin and subsequent deviating detection of DNA damage by cellular components is believed to play a major role in different processing [42].

In general, the development of resistance is always a multifactorial phenomenon, in which decreased response of a tumor to an anti-cancer drug can never be attributed to only one of the mechanisms described briefly below. It is usually a combination of several factors, most of which are rarely obvious [45]. For this reason, finding a solution

to resistance is complicated and the identification of biomarkers that would allow a prediction of therapeutic success before treatment is extremely desirable.

1.4.1 Pre-Target

Pre-target resistance is triggered by mechanisms that precede target (DNA) binding of platinum drugs. This includes reduction of intracellular accumulation due to decreased influx and increased efflux. Even though not entirely elucidated, reduced expression of CTR1 was attributed to cisplatin resistance. CTR1-deficient mouse models were found to be more resistant and pre-treatment with copper salts, the natural substrate of CTR1, suppressed cisplatin-induced cytotoxicity [29]. Internalization of the transporter was observed at clinically relevant concentrations of cisplatin [76]. This, however, could indicate not only the development of resistance but also the irrelevance of this transporter for the uptake of cisplatin in general. Concerning participation of CTR1 expression in the development of oxaliplatin resistance, data is even more contradictory. While downregulation of CTR1 has been shown to promote resistance [77], other research deemed contribution of the transporter to resistance unlikely [54]. Similarly, the role of OCT1-3 is not unambiguously clarified. Taken OCT2, for example, kidney cells stably expressing this transporter showed increased susceptibility towards oxaliplatin and cisplatin, whereas expression could not be correlated with positive clinical outcome in ovarian cancer patients and no difference in uptake by sensitive vs. resistant colorectal cells was found [54,78]. Beside the rather vague results and the uncertainty as to whether platinum enters the cell by active transport to a relevant extent, there is relatively reliable data on increased export of the drug. Here, especially multidrug resistance protein 2 (MRP2) seems to be responsible for an increased efflux of platinum [29]. Additionally, two other transporters, ATPase copper transporting alpha and beta (ATP7A and ATP7B), are supposed to be involved in the outward transport of cisplatin [29]. It was found that these proteins are overexpressed in cisplatin-resistant cell lines [79] and that increased ATP7A and ATP7B expression in patients correlated with disease recurrence and reduced overall survival [80]. The same was detected for ATP7A in oxaliplatin-resistant ovarian cancer cells [81] and for ATP7B in colorectal cancer patients, which featured shorter times to progression than patients with lower mRNA expression levels of the transporter [82].

Once inside the cell, platinum drugs are increasingly bound by molecules such as GSH, MT and other cytoplasmic scavengers with nucleophilic properties. Even though

these interactions may sustain cisplatin's cytoplasmic effects, this also limits the amount of freely available platinum [29]. Moreover, binding to glutathione, catalyzed by glutathione-S-transferase π 1, results in efflux of the platinum-GSH complexes out of the cell via MRP2 [29,53]. Beyond that, GSH has been shown to bind to platinum-DNA monoadducts, thus preventing the formation of bifunctional crosslinks [83,84]. Taken together, it is therefore conclusive that increased levels of GSH have been associated with cisplatin resistance [29].

Furthermore, efflux of toxic substances, including cisplatin-glutathione conjugates, via p-glycoprotein (P-gp, multidrug resistance proteins 1 (MDR1)) has also been observed [85]. However, this is in contrast to findings that demonstrated the transporter to be of minor relevance for cisplatin resistance [39,86].

1.4.2   On-Target

On-target resistance emerges due to alterations of processes that are directly connected to molecular damage induced by platinum. This covers basically all mechanisms that are involved in the recognition of DNA adducts and subsequent cascades, be it apoptotic signaling or DNA repair. As explained before, the MMR system detects platinum-induced DNA base pair mismatches, but repairing of the newly synthesized strand instead of the template leads to failure of long-lasting improvement and a vicious circle of repair, ultimately leading to emission of apoptotic signals. The detection of adducts and following induction of apoptotic signals is impaired in resistant cells and proteins involved in MMR are often mutated or downregulated [29]. MMR deficiency has been proven to be present in many resistant cancer cell lines. Since MMR does not play a role in oxaliplatin resistance [42,53], this might be one reason for the distinctive efficacy of oxaliplatin in cisplatin- and carboplatin-resistant cells. In agreement with this, defects in mutL homolog 1 (MLH1), an MMR-related protein, have been repeatedly linked to increased levels of replicate bypass [29]. Without a functional MMR system, mismatching caused by translesion synthesis polymerases would not be detected and removed, thus, preventing the futile cycles addressed before and enabling completion of replication after replicative bypass of the damage. Interestingly, it has been shown that replicative bypass is increased in cisplatin-resistant cells and that it is selective for cisplatin in comparison to oxaliplatin adducts [66]. This enhanced toleration of DNA lesions is yet another common feature of resistant cells. On the other hand, defects in DNA polymerases involved in the

replicate bypass have been correlated with increased susceptibility towards cisplatin [45].

Another characteristic that platinum-resistant cells can acquire is an increased ability to repair detected DNA lesions via NER. Expression of ERCC1, one of the rate-limiting factors of NER, has been inversely correlated with responsiveness to cisplatin-based treatment regimens and survival on a clinical level in multiple entities [29]. Interestingly, ERCC1 expression has been associated with cisplatin, but not oxaliplatin resistance, while it was the other way around with XPD expression [53]. In that regard, not only low ERCC1, but also XPA and xeroderma pigmentosum type G (XPF) expression has been attributed to the exceptional efficacy of cisplatin in testicular cancer [53].

Finally, it should be noted that cytoplasmic components that may account for extranuclear cytotoxicity of platinum drugs, and of which only few have been identified thus far, are also of great importance and might be responsible for the development of on-target resistance [45].

1.4.3   Post-Target

Post-target resistance mechanisms, that is, modification of signaling pathways induced by DNA damages, are nearly never specific and can be expanded to other DNA-damaging agents and other cytotoxic stimuli [45]. Most commonly, signaling cascades that are normally involved in the regulation of apoptosis, as well as the cell death machinery itself, show malfunctions, which have been linked to various levels of cisplatin resistance [29]. Although not entirely conclusive, many studies show an association between p53 status and the sensitivity of platinum drugs. In many cancer entities, such as breast, lung, colon, kidney and ovarian cancer, p53 inactivation via mutations was found in resistant cell lines in comparison to sensitive cell lines harboring p53 wild-type [68]. Moreover, cisplatin-resistant colon cancer cells, which lacked a functional p53 protein, had reduced levels of Fas and Apaf1, both proteins immensely important in the processes of extrinsic and intrinsic apoptosis, respectively [68]. In ovarian cancer, patients with affirmed p53 wild-type had a higher chance to benefit from cisplatin-based chemotherapy than patients with inactivated p53 [29]. Likewise, a loss of p53 function has also been associated with intrinsic resistance to oxaliplatin in colorectal cancer cells [78].

Considering other pathways usually triggered by treatment with platinum compounds, failure to activate p38 and JNK was determined in resistant cells, which ultimately led to limitation in pro-apoptotic signaling. Furthermore, upregulation of caspase-inhibitor survivin by PI3K/Akt-dependent mechanisms was negatively associated with cisplatin responsiveness in esophageal, lung and ovarian cancer patients. Similarly, upregulation of anti-apoptotic Bcl-2 seems to correlate with cisplatin resistance and recurrent disease [29].

1.4.4   Off-Target

Deviations in signaling pathways that are not directly activated by cisplatin but compensate or disturb cisplatin-induced lethal signals, are considered off-target resistance mechanisms [29]. One example is the v-erb-b2 avian erythroblastic leukemia viral oncogene homolog 2 (ERBB2) protooncogene, also known as human epidermal growth factor receptor 2 (HER2), which codes for an EGFR tyrosine kinase. This protein is amplified or overexpressed in many types of tumors and has been suggested to convey cisplatin and oxaliplatin resistance [29,45,87]. Signals induced by ERBB2 are forwarded via multiple downstream pathways, including the SHC-transforming protein 1 (SHC)/growth factor receptor bound protein 2 (Grb2)/Son of sevenless (Sos) and the PI3K/Akt cascades [29]. Moreover, this oncogene is reputed to regulate the transitory cell cycle arrest, which is initiated in order to enable the repair of platinum-induced damage [45].

1.5   Binding Partner Identification and Its Relevance

Since the early 1980s, cellular fate of cisplatin has been of interest. The necessity of knowing the sites of its localization and accumulation within the cell as well as the molecular species with which it interacts, aiming at understanding the toxic and therapeutic effects, was pointed out [88,89]. It is known that only as little as 1% of intracellular cisplatin reacts with nuclear DNA and similar estimations have been made for its successors carbo- and oxaliplatin [41,48,90]. Based on the repeatedly proven high affinity of platinum drugs for both N- and S-donors, the theory that DNA cannot be the only target has emerged [59,61,91]. Interactions between platinum species and a variety of intracellular nucleophiles, besides the nucleobases, have been examined more closely in the past years [89,92]. Here, proteins possessing preferentially sulfur-containing amino acid side chains such as cysteines and methionines, but also

histidines have come into focus [59,91–93]. It has been shown that while binding to nucleobases requires hydrolytic aquation of cisplatin, relatively strong coordinative binding to sulfur-containing species can take place directly without any prior ligand replacement and generally constitutes a kinetically favored process [40,91,92,94]. Since the formation of aquated platinum species presents the rate-limiting step in DNA platination as opposed to the high reactivity of thiol- and thioether-containing proteins, it is the logical conclusion that cisplatin-protein interactions represent the majority of intracellular adducts [59,91]. Thus, it comes as no surprise that involvement of non-DNA targets in the mechanism of action but also in the development of resistance has been increasingly discussed, even though inter- and intrastrand crosslinks with DNA and subsequent initiation of apoptosis are still considered the major cytotoxic effect of cisplatin.

In this context, the interactions of cisplatin with cysteine and methionine residues of intracellular metallothioneins and glutathione rank amongst the most intensively studied [59]. With about 0.1-10 mM, GSH represents the most abundant intracellular thiol [95]. Naturally, an interaction with cisplatin would be expected. In reality however, the role of GSH in the impact that cisplatin has on cells, is rather contradictory. Certainly, most of the studies conducted confirm that the tripeptide plays an active role in the detoxification of drugs [96]. In line with this, as mentioned earlier, cisplatin is bound to GSH by the enzyme glutathione-S-transferase π 1 (GSTP1) and then removed from the cell by MRP2 efflux transporter [29,53]. As an example, it has been reported that in cisplatin-treated leukemia cells 60% of the intracellular Pt(II) is present bound to glutathione [97]. This way, less free active cisplatin is available in the cell resulting in cytotoxicity decrease. GSH also appears to reduce the reaction rate of cisplatin with DNA [59]. As also addressed before, GSH is able to react with monofunctional DNA adducts and inhibit rearrangement into lethal bifunctional adducts [83]. This is consistent with the fact that the presence of elevated levels of GSH is often associated with cisplatin resistance [98–100]. On the other hand there are also contradictory studies, in which no cisplatin-GSH adducts were found at all [101–103]. Even though GSH is greatly abundant in the cell, reactivity of cisplatin towards MT is about 50 times higher than towards GSH, which makes this class of proteins equally important as binding partners [104]. Indeed, cisplatin has been shown to be bound to a large extent to MT cysteine residues and an overexpression of these highly effective platinum scavengers is known to increase resistance dramatically, thus, resulting in

lower clinical response to the drug and unfavorable prognosis of patients [59,105]. In accordance with this, sensitivity to cisplatin is significantly higher in cells without MT [59,88]. The interaction of cisplatin with MT was accompanied by the simultaneous release of zinc, which is naturally bound to MT but can be replaced by other metals such as platinum [106]. This in turn triggers the biosynthesis of MT-2, one of two major isoforms of metallothioneins, and results in further amplification of cisplatin inactivation [106].

This, of course, raises the logical question of how cisplatin can exert any cytotoxic effect at all despite the vast number of intracellular thiols, which has been addressed several times in the past. In contrast to the interactions triggering resistance, protein binding that enhances the cytotoxic activity of cisplatin and has, therefore, a positive effect on cisplatin efficiency, has also been described. One example is the irreversible inhibition of the enzyme thioredoxin reductase (TrxR). This has the consequence that the intracellular redox homeostasis is strongly disturbed after cisplatin treatment increasing cell death [107,108]. In this context, however, it has also been associated to a possible increase in nephrotoxicity and hepatotoxicity due to the resulting unbalanced redox processes [108]. In general, the connection between cisplatin-protein binding and adverse reactions or lack of efficacy has been documented quite frequently [40,59,89,109]. These findings are in line with the opinion of Karasawa et al., who hypothesized that cisplatin toxicity in slowly proliferating or terminally differentiated cells occurs predominantly due to drug interactions with antioxidant proteins leading to the accumulation of endogenous reactive oxygen species (ROS) and that DNA binding is of rather minor significance when considering toxicities [110]. Other studies even go so far as to hypothesize that platination of DNA in cancer cells might also play a subordinate role and that desired cytotoxicity is mainly initiated by activity in the cytosol, since the level of DNA platination does not correlate with cisplatin-induced apoptosis on the one hand and it has been shown that cisplatin can induce nucleus-independent apoptosis signaling on the other hand [59–61].

In addition to these less generally accepted mechanisms of cell death, influence of protein binding partners on the well-known mechanism of action through DNA platination has been investigated. Studies suggest that cisplatin bound to S- or N-donors such as S-guanosyl-L-homocysteine represent only intermediate species and that platinum is ultimately transferred to N7 of guanines [59,91,93]. It appears that

although interactions with proteins are kinetically preferred, binding to guanine-N7 is thermodynamically favored and DNA adducts thus yield the final reaction product [59,91,93,111]. Concomitantly, it has been discussed that binding to proteins may represent some sort of drug reservoir, enabling a long-term supply of platinum moieties and thereby subsequent DNA platination [41,93,112]. In agreement with this, even years after therapy platinum levels in patients, treated with platinum drugs were >30-fold higher than the mean level in unexposed controls [49]. However, the existence of such a reservoir does not seem to be universal. On the one hand, studies have shown that only Pt-thioether adducts are involved and, on the other hand, a transfer to N7 seems to be limited to guanines [93].

In a previous work, the working groups of Dr. Sabine Metzger, University of Cologne, Germany, and Prof. Ulrich Jaehde, University of Bonn, Germany, successfully identified cytosolic binding partners of CFDA-cisplatin (cisplatin analog featuring a carboxyfluorescein diacetate tag) in ovarian cancer cells [113,114] and showed that pharmacological inhibition of protein disulfide isomerase alpha 1 (PDIA1) results in restored sensitivity of resistant cells to cisplatin [115]. A similar attempt was conducted by Karasawa et al., who synthesized platinum-agarose conjugates to specifically investigate protein binding that might be involved in two common cisplatin side effects, ototoxicity and nephrotoxicity [110]. Furthermore, Messori et al. emphasized that exploration of cisplatin-protein interactions is essential for studying resistance mechanisms and for the development of new therapeutic agents. Therefore, they made an effort to elucidate the critical characteristics of cisplatin binding to proteins and pointed out that this would eventually help to predict possible binding partners [92].

Collectively, all this data shows that the effect of cisplatin interaction with intracellular components other than DNA cannot be exclusively labeled as positive or negative in terms of sensitivity of cancer cells. The outcome is highly dependent on the cellular context and is probably even cancer-entity specific, which is why the study of the cisplatin interactome is crucial for increasing the general understanding of molecular processes as well as pathological mechanisms. Also due to ever increasing incidence and mortality rates of almost all cancer entities [3,6,73], it is vitally important not only to identify possible reasons of therapy failure and underlying mechanisms, but also to determine new biomarkers and novel targets that will help to improve and personalize cancer chemotherapy.

2   Aim and Objectives

As resistance is still the major drawback of platinum-based chemotherapy and frequently leads to failure of treatment, it is of utmost importance to unravel unknown details about resistance development and in doing so identify biomarkers, which would allow early identification of resistant tumors. Additionally, characterization of alternative drug targets may help to expand the possibilities of cancer therapies through development of effective combination treatments of novel and conventional anti-cancer therapies.

In this respect, given the different activity of cisplatin in ovarian and colorectal cancer, this project aimed at identifying cytosolic binding partners of cisplatin in tumor cells of these two entities and at evaluating their relevance for cytotoxicity. It was hypothesized that intracellular binding partners of cisplatin differed between ovarian cancer and colorectal cancer cells, thus partaking in the development of acquired and intrinsic resistance, respectively. As addressed above, protein binding can affect cell sensitivity to platinum drugs on many levels. On the one hand, it may lead to the sequestration in the cytosol, limiting the amount of free platinum that can subsequently reach the nucleus. On the other hand, platinum binding may impair normal function of a protein via inhibition of downstream signaling.

In order to identify protein binding partners of cisplatin, applicability of different identification methods including direct detection with a fluorescent cisplatin analog, immunoprecipitation and copper-catalyzed azide-alkyne cycloaddition for the above-mentioned purpose in terms of simplicity, speed and reliability was to be compared. Subsequently, a selection of the identified protein binding partners of cisplatin was to be examined more closely for their for sensitivity to the drug.

3   Materials and Methods

All materials and methods described below refer to the final compositions and applications. Where applicable, adjustments are described in Chapters 4.1.5, 4.1.6 and 4.1.7.

3.1   Materials

3.1.1   Chemicals and Reagents

Acetonitrile	Sigma Aldrich GmbH, Steinheim
Ammonium Bicarbonate	Sigma Aldrich GmbH, Steinheim
Ammoniumperoxodisulfate (APS)	Roth GmbH & Co., Karlsruhe
BioVision Nuclear/Cytosol Fractionation Kit	BioVision Incorporated, Milpitas, CA, USA
Bis(sulfosuccinimidyl)suberate (BS^3)	Thermo Fisher Scientific, Rockford, IL, USA
Boron-dipyrromethene (BODIPY)-FL-Alkyne	Lumiprobe GmbH, Hannover
BODIPY-FL-Azide	Lumiprobe GmbH, Hannover
Bromophenol Blue (BPB)	AppliChem GmbH, Darmstadt
Bovine Serum Albumin (BSA)	Sigma-Aldrich GmbH, Steinheim
Carboxyl-BODIPY	Lumiprobe GmbH, Hannover
Cell Analysis System (CASY)®-Ton, isotonic diluting solution	Schärfe System, Reutlingen
3-[(3-Cholamidopropyl)dimethylammonio]-1-propanesulfonate (CHAPS)	Serva Electrophoresis, Heidelberg
Chloroform 99%	Grüssing GmbH, Filsum
Copper Sulfate Pentahydrate	Bernd Kraft GmbH, Duisburg
4′,6-Diamidino-2-phenylindole-dihydrochloride (DAPI)	Sigma-Aldrich GmbH, Steinheim
DeStreak™ Reagent	VWR International, Darmstadt
Dimethylformamide (DMF)	Sigma-Aldrich GmbH, Steinheim
Dimethylsulfoxide (DMSO)	Roth GmbH & Co., Karlsruhe
(2S,3S)-1,4-Bis(sulfanyl)butane-2,3-diol (Dithiothreitol, DTT)	Sigma Aldrich GmbH, Steinheim

DryStrip Cover Fluid	VWR International, Darmstadt
Dynabeads™ Protein A Immunoprecipitation Kit	Thermo Fisher Scientific, Rockford, IL, USA
eBioscience™ Annexin V-Fluorescein Isothiocyanate (FITC) Apoptosis Detection Kit	Thermo Fisher Scientific, Rockford, IL, USA
Ethanol 96%	VWR International, Radnor, PA, USA
Ethylenediaminetetraacetic acid (EDTA)	Sigma Aldrich GmbH, Steinheim
Fetal Calf Serum (FCS)	PAN-Biotech GmbH, Aidenbach
Glycerol	AppliChem GmbH, Darmstadt
Glycine	AppliChem GmbH, Darmstadt
4-(2-Hydroxyethyl)piperazine-1-ethanesulfonic acid (HEPES)	Sigma-Aldrich GmbH, Steinheim
Hydrochloric Acid 37% (m/V)	Merck KGaA, Darmstadt
Iodoacetamide (IAA)	VWR International, Darmstadt
Isopropanol 100%	Merck KGaA, Darmstadt
K4® Transfection System	Biontex Laboratories GmbH, Steinheim
10x Laemmli Electrophoresis Buffer	Serva Electrophoresis, Heidelberg
Leupeptin	Sigma-Aldrich GmbH, Steinheim
Magnesium Chloride Hexahydrate	Sigma-Aldrich GmbH, Steinheim
2-Mercaptoethanol	Sigma-Aldrich GmbH, Steinheim
Methanol	VWR International, Darmstadt
Molecular Probes™ SYPRO™ Ruby Protein Gel Stain	Thermo Fisher Scientific, Rockford, IL, USA
3-(4,5-Dimethylthiazol-2-yl)-2,5-diphenyltetrazolium bromide (MTT)	VWR International, Darmstadt
Nonyl Phenoxypolyethoxylethanol (NP)-40	Sigma-Aldrich GmbH, Steinheim
PageRuler™ Plus Prestained Protein Ladder	Thermo Fisher Scientific, Rockford, IL, USA
Penicillin/Streptomycin Solution (P/S)	PAN-Biotech GmbH, Aidenbach
Pepstatin A	Sigma-Aldrich GmbH, Steinheim
Phosphate-buffered Saline (PBS) Solution	PAN-Biotech GmbH, Aidenbach

Pierce™ Bicinchoninic Acid (BCA) Protein Assay Kit	Thermo Fisher Scientific, Rockford, Il, USA
Pierce™ Enhanced Chemiluminescence (ECL) Western Blotting Substrate Kit	Thermo Fisher Scientific, Rockford, IL, USA
Potassium Chloride	Sigma-Aldrich GmbH, Steinheim
Protein Inhibitor Cocktail	Roche AG, Basel, Switzerland
Purelab® Water	Obtained by Purelab® flex 2 Water Purification System, Elga LabWater, Celle
Quick Coomassie® Stain	Serva Electrophoresis, Heidelberg
Rotiphorese® Gel 30	Roth GmbH & Co., Karlsruhe
Roswell Park Memorial Institute (RPMI) 1640 Cell Culture Medium	Thermo Fisher Scientific, Rockford, IL, USA
SERVALYT™ 3-10	Serva Electrophoresis, Heidelberg
Skim Milk Powder	LABC-Labortechnik, Hennef
Sodium Ascorbate	Sigma-Aldrich GmbH, Steinheim
Sodium Azide	Merck Schuchardt OHG, Hohenbrunn
Sodium Chloride	Fisher Scientific, Hampton, VA, USA
Sodium Deoxycholate	AppliChem GmbH, Darmstadt
Sodium Dodecyl Sulfate (SDS)	Roth GmbH & Co., Karlsruhe
Sodium Fluoride	AppliChem GmbH, Darmstadt
Sodium Hydroxide 1.0 M	Sigma-Aldrich GmbH, Steinheim
Sodium Orthovanadate	Sigma-Aldrich GmbH, Steinheim
Sodium Phosphate Dibasic Dihydrate	Sigma-Aldrich GmbH, Steinheim
N,N,N',N'-Tetramethylethylenediamine (TEMED)	VWR International, Darmstadt
Thiourea	VWR International, Darmstadt
Tris(hydroxymethyl)aminomethane (Tris Base)	VWR International, Darmstadt
Tris(hydroxymethyl)aminomethane Hydrochloride (Tris HCl)	AppliChem GmbH, Darmstadt
Triton™ X-100	AppliChem GmbH, Darmstadt
Trypsin-EDTA Solution	Thermo Fisher Scientific, Rockford, IL, USA

| Tween®-20 | VWR International, Darmstadt |
| Urea | Serva Electrophoresis, Heidelberg |

Small interfering RNA (siRNA)

	Catalog Nr.	Supplier
Silencer® Select Vimentin	s14799	Thermo Fisher Scientific, Rockford, IL, USA
Stealth siRNA Glutathione-S-Transferase π 1	HSS104546	Thermo Fisher Scientific, Rockford, IL, USA
Silencer® Select Protein/Nucleic Acid Degylcase DJ-1 (DJ-1)	s22304	Thermo Fisher Scientific, Rockford, IL, USA
Silencer® Select Grb2	s226232	Thermo Fisher Scientific, Rockford, IL, USA
Stealth RNAi™ siRNA Negative Control (NC)	12935112	Thermo Fisher Scientific, Rockford, IL, USA

Primary Antibodies

	Catalog Nr.	Supplier	Dilution
Lamin B1, rabbit, polyclonal IgG	GTX103292	GeneTex, Irvine, CA, USA	1:5,000
Glyceraldehyde 3-phosphate Dehydrogenase (GAPDH), rabbit, polyclonal IgG	GTX100118	GeneTex, Irvine, CA, USA	1:20,000
Vimentin, mouse, monoclonal IgG$_1$	sc-6260	Santa Cruz Biotechnology, Dallas, TX, USA	1:200

DJ-1, rabbit, monoclonal IgG	MA5-29462	Thermo Fisher Scientific, Rockford, IL, USA	1:200
Grb2, mouse, monoclonal IgG$_1$	sc-8034	Santa Cruz Biotechnology, Dallas, TX, USA	1:200
BODIPY FL-antibody, rabbit, polyclonal IgG	A-5770	Thermo Fisher Scientific, Rockford, IL, USA	4 µL ≙ 12 µg/IP

Secondary Antibodies

	Catalog Nr.	Supplier	Dilution
Goat Anti-Rabbit IgG-Horseradish Peroxidase (HRP)	4030-05	Southern Biotech, Birmingham, AL, USA	1:1,000
Goat Anti-Mouse IgG, Human ads-HRP	1030-05	Southern Biotech, Birmingham, AL, USA	1:1,000

Platinum Complexes

Cisplatin (cis-diamminedichloridoplatinum(II))	Sigma-Aldrich GmbH, Steinheim
Oxaliplatin ([(1R,2R)-cyclohexane-1,2-diamine] (ethanedioato-O,O')platinum(II))	Sigma-Aldrich GmbH, Steinheim
BODIPY-cisplatin	Synthesis according to the literature procedure [116] by PD Dr. Ganna V. Kalayda.
Cisplatin-Azide	Synthesis according to the literature procedure [117] by PD Dr. Ganna V. Kalayda.
Cisplatin-Alkyne	Synthesis according to the literature procedure [118] by PD Dr. Ganna V. Kalayda.

Pharmacological Inhibitors

DJ-1 Inhibitor (5-Fluoro-1-(2-phenylethyl)-1H-indole-2,3-dione)	AKos Consulting & Solutions GmbH, Lörrach
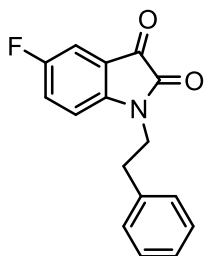
Ezatiostat-HCl	BIOTREND Chemikalien GmbH, Cologne
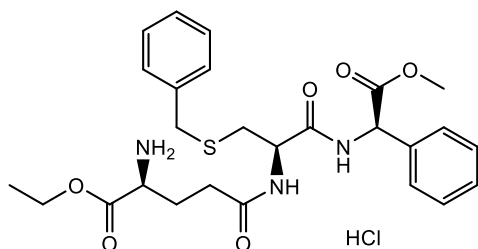
FOXC2-inhibiting Vimentin effector 1 (FiVe1)	BIOTREND Chemikalien GmbH, Cologne
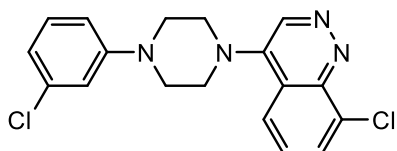
Grb2 Inhibitor A (1-(3-(4-(3-Aminophenyl)butyl)phenyl)-6,6-dimethyl-1,6-dihydro-1,3,5-triazine-2,4-diamine HCl)	NCI/DTP Open Chemical Repository, National Cancer Institute, Rockville, IL, USA
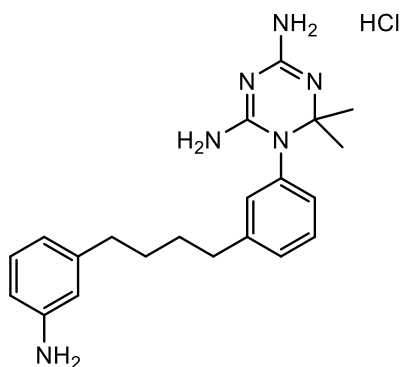
| Grb2 Inhibitor B (6,6-Dimethyl-1-(3-((1E,3E)-4-(3-nitrophenyl)buta-1,3-dien-1-yl)phenyl)-1,6-dihydro-1,3,5-triazine-2,4-diamine HCl) | NCI/DTP Open Chemical Repository, National Cancer Institute, Rockville, IL, USA |
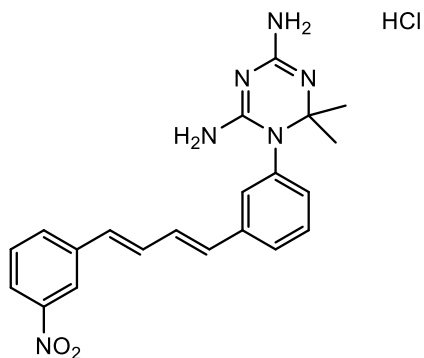
3.1.2   Solutions and Buffers

3.1.2.1   Cell Incubation Experiments

Cell Culture Medium for Cultivation	RPMI 1640 Cell Culture Medium	500.0 mL
	FCS	50.0 mL
	P/S	5.0 mL
Cell Culture Medium for Incubation Experiments	RPMI 1640 Cell Culture Medium	500.0 mL
	P/S	5.0 mL
Cisplatin Stock Solution [5 mM]	Cisplatin	15.0 mg
	PBS	10.0 mL
Oxaliplatin Stock Solution [10 mM]	Oxaliplatin	39.7 mg
	Purelab® Water	10.0 mL
BODIPY-cisplatin Stock Solution [50 mM]	BODIPY-cisplatin	12.18 mg
	DMF	387.16 µL
Carboxyl-BODIPY [50 mM]	Carboxyl-BODIPY	25.0 mg
	DMF	1711.8 µL

FiVe1 Stock Solution [100 mM]	FiVe1	10.0 mg
	DMF	278.4 µL
Ezatiostat-HCl Stock Solution [100 mM]	Ezatiostat-HCl	25.0 mg
	DMF	441.61 µL
DJ-1 Inhibitor Stock Solution [100 mM]	DJ-1 Inhibitor	25.0 mg
	DMF	242.5 µL
Grb2 Inhibitor A Stock Solution [100 mM]	Grb2 Inhibitor A	20.0 mg
	DMF	546.0 µL
Grb2 Inhibitor B Stock Solution [100 mM]	Grb2 Inhibitor B	20.0 mg
	DMF	511.0 µL
Cisplatin-azide Stock Solution [100 mM]	Cisplatin-azide	21.53 mg
	DMF	564.9 µL
Cisplatin-alkyne Stock Solution [100 mM]	Cisplatin-alkyne	25.38 mg
	DMF	564.9 µL
BSA Solution [0.1%]	BSA	1.0 mg
	Purelab® Water	ad 1.0 mL
MTT Solution	MTT	50.0 mg
	PBS	ad 10.0 mL
siRNA Stock Solution [20 µM]	siRNA (against vimentin, GSTP1, DJ-1, Grb2 or NC)	5 nmol
	Ribonuclease (RNAse)-free water	250.0 µL

Transfection Solution "Knockdown-Sample Preparation"	RPMI 1640 Medium (w/out FCS and P/S)	250.0 µL
	K4® Transfection Reagent	27.0 µL
	RPMI 1640 Medium (w/out FCS and P/S)	250.0 µL
	siRNA [20µM]	10.0 µL
Add	Diluted siRNA	260.0 µL
to	Diluted K4® Transfection Reagent	260.0 µL
Transfection Solution "Knockdown-Cytotoxicity Experiments"	RPMI 1640 Medium (w/out FCS and P/S)	300.0 µL
	K4® Transfection Reagent	32.4 µL
	RPMI 1640 Medium (w/out FCS and P/S)	300.0 µL
	siRNA [20µM]	24.0 µL
Add	Diluted siRNA	300.0 µL
to	Diluted K4® Transfection Reagent	300.0 µL
DAPI Stock Solution	DAPI	1.0 mg
	Methanol	1.0 mL
DAPI Working Solution	DAPI Stock Solution	5.0 µL
	Purelab® Water	1.0 mL
Cryogenic Medium	FCS	45.0 mL
	DMSO	5.0 mL

3.1.2.2 Gel Electrophoresis

Pepstatin A Stock Solution [2 mM]	Pepstatin A	1.37 mg
	Methanol	1.0 mL
Leupeptin Stock Solution [11.7 mM]	Leupeptin	5.0 mg
	Purelab® Water	1.0 mL

Cell Lysis Buffer (CLB) IV	HEPES	0.238 g
	KCl	0.298 g
	$MgCl_2$ x 6 H_2O	0.061 g
	Glycerol	5.0 mL
	Nonylphenoxypolyethoxylethanol-40 (NP-40)	0.5 mL
	Purelab® Water	ad 100.0 mL
	pH adjusted to 7.4 using NaOH 1.0 M	
	per 1.0 mL aliquot:	
	Pepstatin A	5.0 µL
	Leupeptin	2.0 µL
Radioimmunoprecipitation Assay (RIPA) Buffer	Tris-HCl	0.788 g
	NaCl	0.876 g
	Triton™ X-100	1.0 mL
	Sodium Deoxycholate	1.0 g
	EDTA	0.0326 g
	Purelab® Water	ad 100.0 mL
	pH adjusted to 7.4 using NaOH 1.0 M	
RIPA Lysis Buffer	RIPA Buffer	1.0 mL
	Pepstatin A	5.0 µL
	Leupeptin	2.0 µL
	Sodium Fluoride	5.0 µL
	Sodium Orthovanadate	10.0 µL
	Protease Inhibitor Cocktail	1.0 µL
BCA Working Reagent	BCA Reagent A	20.0 mL
	BCA Reagent B	0.4 mL
	Both included in Pierce™ BCA Protein Assay Kit	

Sample Loading Buffer, 5x	Stacking Gel Buffer	1.75 mL
	Glycerol	1.5 mL
	SDS Solution 10%	5.0 mL
	BPB	0.025 g
APS Solution [10%]	APS	100.0 mg
	Purelab® Water	ad 1000.0 µL
SDS Solution [10%]	SDS	1.0 g
	Purelab® Water	ad 10.0 mL
Laemmli Electrophoresis Buffer, 1x	Laemmli Electrophoresis Buffer 10x	100.0 mL
	Purelab® Water	ad 1000.0 mL
Stacking Gel Buffer pH 6.8	Tris Base	12.11 g
	Purelab® Water	ad 100.0 mL
	pH adjusted to 6.8 using HCl 37%	
Solubilization Buffer	Urea	8.41 g
	Thiourea	3.05 g
	CHAPS	0.4 g
	Purelab® Water	ad 20.0 mL
	Per 1.0 mL of aliquot:	
	DeStreak™ Reagent	12 µL
	SERVALYT™ 3-10	5 µL

Equilibration Buffer	Tris HCl pH 8.8	3.33 mL
	SDS	0.8 g
	Urea	7.21 g
	Glycerol	6 mL
	BPB	
	Purelab® Water	ad 20.0 mL
	Per 10.0 mL of aliquot:	
	DTT	100.0 mg
	or	
	IAA	250.0 mg

3.1.2.3 Western Blot

Tris-buffered Saline (TBS)	NaCl	40.0 g
Solution, 10x	Tris Base	6.06 g
	Purelab® Water	ad 500.0 mL
	pH adjusted to 7.3 using HCl 37%	

| TBS Solution, 1x | TBS Solution, 10x | 10.0 mL |
| | Purelab® Water | ad 100.0 mL |

Tris-buffered Saline with	TBS Solution, 10x	100.0 mL
Tween®-20 (TBS-T)	Tween®-20	2.0 mL
Solution	Purelab® Water	ad 1000.0 mL

Transfer Buffer, 10x	Glycine	144.0 g
	Tris Base	30.0 g
	Purelab® Water	ad 1000.0 mL
	pH should be between 8.2 to 8.4	

| Transfer Buffer, 1x | Transfer Buffer, 10x | 100.0 mL |
| | Purelab® Water | ad 1000.0 mL |

| Blocking Solution | Skim Milk Powder | 5.0 g |
| | TBS-T | ad 100.0 mL |

Primary Antibody Solution	Sodium Azide	10.0 mg
	BSA	500.0 mg
	Primary Antibody	as required
	TBS-T	10.0 mL
Secondary Antibody Solution	Skim Milk Powder	500.0 mg
	Secondary Horseradish Peroxidase-conjugated Antibody	as required
	TBS-T	10.0 mL
Luminol-Peroxide Working Solution	Detection Reagent 1	1.0 mL
	Detection Reagent 2	1.0 mL
	Both included in Pierce™ ECL Western Blotting Substrate Kit	

3.1.2.4   Immunoprecipitation

Phosphate-buffered Saline with Tween®-20 (PBS-T) [0.1%]	Tween®-20	0.5 mL
	PBS	500.0 mL
BS^3 Stock Solution [100 mM]	BS^3	2.0 mg
	BS^3 Conjugation Buffer	34.94 mL
BS^3 Conjugation Buffer	Sodium Phosphate Dibasic Dihydrate	17.8 mg
	Sodium Chloride	43.83 mg
	Purelab® Water	ad 5.0 mL
	pH should be between 7 to 9	
BS^3 Quenching Buffer	Tris HCl	121.14 mg
	Purelab® Water	ad 1.0 mL
	pH adjusted to 7.5 using HCl 37%	

3.1.2.5   Copper-Catalyzed Azide-Alkyne Cycloaddition

BODIPY-FL-azide Stock Solution [100 mM]	BODIPY-FL-Azide	5.0 mg
	DMF	133.62 µL
BODIPY-FL-alkyne Stock Solution [100 mM]	BODIPY-FL-Alkyne	5.0 mg
	DMF	151.90 µL
Cisplatin-Azide Stock Solution [100 mM]	Cisplatin-Azide	21.53 mg
	DMF	564.90 µl
Cisplatin-Alkyne Stock Solution [100 mM]	Cisplatin-Alkyne	25.38 mg
	DMF	564.90 µl
Azide Stock Solution [100 mM] Synthesis of Azide according to the literature procedure [119] by PD Dr. Ganna V. Kalayda.	Azide	5.0 mg
	DMF	158.54 µL
Alkyne Stock Solution [100 mM] Synthesis of Azide according to the literature procedure [118] by PD Dr. Ganna V. Kalayda.	Alkyne	5.0 mg
	DMF	130.38 µL
Tris(3-hydroxypropyltriazolylmethyl)amine (THPTA) Stock Solution [100 mM]	THPTA	43.45 mg
	Purelab® Water	1.0 mL
Copper Sulfate Pentahydrate Stock Solution [50 mM]	Copper Sulfate Pentahydrate	124.8 mg
	Purelab® Water	10.0 mL
Sodium Ascorbate Stock Solution [300 mM]	Sodium Ascorbate	59.43 mg
	Purelab® Water	1.0 mL

3.1.3 Consumables

CASY® Tubes	Schärfe System, Reutlingen
Cell Culture Flasks T25	Sarstedt AG & Co., Nümbrecht
Cell Culture Flasks T75	Sarstedt AG & Co., Nümbrecht
Cell Culture Flasks T175	Sarstedt AG & Co., Nümbrecht
Cell Culture Plates, 96 Wells	Sarstedt AG & Co., Nümbrecht
Cell Culture Plates, 6 Wells	Sarstedt AG & Co., Nümbrecht
Cell Scraper 25 cm	Sarstedt AG & Co., Nümbrecht
Cell Scraper 39 cm	Sarstedt AG & Co., Nümbrecht
Cellulose Wadding	LABC-Labortechnik Zillger KG, Hennef
Centrifugation Tubes 15 mL	Sarstedt AG & Co., Nümbrecht
Centrifugation Tubes 50 mL	Sarstedt AG & Co., Nümbrecht
Cover Slips	Roth GmbH & Co., Karlsruhe
Cryovials	Sarstedt AG & Co., Nümbrecht
Disposal Bags	VWR International, Darmstadt
Glass Bottom Cell Culture Dishes	Willco Wells B.V., Amsterdam, the Netherlands
Microscope Slides	Roth GmbH & Co., Karlsruhe
Paper Electrode Wicks	Bio-Rad Laboratories GmbH, Munich
Pasteur Pipettes	Brand GmbH & Co., Wertheim
Petri Dishes	Greiner Labortechnik, Frickenhausen
pH-Indicator Strips	VWR International, Darmstadt
Pipette Tips	Mettler-Toledo GmbH, Gießen; Brand GmbH & Co., Wertheim
Pipette Tips, RNAse-free	Thermo Fisher Scientific, Rockford, IL, USA
Polyvinylidene Fluoride (PVDF) Membranes	Roth GmbH & Co., Karlsruhe
Reaction Tubes 0.5 mL	VWR International, Darmstadt
Reaction Tubes 1.5 mL	VWR International, Darmstadt
Reaction Tubes 1.5 mL, RNAse-free	Thermo Fisher Scientific, Rockford, IL, USA
Reaction Tubes 2.0 mL	VWR International, Darmstadt
Reaction Tubes 5.0 mL	Eppendorf AG, Hamburg

Reagent Solution Reservoirs	VWR International, Darmstadt
Serological Pipettes	LABC-Labortechnik Zillger KG, Hennef
SERVAGel™ TG PRiME™ 12%	Serva Electrophoresis GmbH, Heidelberg
SERVAGel™ TG PRiME™ 4-20%	Serva Electrophoresis GmbH, Heidelberg
SERVAGel™ TG PRiME™ 8-16%	Serva Electrophoresis GmbH, Heidelberg
SERVA IPG BlueStrip 3-10, 7 cm	Serva Electrophoresis GmbH, Heidelberg
Western Blotting Filter Paper	Thermo Fisher Scientific, Rockford, IL, USA

3.1.4   Equipment

AccuJet®	Brand GmbH & CO., Wertheim
Axiovert® 25 Inverted Microscope	Carl Zeiss AG, Oberkochen
Beckman Microfuge® Lite	Beckman-Coulter, Fullerton, CA, USA
CASY®1 Cell Counter, Modell TT	OMNI Life Science GmbH & Co. KG, Bremen
Centrifuge Universal 32R	Hettich GmbH & Co. KG, Tuttlingen
Centrifuge Mikro 200R	Hettich GmbH & Co. KG, Tuttlingen
ChemiDoc™ MP Imaging System	Bio-Rad Laboratories, Munich
ChemiDoc™ XRS+ System	Bio-Rad Laboratories, Munich
Compact Shaker KS 15 Control	Edmund Bühler GmbH, Bodelshausen
Drying and Heating Chamber FD 115 E2	Binder GmbH, Tuttlingen
DynaMag™-2 Magnet	Thermo Fisher Scientific, Rockford, IL, USA
E4 Electronic Pipette, LTS E4-10XLS+ (variable volume, 0.5-10 µL)	Mettler-Toledo GmbH, Gießen
E4 Electronic Pipette, LTS E4-100XLS+ (variable volume, 10-100 µL)	Mettler-Toledo GmbH, Gießen

E4 Electronic Pipette, LTS E4-1000XLS+ (variable volume, 100-1000 µL)	Mettler-Toledo GmbH, Gießen
E4 Electronic Pipette LTS E4-5000XLS (variable volume, 500-5000 µL)	Mettler-Toledo GmbH, Gießen
E4 Multi Pipette Multi E12-20XLS+ (variable volume, 2-20 µL)	Mettler-Toledo GmbH, Gießen
Electrophoresis Power Supply E865	Consort bvba, Turnhout, Belgium
Freezer (-20 °C)	Robert Bosch GmbH, Gerlingen
Freezer (-80 °C)	National Lab GmbH, Mölln
Guava® easyCyte™ HT	Luminex Corporation, Austin, TX, USA
InoLab® pH Level 2 pH Meter	Wissenschaftlich-Technische Werkstätten GmbH, Weilheim
Kern 770 Analytical Balance	Kern & Sohn GmbH, Balingen
Kern EW6000-1M Precision Balance	Kern & Sohn GmbH, Balingen
Laminar Air Flow Workstation Herasafe HSP 12	Heraeus Holding GmbH, Hanau
Laminar Air Flow Workstation Holten Maxi Safe 2010	Thermo Electron Corporation, Waltham, MA, USA
Liquid Nitrogen Tank MVE CryoSystem 4000	Chart Industries, Ball Ground, GA, USA
MCO-170AICUV-PE IncuSafe CO_2 Incubator	Panasonic Healthcare Co., Ltd., Osaka, Japan
Microfuge® Lite Centrifuge	Beckman Coulter, Brea, CA, USA
MT Classic AB135-S Analytical Balance	Mettler-Toledo GmbH, Gießen
Multi-channel micropipette Transferpette® -12 electronic (variable volume, 10-200 µL)	Brand GmbH & Co., Wertheim
Multiskan® EX Microplate Reader	Thermo Fisher Scientific, Rockford, IL, USA
Nikon A1 Eclipse Ti® Confocal Microscope	Nikon, Kingston, UK
omniBLOT Blotter	Cleaver Scientific Ltd., Warwickshire, UK

omniPAGE Mini Vertical Protein Electrophoresis System	Cleaver Scientific Ltd., Warwickshire, UK
Pipet-Lite LTS Pipette L-10XLS+ (variable volume, 0.5-10 µL)	Mettler-Toledo GmbH, Gießen
Pipet-Lite LTS Pipette L-100XLS+ (variable volume, 10-100 µL)	Mettler-Toledo GmbH, Gießen
Pipet-Lite LTS Pipette L-1000XLS+ (variable volume, 100-1000 µL)	Mettler-Toledo GmbH, Gießen
Pipet-Lite LTS Pipette L-2XLS+ (variable volume, 0.1-2 µL)	Mettler-Toledo GmbH, Gießen
Pipet-Lite LTS Pipette L-200XLS+ (variable volume, 20-200 µL)	Mettler-Toledo GmbH, Gießen
Platform Shaker Unimax® 1010	Heidolph Instruments GmbH & CO. KG, Schwabach
PROTEAN® Isoelectric Focusing (IEF) Cell System	Bio-Rad Laboratories, Munich
PTR-35 Vertical Multi-function Rotator	Grant Instruments Ltd., Shepreth, UK
Purelab® flex 2 Water Purification System	ELGA LabWater, Celle
Refrigerator Comfort	Liebherr, Bulle FR, Switzerland
Single Channel micropipette Transferpette® S (variable volume, 2-20 µL)	Brand GmbH & Co., Wertheim
Single Channel micropipette Transferpette® S (variable volume, 10-100 µL)	Brand GmbH & Co., Wertheim
Single Channel micropipette Transferpette® S (variable volume, 100-1000 µL)	Brand GmbH & Co., Wertheim
Sonicator Bandelin HD2070/UW2070	Bandelin Electronic GmbH, Berlin
Systec V95 Autoclave	Systec GmbH, Linden
Thermomixer Comfort	Eppendorf AG, Hamburg
Ultrasonic Bath SONOREX SUPER RK 102 H	Bandelin electronic GmbH & Co. KG, Berlin

Vacuum Pump DOA-V155-BN	Gast Manufacturing, Inc., Benton Harbor, MI, USA
VarioMAG Monotherm Magnetic Stirrer	HP Labortechnik GmbH, Oberschleißheim
Vortexer RS-VA10	Phoenix Instrument GmbH, Garbsen
Vortexer Zx³	VELP Scientifica Srl, Milan, Italy
Wilovert S Inverse Microscope	Helmut Hund GmbH, Wetzlar

3.1.5 Software

Ascent Software (Multiskan® EX)	Thermo Fisher Scientific, Rockford, IL, USA
CompuSyn® 1.0	ComboSyn Incorporated, Paramus, NJ, USA
Delta 2D 4.8	Decodon, Greifswald
GraphPad Prism® 6.0	GraphPad Software, San Diego, CA, USA
Guava® InCyte™ 3.3	Luminex Corporation, Austin, TX, USA
ImageJ 1.52a	National Institutes of Health, Bethesda, MD, USA
Image Lab™ 5.1	Bio-Rad Laboratories, Munich
Microsoft® Office 2019	Microsoft Corporation, Redmond, WA, USA
NIS-Elements AR 3.2	Nikon Corporation, Tokyo, Japan

3.2 Cell Culture

In the experiments described below, the cell line A2780, and its cisplatin-resistant subtype A2780cis as well as the cell line HCT-8, and its oxaliplatin-resistant subtype HCT-8ox were used.

The human ovarian carcinoma cell line A2780 (catalog nr. 93112519) and its cisplatin-resistant subline A2780cis (catalog nr. 93112517) were obtained from the European Collection of Authenticated Cell Cultures (ECACC), UK. While A2780 cells originate from tumor tissue of untreated patients, the resistant sub-cell line A2780cis was generated by chronic exposure to steadily increasing cisplatin concentrations.

The human ileocecal colorectal adenocarcinoma cell line HCT-8 and its oxaliplatin-resistant sub-cell line HCT-8ox were kindly provided by Dr. R. A. Hilger, University of Essen, Germany. Equivalent to A2780cis cells, the resistant sub-cell line HCT-8ox was also obtained by chronic exposure to constantly increasing oxaliplatin concentrations. All cell lines were cultured in RMPI 1640 medium at 37 °C and 5% CO_2. The culture media were supplemented with 10% fetal bovine serum, 100 I.E./mL penicillin and 0.1 mg/mL streptomycin.

3.2.1 Storage

At 80-90% confluence, cells were washed with PBS and trypsinated for two minutes at 37 °C and 5% CO_2 to ensure complete detachment from the cell culture flask. After that, the reaction was terminated with RPMI 1640 cell culture medium and the solution was centrifuged (4 °C, 1,000 g) for four minutes. Then, the supernatant was removed and the cell pellet was put together with a certain amount of cryogenic medium (FCS with 10% DMSO) to a final concentration of 1-2x 10^{-6} cells/mL to be filled in cryogenic tubes. DMSO hereby acts as a cryoprotectant and is used to protect cells from damage such as ice recrystallization and therefore to enhance cell viability post-freeze-thaw. At room temperature (RT), though, DMSO is cytotoxic and all steps had to be carried out quickly. After 15 minutes in the refrigerator, the cell suspension was cooled down to -20 °C for about two hours. Finally, after storage at -80 °C overnight, the cryogenic tubes were transferred to the liquid nitrogen tank where they were stored in the gas phase at -150 to -160 °C for longer periods.

3.2.2 Thawing

Just as for the freezing process, all steps concerning thawing had to be conducted quickly to minimize exposure of cells to the cytotoxic DMSO. In order to do so, 10 mL of pre-warmed RPMI 1640 medium were put in a centrifugation tube and combined with the previously frozen cell suspension by carefully pipetting up and down. Subsequently, the cell suspension was centrifuged (4 °C, 1,000 g, 4 minutes), the DMSO-containing supernatant was aspirated, the cell pellet was resuspended in warm medium and transferred into a cell culture flask.

3.2.3 Cultivation

In order to ensure fast further growth, cells were subcultivated at a maximum confluence of 90%. For this purpose, adherent cells were washed with PBS and

exposed to trypsin for two minutes at 37 °C and 5% CO_2. Then, the reaction was stopped by adding cell medium and the cell suspension was centrifuged (4 °C, 1,000 g) for 4 minutes to enable the aspiration of the supernatant. Following this, the cell pellet was resuspended in 10 mL of warm RPMI 1640 medium. The desired quantity of cell suspension was combined with additional cell medium and put in a new cell culture flask. Until further use, the cells were cultivated at 37 °C and 5% CO_2.

3.2.4   Cell Counting

As described before, cells were detached from the cell culture flask by means of trypsination, centrifuged (4 °C, 1,000 g, 4 minutes) afterwards and finally resuspended in 10 mL of pre-warmed medium. 20 µL of the suspension were then added to 10 mL of sterile CASY®-Ton solution and measured with the CASY®1 cell counter and analyzer (Figure 3.1). Each particle or cell that passes through the measuring capillary generates a change of electrical resistance proportional to their size and conductivity. The measurement provides information about cell counts per milliliter, cell size distribution, aggregation and viability.
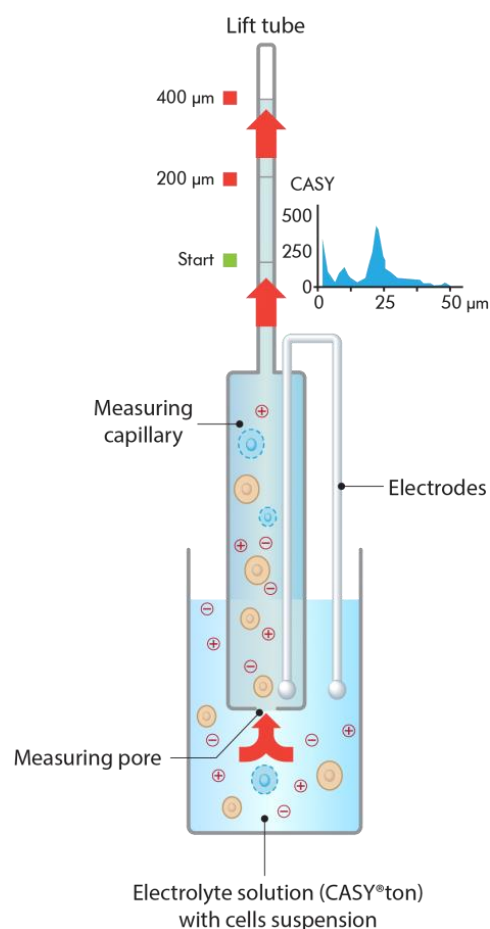
Figure 3.1 Principle of measurement of the CASY®1 cell counter [120].

3.2.5 Mycoplasma Test

Mycoplasma are small bacteria lacking a cell wall, which pose a major risk of contamination in cell culture. They cannot be detected under a light microscope and are resistant towards common antibacterial agents, which is why they often remain unrecognized. Nevertheless, mycoplasma infections can induce changes in cell growth, protein expression and metabolism amongst others, severe infections can even result in cell death. Therefore, to ensure comparability of all cells employed in the experiments and subsequent results, all cell lines were screened regularly for mycoplasma contamination using DAPI. DAPI is a fluorescence dye, which binds to DNA (both cellular as well as mycoplasmic).

To do so, cells were cultivated in antibiotics-free medium on a microscope slide in a petri dish for 3 days. Then, the medium was removed, cells were washed in PBS and 2 mL methanol was added to fix the cells. Then 80 µL DAPI working solution was added for 5 minutes at RT. The slide was then washed with methanol in the dark and cover slips were mounted on the slides using mounting medium. In the final step, possible mycoplasma contamination was analyzed using a *Nikon Eclipse Ti®* *fluorescence microscope*. If the culture is positive for mycoplasma, besides nuclear staining there will also be extra-nuclear fluorescence, identifiable by small scattered blue spots.

3.3 Cell Culture Experiments

All cell incubation experiments were conducted at a confluence of approximately 80-90%. In order to prevent contamination due to external influence, all relevant steps were executed under sterile conditions under a laminar airflow work bench.

The specific experimental and treatment procedures of the respective experiments are described more precisely in the corresponding chapters.

3.3.1 Cell Lysis and Fractionation

The efficiency of fractionation by CLB IV and the *BioVision Nuclear/Cytosol Fractionation Kit* were verified by the detection of marker proteins via Western Blot (Chapter 3.11). Therefore, primary antibodies against the nuclear matrix protein Lamin B1 for the nuclear fraction and against GAPDH for the cytosolic fraction were used to detect possible occurrence of cross-contamination of fractions. In this project, only the

cytosolic fraction was investigated. On the one hand, fractionation reduced the complexity, which would obstruct the identification methods further on. On the other hand, though, the interaction of platinum with intracellular proteins, but also the toxicities and putative mechanisms of action of platinum drugs, are associated largely with cytosolic proteins. Therefore, only the cytosolic fraction was evaluated for cross-contamination.

3.3.1.1   Basics

In order to allow the investigation of different cellular compartments, such as cytosol vs. nucleus, it is necessary to fractionate the cell. Cell fractionation is always preceded by cell lysis, which can be performed either with detergents, such as Triton™ X-100 or NP-40, or by means of physical methods, such as sonication. The latter leads to disruption of the lipid membrane of the intact cell by applying high frequency sound waves to the sample. Detergents are able to effectively penetrate into the membrane bilayer, which will, also ultimately result in rupture of the membrane. Cell lysis with detergents is usually gentler, but the sample may need to be purified before downstream analysis since high detergent concentrations may be incompatible with downstream applications. On the other hand, physical disruption may evoke protein denaturation and aggregation due to localized heating within the sample. Keeping the sample on ice at all times may help to avoid this problem, though. To ensure minimal proteolysis of proteins, all buffers have been supplemented by protease inhibitors, independent of the lysis method used [121].

By a suitable combination of lysis methods and centrifugation steps it is possible to separate the nuclear and cytosolic fraction from each other. This can be achieved by taking advantage of the fact that the nucleus has its own membrane. After the initial disruption of the outer cell membrane, cell nuclei can be separated by centrifugation and lysed in a separate step [121].

3.3.1.2   CLB IV

Ready-to-use CLB IV was prepared freshly at all times by adding Pepstatin A and Leupeptin to the basic CLB IV solution (Chapter 3.1.2.2). The composed buffer was then put on ice until use.

After treatment, cells were washed with PBS twice and then harvested in 1 mL PBS using a cell scraper. The cell suspension was subsequently transferred to a 15 ml

centrifugation tube and centrifuged at 160 g (4 °C, 4 minutes). Next, PBS was removed and the pellet was dissolved in 1 mL CLB IV and incubated on ice for 5 minutes. To ensure proper lysis, the cell suspension was sonicated 3 times (25% power, 30 seconds – 5 seconds pause) on ice. The lysate was then transferred to 1.5 mL reaction tubes and centrifuged at 700 g for 15 minutes (4 °C). After centrifugation, the supernatant was pipetted into a new reaction tube and the remaining pellet was labeled 'nuclear fraction' and stored at -80 °C. The reaction tube with the supernatant was yet again centrifuged (4 °C, 15,000 g, 20 minutes) and once again the supernatant, which contained the cytosolic fraction was transferred to a new reaction tube, while the remaining pellet was labeled 'mitochondrial fraction' and also stored at -80 °C. Both the nuclear as well as the mitochondrial fraction could be further processed if needed.

3.3.1.3   *BioVision Nuclear/Cytosol Fractionation Kit*

Again, after treatment, cells were washed with PBS and detached from the cell culture flask using trypsin. Trypsination was stopped with culture medium and the suspension was centrifuged (4 °C, 1,000 g, 4 minutes). Thereupon, the supernatant was aspirated and aiming at achieving full removal of the excessive treatment substances the cell pellet was washed with cold PBS twice, followed by the transfer of the cell suspension to a 1.5 mL reaction tube and subsequent centrifugation. Next, once again the supernatant was aspirated and the cell pellet was further treated according to the *BioVision Nuclear/Cytosol Fractionation Kit* protocol, with only minor changes. First, the cell pellet was resuspended in 400 µL *CEB-A Mix*, vortexed thoroughly and incubated on ice for 10 minutes. Afterwards, 22 µL of *CEB-B* were added to the suspension, the mix was vortexed again and incubated on ice for one minute this time. Following a quick vortexing step, the suspension was then centrifuged at 16,000 g (4 °C, 5 minutes) and the supernatant, which contained the cytosolic fraction, was transferred to a pre-cooled 1.5 mL reaction tube. The fraction was stored at -80 °C. The remaining cell pellet, representing the nuclear fraction, could be resuspended in 200 µL ice-cold *NEB-Mix* and further processed, if needed.

3.3.1.4   **RIPA Buffer for Whole Cell Lysate**

The final RIPA lysis buffer was prepared freshly at all times by adding Pepstatin A, Leupeptin, NaF, Na_3VO_4 and protease inhibitor cocktail to the basic RIPA buffer (Chapter 3.1.2.2). The composed buffer was then put on ice until use.

For cell lysis, the cell culture medium was removed and cells were washed with 1 mL PBS per well of a 6-well plate. After PBS had also been removed, 250 μL lysis buffer/well was added, cells were detached with the aid of a cell scraper and the suspension was transferred to a 15 mL centrifugation tube, which was then put on ice for a minimum of 30 minutes. Subsequently, the cell suspension was subjected to ultrasonic treatment (50% power; 5 seconds – 30 seconds pause; 3x) on ice to ensure complete solubilization. Last of all, the lysate was transferred to a reaction tube and centrifuged for 15 minutes (4 °C, 14,000 rpm), after which the supernatant was then stored at -80 °C until further use.

3.4   Cytotoxicity Assay (MTT Assay)

3.4.1   Basics

Based on the reduction of the yellow tetrazolium dye MTT to purple formazan by mitochondrial dehydrogenases of living cells (Figure 3.2), an MTT assay presents a simple method to determine the cytotoxicity of various substances. The higher the cytotoxic impact of the investigated substance the lower is the number of viable cells and therefore the amount of generated formazan. The analysis of the colored product was carried out with the spectrometer *Multiskan® EX Microplate Photometer* at 570 nm and afterwards at 690 nm for background subtraction of non-converted MTT and cellular components. The measured absorption difference is proportional to the amount of generated formazan, and hence to the number of living mitochondrially active cells. The half maximal effective concentration (EC_{50}) and pEC_{50} (pEC_{50} = -$logEC_{50}$) were determined using non-linear regression analysis with GraphPad Prism® (sigmoidal dose-response, variable slope).
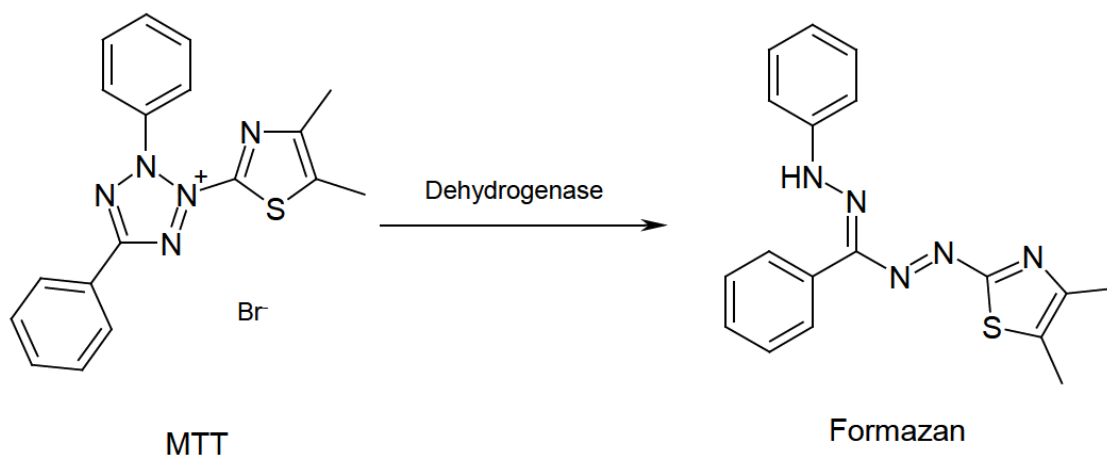
Figure 3.2 Conversion of the tetrazolium salt MTT to the purple formazan product.

3.4.2   Experimental Procedure

At the beginning of the experiment, cells were seeded in 96-well plates so that the untreated growth control would be at approximately 90% confluence on the day of evaluation. A density of 3,000 cells/well for HCT-8 cells and 10,000 cells/well for A2780 cells proved suitable for this purpose. The corresponding number of cells were seeded in 100 µL of full cell culture medium and allowed to attach overnight at 37 °C and 5% CO_2. To account for possible evaporation, the outer wells were filled with PBS only. The following day, the growth medium was removed and the cells were exposed to increasing concentrations of substances (either platinum drug alone, inhibitor alone, a combination of both or NC treatments), beginning with only medium as growth control for 72 hours (Figure 3.3). All experiments were conducted in triplicate. After expiry of the 72 hours, cells were treated with 20 µL/well MTT for 1 hour. The supernatant was subsequently removed and the purple formazan crystals produced by viable cells were dissolved in 100 µL DMSO. The absorbance was quantified as described in Chapter 3.4.1.

Cytotoxicity experiments after knockdown followed a slightly different procedure: after seeding the cells and overnight incubation, they were treated with protein-specific siRNA (8 pmol/well) for either GSTP1, vimentin, DJ-1, Grb2 or NC siRNA for 24 hours and the *K4® Transfection System*, composed of the *K4® Transfection Reagent* and the *K4® Multiplier*, according to the manufacturer's instructions (Chapter 3.1.2.1). Then the cells were exposed to the specific substance for 48 hours. The further procedure was the same as described above.
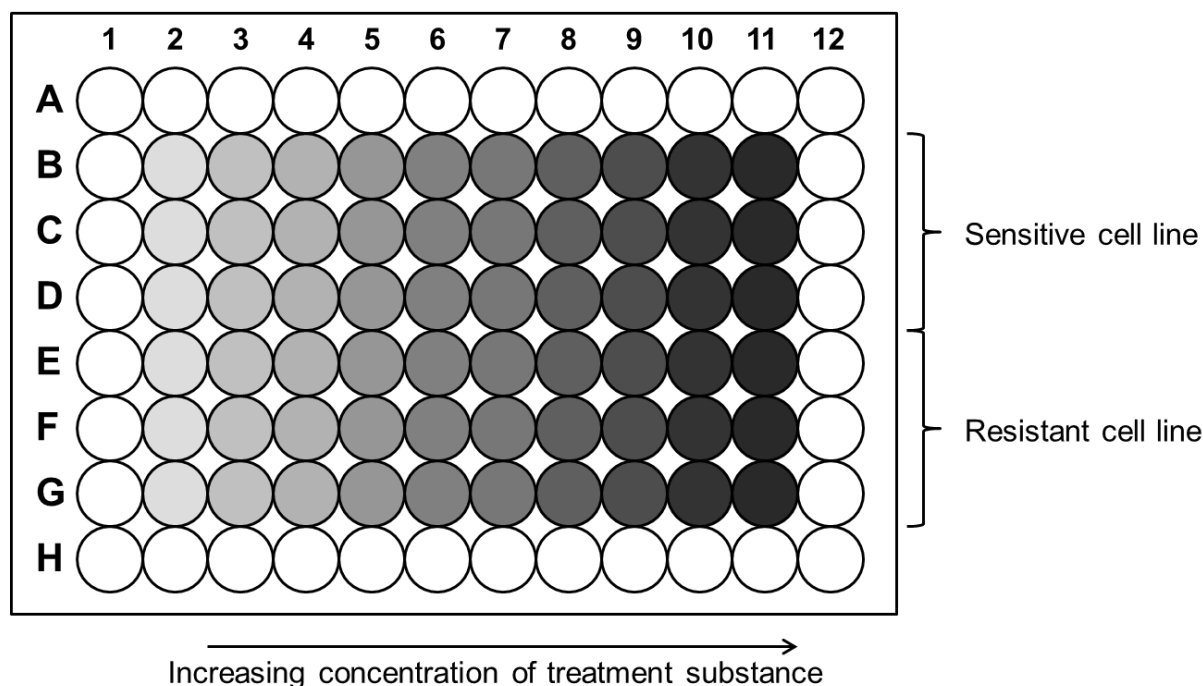
Figure 3.3 Exemplary illustration of the treatment scheme of a 96-well plate in the course of an MTT assay.

3.4.3   Determination of the Resistance Factor (RF)

The resistance factor was calculated by dividing the EC_{50} value of resistant cells by the EC_{50} value of sensitive cells (Equation 3.1). Thereby, it shows the relation of the EC_{50} value of the resistant to the sensitive cell line.

$$RF = \frac{EC_{50}(\text{resistant})}{EC_{50}\ (\text{sensitive})}$$

Equation 3.1

For assessment of the calculated RF, the confidence intervals of the $logEC_{50}$ values have to be taken into account. In the case of any overlap, there is no resistance.

3.5   Apoptosis Assay

3.5.1   Basics

Different stages of apoptosis can be detected using fluorescently labeled Annexin V and a so-called DNA-binding viability dye, such as propidium iodide (PI). Annexin V has the ability to bind to phospholipids of the cell membrane, preferentially to phosphatidylserines. Under normal conditions, when the cell is fully viable, phosphatidylserines are located mainly on the cytosolic side of the plasma membrane. In case of initiated apoptosis, though, phosphatidylserines relocate from the intracellular to the extracellular side. Now, Annexin V is able to specifically detect and bind to the phospholipid. By fluorescent labeling Annexin V with FITC, early apoptotic

cells can be visualized by flow cytometry. PI is not able to penetrate membranes of fully viable or early apoptotic cells. But at later stages of apoptosis, cell membranes lose their integrity and allow for both PI and Annexin V-FITC to enter the cellular interior (Figure 3.4). This way, the assay makes it possible to differentiate between earlier apoptotic and late apoptotic/necrotic cells.
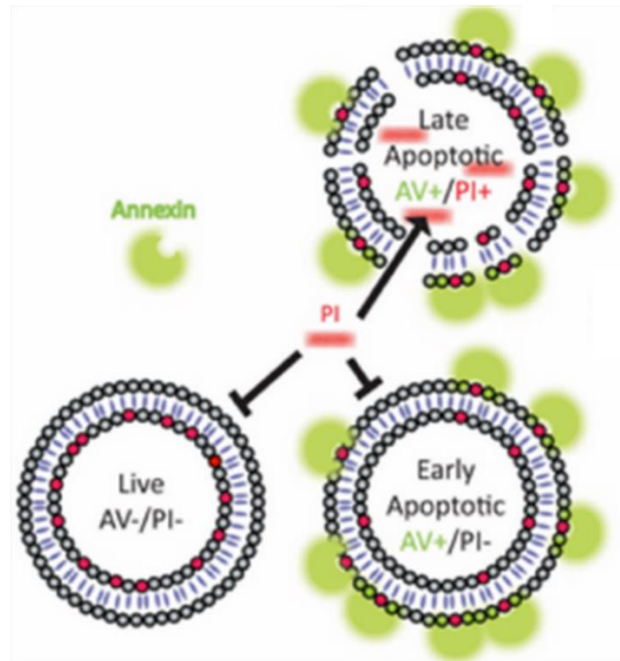
Figure 3.4 Dual Staining with Annexin V-FITC and propidium iodide to detect the stage of apoptosis [122].

3.5.2   Experimental Procedure

Apoptosis was assessed using the *eBioscience™ Annexin V-FITC Apoptosis Detection Kit* according to the manufacturer's instructions. A2780 and HCT-8 cells were seeded in 6-well plates at a density of 1x 10^5 cells/well and after attaching overnight at 37 °C and 5% CO_2, they were exposed to either platinum drug/inhibitor combinations for 72 h or siRNA for 24 h followed by platinum drug exposure for 48 h. Treated cells were then washed once with PBS and afterwards with 1x *Binding Buffer*. After centrifugation (4 °C, 200 g, 5 minutes), the cell pellet was resuspended in 200 µL *Binding Buffer* and incubated with 10 µL PI and 5 µL Annexin V-FITC for 15 minutes at RT in the dark. Measurements were performed right after by flow cytometry (Guava® easyCyte™ HT). Subsequent analysis was conducted with Guava® InCyte™ (version 3.3). Annexin V-FITC negative/PI negative cells were considered alive, Annexin V-FITC positive/PI negative cells were considered early apoptotic and Annexin V-FITC negative/PI positive and Annexin V-FITC positive/PI positive cells

were combined and considered late apoptotic/necrotic. Cellular debris was excluded using forward and side scatter.

3.6   Protein Quantification (BCA Assay)

3.6.1   Basics

Based on the biuret reaction, which represents the reduction of copper in the presence of peptides and the subsequent formation of a chelate complex, the amount of protein in lysates could be determined using BCA. Here, Cu^{2+} is reduced to Cu^+ by amino acids such as cysteine, cystine, tryptophan and tyrosine and then reacts with two molecules of BCA to form a purple-colored chelate complex (Figure 3.5). Notably, the amount of reduced Cu^{2+} is proportional to the amount of protein in the lysate, as is the absorption of the complex. The latter could easily be detected at a wavelength of 570 nm using the *Multiskan® EX Microplate Photometer*.

Quantification of proteins was achieved by simultaneous measurement of protein standards and generation of a calibration curve.
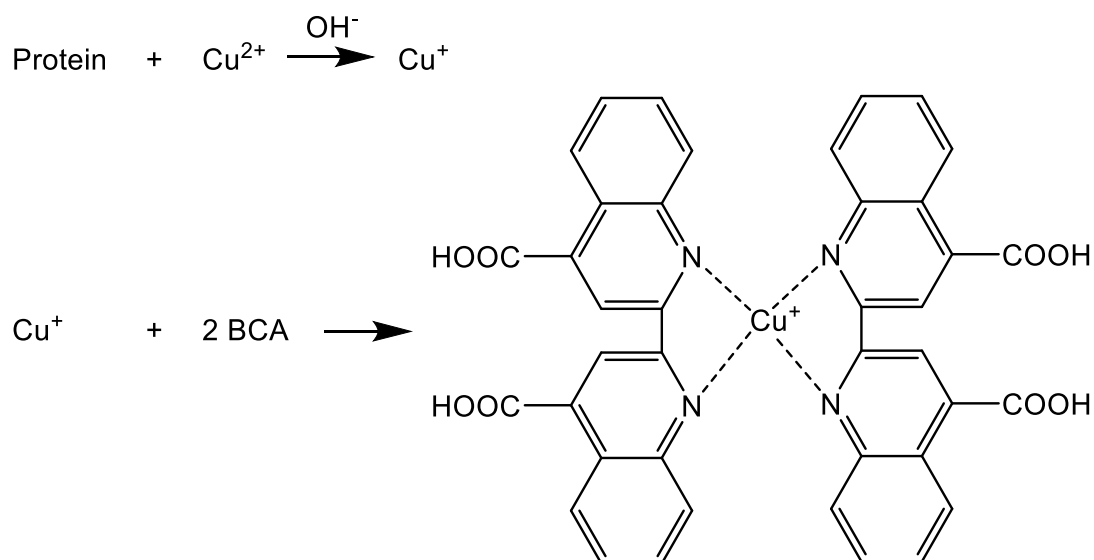
Figure 3.5 Biuret reaction for protein quantification.

3.6.2   Preparation of Standard Solutions and Quality Control Samples

Standard solutions as well as quality control samples were prepared by means of various dilutions of a 2 mg/mL BSA stock solution from the *Pierce™ BCA Protein Assay Kit* with Purelab® water according to the internal Standard Operating Procedure (Table 3.1).

All solutions were aliquoted and stored at -20 °C. If not used up, possibly remaining residues of aliquots were discarded.

Table 3.1 Preparation of standard solutions and quality control samples.

	BSA 2 mg/mL [µL]	Purelab® water [µL]
Standard Solutions		
S1 [50 µg/mL]	50	1,950
S2 [75 µg/mL]	75	1,925
S3 [100 µg/mL]	100	1,900
S4 [200 µg/mL]	200	1,800
S5 [300 µg/mL]	300	1,700
S6 [400 µg/mL]	400	1,600
Quality Control Samples		
Q1 [150 µg/mL]	150	1,850
Q2 [250 µg/mL]	250	1,750
Q3 [350 µg/mL]	350	1,650

3.6.3 Experimental Procedure

To ensure that all measurements fit into the calibration range, lysates were diluted with Purelab® water, if necessary. In most cases, a 1:20 dilution was appropriate.

20 µL/well of the standard solutions, as well as the quality control samples and lysates, were pipetted in 96-well plates. Standards were measured in triplicates, quality control samples and lysates in duplicates. In order to initiate proper development of the assay, 200 µL of the BCA working solution (Chapter 3.1.2.2) was applied to each well, according to the instructions provided by the manufacturer. Afterwards, the 96-well plate was incubated for 0.5 hours at 60 °C and the absorbance was quantified at 570 nm as described in Chapter 3.6.1.

The result was considered valid when the following criteria were met:

- The deviation of standards from the nominal value was ≤15% and the deviation of the Lower Limit of Quantification (LLOQ) was ≤20%.
- At least 4 out of 6 standards, including the LLOQ and the Upper Limit of Quantification (ULOQ), met the aforementioned criteria.
- The coefficient of correlation r was ≥0.99 (weighted linear regression).
- At least 2 out of 3 quality control samples were within ± 15% deviation from their respective nominal value.

3.7   Protein Precipitation

3.7.1   Basics

With the aim of removing interfering components that might inhibit downstream applications, such as isoelectric focusing, immunoprecipation or copper-catalyzed azide-alkyne cycloaddition (Chapters 3.8.2, 3.13 and 3.14, respectively), and, in consequence, of obtaining total protein as clean as possible, lysates were subjected to precipitation procedures. The basic principle of protein precipitation is the alteration of solubility of proteins in solution. Amongst other approaches, this can be achieved with the method of Wessel and Flügge [123]. At first, proteins are exposed to a homogenous mixture of water, methanol and chloroform. By adding more water, the lipophilic organic chloroform phase separates, thus, forming a two-phase system. As proteins are amphiphilic, their hydrophilic residues align with the upper aqueous phase, whereas their lipophilic residues align with the bottom organic phase. This way, proteins generate an interphase. Next, the upper phase, containing salts, detergents, etc. is removed and after the addition of another portion of methanol and a centrifugation step, the remaining liquid, containing lipids, is removed as well, leaving behind the precipitated protein as a dry pellet.

3.7.2   Experimental Procedure

An appropriate volume of lysate corresponding to the desired amount of protein was mixed with Purelab® water to make up 100 µL. Then, 400 µL methanol was added and the samples were vortexed for 5 seconds and centrifuged (RT, 9,000 g, 10 seconds). In the next step, 100 µL of chloroform was added and the mix was vortexed (5 seconds) and centrifuged (RT, 9,000 g, 10 seconds) again. In order to achieve a phase separation and to precipitate the purified proteins, 300 µL Purelab® water was transferred to the reaction tube and mixed gently. Following this, the solution was centrifuged for 1 minute (RT, 22,000 g) and then the upper phase was aspirated carefully, while the interphase that contained proteins, and the lower chloroform phase remained. Once an additional 300 µL of methanol was added, the reaction tube was inverted with caution and a final centrifugation (RT, 22,000 g, 2 minutes) allowed the removal of the supernatant. At last, the cell pellet was air dried for 10 minutes.

3.8 Gel Electrophoresis

3.8.1 One-Dimensional (1D) Gel Electrophoresis

3.8.1.1 Basics

In the course of some experiments, such as prior to Western Blotting (Chapter 3.11), after immunoprecipitation (Chapter 3.13) or after the copper-catalyzed azide-alkyne cycloaddition (Chapter 3.14), the previously prepared lysates were separated by means of one-dimensional polyacrylamide gel electrophoresis (SDS-PAGE, sodium dodecyl sulfate polyacrylamide gel electrophoresis) according to the principles of Laemmli [124]. This approach makes use of the denaturizing effect of SDS and heating during sample preparation, which leads not only to disruption of the three-dimensional protein structure but also to the formation of negatively charged SDS-protein micelles. These micelles in turn render the intrinsic charge of the proteins negligible. This way, the ratio of charge to mass of each protein is considered roughly equal and upon application of electric current the SDS-protein micelles migrate towards the anode with different speed depending on their molecular weight only, first through the stacking gel and subsequently through the separating gel. Stacking gels and separating gels differ by pore size, pH value (pH 6.8 vs. pH 8.8) and ionic strength and are based on a tris-glycine buffer system. Glycines, which are mostly present in the zwitterionic form at neutral pH, become mainly anionic at basic pH, which allows their role as trailing ions in the stacking gel and as leading ions in the separating gel. The pH gradient between the two gels causes the shift of charge of the glycines and the overhauling of the proteins of interest, which thus leads to accumulation or stacking of these proteins at the end of the stacking gel. Then, the actual separation takes place in the separating gel according to their respective molecular weight [125].

Through the use of a comparative sample with proteins of known masses (the so-called protein standard), it is possible to estimate the approximate molecular weight of the proteins of interest after the run.

3.8.1.2 Experimental Procedure

At first, all protein samples were diluted with 5x sample loading buffer and heated to 95 °C for 5 minutes, so that 20 µg of denaturized total protein could be applied to each gel pocket afterwards. Depending on the grade of polymerization (either 12% or 4-20% SERVAGel™ TG PRiME™ ready-made gels) of the separating gel, the samples were

then electrophoretically separated for at least 1 hour at about 200 V using the *omniPAGE Mini Vertical Protein Electrophoresis System.* After successful completion of the electrophoresis, the gels were then removed from the apparatus and further treated according to one of the following protocols.

3.8.2   Two-Dimensional (2D) Gel Electrophoresis

3.8.2.1   Basics

Especially with rather complex protein mixtures, where sufficient separation via one-dimensional gel electrophoresis is not likely, two-dimensional gel electrophoresis is a powerful tool to separate and detect a broad variety of proteins in one gel. Since the method is composed of variable experimental steps, it is of utmost importance to standardize wherever possible in order to minimize variability of results. This includes a mandatory precipitation step of the lysate before the experiment is started to get rid of all unwanted, but influential components.

As the name suggests, two-dimensional gel electrophoresis is made up of two separate dimensions. In the first dimension, called IEF, proteins are strictly separated according to their isoeletric point. This step has to be performed at constant temperatures to avoid shifting of spots [125]. Basically, proteins wander in the pH gradient until the sum of the negative and positive charges of their amino acid chain (net charge) is zero (Figure 3.6). Nowadays, the pH gradient usually is embedded in a ready-made gel strip, called an immobilized pH gradient (IPG) strip, which is another factor of standardization on the one hand, and simplifies handling on the other. Amongst others, the reswelling of these dry strips can be combined with the application of the sample proteins during strip rehydration via in-gel rehydration, where the sample is solubilized within the rehydration solution and exposed to the strip overnight or at least 6 hours [126]. In this case the rehydration buffer would also act as solubilization buffer and the two steps would be carried out simultaneously. Additives such as urea, thiourea or detergents like CHAPS enhance solubility of hydrophobic proteins. Carrier ampholytes are used to further increase the solubility of proteins and usually do not interfere with the IEF run, since their net charge at the isoelectric point is zero. Nevertheless, if the concentration of salt or buffer ions from the sample or the rehydration buffer exceeds a certain amount, anions and cations wander to their respective electrodes and form areas with high conductivity. In these areas, the electric field strength is very low, while

the areas with low ion concentration exhibit high electric field strength. If this is the case, proteins will only be separated in the central areas of the IPG strip and may explain lower volt hours during focusing, which are an indicator of the quality of the separation [125]. Furthermore, all solubilization buffers contain reducing agents, such as DTT, to ensure uniform oxidation state of the proteins. Yet, DTT, being a weak acid, ultimately wanders towards the anode and thiol groups of basic proteins are oxidized and partly reform intra- and intermolecular disulfide bridges, which then results in visible streaks. By application of hydroxyethyldisulfide (HED) instead of DTT, all thiol groups are conversed deliberately, preventing the presence of multiple protein species [127].
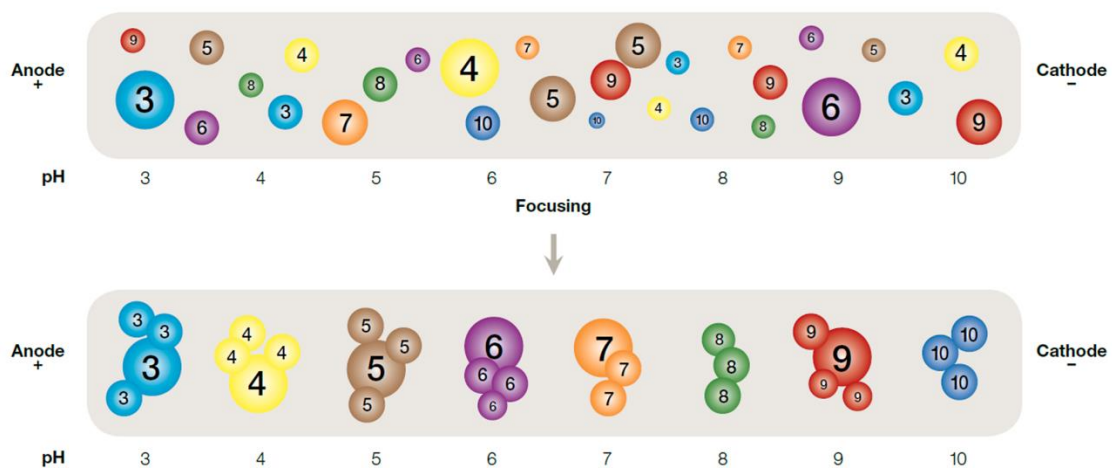
Figure 3.6 Separation of proteins according to isoeletric point [128].

As soon as the IEF is finished, the strips have to be equilibrated for further steps. Separated proteins have to be reduced, alkylated and coated by SDS to make them accessible for separation in the second-dimensional, which is comparable to conventional one-dimensional SDS-PAGE. The difference here is that proteins are not in solution anymore but incorporated in the processed IPG strip. This way, the strip has to be placed tightly on top of a separating gel, to allow for the protein migration out of the strip into the separating gel towards the anode at a right angle (Figure 3.7). Here as well, a protein standard enables the estimation of the approximate molecular weight of the proteins of interest after the run.
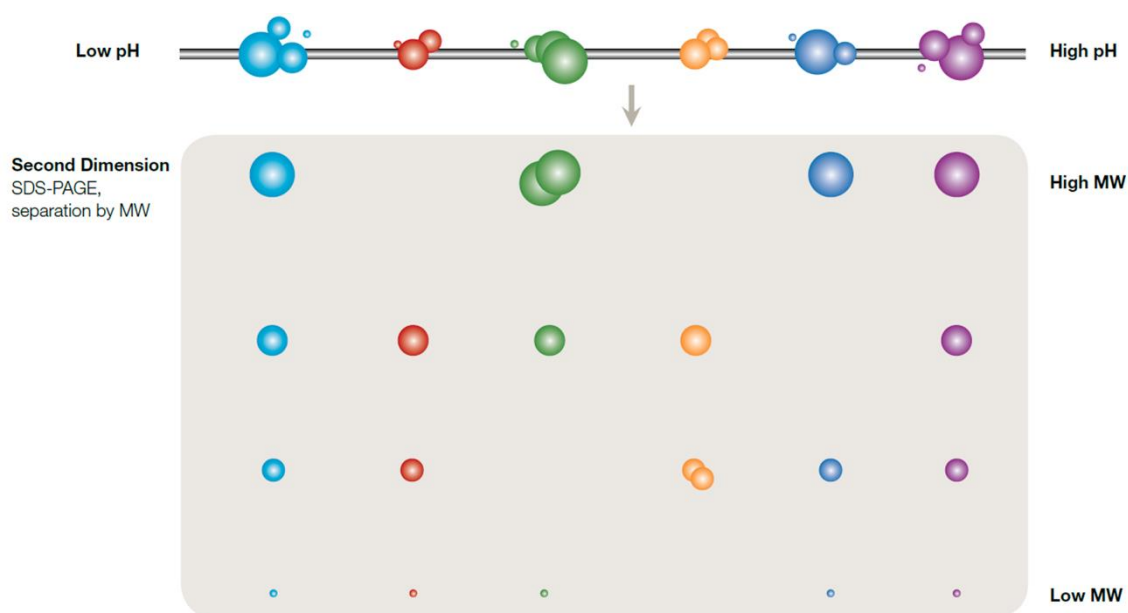
Figure 3.7 Transfer of proteins separated by isolectric point into the second dimension SDS PAGE [128].

3.8.2.2   Experimental Procedure

Cells were treated with 25 µM BODIPY-cisplatin (Figure 3.8) or the negative controls carboxyl-BODIPY (Figure 3.8) or DMF in serum-free medium for 2 hours and fractionated using *BioVision Nuclear/Cytosol Fractionation Kit* prior to subjecting the lysates to electrophoretic separation.
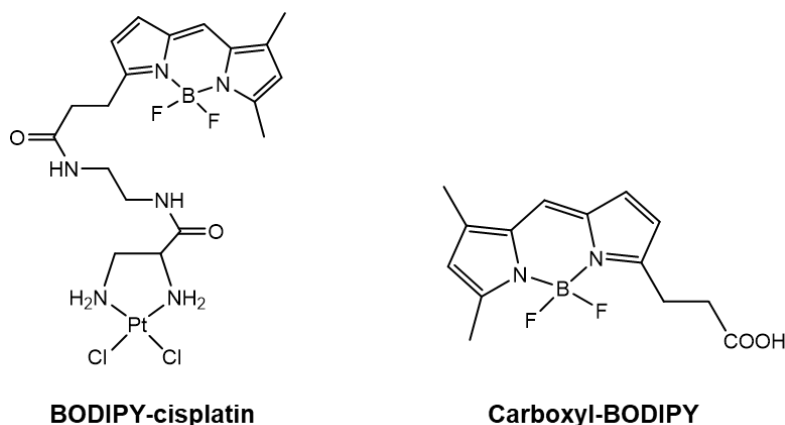
Figure 3.8 Chemical structures of the cisplatin analog BODIPY-cisplatin and the platinum-free label carboxyl-BODIPY.

Two-dimensional gel electrophoresis and all associated procedures (such as isoelectric focusing and staining) were carried out based on Kotz et al. [113] with some modifications to the protocol. After precipitation, 150 µg of total protein was solubilized in solubilization buffer (Chapter 3.1.2.2) for 1 hour and via subsequent overnight in-gel rehydration applied to pH 3-10 IPG strips (70 x 3 x 0.5 mm). After approximately

24 hours, IEF was carried out at a maximum current of 50 µA and a total of 17-18 kVh according to Table 3.2.

Table 3.2 Settings of the *PROTEAN® IEF Cell* system during isoelectric focusing.

Final Voltage [V]	Time [h]	Voltage Ramping Method [129]
300	12	Rapid
1,000	0.5	Linear
3,000	1.5	Linear
3,000	3.5	Rapid

All focused strips were stored at -80 °C until equilibration: second-dimensional SDS-PAGE was preceded by reduction and alkylation by 1% DTT and 2.5% IAA in 10 ml equilibration solution (6 M Urea, 50 mM Tris-HCl (pH 8.8), 30% glycerol and 4% SDS) for 15 minutes per strip. Afterwards the strip was put onto a ready-made 8-16% separation gel flanked by two electrode wicks soaked with protein marker and sealed with a 5% stacking gel (Table 3.3) to prevent the strip from moving and ensure exact and air bubble-free contact of the IPG strip and the separation gel. Proteins were separated for approximately 1.5 hours, starting at 80 V for 0.5 hours, followed by 140 V until the running front reached the bottom of the gel. All experiments were conducted with the *PROTEAN® IEF Cell* system in the first dimension, followed by *omniPAGE Mini Vertical Protein Electrophoresis System* in the second dimension SDS-PAGE.

Table 3.3 Preparation of 5% stacking gel solution for second dimension of two-dimensional gel electrophoresis.

Stacking Gel Solution	
Rotiphorese® Gel 30	833.0 µL
Purelab® Water	3.445 mL
Stacking Gel Buffer	625.0 µL
SDS (10%)	50.0 µL
TEMED*	5.0 µL
APS (10%)*	20.8 µL

* addition shortly before casting the gel in order to initiate polymerization

After the gels were scanned using the *ChemiDoc™ MP Imaging System* to detect fluorescence at 460-490/518-546 nm (excitation/emission), they were stained with Coomassie overnight to visualize all proteins. On the next day, the gels were scanned again and Delta2D (version 4.8) was used to warp the fluorescence and Coomassie-

stained pictures. Spots with both BODIPY-cisplatin and protein staining were detected, cut out and prepared for mass spectrometry (MS).

3.9 Staining

3.9.1 Coomassie Brilliant Blue (CBB)

First introduced for use in protein staining by Diezel et al. in 1972 [130], Coomassie Brilliant Blue G250, a triphenylmethane dye of greenish tint, was and still is the most widely used staining method for post-polyacrylamide gel electrophoresis staining processes. CBB G250 binds to the amino groups of proteins primarily through electrostatic and hydrophobic interactions. Being superior to its derivate CBB R250 in terms of solubility and, subsequently, less background staining, it enables visualization even of weaker protein bands shortly after its application. While Diezel and colleagues simply attributed this property to a lower penetration of the gel by the dye through conversion of CBB G250 into a colloidal state by the solvent trichloroacetic acid (TCA), Hoffmann et al. carried out further thorough investigations and optimized the composition throughout the years [131,132]. Nowadays, basically all colloidal Coomassie G250 staining methods are based upon these findings, including a variety of commercial kits.

Here, the *Quick Coomassie® Stain Kit*, which is a reusable, ready-to-use colloidal CBB G250 solution was used. After electrophoresis, gels were removed from the apparatus and soaked in the dye solution for just 15 minutes, without any prior or subsequent treatment. As staining with CBB is an endpoint method and oversaturation is not a problem, staining overnight for convenience was also possible. According to the manufacturer, the solution features a sensitivity of up to 5 ng per protein band.

3.9.2 Cy5

Cy5 is a cyanine-based dye that binds covalently to the amino group of lysines within the protein sample. Used for fluorescent labeling of proteins prior to gel electrophoresis (both one- or two-dimensional), the dye was designed to match the charge of the protein residue that it modifies. This means that it has basic buffering groups with pK values similar to those of the amino group of the lysines it binds to. Therefore, the isoelectric point of the protein is not altered and IEF can be performed without any changes to the result. Other than that, binding of the dye to the protein leads to an

addition of approximately 0.5 kDa per protein resulting in a separation of tagged and non-tagged proteins in the low molecular range. This could be a problem when subsequent protein identification of deviating protein patterns via mass spectrometry followed by additional post-run staining is planned. It should also be noted that labeling could cause decrease in protein solubility during electrophoresis induced by the hydrophobicity of the dye. To prevent multiple labeling of lysine residues in each protein, and thereby keeping hydrophobic properties within limits, the dye/protein ratio is kept deliberately low ('minimal labeling') [133,134].

The *SERVA Lightning Sci5 Kit* was applied according to the manufacturer's instructions. After the volume of protein lysate equivalent to 50 μg of total protein was adjusted to pH 8.5 with 50 mM NaOH, 1 μL of Sci5 working solution (400 pmol) was added. The solution was mixed and centrifuged at 12,000 g (4 °C, 30 seconds). Next, the mixture was incubated on ice for 30 minutes and then the labeling was stopped by adding 10 mM lysine solution. After vortexing and centrifugation (4 °C, 12,000 g, 20 seconds), the labeled proteins were put on ice for another 10 minutes in the dark. The samples were stored at -80 °C until needed. Excitation and emission were recorded at 625-650 nm and 675-725 nm, respectively.

3.9.3 SYPRO™ Ruby

There are several fluorescent SYPRO™ dyes available these days. Yet, while SYPRO™ Red and Orange, for example, attach to the detergent coat surrounding proteins in SDS denaturing gels, SYPRO™ Ruby binds to the basic amino acids of proteins and the polypeptide backbone through direct electrostatic interaction [135]. The mechanism, by which this ruthenium metal chelate interacts with the amino acid residues, is similar to CBB and does not involve intercalation into SDS micelles [136]. SYPRO™ Ruby features a broad linear quantitation range and is readily compatible with downstream mass spectrometry analysis [137].

In this project, a ready-to-use staining kit was applied. All solutions needed were included in the *SYPRO™ Ruby Protein Gel Stain Kit* by Thermo Fisher Scientific. After gel electrophoresis, the gels were placed in clean, opaque containers and treated with the fix solution for 0.5 hours twice. Next, the solution was discarded, the gel was subjected to the stain, and agitated smoothly overnight. On the next day, the gels were transferred to new containers and washed with the washing solution for 0.5 hours.

Then the gels were rinsed with Purelab® Water right before imaging at 302/535-645 nm (excitation/emission) to prevent corrosive damage to the device. According to the manufacturer, the stain achieves sensitivity up to the 1 ng.

3.10 RNA Interference (RNAi)

3.10.1 Basics

RNAi represents a potent approach for the elucidation of yet unknown functions of certain genes and their coded proteins. In the cell, double-stranded RNA (dsRNA) is cleaved by the enzyme Dicer, resulting in short double-stranded fragments of about 20 to 25 base pairs in length. Next, these short dsRNA are incorporated in the RNA-induced silencing complex (RISC), forming the pre-RISC. In this preliminary complex, each bound dsRNA is unwound into two single-stranded RNA, called the guide strand and the passenger strand. The latter is then degraded, while the former remains a part of the RISC and now functions as template for the targeted messenger RNA (mRNA). As soon as the complementary mRNA is found, it is dismantled or inhibited for subsequent translation (Figure 3.9). However, RNAi does not abolish gene expression completely, which is why this process is sometimes referred to as knockdown to distinguish it from knockout processes, where gene expression is blocked in its entirety.
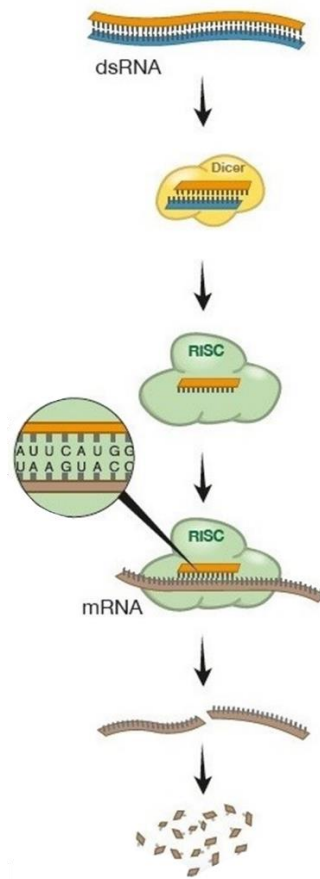
Figure 3.9 The mechanism of RNA interference [138].

While the regulation of proteins through this mechanism is a naturally occurring process, it can also be initiated via the introduction of exogenous siRNA. Provided that the nucleotide sequence of the gene of interest is known, synthesized siRNA molecules can be transfected into cells via different techniques. Here, all gene-silencing experiments were conducted by means of transient, i.e. only temporary, transfection of specific siRNA via lipofection on the basis of cationic lipids. Initiated by the spontaneous formation of so-called lipoplexes (liposomes formed by positively charged lipids and negatively charged siRNA, that can easily merge with the phospholipid bilayer of the cell membrane) and their uptake into the cell through endocytosis, the release of siRNA is caused by disruption of the endosome membrane or the fusion of the endosome membrane with the liposome.

3.10.2 Experimental Procedure

Cells were seeded in 6-well plates at a density of $5x\ 10^5$ cells/well for A2780 cells and 2.5×10^5 cells/well for HCT-8 cells and were allowed to attach overnight at 37 °C and 5% CO_2. On the next day, cells were treated with 100 pmol protein-specific siRNA

(Table 3.4) for either GSTP1, Vimentin, DJ-1, Grb2 or NC siRNA and the *K4®*
Transfection System, composed of the *K4® Transfection Reagent* and the *K4®*
Multiplier, according to the manufacturer's instructions (Chapter 3.1.2.1). Hereby, the
reagent is based on cationic lipids to ensure proper lipoplex formation and the multiplier
is applied to minimize the cell's ability to detect non-cellular nucleic acids and their
subsequent initiation of defensive measures. First, cells were pre-treated with 10 µL
K4® Multiplier per well. For two wells of a 6-well plate, 10 µL of siRNA stock (20 µM)
was mixed with 250 µL medium, without serum and antibiotics. In another tube, 27 µL
of *K4® Transfection Reagent* was mixed with 250 µL of serum- and antibiotic-free
medium. Then, 260 µL of the transfection reagent dilution was added to 260 µL of the
siRNA dilution and incubated at RT for 15 minutes. A total of 250 µL of the mixture per
well was added to the cells, and the plate was gently swayed to ensure an equal
distribution of the transfection complex. After 24 hours, siRNA-containing antibiotic-
free medium was removed and replaced by fresh full medium. After another 48 hours,
cells were lysed with freshly prepared RIPA lysis buffer and sonicated, as described
before, to ensure protein solubilization. Next, lysates were centrifuged and the
supernatant was stored at -80 °C until further use.

Table 3.4 Base sequences of the siRNA used.

Protein	Sense sequence (5'→ 3')	Antisense sequence (5'→ 3')
Vimentin	GGUUGAUACCCACUCAA AAtt	UUUUGAGUGGGUAUCAACC ag
GSTP1	ACCAGAUCUCCUUCGCU GACUACAA	UUGUAGUCAGCGAAGGAGA UCUGGU
DJ-1	GGUUUUGGAAGUAAAGU UAtt	UAACUUUACUUCCAAAACCt a
Grb2	GGUGGAUUAUCACAGAU CUtt	AGAUCUGUGAUAAUCCACC ag
NC	Scrambled sequence	

For the experimental procedure concerning cytotoxicity tests after knockdown see
Chapter 3.4.2.

3.11 Western Blot

3.11.1 Basics

Western Blotting is a molecular biological method used to identify the presence of proteins of interest in a complex sample. Preceded by electrophoretic separation of this mixture and a protein standard, all proteins are electrophoretically transferred to a membrane (usually made of PVDF or nitrocellulose) to make them accessible to detection via antibodies. During this process, called 'electroblotting', negatively charged proteins are pulled from the gel towards the anode into the membrane. All proteins thereby stay at the same position they were at in the gel, so that the distribution of bands on the membrane is basically an exact mirror image of the separation in the gel. Next, the membrane has to be treated with a blocking agent (milk for instance) to prevent unspecific bindings of primary antibodies and only then the membrane is incubated with the primary antibody solution under gentle agitation for a time period of a couple of hours to overnight. Following this, depending on the antibody the membrane is to be washed several times in TBS-T to get rid of any excess antibody. In the next step, the membrane is exposed to a secondary antibody, which recognizes the species-specific epitope of the primary antibody. There are several ways to finally detect the target protein, for example via chemiluminescence, if the secondary antibody is coupled to a reporter enzyme such as HRP. After incubation with the secondary antibody and a number of washing steps, the membrane is subjected to an appropriate chemiluminescent substrate. HRP causes the oxidization of the substrate and subsequently the generation of luminescence, which can be detected with suitable imagers (Figure 3.10). The intensity of luminescence is thereby proportional to the amount of HRP-conjugated secondary antibody, which in turn correlates with the amount of the protein of interest. An additional detection of a protein which is constitutively and steadily expressed in cells ('loading control'), for example GAPDH, actin or tubulin, is used to enable normalization of amounts of target protein and therefore allows for a semi-quantitative determination of the target protein in different samples.
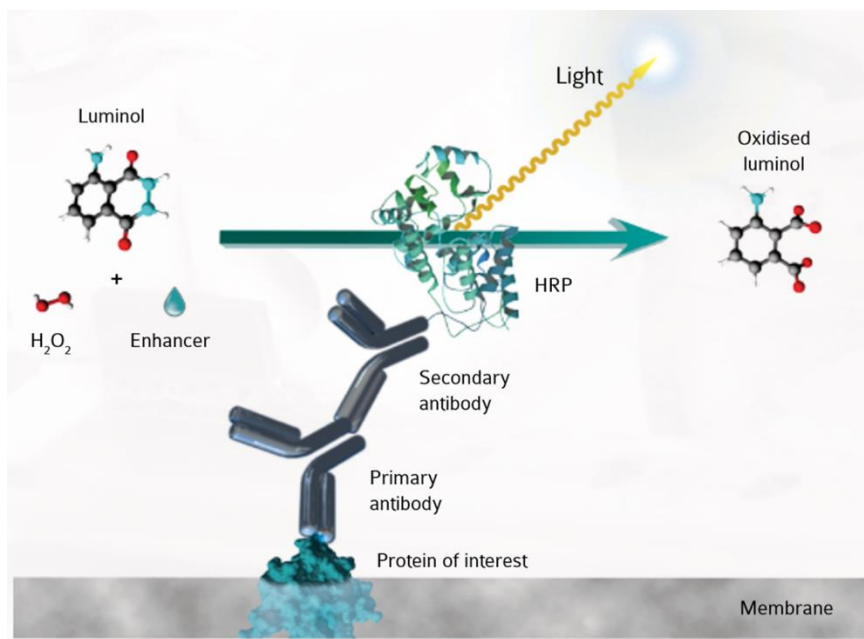
Figure 3.10 Chemiluminescent detection of the membrane-bound antigens [139].

3.11.2 Experimental Procedure

After successful one-dimensional gel electrophoresis, the separation gels were equilibrated in transfer buffer for about 5 minutes. At the same time, the required number of PVDF membranes were swiveled in methanol for 20 seconds to make them more hydrophilic for blotting and afterwards also placed in the transfer buffer. In the next step, the separating gel and membrane were incorporated in the blot sandwich and blotted for two hours at 100 V, 350 mA and about 4 °C. The membrane was subsequently treated with 5% skim milk in TBS-T (blocking solution) for 1 hour to prevent unspecific binding of the primary antibody afterwards. After several washing steps in TBS-T solution, the membrane was incubated overnight at 4 °C with the respective primary antibody against vimentin, GSTP1, DJ-1 or Grb2. The dilution of the respective antibodies for the respective target proteins was hereby based on the manufacturer's recommendations (Chapter 3.1.1). The next morning, the antibody solution was removed from the membrane, followed by several washing steps in order to remove all excessive unbound antibodies. After this was completed, the membrane could then be incubated for about 1.5 hours with the secondary antibody, which carries the enzyme HRP and is directed against the Fc region, in others words the tail region, of the primary antibody. Using a mixture of luminol and peroxide buffer (prepared according to the manufacturer's instructions, *Pierce™ ECL Western Blotting Substrate*), HRP and thereby the target antigen could then be detected by chemiluminescence in the final step. The image was recorded using the *ChemiDoc™*

XRS+ system, the bands were densitometrically evaluated using *ImageLab™* (version 5.1). GAPDH expression was used as a loading control.

3.12 Combination Index (CI)

3.12.1 Basics

In order to characterize the pharmacological interaction between a combination of multiple drugs and facilitate the determination of whether the combination results in synergism, additivity or antagonism, Chou and Talalay have introduced the CI method in 1984 [140]. Based on the idea that a combination of two drugs behaves like a third drug, the cells are treated with both single drugs and a serial dilution of the mixture (usually 2-fold with several concentration points above and below the EC_{50} values to make the assay more accurate). This way, all parameters needed for the determination of the CI according to the *Combination Index Equation of Chou-Talalay* (Equation 3.2), including the drugs' different potencies and their dose-effect curves, can be calculated [141]. All of the respective calculations were performed by means of the computer software *CompuSyn®* by simply adding the constant combination ratio of both drugs and the given degrees of effect after treatments [142]. It should be noted that the minimum of data points for drug combination studies conducted as described by Chou et al. is 5. Nevertheless, to avoid difficulties associated with technical or biological variabilities, there should always be more than the required minimum [141]. As specified by Chou et al., CI values >1, =1 and <1 correspond to antagonism, additivity and synergism, respectively [140].

$$CI = \frac{(D)_1}{(D_x)_1} + \frac{(D)_2}{(D_x)_2}$$
Equation 3.2

$(D)_1$: Concentration of drug 1 in the combination with drug 2 that inhibits a system by x%
$(D)_2$: Concentration of drug 2 in the combination with drug 1 that inhibits a system by x%
$(D_x)_1$: Concentration of drug 1 alone that inhibits a system by x%
$(D_x)_2$: Concentration of drug 2 alone that inhibits a system by x%

3.12.2 Experimental Procedure

A2780 cells were seeded in 96-well plates at a density of 10,000 cells/well and incubated overnight at 37 °C and 5% CO_2. On the following day, they were treated with either 0-100 µM cisplatin or FiVe1 alone or with combinations of 10, 20, 40, 60, 80, 100, 200, 400 and 800% of the previously determined EC_{50} concentrations of cisplatin and FiVe1 (Table 3.5). The ratio of cisplatin to FiVe1 in A2780 cells was 1.247 and in

A2780cis cells 6.225. After 72 h, the modalities of the combinations were assessed via the MTT assay (Chapter 3.4).

Table 3.5 Concentrations [µM] of cisplatin and FiVe1 used in combination treatments.

Concentration [% of EC$_{50}$]	Concentration [µM]			
	A2780		A2780cis	
	Cisplatin	FiVe1	Cisplatin	FiVe1
10	0.116	0.093	0.498	0.080
20	0.232	0.186	0.996	0.160
40	0.464	0.372	1.992	0.320
60	0.696	0.558	2.988	0.480
80	0.928	0.744	3.984	0.640
100	1.160	0.930	4.980	0.800
200	2.320	1.860	9.960	1.600
400	4.640	3.720	19.920	3.200
800	9.280	7.440	39.840	6.400

3.13 Immunoprecipitation (IP)

3.13.1 Basics

By means of immunoprecipitation it is possible to separate complex samples, detect certain target proteins and further investigate these according to the respective objective. It is also possible to isolate larger complexes such as target protein-protein or target protein-ligand complexes, provided that these bonds are sufficiently strong. Previously unknown binding partners can be identified by this so-called "pull-down". The method is hereby based on classical antigen-antibody reactions, which are expanded by varying solid, insoluble supports (so-called beads), onto which antibodies specific for the target protein are immobilized. Solid supports can be agarose resins or magnetic particles, amongst others, coated with protein A or protein B (or a combination of both) for instance, to enable antibody binding. Particularly, protein A binds specifically to the heavy chains of the Fc region, which conversely directs the antigen-binding sites outwards [143]. By the application of so-called crosslinking agents like disuccinimidylsuberate (DSS), dimethylpimelimidate (DMP) or BS^3 it is possible to covalently link an antibody and beads and therefore prevent co-elution of antibody fragments, which would complicate a subsequent detection of the target protein [144,145]. Hereby, N-hydroxysuccinimidyl (NHS) ester groups of the crosslinkers react covalently with primary amines from proteins, both protein A or B of the solid support as well as the antibody [143]. In general, magnetic beads are

considered superior to agarose resins, since they allow not only fast, reproduceable results, but also simplified handling. Especially when dealing with rather weak antibody-antigen binding, the lack of physical stress by omitting centrifugation steps can increase the yield of detectable targets.

In brief, there are two distinct approaches to the application of immunoprecipitation: direct and indirect ('pre-immobilized antibody approach' and 'free antibody approach', respectively, Figure 3.11). When using the former, specific antibodies are firstly immobilized onto the beads. Then, the antibody-beads complexes are added to the lysate and during gentle agitation the target antigen binds to the immobilized antibody. In contrast, the indirect method involves incubation of free, unbound antibody and antigen in the lysate. Thereupon, the beads are added and the antigen-antibody complexes are captured by the beads. This approach is mostly used if the concentration of target protein is low or the specific affinity of the antibody to the antigen is expected to be weak. Furthermore, if binding kinetics of the antibody to the antigen appears to be slow, the indirect immunoprecipitation should be selected. Following the formation of the antigen-antibody-bead complexes, all further steps, such as their collection and the elution of the target antigen, are independent of the method employed. Typically, the immobilized immune complexes are heated in sample loading buffer containing SDS, which denaturizes proteins for the subsequent SDS PAGE. In doing so, the beads are irreparably destroyed and hence disposed of [143].
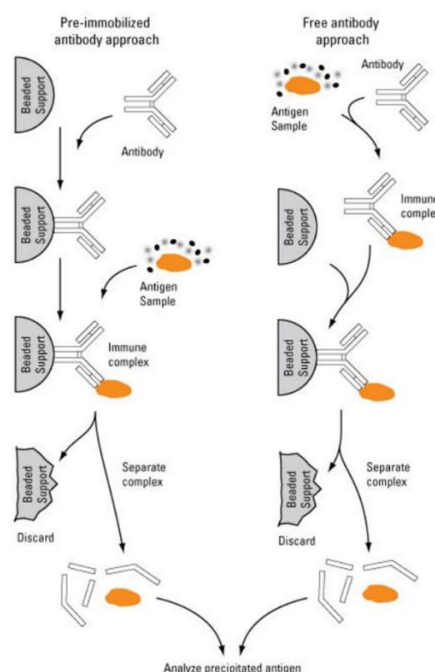
Figure 3.11 Schematic diagram of direct (left panel) and indirect (right panel) immunoprecipitation [143].

3.13.2 Experimental Procedure

Following treatment with 25 µM BODIPY-cisplatin (Figure 3.8) or its negative control DMF in serum-free medium for 2 hours and subsequent lysis with *BioVision Nuclear/Cytosol Fractionation Kit*, lysates were subjected to immunoprecipitation in order to achieve separation of the sample before two-dimensional gel electrophoresis. Via immunoprecipitating potential BODIPY-cisplatin protein binding partners with a BODIPY FL-antibody bound to magnetic beads ('eluate'), the lysate was supposed to be cleared of all other components and therefore allow for electrophoretic separation of exclusively the proteins of interest, i.e. those carrying BODIPY-cisplatin moieties. Prior to acquiring the eluate, the bead-antibody-antigen complexes were washed several times with washing buffer to get rid of unspecific binding, generating the 'washing fraction'. As the affinity and binding capacity of the antibody was unknown, the 'unbound fraction' was intended to provide information on possibly uncaptured antigens.

By using magnetic beads, it was possible to separate beads and solutions after respective incubation steps without the risk of aspirating immune complexes in the process. Since the affinity and binding kinetics of the antibody to the antigen were unknown and the complex of interest (beads-antibody-antigen-protein complex) was rather large and binding properties were also unfamiliar, the application of a high-power magnet and therefore the omission of centrifugation was considered beneficial. In parallel, every immunoprecipitation of a BODIPY-cisplatin-treated sample, samples treated with just the solvent (DMF) were subjected to the same protocol to compare specificity and efficiency.

All experiments were carried out according to the manufacturer's instructions of the *Immunoprecipitation Kit Dynabeads™ Protein A* with minor changes to the protocol along the way. It is pointed out that longer incubation times can be advantageous, especially when using low affinity antibodies. Unless otherwise stated, all steps were performed at RT. Yet, cooling to 4 °C during experiments helps with sensitive protein complexes, as dissociations and enzymatic activity are reduced.

3.13.2.1 Indirect Immunoprecipitation

Here, the volume of pre-treated lysate equivalent to 100 µg of total protein was precipitated as described in Chapter 3.7. After air drying the cell pellet, it was

resuspended in 100 µL of PBS-T (0.1%). 3 µL of primary anti-BODIPY-FL antibody stock solution (equal to 9 µg antibody) was simultaneously diluted in 200 µL *Binding and Washing Buffer* provided with the kit. After uniting the sample and antibody solutions, the mix was incubated for 0.5 hours at RT on a 360° rotation mixer (50 rpm) in order to allow formation of the immune complexes. Next, 50 µL (equal to 1.5 mg) Dynabeads™ magnetic beads were separated from their supernatant on the magnet and incubated with the immune complex solution for 10 minutes at RT on the 360° rotation mixer (50 rpm). The complexes were washed 3 times in *Washing Buffer*, each time followed by separation on the magnet and aspiration of the supernatant. Then, the beads-antibody-antigen-protein complexes were resuspended in 100 µL *Washing Buffer* and transferred to a clean reaction tube to avoid co-elution of proteins bound to the tube wall. After another magnetic separation, the immune complexes were exposed to 20 µL *Elution Buffer* and 5 µL 5x sample loading buffer and heated to 95 °C for 5 minutes. Finally, the supernatant obtained by one last separation step was loaded onto a 4-20% ready-made separating gel and subjected to one-dimensional gel electrophoresis.

3.13.2.2 Direct Immunoprecipitation

All steps of the direct immunoprecipitation protocol were executed at 4 °C to avoid protein complex dissociation and minimize enzymatic activity. In contrast to the indirect immunoprecipitation, 1.5 mg (equals 50 µL) Dynabeads™ magnetic beads were first incubated with 3 µL (equals 9 µg) primary anti-BODIPY-FL antibody diluted in 200 µL PBS-T (0.1%) for 10 minutes (RT, 360° rotation). After subsequent removal of the supernatant, coupled beads were then washed with 200 µL PBS-T (0.1%) and twice with Conjugation Buffer (Chapter 3.1.2.4). The solution and the beads were separated on the magnet and the supernatant was discarded. Next, the beads were resuspended in 250 µL 5 mM BS^3 and incubated for 0.5 hours (360° rotation). The crosslinking of beads and antibody was stopped by adding 12.5 µL Quenching Buffer (Chapter 3.1.2.4) and ensuing incubation for 15 minutes (360° rotation). The crosslinked Dynabeads™ were washed 3 times with PBS-T (0.1%) and after discarding of the supernatant, 300 µg lysate stocked up on 100 µL PBS-T (0.1%) were added. The mixture was incubated for 2 hours (360° rotation) to allow the formation of the immune complexes. Then, the complexes were washed 3 times with *Washing Buffer* and all following steps were performed just as with the direct approach.

3.14 Copper-Catalyzed Azide-Alkyne Cycloaddition (CuAAC)

3.14.1 Basics

Since its first independent introduction by Rostovtsev et al. and Tornøe and colleagues in 2002 on the basis of the azide-alkyne Huisgen cycloaddition, CuAAC has emerged as the most popular approach of a group of methods termed "*Click Chemistry*" for a variety of purposes [146]. The concept of *Click Chemistry* was initially defined as a group of reactions demonstrating the following properties: amongst other factors they had to be wide in scope, give very high yields, generate only inoffensive byproducts, present simple and easy reproducible reaction conditions and include only easy accessible reaction materials and reagents [147]. During CuAAC, azides and alkynes are assembled rapidly, leading to regiospecific 1,4-disubstituted 1,2,3-triazoles (Figure 3.12). Thereby it is of advantage that the reaction is unaffected by most organic and inorganic functional groups attached to the azide and the alkyne. Catalyzation by Cu^+ can be induced by several sources of Cu^+, one being the addition of Cu^{2+} (in the form of $CuSO_4$) and a supplementary reducing agent, such as sodium ascorbate. To ensure the inhibition of re-oxidation of reduced Cu^+ through oxygen radicals, the catalyst needs to be chelated by a stabilizing ligand. Due to its solubility in water, THPTA has proven to be superior to other ligands. After the alkyne and azide are mixed and both THPTA and $CuSO_4$ are included in the solution, the click reaction is finally initiated by the addition of a reducing agent.
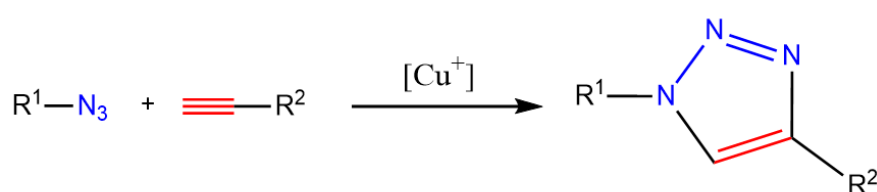
Figure 3.12 Copper-catalyzed azide-alkyne cycloaddition.

3.14.2 Experimental Procedure

Cells treated with 25 µM cisplatin-azide or cisplatin-alkyne (Figure 3.13) in serum-free medium for 2 hours, as well as control samples treated with DMF, serum-free medium, or unplatined azides/alkynes (Figure 3.13) were harvested by trypsination, washed with PBS twice to remove excessive compound and centrifuged (4 °C, 1,000 g, 4 minutes). The cell pellet was resuspended in 1 mL PBS and pipetted in a 1.5 mL reaction tube. After lysis using the *BioVision Nuclear/Cytosol Fractionation Kit*, a

volume of lysate equivalent to 30 µg total protein was transferred to a separate reaction tube and filled up with PBS to a total volume of 100 µL (deviations of total protein used are indicated, if applicable). From this point forward, CuAAC-treatment concentrations were partly adjusted in order to work out the most appropriate conditions for the objectives set, pre-treatment with IAA for 0.5 hours proved to be valuable to some extent (Chapter 4.1.7). First off, depending on the preceding treatment of cells, the sample was subjected to the treatment with the corresponding azide or alkyne (5-500 µM), linked to a fluorophore for subsequent detection (BODIPY-azide/-alkyne, Figure 3.13), and vortexed briefly.
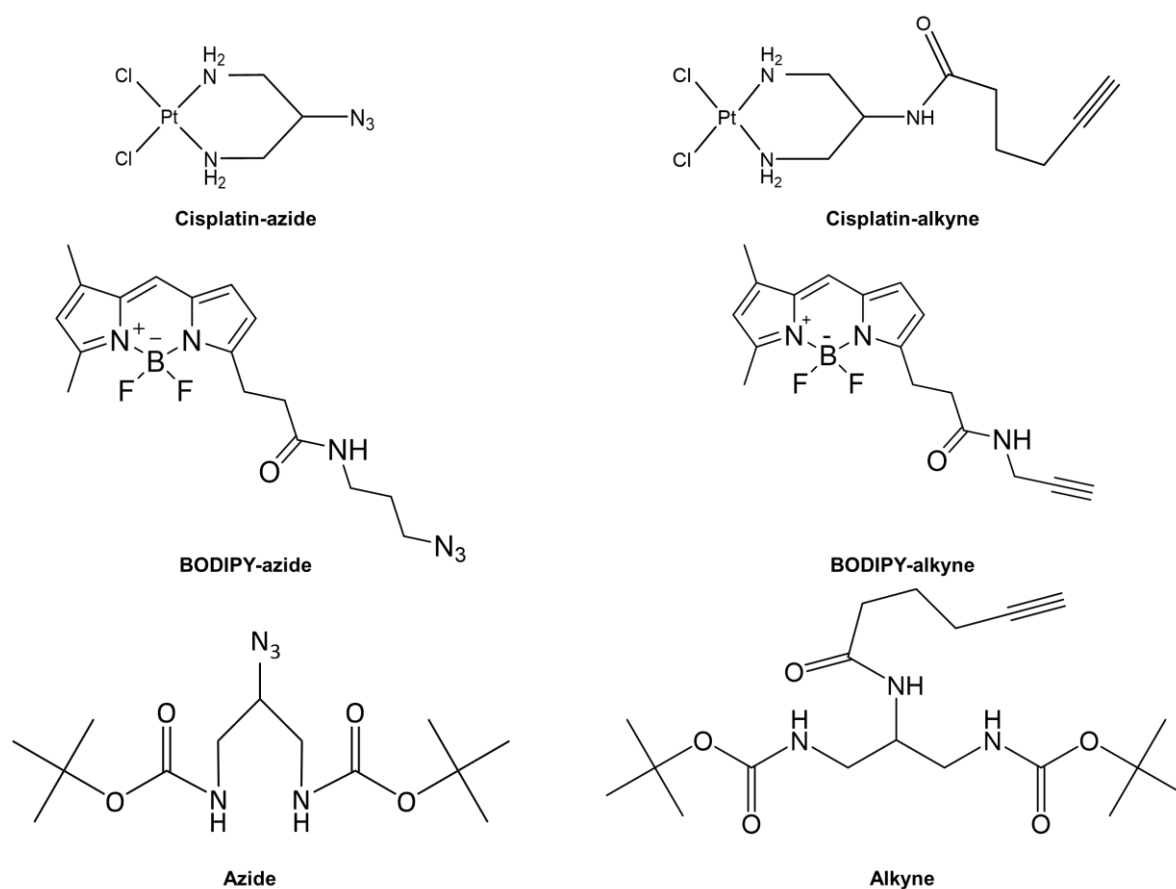
Figure 3.13 Molecular structures of cisplatin-azide, -alkyne, BODIPY-azide, -alkyne and their respective unplatinated non-fluorescent tags azide and alkyne.

Next, THPTA (2-10 mM) was added and the mixture was vortexed again for only a couple of seconds. Without much delay, $CuSO_4$ (1-2 mM) was pipetted into the reaction tube and, once again, the mixture was vortexed. Lastly, the addition of sodium ascorbate followed by one last vortexing activated the reduction of Cu^{2+} to Cu^+ and therefore the click reaction. The sample was incubated for 1 hour in the dark and was then ready for further procedures. After electrophoresis, gels were scanned using the

ChemiDoc™ MP Imaging System to detect BODIPY fluorescence at 460-490/518-546 nm (excitation/emission).

3.15 Mass Spectrometry

All mass spectrometry-related experiments, such as sample preparation, the liquid chromatography coupled mass spectrometry (LC-MS) analysis itself and subsequent protein identification were conducted by Dr. Marc Sylvester and Bernd Gehrig from the Mass Spectrometry Core Facility, Institute of Biochemistry and Molecular Biology at the University of Bonn.

3.15.1 Basics

Mass spectrometry is an analytical technique to detect the mass-to-charge ratio (m/z) of charged molecules. By analyzing the mass spectra, it is possible to determine diverse characteristics of the sample, amongst others the chemical identity or structure of the sample molecules (e.g. proteins). The prototypic mass spectrometer basically consists of three consecutive units: an ion source, a mass analyzer and a detector (Figure 3.14).
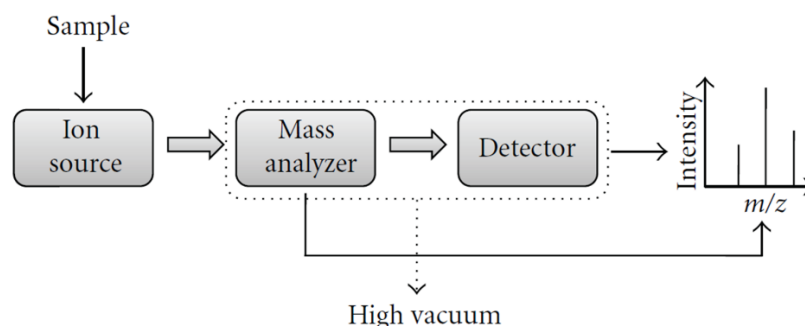
Figure 3.14 The basic components of an mass spectrometer [148].

Each MS analysis starts with the ionization of the analyte and, besides several more methods to achieve this, this can be done with electrospray ionization (ESI). Here, the liquid containing the sample is subjected to high voltage, thus, producing a fine aerosol. This aerosol is introduced into a vacuum and as the solvent evaporates, the droplets become more and more charged. Upon exceeding a certain charge threshold, the droplets explosively dissociate, resulting in the formation of charged ions. Next, it is possible to combine both mass analyzer and detector by employing an Orbitrap ion trap mass analyzer. An Orbitrap consists of two outer electrodes and one central electrode. As soon as the ions are inserted, they start to oscillate around the inner

cathode and, depending on their m/z, they spin around at different frequencies, which can be measured and will result in signals leading to mass spectra.

Additionally, it is possible to carry out chromatographic separation, e.g. high-performance liquid chromatography (HPLC), prior to MS to decrease complexity of the sample. However, a major problem is the transfer of the separated sample into the MS, which requires an almost complete removal of the solvent. When using a Nano High-performance Liquid Chromatography (nanoHPLC), the chromatographic separation is performed at a significantly lower flow rate making it feasible to omit the carrier gas that is usually applied to get rid of the excess sample volumes and solvent but is prone to generating contaminations.

3.15.2 Experimental Procedure

3.15.2.1 Sample Preparation for MS

For protein identification gel slices were first subjected to in-gel digestion [149,150]. In brief, slices were washed consecutively with water, 50% acetonitrile (ACN), and 100% ACN. Proteins were reduced with 20 mM DTT in 50 mM ammonium bicarbonate and alkylated with 40 mM acrylamide (in 50 mM bicarbonate) for 0.5 hours. The slices were washed again and dehydrated with ACN. Dried slices were incubated with 330 ng trypsin at 37 °C overnight. The peptide extract was separated and remaining peptides extracted with 50% ACN. Peptides were dried in a vacuum concentrator and stored at -20 °C.

3.15.2.2 Protein Identification by MS

Peptides were dissolved in 0.1% formic acid (solvent A, FA) and 1/3 was injected onto a C18 trap column (20 mm length, 100 µm inner diameter, ReproSil-Pur 120 C18-AQ, 5 µm, Dr. Maisch GmbH, Ammerbuch-Entringen, Germany) made in-house. Bound peptides were eluted onto a C18 analytical column (200 mm length, 75 µm inner diameter, ReproSil-Pur 120 C18-AQ, 3 µm). Peptides were separated during a linear gradient from 2% to 35% solvent B (90% acetonitrile, 0.1% FA) within 20 min at 300 nl/min. The nanoHPLC was coupled online to an LTQ Orbitrap Velos mass spectrometer (Thermo Fisher Scientific, Bremen, Germany). Peptide ions between 330 and 1,600 m/z were scanned in the Orbitrap detector with a resolution of 30,000 (maximum fill time 400 ms, AGC target 106). The 20 most intense precursor ions (threshold intensity 3,000, isolation width 1.1 Da) were subjected to collision induced

dissociation (normalized energy 35) and analyzed in the linear ion trap. Fragmented peptide ions were excluded from repeat analysis for 13 seconds.

Raw data processing and analysis of database searches were performed with Proteome Discoverer software 2.2.0.388 (Thermo Fisher Scientific). Peptide identification was done with an in-house Mascot server version 2.6.1 (Matrix Science Ltd, London, UK). MS2 data were searched against human sequences in SwissProt (release 2018_10) and common contaminants. m/z tolerance was 10 ppm (precursor ions) and 0.6 Da (fragment ions) respectively. Tryptic peptides with up to two missed cleavages were searched. Propionamide, PtBDP (BC17F2H26N5O2Pt mass shifts 576.178992 and 557.160602 with and without water) were set as dynamic modifications on cysteines. PtBDP modifications as above but without one hyrdrogen were searched dynamically on cysteine, histidine, and methionine. Oxidation of methionine and N-terminal protein acetylation were also allowed as dynamic modifications. Mascot results were assigned q-values by the percolator algorithm [151] version 3.00 as implemented in Proteome Discoverer. Localization of modifications was scored with the ptmRS 2.0 node [152]. Proteins were included if at least two peptides were identified with q ≤ 0.01. Actual false positive rates were typically ≈1% on peptide spectrum matches (PSM), peptide, and protein level.

3.16 Statistical Analysis

Experiments were executed at least in triplicate with independent samples and the results are presented as mean (Equation 3.3) and standard error of the mean (SEM, Equation 3.4).

$$\text{Mean } (\overline{x}) = \frac{\sum_{x=1}^{n} x_i}{n}$$

Equation 3.3

n: number of measurements
x_i: individually measured value

$$\text{SEM} = \frac{\frac{\sum_{x=1}^{n} (x_i - \overline{x})^2}{n-1}}{\sqrt{n}} = \frac{\text{SD}}{\sqrt{n}}$$

Equation 3.4

n: number of measurements
x_i: individually measured value
SD: standard deviation

As experiments were performed with a small sample size, data could not be tested for normal distribution and this was simply assumed.

In case of co-incubation cytotoxicity experiments, statistical comparison between differentially treated cell lines of each cell line separately was carried out using an unpaired t-test. Cytotoxicity experiments of cells pre-treated with specific, NC or no siRNA were compared using one-way analysis of variance (ANOVA) with Sidak post-hoc test in the event of significant results.

All apoptosis assays were analyzed by applying two-way ANOVA with Tukey's multiple comparison's test.

All data was analyzed employing GraphPad Prism® 6 Software. Differences were considered statistically significant for $p < 0.05$ with specified settings according to Table 3.6.

Table 3.6 p-values and their corresponding specific statistical significance.

p value	Specification
$0.01 < p < 0.05$	*, low statistical significance
$0.001 < p < 0.01$	**, average statistical significance
$0.0001 < p < 0.001$	***, strong statistical significance
$p < 0.0001$	****, very strong statistical significance

4   Results

4.1   Method Development

4.1.1   Comparative Cytotoxicity of Labelelled and Unlabelled Compounds

To confirm the expected properties of the employed ovarian cancer and colorectal cancer cell lines (A2780/A2780cis and HCT-8/HCT-8ox cells, respectively) with regards to sensitivity and resistance, MTT assays were performed routinely before the start of the project (Figure 4.1, Table 4.1) and as control runs to all respective experiments. Hereby, cells were treated with either 0.1-1000 µM of cisplatin or oxaliplatin. In order to assess the antitumor properties of the cisplatin analogs used prior to two-dimensional separation and immunoprecipitation, cells were treated with 0.2-1000 µM of BODIPY-cisplatin or 0.2-500 µM carboxyl-BODIPY. While A2780 cells were sensitive towards both cisplatin and oxaliplatin, A2780cis cells featured resistance especially in the case of cisplatin (RF = 4.2 for cisplatin and RF = 3.1 for oxaliplatin). In both HCT-8 and HCT-8ox cells, on the other hand, cisplatin was rather ineffective (RF = 1.7). Treatment with oxaliplatin then again was only effective in oxaliplatin-sensitive HCT-8 cells (RF = 31.0) (Figure 4.1, Table 4.1). These results clearly reflected the existing acquired resistance of A2780cis cells and intrinsic resistance of HCT-8/HCT-8ox cells to cisplatin and natural sensitivity to oxaliplatin in the case of HCT-8 cells, so that work could be continued as planned.

Figure 4.1 Cytotoxicity of cisplatin and oxaliplatin in A2780/A2780cis (A,B) and HCT-8/HCT-8ox (C,D) cells, respectively (mean ± SEM, n = 6-8). The left panel represents cell-viability data from all experiments, the right panel the respective pEC_{50} values. **, $p < 0.01$; ****, $p < 0.0001$.

Table 4.1 Cytotoxicity (pEC$_{50}$, mean ± SEM, n = 5-8) of cisplatin, oxaliplatin, BODIPY-cisplatin and carboxyl-BODIPY in A2780, A2780cis, HCT-8 and HCT-8ox cells (the respective EC$_{50}$ values are given in parentheses).

Compound	A2780	A2780cis	HCT-8	HCT-8ox
Cisplatin	5.932 ± 0.037 (1.17 µM)	5.312 ± 0.021 (4.88 µM)	5.259 ± 0.031 (5.51 µM)	5.037 ± 0.047 (9.18 µM)
Oxaliplatin	6.370 ± 0.093 (0.43 µM)	5.883 ± 0.085 (1.31 µM)	6.059 ± 0.027 (0.87 µM)	4.569 ± 0.060 (26.98 µM)
BODIPY-cisplatin	4.742 ± 0.034 (18.11 µM)	4.007 ± 0.002 (98.40 µM)	4.028 ± 0.052 (93.76 µM)	3.781 ± 0.028 (165.58 µM)
Carboxyl-BODIPY	<3.301 (>500 µM)	<3.301 (>500 µM)	<3.301 (>500 µM)	<3.301 (>500 µM)

Furthermore, it could be shown that BODIPY-cisplatin acts similarly to its parent compound cisplatin with regard to cytotoxicity, even though it was reduced due to the introduction of the tag (Figure 4.2, Table 4.1). Cisplatin-resistant A2780cis ovarian cancer cells exhibited resistance towards BODIPY-cisplatin (RF was 4.2 for cisplatin and 5.4 for BODIPY-cisplatin). Cytotoxicity of BODIPY-cisplatin was much lower in colorectal cancer cells, both in the oxaliplatin-sensitive HCT-8 and oxaliplatin-resistant HCT-8ox cell lines, which are intrinsically resistant to cisplatin. In HCT-8 cells, cisplatin was 4.7 times less active than in A2780 ovarian cancer cells. The cytotoxicity of BODIPY-cisplatin was reduced 5.2-fold. The platinum-free label carboxyl-BODIPY showed no antitumor activity in both entities up to 500 µM, in case of HCT-8 cells calculation of EC$_{50}$ was not even possible (Figure 4.2).
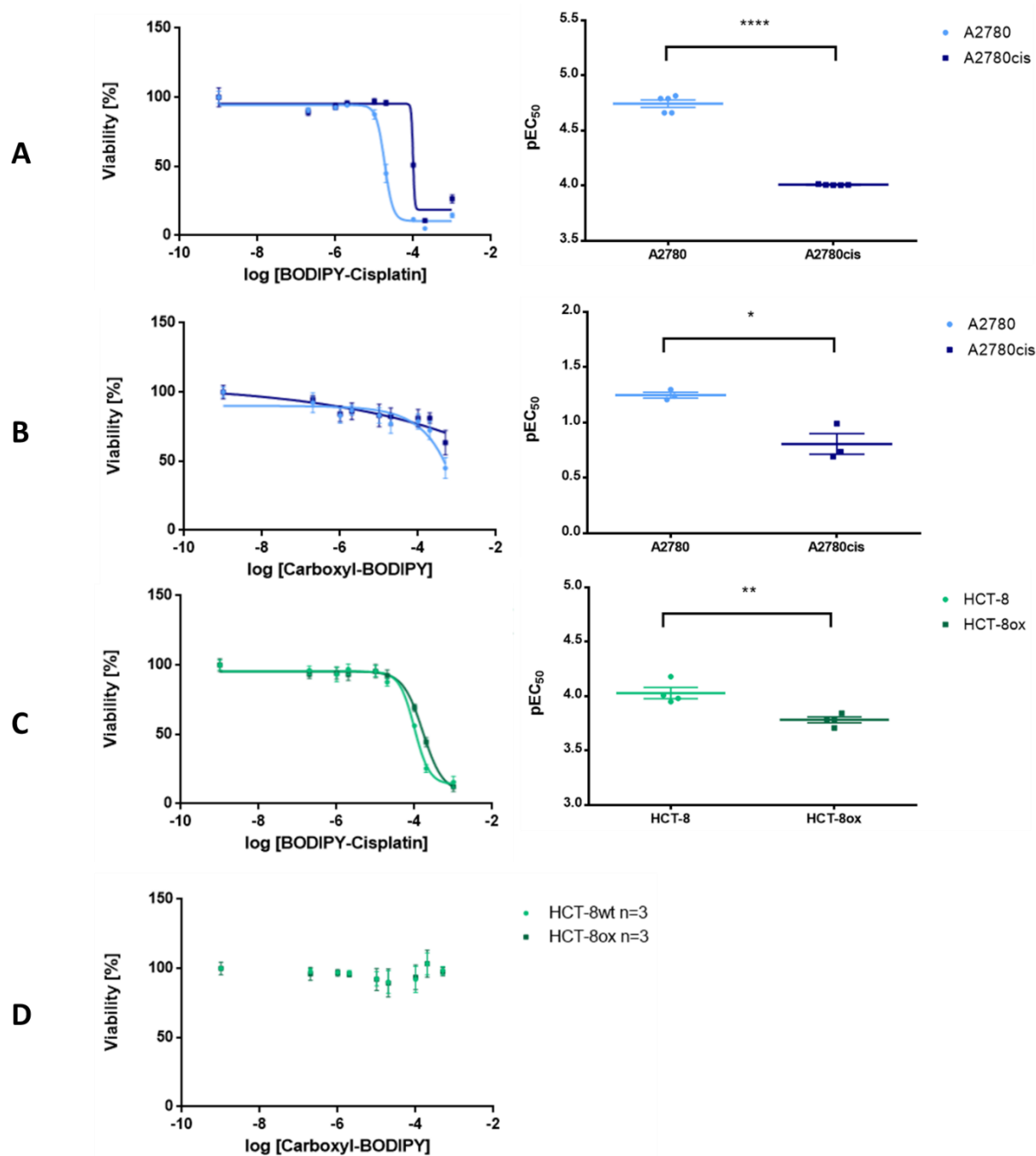
Figure 4.2 Cytotoxicity of BODIPY-cisplatin and carboxyl-BODIPY in A2780/A2780cis (A,B) and HCT-8/HCT-8ox (C,D) cells, respectively (mean ± SEM, n = 3-5). The left panel represents cell-viability data from all experiments, the right panel the respective pEC_{50} values. *, $p < 0.05$; **, $p < 0.01$; ****, $p < 0.0001$.

In addition to the performed MTT assays to evaluate the antitumor properties of the cisplatin analogs used prior to two-dimensional separation and immunoprecipitation in all employed cell lines (A2780/A2780cis and HCT-8/HCT-8ox) as shown in Figure 4.1 and Table 4.1, antitumor activity of all cisplatin analogs used during CuAAC was assessed. Cells were hereby treated with cisplatin-azide, cisplatin-alkyne, azide or alkyne tag in the concentration range 0.2-500 µM.

In both ovarian cancer cells used, cisplatin-azide exerted cytotoxicity very similar to its parent drug (EC_{50} was 4.72 µM/1.17 µM for A2780 cells and 20.47 µM/4.88 µM for A2780cis cells; Figure 4.3A, Table 4.2). Even though the cytotoxic effects were slightly less pronounced, the RF was approximately the same as that for cisplatin (RF was 4.3 vs. 4.2, respectively), proving that cisplatin-resistant A2780cis cells presented resistance to the azide-bearing analog akin to the parent compound. As far as treatment with cisplatin-alkyne is concerned, exhibited cytotoxicity in ovarian cancer cells was also satisfactory, although it was somewhat lower compared to both cisplatin as well as cisplatin-azide (EC_{50} was 8.41 µM and 52.50 µM for A2780 and A2780cis cells, respectively; Figure 4.3B, Table 4.2). Nevertheless, due to a more distinctive resistance of A2780cis cells towards cisplatin-alkyne than to cisplatin, the RF increased to 6.2.

As was the case with cisplatin, cisplatin-azide was less cytotoxic in HCT-8 cells than in A2780 cells (4 times less, Table 6.1), confirming intrinsic resistance of colorectal cancer cells. EC_{50} of cisplatin-azide was hereby quite similar in both HCT-8 and HCT-8ox cells (EC_{50} was 19.10 µM and 14.49 µM for HCT-8 and HCT-8ox cells, respectively; Figure 4.3C, Table 4.2). Again, cytotoxicity of cisplatin-alkyne was lower as compared to the azide analog and did not differ between HCT-8 and its oxaliplatin-resistant subline HCT-8ox (EC_{50} was 92.9 µM and 95.06 µM for HCT-8 and HCT-8ox cells, respectively, Figure 4.3D, Table 4.2).
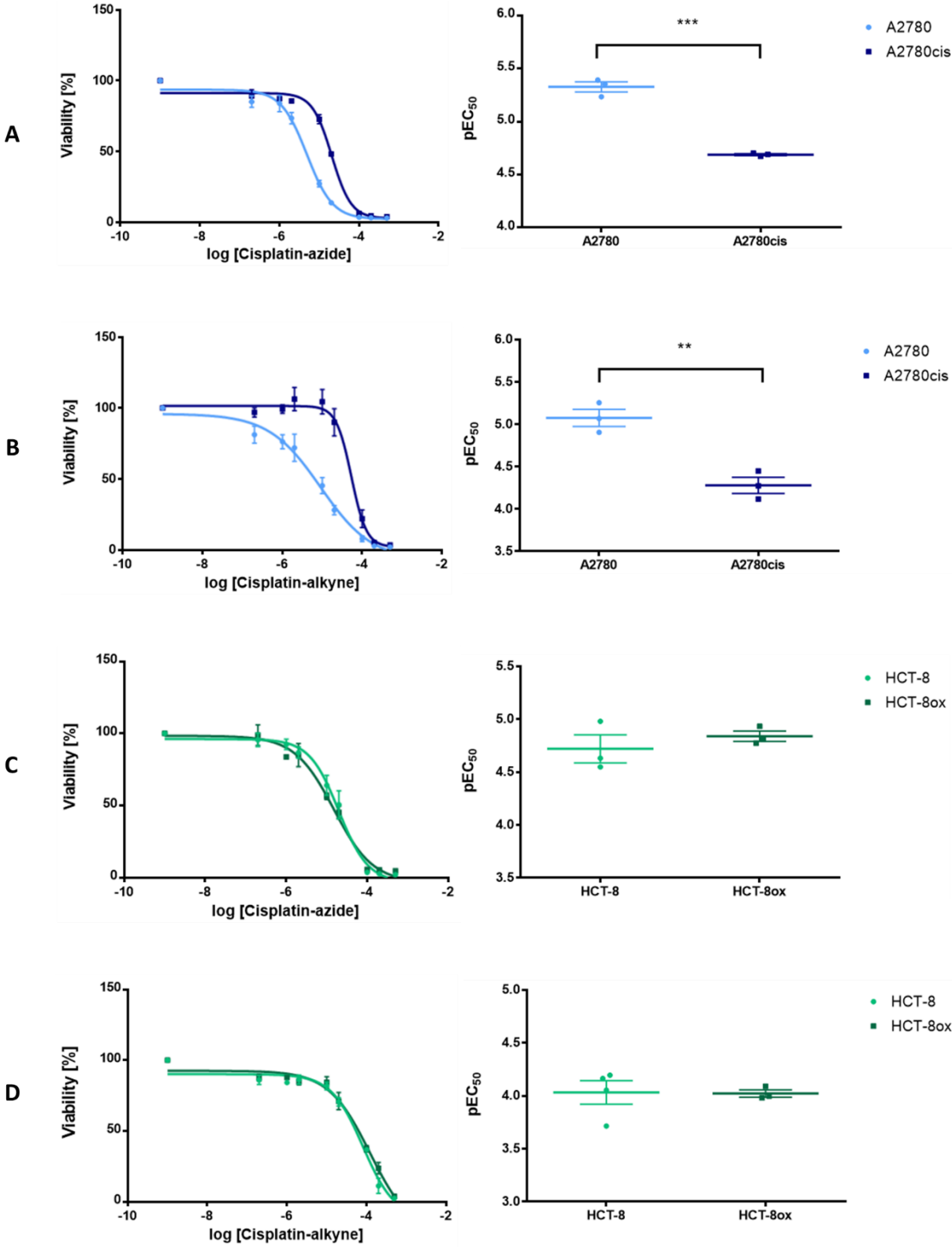
Figure 4.3 Cytotoxicity of cisplatin-azide and cisplatin-alkyne in A2780/A2780cis (A,B) and HCT-8/HCT-8ox (C,D) cells, respectively (mean ± SEM, n = 3-4). The left panel represents cell viability data from all experiments, the right panel the respective pEC_{50} values. **, $p < 0.01$; ***, $p < 0.001$.

Table 4.2 Cytotoxicity (pEC$_{50}$, mean ± SEM, n = 3-8) of cisplatin, oxaliplatin, cisplatin-azide and cisplatin-alkyne in A2780, A2780cis, HCT-8 and HCT-8ox cells (the respective EC$_{50}$ values are given in parentheses).

Compound	A2780	A2780cis	HCT-8	HCT-8ox
Cisplatin	5.932 ± 0.037 (1.17 µM)	5.312 ± 0.021 (4.88 µM)	5.259 ± 0.031 (5.51 µM)	5.037 ± 0.047 (9.18 µM)
Oxaliplatin	6.370 ± 0.093 (0.43 µM)	5.883 ± 0.085 (1.31 µM)	6.059 ± 0.027 (0.87 µM)	4.569 ± 0.060 (26.98 µM)
Cisplatin-azide	5.326 ± 0.048 (4.72 µM)	4.689 ± 0.009 (20.47 µM)	4.719 ± 0.132 (19.10 µM)	4.839 ± 0.048 (14.49 µM)
Cisplatin-alkyne	5.075 ± 0.101 (8.41 µM)	4.280 ± 0.095 (52.50 µM)	4.032 ± 0.110 (92.90 µM)	4.022 ± 0.034 (95.06 µM)
Azide	3.884 ± 0.164 (130.6 µM)	4.153 ± 0.119 (70.31 µM)	<3.3 (>500 µM)	<3.3 (>500 µM)
Alkyne	3.783 ± 0.089 (164.8 µM)	3.68 ± 0.234 (208.9 µM)	<3.3 (>500 µM)	<3.3 (>500 µM)

In order to make sure that cytotoxicity of the cisplatin analogs intended for CuAAC was not exerted mainly by their tags, viability of all cells employed was evaluated after treatment with the labels alone. Even though both the azide as well as the alkyne label showed cytotoxic effects in A2780/A2780cis cells, EC$_{50}$ values of 130.6/70.31 µM and 164.8/208.9 µM, respectively, were far from the concentrations applied to cells in all experiments (Figure 4.4A,B, Table 4.2), which is why they were considered non-toxic in the concentration ranges used in this project. In both colorectal cancer cell lines, no cytotoxicity of the azide and the alkyne tags alike was determined (EC$_{50}$ was >500 µM in both HCT-8 and HCT-8ox cells, Figure 4.4C,D, Table 4.2).
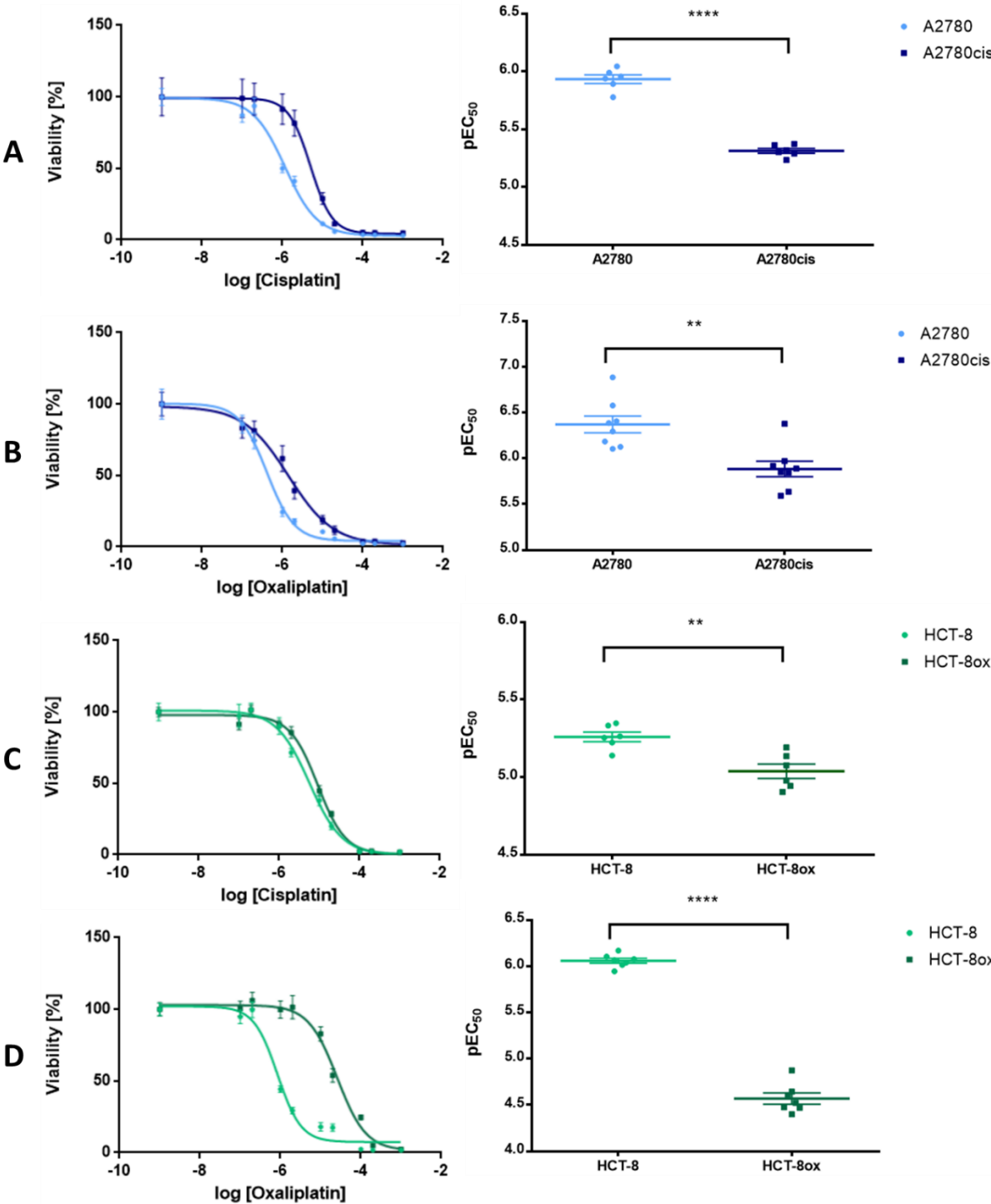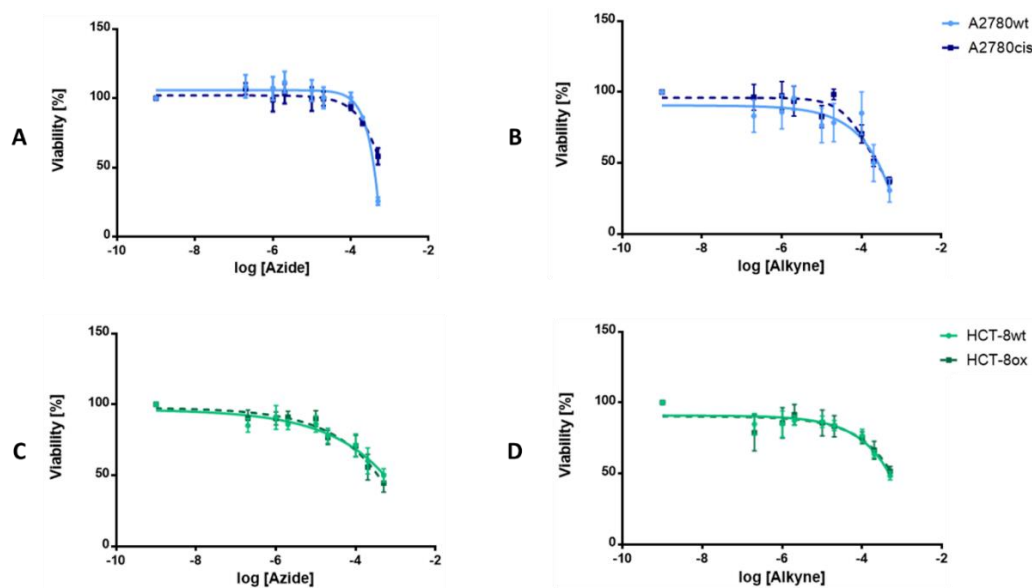
Figure 4.4 Cytotoxicity of platinum-free azide and alkyne in A2780/A2780cis (A,B) and HCT-8/HCT-8ox (C,D) cells, respectively (mean ± SEM, n = 3). Represented are cell viability data from all experiments.

4.1.2   Cellular Distribution of BODIPY-cisplatin

Additionally to cytotoxicity, BODIPY-cisplatin was also tested for cellular distribution patterns in A2780/A2780cis and HCT-8/HCT-8ox cells, which was possible due to its fluorescent properties. Cells were hereby treated with the same amount of drug and for the same period of time as intended for subsequent experiments to investigate protein binding partners. It could be clearly shown that BODIPY-cisplatin uptake was most prominent in A2780 cells, where fluorescence could also be detected in the cell nucleus (Figure 4.5A). In both A2780cis cells and either colorectal cancer cell line (HCT-8 and HCT-8ox) on the other hand, little compound could be observed and most fluorescence was seen in the cell membrane (Figure 4.5B-D), which is another indicator that BODIPY-cisplatin mimics its parent drug well.
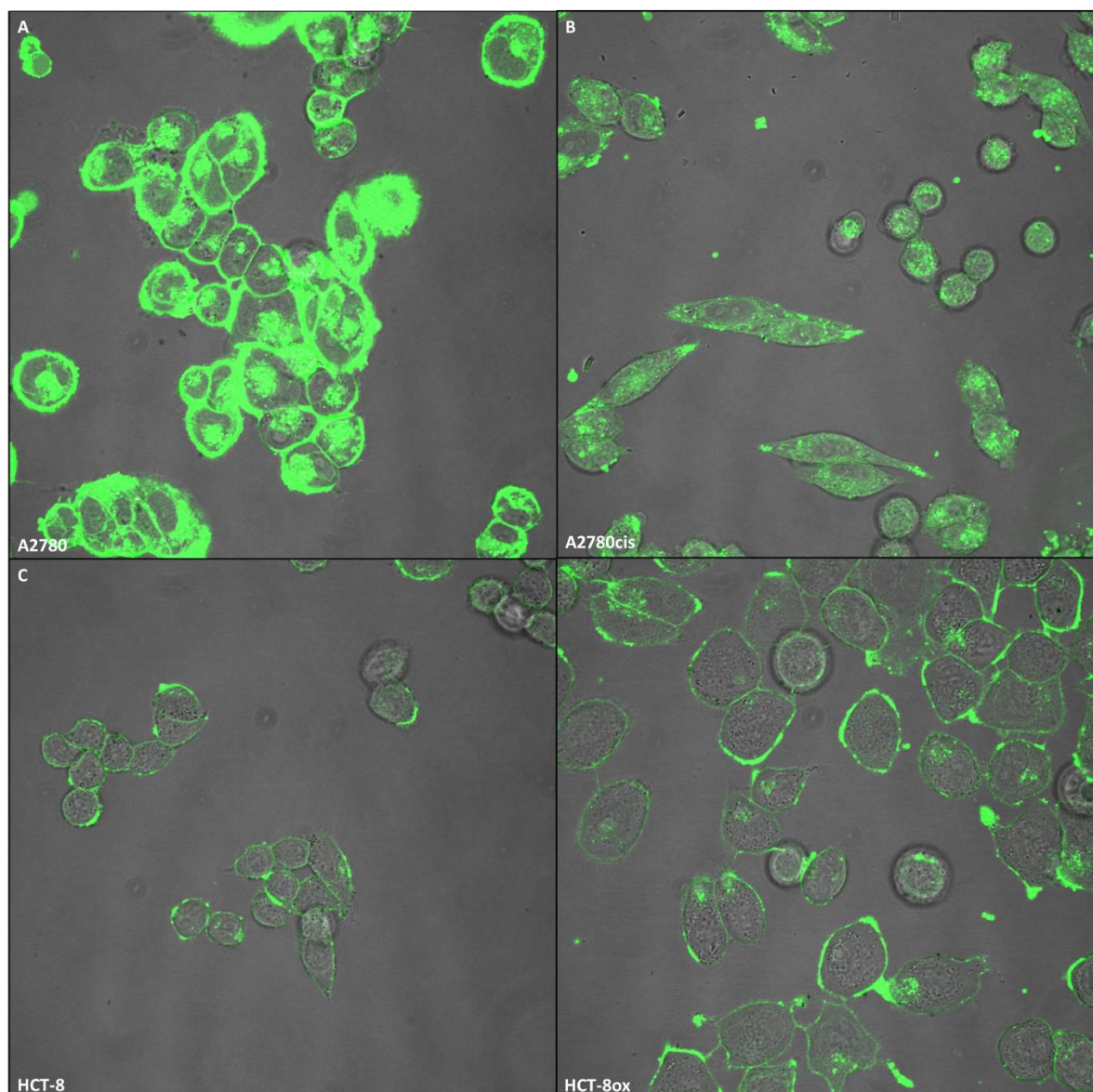
Figure 4.5 Cellular distribution of BODIPY-cisplatin in A2780 (A), A2780cis (B), HCT-8 (C) and HCT-8ox (D) cells. Images were kindly provided by Dr. Ganna Kalayda. Green indicates fluorescence of BODIPY-cisplatin (excited at 488 nm).

4.1.3   Specificity of BODIPY-cisplatin

One-dimensional gel electrophoretic runs of negative control lysates (of cells treated with either the fluorescent label BODIPY or the solvent DMF alone) were carried out to make sure that fluorescent signals detected after treatment were not caused by any kind of unspecific binding to cytoplasmic proteins. If such false positive signals were detected, all cisplatin-protein binding partners found later on could not have been accepted as valid. Yet, with both negative controls little to no fluorescence bands were detected as in comparison to treatment with BODIPY-cisplatin (Figure 4.6), while protein detection via Coomassie staining was even clearer in the negative controls, which both displays the specificity of the cisplatin analog with regard to protein binding.
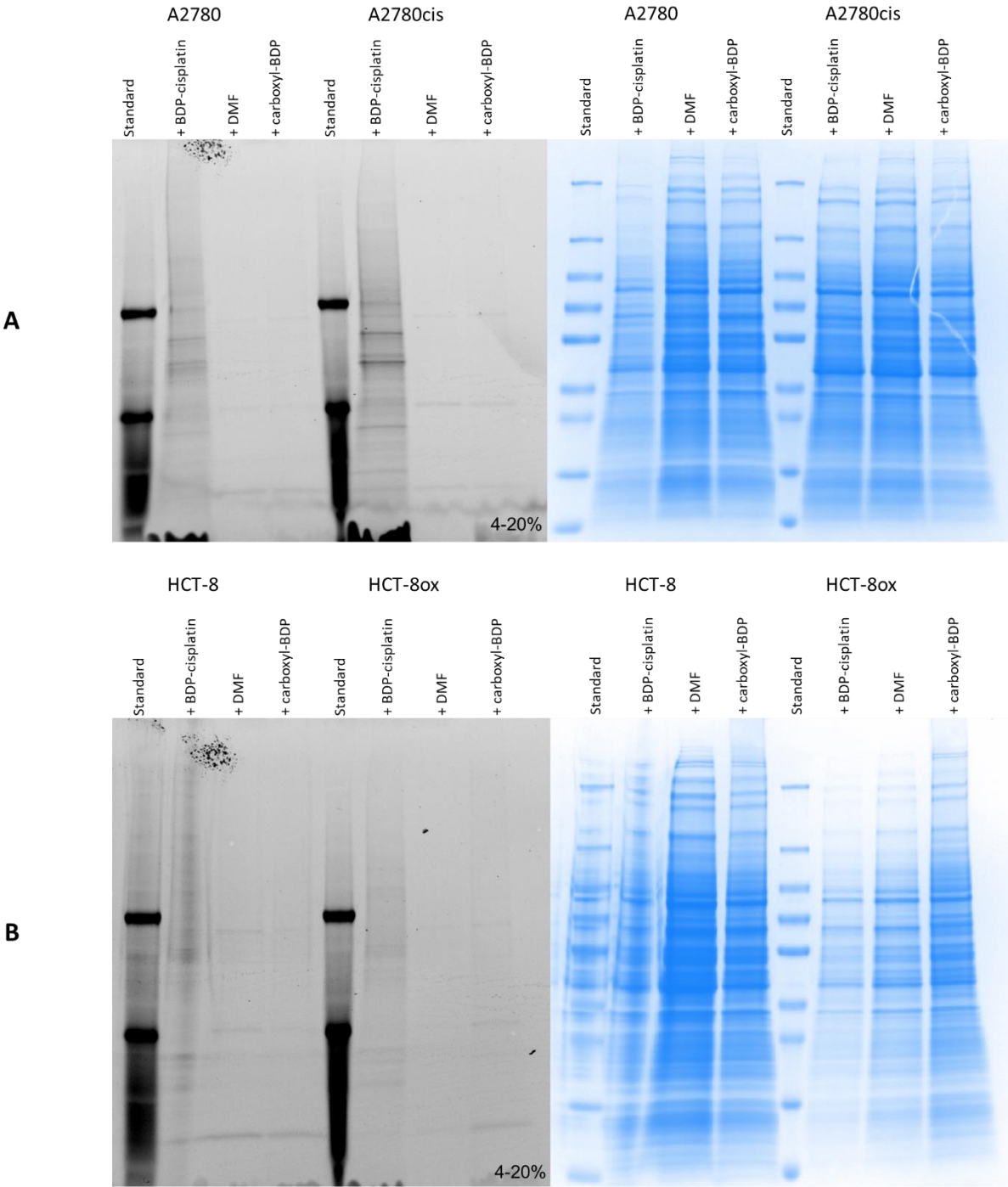
Figure 4.6 One-dimensional gel electrophoresis of the lysates of A2780/A2780cis (A) and HCT-8/HCT-8ox (B) cells treated with DMF, 25 µM carboxyl-BODIPY or 25 µM BODIPY-cisplatin for 2 h. Shown are fluorescence and Coomassie stained pictures (left and right panel, respectively).

4.1.4   Optimization of Cell Fractionation

Cell fractionation was performed in order to isolate the cytosolic fraction and therefore be able to identify cytosolic protein binding partners of cisplatin in a much less complex sample. To do so, firstly fractionation was done by means of the CLB IV protocol and the lysates were separated via one-dimensional gel electrophoresis. After the run, the gel was blotted on a membrane and proteins were subjected to primary antibodies against Lamin B1 and GAPDH to verify the efficiency of fractionation. As can be seen in Figure 4.7A, the protocol using cell lysis buffer IV achieved complete separation of cytosolic and nuclear fractions neither in A2780 cells (conducted by Dr. Maximilian Kullmann [153]) nor in HCT-8 cells, as Lamin B1 could be detected in cytosolic lysates. Thus, the *BioVision Nuclear/Cytosol Fractionation Kit* was evaluated as an alternative method. Here, a clear separation of cytosolic and nuclear fractions in both A2780 cells (conducted by Dr. Shahana Dilruba) and HCT-8 cells was accomplished (Figure 4.7B), and therefore this approach was chosen for all sample preparations for identification of cytosolic protein binding partner.
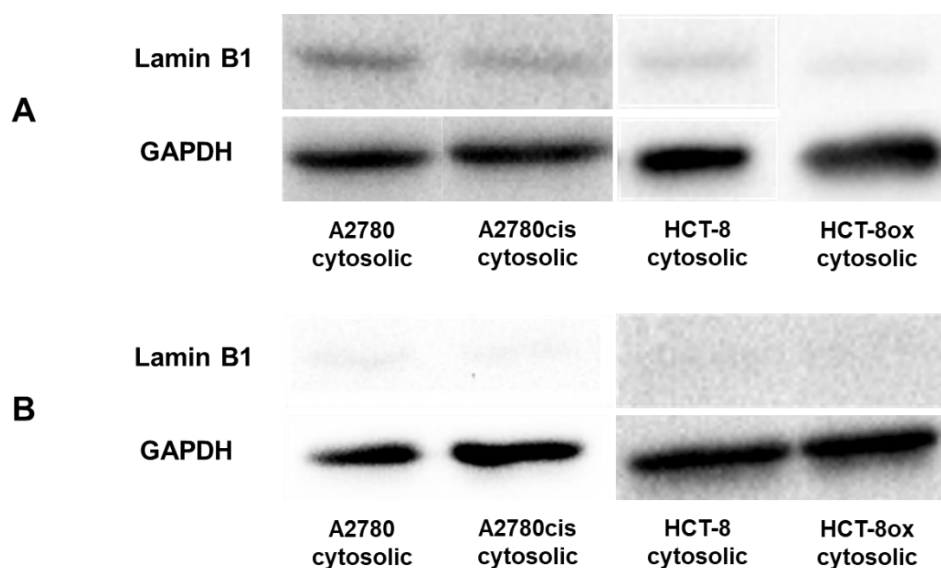
Figure 4.7 Representative Western Blots after fractionation of A2780, A2780cis, HCT-8 and HCT-8ox cells with CLB IV (A) and *BioVision Nuclear/Cytosol Fractionation Kit* (B). Nuclear marker protein Lamin B1 and cytosolic marker protein GAPDH were detected as markers for the respective fraction. Image A (left panel) was acquired by Dr. Maximilian Kullmann [153], image B (left panel) by Dr. Shahana Dilruba.

4.1.5   Protein Detection by Two-Dimensional Gel Electrophoresis

All experiments performed to identify protein binding partners via two-dimensional gel electrophoresis started by treatment of the cells with 25 µM of the fluorescent cisplatin analog tagged with boron-dipyrromethene (BODIPY-cisplatin, Figure 3.8) in serum-free medium for 2 hours. Control treatments with the solvent DMF or carboxyl-BODIPY (Figure 3.8) were carried out at the same time.

Since the protocol by Kotz et al. allowed the detection of protein binding partners of CFDA-cisplatin satisfactorily [113], an attempt was made to apply this protocol for BODIPY-cisplatin. Using 150 µg precipitated protein solubilized in 7 M urea, 2 M thiourea, 2% CHAPS, 65 mM DTT and 2% SERVALYT™ 4-7 for 1 hour, followed by in-gel rehydration of pH 4-7 IPG strips, IEF for approximately 14.4 kVh and separation on a 12% self-made separating gel in the second dimension, Kotz and colleagues achieved visualization of spots that were largely well-focused. However, following that protocol in detail did not give the same outcome. As only a total of about 8 kVh was achieved in each IEF run, resolution was poor in the first few runs. Additionally, either the transfer from the focused IPG strip into the separating gel did not work properly or the amount of protein applied was not suitable for the experiment, as only very little protein was detected via Coomassie staining of the 2D gel (Figure 4.8A).
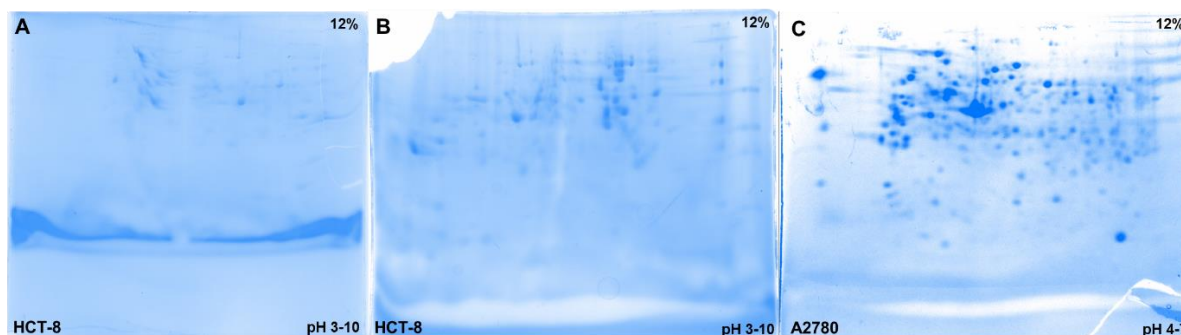
Figure 4.8 Representative Coomassie stained 2D gels after following protocol according to Kotz et al. (A) [113] and after reducing the amount of carrier ampholytes in the solubilization buffer in HCT-8 (B) and A2780 (C) cells.

To avoid uneven separation during IEF due to high ampholyte amounts, the concentration of SERVALYT™ was reduced from 2% to 0.5%, which resulted in a higher amount of volt hours of ca. 12 kVh and a better resolution of the sample (Figure 4.8B).

Still, especially in the lower molecular weight range, protein detection was insufficient. This was largely independent of the cell line and pH range employed, which was

intermittently switched from the initially pursued pH 3-10 nonlinear (NL) to pH 4-7 range established by Kotz et al. [113] in order to compare results more efficiently. Nonetheless, the results in A2780 cells were somewhat more satisfactory (Figure 4.8B vs. Figure 4.8C). Additionally, it could be clearly seen that A2780 cells feature a visibly higher protein diversity in comparison to HCT-8 cells (Figure 4.8C). The idea that the prior precipitation step led to the loss of smaller proteins was quickly ruled out, though, as in both precipitated and unprecipitated lysates similar band patterns could be detected after one-dimensional gel electrophoresis (Figure 4.9).
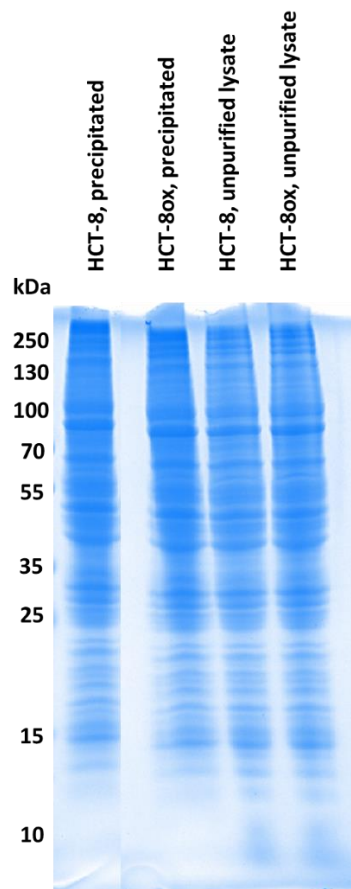
Figure 4.9 Representative Coomassie stained 1D gel of HCT-8 cancer cell lysates that were either precipitated before the run or not purified at all.

Even though ready-made *Quick Coomassie® Stain* has quite good sensitivity according to the manufacturer, the absence of the low protein band in the low molecular weight range, or rather the incapability of detecting these, was thought to be related to sensitivity of the stain. However, since Coomassie presented by far the easiest and cheapest staining method, which is also compatible with subsequent MS, a change of stain was considered the last resort. Therefore, it was tested whether a higher quantity of total protein (200 µg and 300 µg) applied to IPG strips could counteract a possible

loss during or faulty detection after the 2D run. Unfortunately, this approach was clearly disadvantageous as resolution and amount of detected protein were even lower than before (Figure 4.10), which is why all further experiments were conducted with 150 µg total protein.
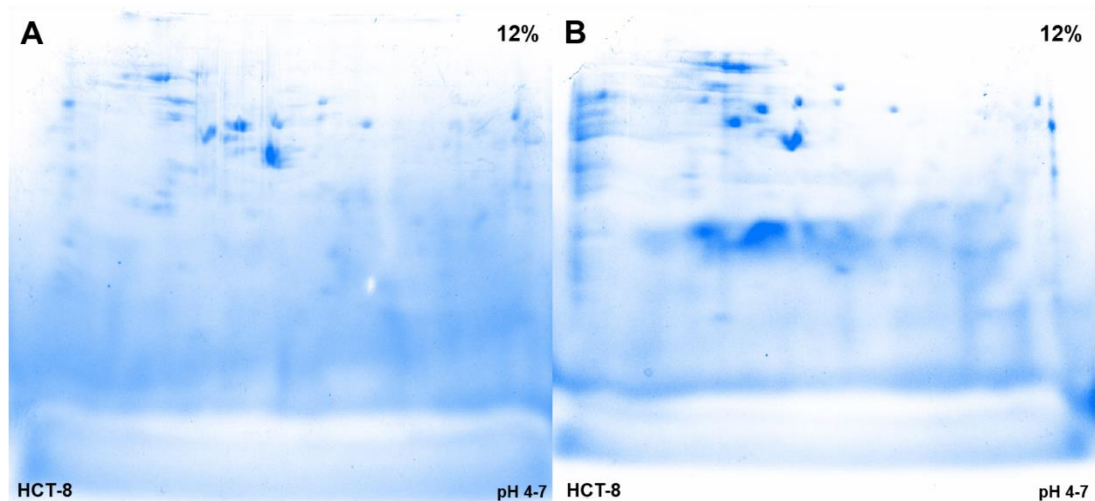
Figure 4.10 Representative Coomassie stained 2D gels of lysates of HCT-8 cells treated with 25 µM BODIPY-cisplatin for 2 h after increasing the quantity of total protein applied to the IPG strip to 200 µg (A) and 300 µg (B).

Another option to achieve better results in the low molecular weight range without the simultaneous loss of resolution in the high molecular weight ranges is the use of gradient separating gels. Due to gradient pore size reduction throughout the gel, the range of proteins with diverse molecular weights that can be separated in a single gel is increased. Moreover, proteins that are similar in molecular weight can be separated much better in a gradient gel and thus the visualization of proteins in a sample is visibly better. Accordingly, by using an 8-16% gel, separation of the cytosolic fraction could be achieved with much greater success (Figure 4.11).
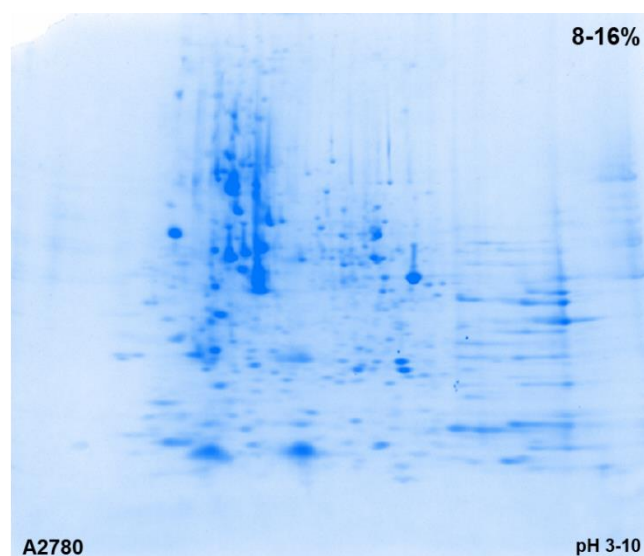
Figure 4.11 Representative Coomassie stained 2D gel of lysates of A2780 cells treated with 25 µM BODIPY-cisplatin for 2 hours after adjustment of gel polymerization from 12% to 8-16% in the second dimension.

While separation and resolution in the acidic and neutral pH ranges became satisfactory, the basic range was dominated by horizontal and vertical streaking. These problems are well known in two-dimensional gel electrophoresis, which is why several approaches to troubleshooting are available. Whereas vertical streaking is mostly associated with protein solubility problems, horizontal streaking is mainly linked to deprotonation of the reducing agent or the lack of complete focusing in the first dimension. In order to address the horizontal streaking problem, in a first attempt focusing was prolonged by an additional 12-hour-desalting step (at 300 V, 50 µA) at the beginning of the IEF to maximize the total volt hours and thereby to allow all proteins to be focused fully. Furthermore, the SDS concentration in the equilibration buffers was increased to 4% to prevent vertical streaking. These measures seemed to be at least partly successful as spots in the basic range were a little sharper and better separated (Figure 4.12A, right panel). Thus, the prolonged IEF and increased SDS concentration were implemented in the protocol henceforth. In contrast to the previous runs (where IPG strips were rehydrated by adding the sample resolved in solubilization buffer), it was also tested to what extent a differentiation of solubilization buffer for sample resolving and rehydration buffer for the dried IPG strip could be of advantage. Here, the precipitated sample was resolved in solubilization buffer featuring DTT, followed by exposure of the dried IPG strip to the solubilized sample at the anode and rehydration buffer containing *DeStreak™ Reagent* (≙ HED) over the remaining strip length. This way, the phenomenon of negatively charged DTT molecules wandering towards the anode away from the proteins, resulting in horizontal streaks caused by

reformation of disulfide bridges, should be diminished. All in all, this alternation led to a real improvement of resolution in comparison to DTT treatment alone (Figure 4.12B, right panel).

The overall aim was to detect both BODIPY-cisplatin fluorescence and total protein via Coomassie staining after 2D gel electrophoresis, then to superimpose these two images and thus draw conclusions about possible binding partners. So, from this point on, besides the Coomassie staining, the gels were also examined for their fluorescence patterns of BODIPY-cisplatin. What was most noticeable, is the seeming disappearance of fluorescence when applying DTT alone in the solubilization and/or rehydration buffers as compared to HED application (Figure 4.12, arrows).
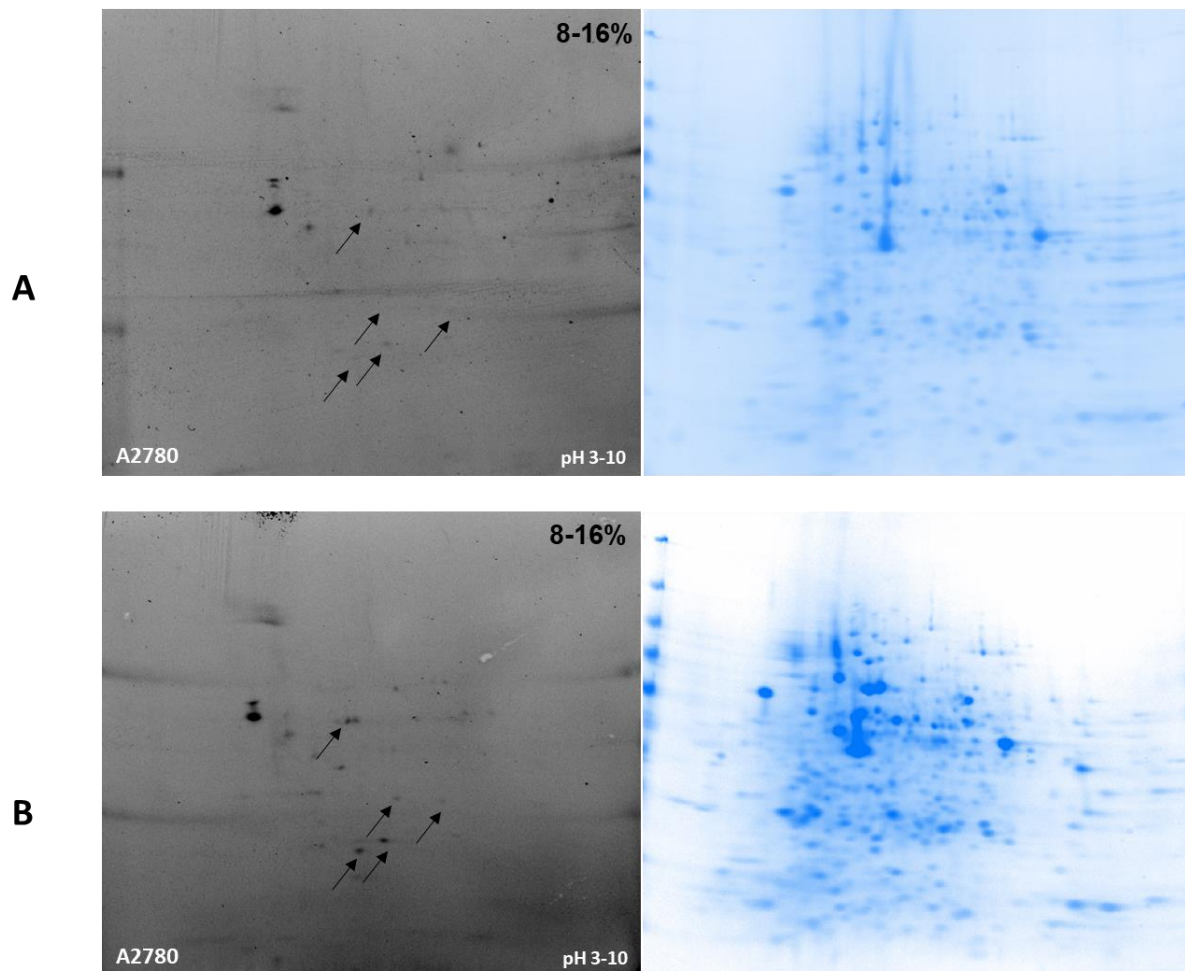
Figure 4.12 Representative fluorescence (left panel) and Coomassie stained (right panel) gel pictures after simple prolongation of focusing time in combination with 4% SDS in equilibration buffer (A) and prolongation of focusing time in combination with 4% SDS in equilibration buffer in addition to differentiation of solubilization and rehydration buffers (B). Arrows indicate fluorescent spots missing in (A) and present in (B).

As resolution with extended focusing time and the addition of HED was superior to the sole use of DTT, solubilization and rehydration with HED-containing solubilization buffer in addition to a paper wick soaked in DTT placed at the cathode was tested next. This was performed in comparison to DTT-containing solubilization buffer also with the DTT-soaked wick placed at the cathode. According to Dépagne et al. [154], the idea here was that the DTT in the wick should replenish the IPG strip with new DTT during IEF. This way the migration of deprotonated DTT should be inhibited, preventing horizontal streaks. Surprisingly, this time, the combination of HED in the buffer and DTT at the cathode did not result in a same degree of resolution as seen before (Figure 4.13, right panel) and a much better outcome considering the separation efficiency was achieved by the DTT buffer/DTT wick-combination (Figure 4.13B, right panel). The former could be explained by the possible reduction of HED to β-mercaptoethanol by the concurrently present DTT. β-mercaptoethanol has a high buffering capability at pH 8-9, which leads to horizontal streaks instead of spots in this pH range as Figure 4.13A (right panel) shows [125]. Apart from this, the loss of fluorescence with the use of DTT noticed with the last protocol was, again, evident.
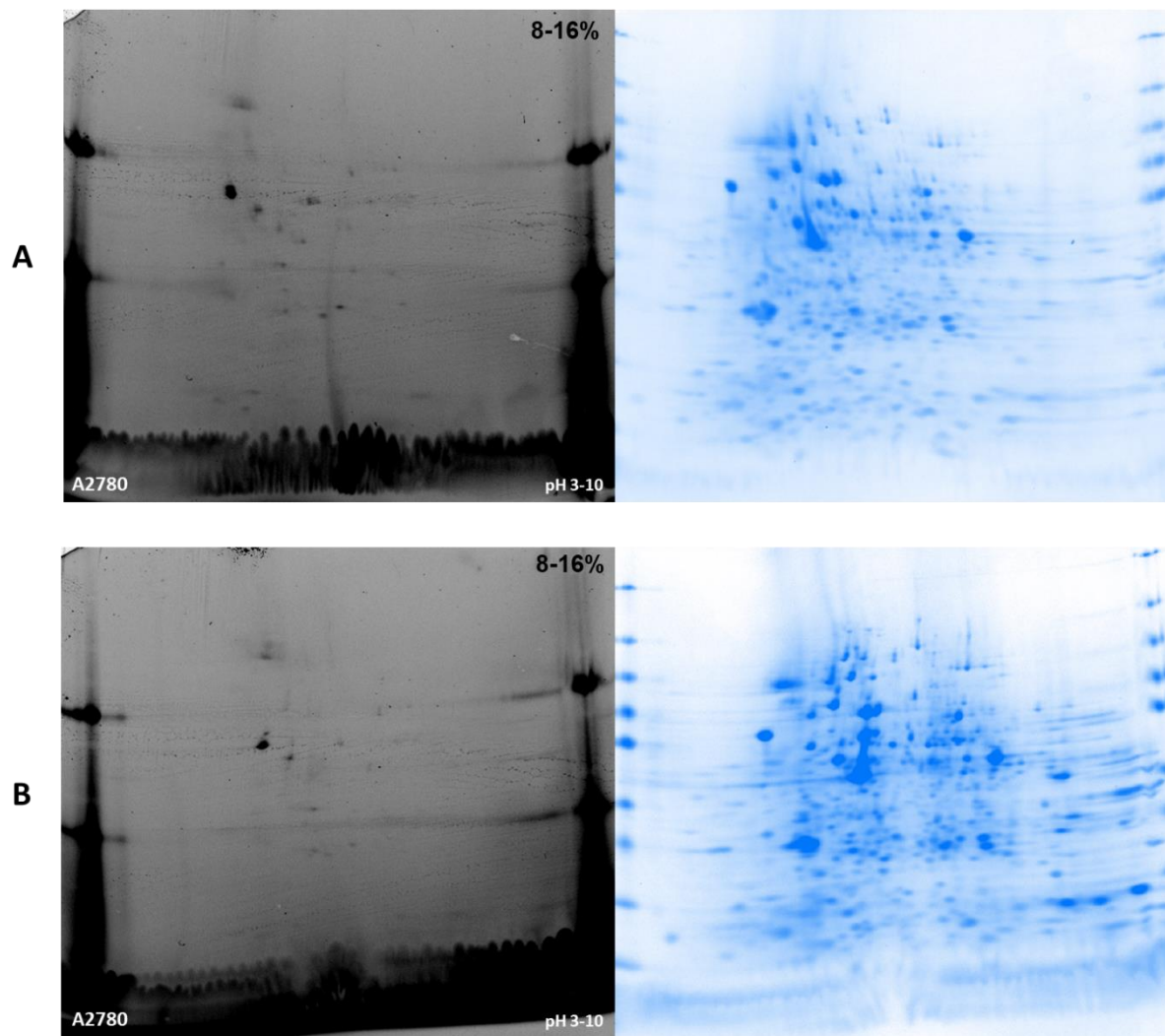
Figure 4.13 Representative fluorescence (left panel) and Coomassie stained (right panel) gel pictures after rehydration with HED and a supplementary DTT-soaked wick placed at the cathode (A) and rehydration with DTT and a supplementary DTT-soaked wick placed at the cathode (B).

All in all, seeing that HED in general provides good resolution in the basic pH range when not directly combined with DTT and the obviously better fluorescence imaging in comparison to the protocols where DTT is involved, led to an attempt to forego DTT completely and thereby to simplify the protocol in total. While forfeiting maximum separating efficiency as seen with the combination of DTT in the solubilization buffer and the DTT-soaked wick at the cathode (Figure 4.13B), the result obtained with that last change of protocol was considered the most expedient in all four cell lines (Figure 4.14).
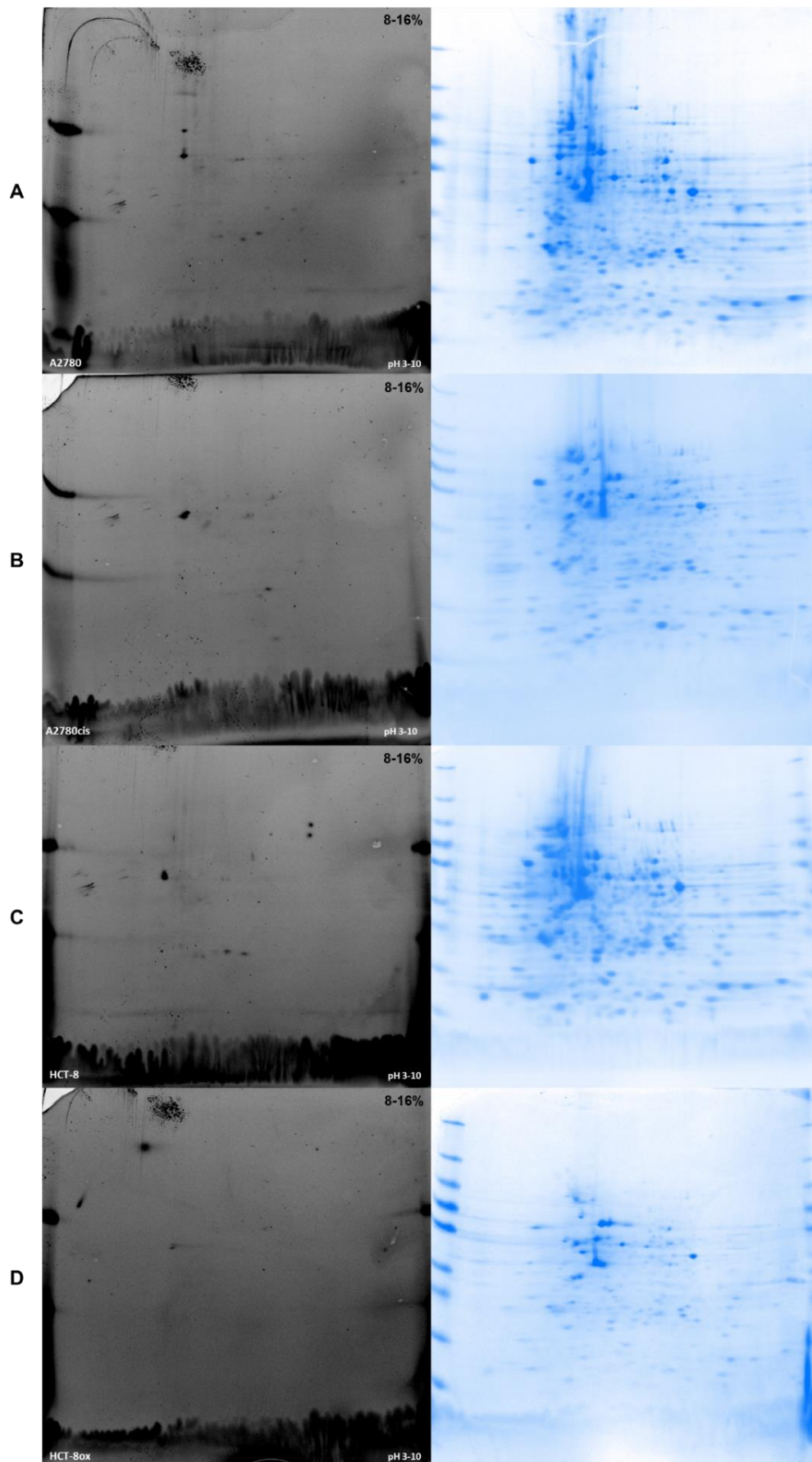
Figure 4.14 Representative fluorescence (left panel) and Coomassie stained (right panel) gel pictures after forfeiting DTT and switching to the use of HED in the rehydration buffer instead of DTT in A2780 (A), A2780cis (B), HCT-8 (C) and HCT-8ox (D) cells.

In summary, the final two-dimensional gel electrophoresis protocol was carried out as follows: After precipitating 150 µg of total protein, the pellet was solubilized in solubilization buffer (7 M urea, 2 M thiourea, 2% CHAPS, 0.5% SERVALYT™ 3-10 and 12 µL/mL buffer *DeStreak™ Reagent*) for 1 hour. Next, pH 3-10 NL IPG strips were subjected to the solution and in-gel rehydration was performed overnight. The IEF was extended by a 12-hour-desalting step, which resulted in a total of about 17-18 kVh. Equilibration buffers were modified only slightly by increasing the amount of SDS to 4%. In contrast to Kotz et al. [113], the second dimension was performed with an 8-16% ready-made separating gel and subsequent staining was done with the ready-made *Quick Coomassie® Stain* to avoid obtaining different results due to variability of materials and chemicals.

4.1.6   Protein Detection by Immunoprecipitation

In order to further reduce the complexity of the cancer cell lysates, the optimized two-dimensional gel electrophoresis was to be amended by an additional immunoprecipitation step. This would allow the detection of cisplatin-protein complexes with higher precision, rigorous work under light exclusion could be neglected and the subsequent time-consuming overlay of fluorescent and Coomassie-stained images could be eliminated.

Since immunoprecipitation was considered to be a simplifying extension of the protein binding partner identification approach via two-dimensional gel electrophoresis, treatment of the cancer cells employed was identical as described in Chapter 4.1.5.

4.1.6.1   Indirect Immunoprecipitation

Due to a presumably rather low antigen concentration in the sample and unknown binding strength of formed beads-antibody-antigen-protein complexes, the indirect immunoprecipitation appeared more promising and was conducted first. Using 50 µg of total protein, no difference between the eluates of the sample treated with BODIPY-cisplatin and the DMF treated control could be observed after incubation with the antibody for 0.5 hours followed by one-dimensional electrophoretic separation in combination with colloidal Coomassie staining afterwards (Figure 4.15). What can clearly be seen, though, is the interference of detection of potential proteins by antibody fragments at approximately 25 and 50 kDa (Figure 4.15, arrows).
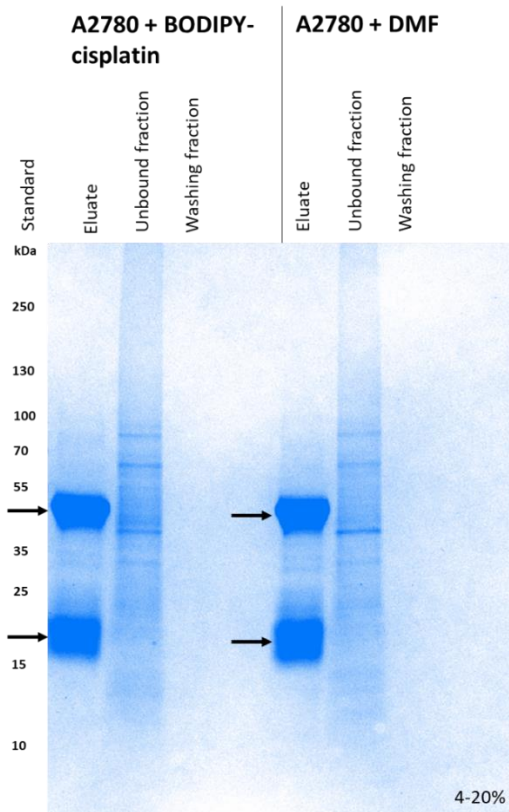
Figure 4.15 Representative Coomassie stained gel picture after indirect immunoprecipitation at RT of 50 µg of total protein of A2780 cells after 0.5 h incubation with the anti-BODIPY antibody. Arrows indicate possible antibody fragments.

Next, it was tested whether an increase of total protein to 100 µg could improve the detection of the antigen. Furthermore, a switch from *Quick Coomassie® Stain* to *SYPRO™ Ruby Protein Staining* for protein staining was thought to increase the protein detection limit (according to the manufacturers 5 ng vs. 0.25-1 ng, respectively). This time, additionally to the DMF control, BSA after treatment with both BODIPY-cisplatin or DMF served as a positive or negative control, respectively (10 µg each). The BSA controls were used to demonstrate the general potential of the immunoprecipitation approach before further optimization was considered.

As a proof-of-principle for this method, pull down of BODIPY-cisplatin-labeled BSA was detected, while no protein could be found in the DMF-treated BSA control (Figure 4.16A). Just as well, the increase of protein amount and the change of the staining method resulted in observation of minimally different protein binding patterns in cells treated with BODIPY-cisplatin and DMF (Figure 4.16B). Nevertheless, the detection of antibody fragments prevented optimal protein visualization, as any existing bands would be superimposed making detection in these molecular weight ranges almost impossible.
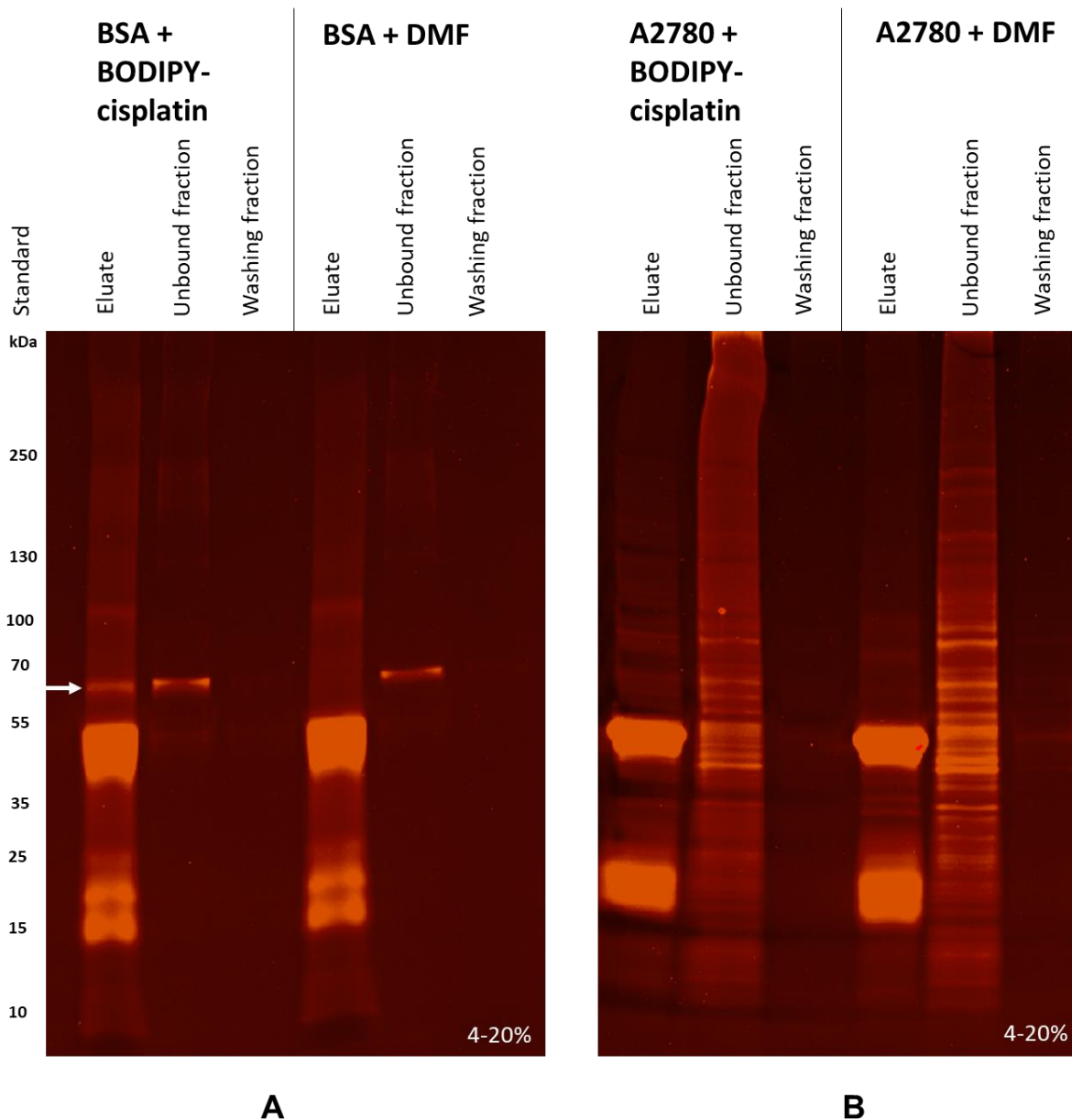
Figure 4.16 Representative SYPRO™ Ruby stained gel pictures after indirect immunoprecipitation at RT of 10 µg of BSA samples (A) and 100 µg of total protein of A2780 cancer cell samples (B) treated with 25 µM BODIPY-cisplatin for 2 hours after 0.5 h incubation with the anti-BODIPY antibody. The arrow indicates successful pull-down of BODIPY-cisplatin-labeled BSA.

4.1.6.2   Direct Immunoprecipitation

Since the simultaneous detection of antibody fragments posed a major problem, a switch from the indirect to the direct immunoprecipitation was considered. Here, the linkage of the magnetic beads with the anti-BODIPY antibody by cross-linking with BS[3] was possible and, thus, co-elution of antibody fragments later on could be prevented. In a first run, 100 µg total protein of both A2780 cancer cell samples treated either with BODIPY-cisplatin or DMF were compared. While no differences could be detected in the very poorly visible eluates of cellular lysates (Figure 4.17A), the simultaneously

performed run of BSA controls, again, showed that the method worked in principle. Whereas the BSA band of the positive control was much clearer after the indirect immunoprecipitation, at least a blurry BSA band could be seen at approximately 67 kDa in the BODIPY-cisplatin treated sample (Figure 4.17B, arrow). It is noticeable that much of the antigen has already been washed off of the beads before the deliberate elution of such (Figure 4.17B, washing fraction).
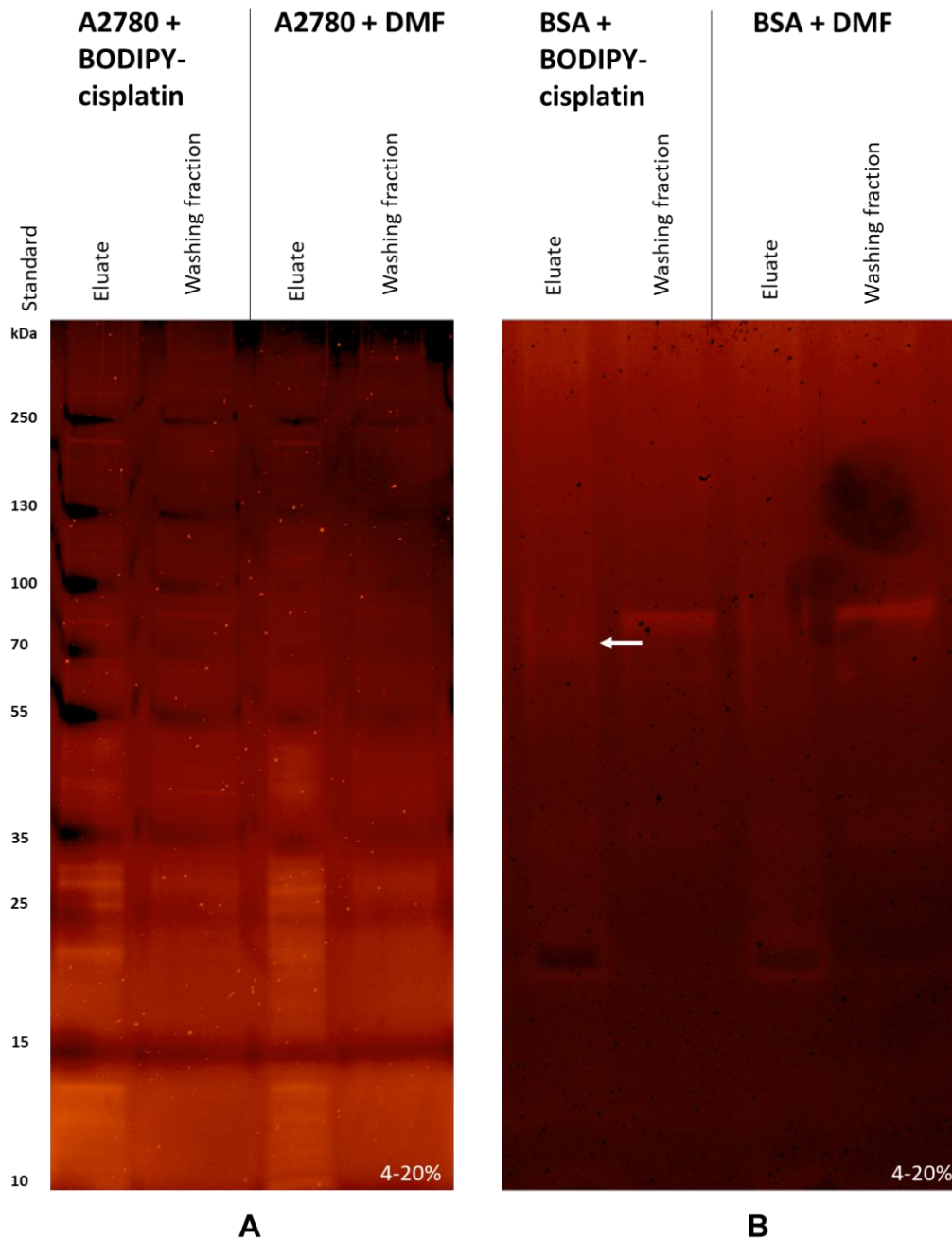
Figure 4.17 Representative SYPRO™ Ruby stained gel pictures after direct immunoprecipitation at RT of 100 µg of total protein of A2780 cancer cell samples (A) and 10 µg of BSA samples (B) treated with 25 µM BODIPY-cisplatin for 2 hours after 0.5 h incubation with the anti-BODIPY antibody. The arrow indicates successful pull-down of BODIPY-cisplatin-labeled BSA.

In order to improve the visibility of detected bands of eluted proteins, total protein was increased to 300 µg per sample. Furthermore, with the aim of improving yield, incubation time of beads-antibody complexes with the solution bearing the antigen was prolonged from 0.5 to 2 hours. Apart from this, the isolation protocol including elution was performed at 4 °C, which is supposed to be beneficial especially for sensitive proteins. After introducing all these changes to the protocol, obvious differences of BODIPY-cisplatin-treated samples to DMF-treated samples were noted. Even though the DMF eluate still exhibited a substantial overlap of bands, the eluate of the BODIPY-cisplatin-treated lysate showed many additional bands on top of probably unspecific binding (Figure 4.18A, arrows). Unfortunately, despite applying the exact same protocol to another set of samples, the results could not be reproduced and when taking a closer look, it even seems like the negative DMF control shows a higher number of eluted proteins in another run (Figure 4.18B, arrows).
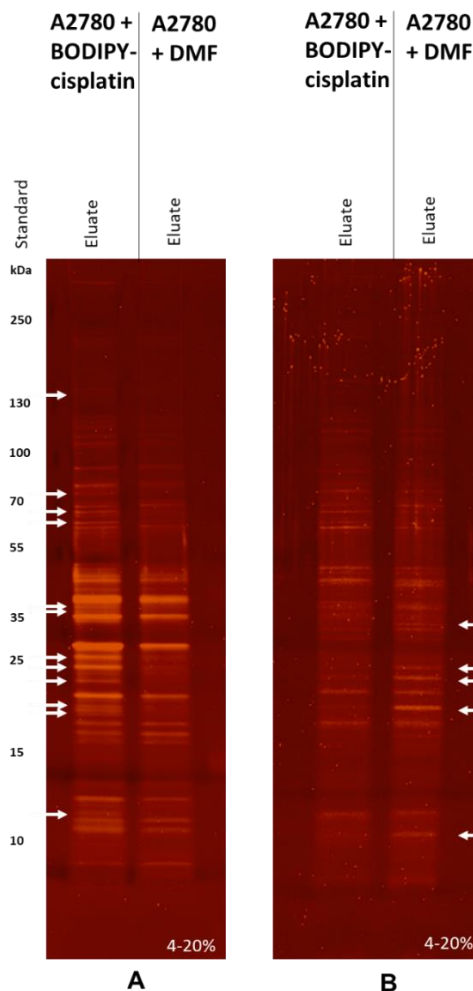
Figure 4.18 Representative SYPRO™ Ruby stained gel pictures from two independent experiments after direct immunoprecipitation at 4 °C of 300 µg of total protein of A2780 cancer cell samples after 2 h incubation with the anti-BODIPY antibody. Arrows indicate differences in eluted proteins of BODIPY-cisplatin- and DMF-treated samples.

In conclusion, it has to be recognized that even though the extension of the two-dimensional electrophoretic identification of cisplatin protein binding partners by a prior immunoprecipitation holds great potential, the method itself needs much optimization and extensive improvement before it can be applied routinely. This being said, even though an additional immunoprecipitation may be an elegant way to simplify the identification of protein binding partners via two-dimensional gel electrophoresis through omitting fluorescence detection of BODIPY-cisplatin and following overlay of diverse images, due to the above-mentioned benefit-effort ratio it was not further elaborated in this project.

4.1.7   Protein Detection by CuAAC

All experiments performed to identify protein binding partners via copper-catalyzed azide-alkyne cycloaddition were started off by treatment of the cells with 25 µM of either cisplatin-azide or cisplatin-alkyne (Figure 3.13) in serum-free medium for 2 hours, comparable to the procedure for protein identification by means of two-dimensional gel electrophoresis (Chapter 4.1.5). Control treatments without any additives, with the solvent DMF or unplatinated azide or alkyne (Figure 3.13) were carried out to detect unspecific reactions.

After binding of the platinum analog (cisplatin-azide or cisplatin-alkyne) to cytosolic proteins, fluorophore-tagged azides or alkynes, (BODIPY-azide or BODIPY-alkyne, respectively; Figure 3.13), were applied to enable identification of binding partners via CuAAC according to Figure 4.19.
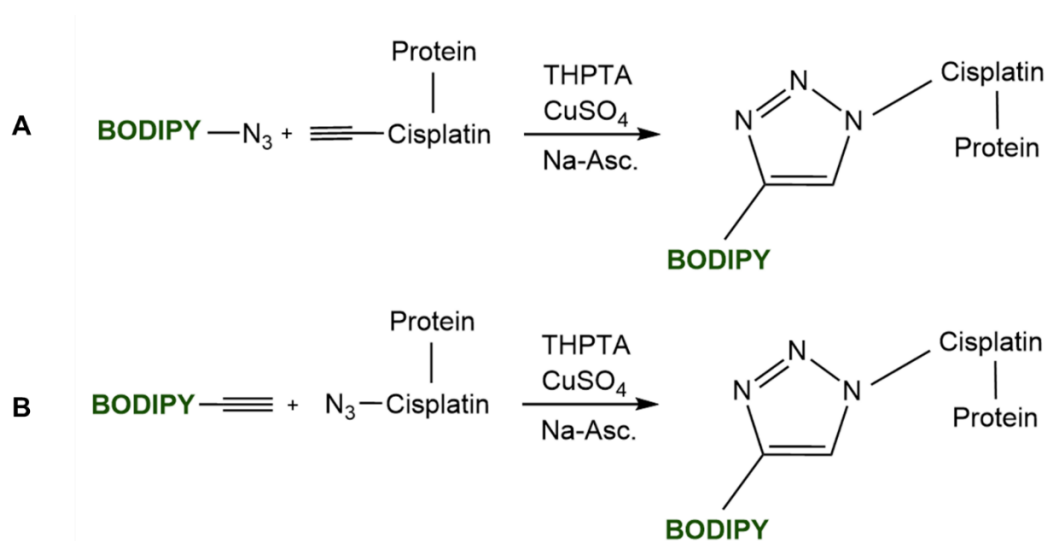
Figure 4.19 Copper-catalyzed click reaction of an alkyne and an azide to a triazole ring. On the basis of the reaction of BODIPY-azide with a protein-cisplatin-alkyne complex (A) or of BODIPY-alkyne with a protein-cisplatin-azide complex (B).

4.1.7.1 Cellular Treatment with Cisplatin-Azide

After treatment of A2780 cancer cells with cisplatin-azide and lysis by means of the *BioVision Nuclear/Cytosol Fractionation Kit,* 30 µg of total protein from cytosolic fraction diluted in PBS were subjected to CuAAC. Initially, 500 µM BODIPY-alkyne, 10 mM THPTA, 2 mM $CuSO_4$ and 30 mM sodium ascorbate were applied to the sample. Besides differently treated cancer cells, a positive control of BSA treated with 25 µM cisplatin-azide for 2 hours was prepared to check whether protein detection after click-chemistry between cisplatin-azide and BODIPY-alkyne was feasible. Immediately after separation via one-dimensional gel electrophoresis (12% separating gel), the fluorescence image was recorded. Unfortunately, in all lysates, either treated with cisplatin-azide or not, similar protein band patterns with almost identical intensities were detected (Figure 4.20A). Evaluation of the positive BSA control treated with the analog turned out to be quite difficult due to the very intense fluorescence signal (Figure 4.20B). Still, the most prominent band appeared at approximately 70 kDa, which is where BSA would be expected (67 kDa) and therefore indicated that click-chemistry worked.
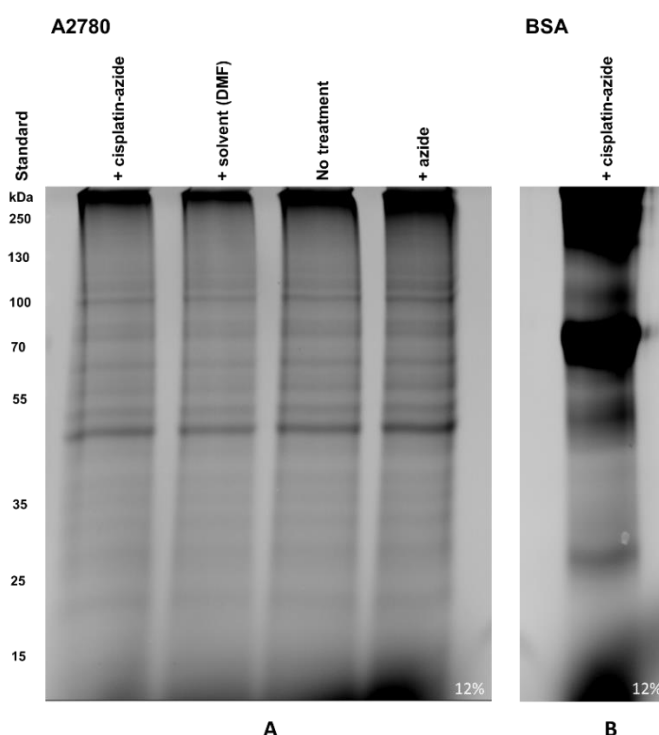
Figure 4.20 Representative fluorescence images after CuAAC with 500 µM BODIPY-alkyne, 10 mM THPTA, 2 mM $CuSO_4$ and 30 mM sodium ascorbate applied to 30 µg of total protein of A2780 cancer cell samples (A) and BSA sample (B) previously treated with 25 µM cisplatin-azide, solvent (DMF) or platinum-free azide for 2 hours or not treated at all.

Next, as was done in the establishment of the final 2D gel electrophoresis protocol, separation of lysates was adjusted and 4-20% ready-made gradient gels were used instead of 12% gels to ensure maximal separation efficiency in all molecular weight ranges. Since protein bands were rather weakly visible in the first run, total protein amount was increased to 100 µg per sample. Apart from this, samples were treated with various concentrations of BODIPY-alkyne (5-100 µM) based on the protocol of Yang et al. [155] to determine an optimal concentration ensuring clear visibility of protein bands with minimal unspecific background fluorescence. In accordance with the protocol deployed from Yang and colleagues, all other CuAAC components were also added in much lower concentrations: 2 mM THPTA, 1 mM $CuSO_4$ and 1 mM sodium ascorbate. Application of these changes produced the following results. First off, protein separation improved as expected and in all molecular weight ranges sharp protein bands could be detected (Figure 4.21). Furthermore, the decreased amounts of reactants did not seem to have influenced the CuAAC negatively as in both cell lysates as well as positive controls with BSA fluorescence bands could be observed (Figure 4.21A,B). Also, the reduction of BODIPY-alkyne concentration to 5 µM was chosen for further modifications to the protocol, because it obviously entailed the lowest background fluorescence in the positive control (Figure 4.21A), while still enabling sufficient fluorescence detection in the sample (Figure 4.21B). However, despite the small progress made, protein band patterns of cisplatin-azide treated A2780 cancer cell samples and negative controls with DMF did not differ. In order to prove that concentration-dependent decrease in fluorescence intensities was not due to varying protein amounts, all gels were additionally stained with Coomassie (Figure 4.21, lower panel).
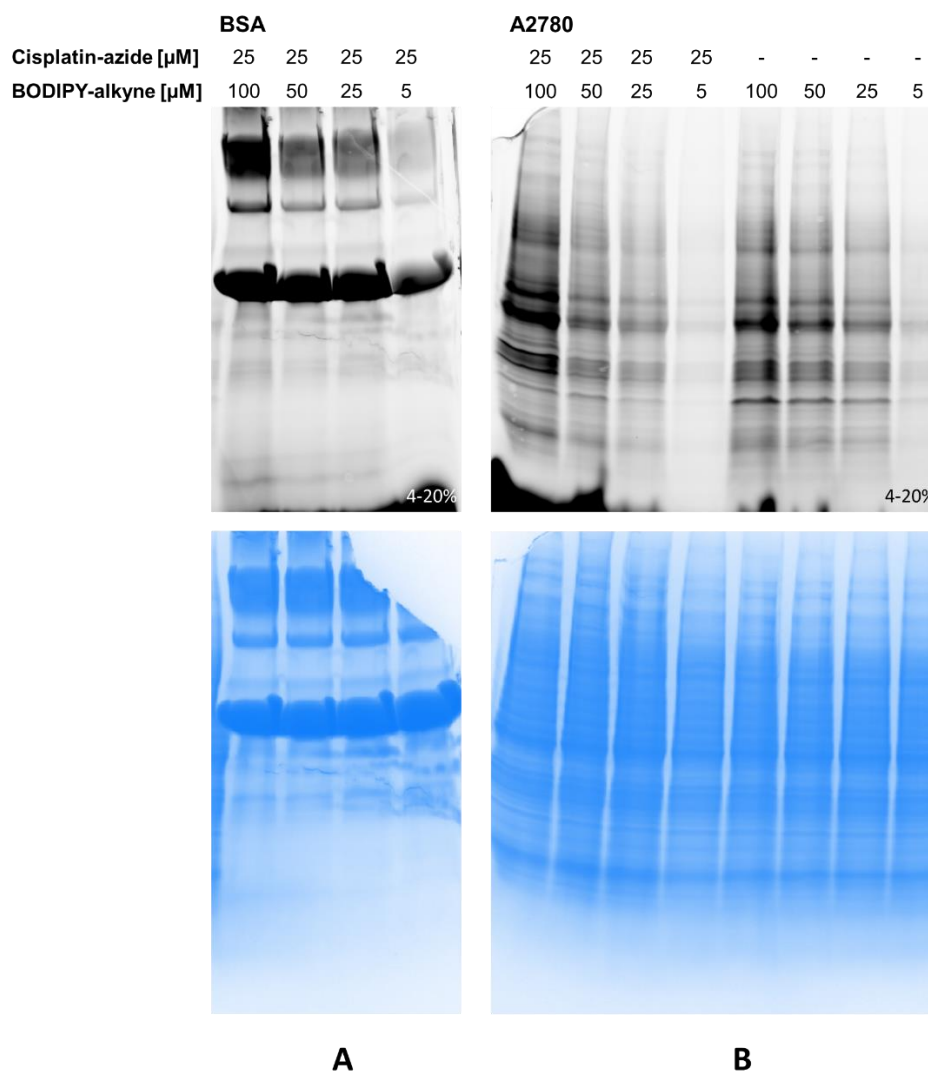
Figure 4.21 Representative fluorescence (upper panel) and Coomassie stained (lower panel) images after CuAAC with 5-100 µM BODIPY-alkyne, 2 mM THPTA, 1 mM CuSO$_4$ and 1 mM sodium ascorbate to 100 µg of total protein of BSA samples (A) and A2780 cancer cell samples (B) previously treated with 25 µM cisplatin-azide for 2 hours.

Subsequently, in order to address the lack of specific bands, probably due to high unspecific background binding, BSA positive controls were pre-treated with differing amounts of IAA which was supposed to alkylate free thiols [156] and, thus, prevent binding of BODIPY-alkyne to anything other than the cisplatin analog. Indeed, when pre-treated with 50 mM IAA for 0.5 hours, a slight decrease of background fluorescence can be noted in comparison to pre-treatment without or with 5 mM IAA (Figure 4.22).

Figure 4.22 Representative fluorescence (upper panel) and Coomassie stained (lower panel) pictures after CuAAC whereby applying 5-50 mM IAA prior to treatment with 5 μM BODIPY-alkyne, 2 mM THPTA, 1 mM CuSO₄ and 1 mM sodium ascorbate to 100 μg of total protein of BSA samples previously treated with 25 μM cisplatin-azide for 2 hours.

Thereafter, in addition to standardizing pre-treatment with IAA, proteins in all samples and controls were precipitated twice to purify the sample as much as possible and, thus, make binding more specific. The first precipitation step was performed right before treatment with 50 mM IAA to get rid of excessive cisplatin-azide and the second following CuAAC, but before electrophoresis, to remove unbound BODIPY-alkyne. Unexpectedly, reduction of background binding as seen in positive BSA controls (Figure 4.23A) could not be reproduced in cancer cell samples. Here, pre-treatment with 50 mM IAA even led to an increase of fluorescence intensity (Figure 4.23B). Interestingly, in A2780 cancer cell lysates pre-treated with IAA several bands could be detected that were not visible in the pre-treated negative control. However, due to an inordinate overlap of proteins, the identification of cisplatin binding partners cannot be guaranteed and a more specific detection method must be pursued.

Figure 4.23 Representative fluorescence (upper panel) and Coomassie stained (lower panel) pictures after CuAAC whereby applying no or 50 mM IAA prior to treatment with 5 µM BODIPY-alkyne, 2 mM THPTA, 1 mM CuSO$_4$ and 1 mM sodium ascorbate to 100 µg of total protein of BSA samples (A) and A2780 cancer cell samples (B) previously treated with 25 µM cisplatin-azide for 2 hours.

4.1.7.2   Cellular Treatment with Cisplatin-Alkyne

As the aim was to evaluate whether the detection of cisplatin-alkyne with a fluorescent azide is more specific, cancer cells were treated alternatively with a cisplatin-alkyne and detection was performed with a BODIPY-azide. Literature evidence suggested that bioconjugation with a fluorophore-tagged azide results in lower background fluorescence than the one with a fluorophore-labeled alkyne [157]. First off, different BODIPY-azide concentrations (5-100 µM) were applied to determine the optimal conditions. Just as established before, proteins in samples were always precipitated twice: before pre-treatment with IAA and post CuAAC. What could be learned from the experiment was that treatment with 50 µM BODIPY-azide offered the best results in positive controls (Figure 4.24A) as well as A2780 cancer cell samples (Figure 4.24B).

Increasing the concentration to 100 µM BODIPY-azide did not lead to better results on the one hand, while reduction to 5 µM made fluorescence detection practically impossible. Unfortunately, again no difference of binding patterns was found between treated samples and negative controls.
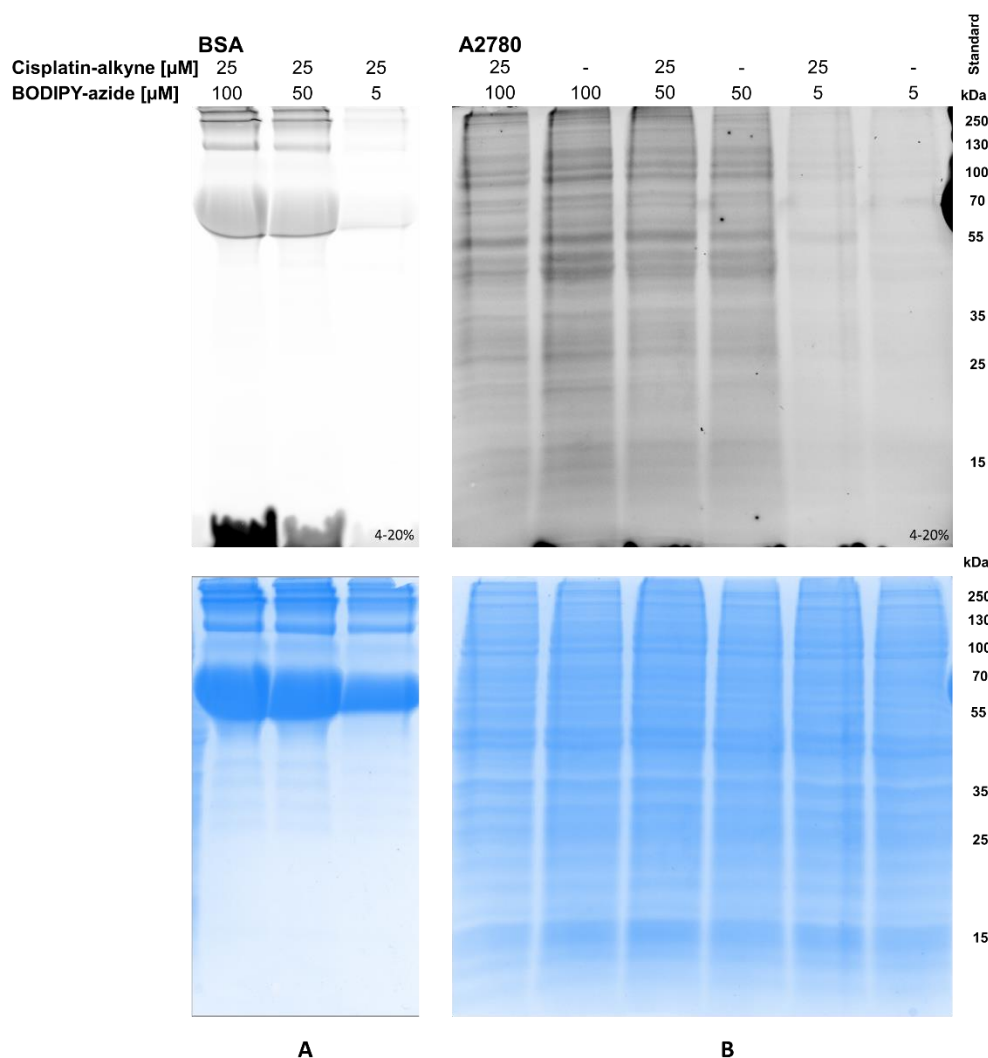
Figure 4.24 Representative fluorescence (upper panel) and Coomassie stained (lower panel) pictures after CuAAC whereby applying no or 50 mM IAA prior to treatment with 5-100 µM BODIPY-azide, 2 mM THPTA, 1 mM CuSO$_4$ and 1 mM sodium ascorbate to 100 µg of total protein of BSA samples (A) and A2780 cancer cell samples (B) previously treated with 25 µM cisplatin-alkyne for 2 hours.

Just like alkynes, azides are also capable of binding to residual thiols [158], which is why pre-treatment with IAA was performed as well and results of exposure to different IAA concentrations (0-50 mM) were compared. In the case of the DMF-treated, negative BSA controls, fluorescence intensity of BSA detection at approximately 76 kDa clearly decreased with increasing amounts of IAA (Figure 4.25A). The fact that BSA can be detected in the DMF controls in the first place is an explicit example of

unspecific binding of BODIPY-azide, which can fortunately be reduced during pre-treatment with 50 mM IAA (Figure 4.25A).

Consequently, from now on all lysates were pre-treated with 50 mM IAA to keep background fluorescence to a minimum. The effect of this measure could luckily be transferred to A2780 cells. Whereas A2780 cancer cell samples without pre-treatment transmitted much fluorescence and showed no difference of binding patterns, cisplatin-alkyne-treated cells that were additionally pre-treated with IAA demonstrated not only less background fluorescence but also distinct fluorescence bands that were non-existent in DMF controls (Figure 4.25B, arrows). Here, bands at approximately 20 kDa and 50 kDa were the most pronounced, which was comparable to results obtained after treatment with cisplatin-azide (Figure 4.23).
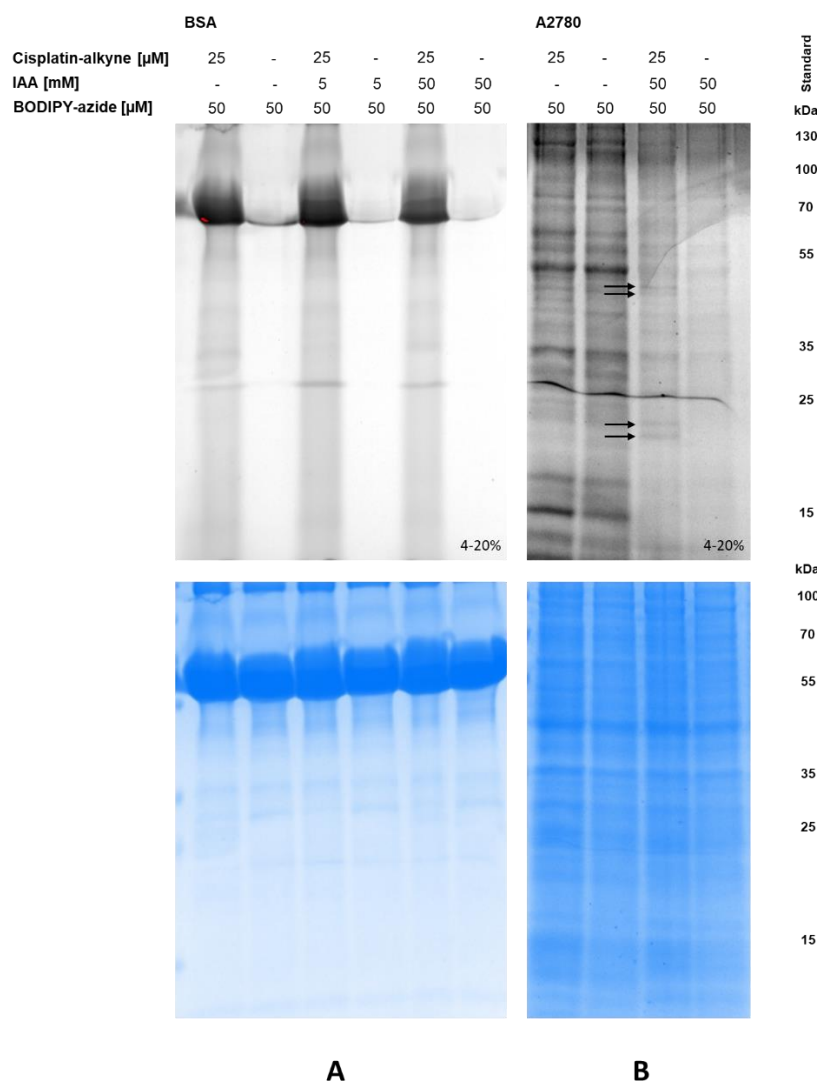
Figure 4.25 Representative fluorescence (upper panel) and Coomassie stained (lower panel) pictures after CuAAC whereby applying 5-50 mM IAA prior to treatment with 50 µM BODIPY-azide, 2 mM THPTA, 1 mM CuSO₄ and 1 mM sodium ascorbate to 100 µg of total protein of BSA samples (A) and A2780 cancer cell samples (B).

Based on these results, fluorescence patterns of cisplatin-alkyne-treated cells were then compared to controls treated either with DMF, with the alkyne-tag or treated with pure medium. This way it should be reliably ruled out that the different binding profiles were caused by the alkyne tag or the solvent and not by the cisplatin analog. As established before, the addition of 50 mM IAA before CuAAC resulted in reproducible reduction in background binding in all samples (Figure 4.26). Additionally, while there was a high number of fluorescence bands in IAA-free samples, IAA-treated negative controls were practically free of unspecific binding. Thus, the detection of specific bands in A2780 cancer cell lysates at circa 20 kDa and 50 kDa was much more definite in IAA-treated samples than it was in IAA-free samples.

A2780

Cisplatin-alkyne [µM]	25	-	-	-	25	-	-	-
Solvent (DMF)	-	+	-	-	-	+	-	-
Alkyne [µM]	-	-	-	25	-	-	-	25
IAA [mM]	-	-	-	-	50	50	50	50
BODIPY-azide [µM]	50	50	50	50	50	50	50	50
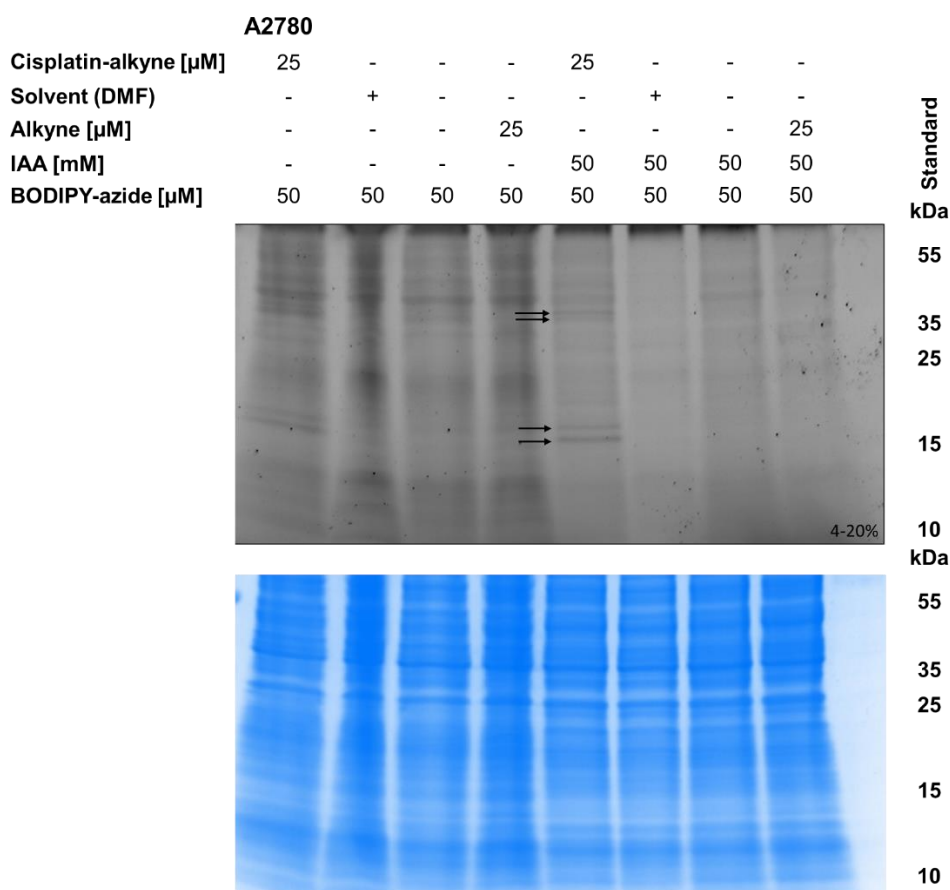
Figure 4.26 Representative fluorescence (upper panel) and Coomassie stained (lower panel) pictures after CuAAC whereby applying no or 50 mM IAA prior to treatment with either cisplatin-alkyne, DMF, alkyne tag or no treatment at all and 50 µM BODIPY-azide, 2 mM THPTA, 1 mM CuSO$_4$ and 1 mM sodium ascorbate to 100 µg of total protein of A2780 cancer cell samples.

Finally, the optimized protocol was applied to all cell lines employed in this study, each time in comparison to negative controls (solvent, no treatment, platinum-free alkyne). The fluorescence pattern of the cisplatin-alkyne-treated A2780cis cancer cell lysate thereby resembled the A2780 cancer cell lysate a lot. In both cisplatin-sensitive as well as cisplatin-resistant cells specific protein bands could be detected in the molecular

weight range around 20 kDa and around 50 kDa, Figure 4.27). Still, differences albeit very few, could be spotted. In general, fluorescence intensity seemed to be lower in A2780cis cancer cell samples than in its parent cell line. Additionally, A2780 cancer cell samples showed blurred bands at approximately 100 kDa as well as a second band at ca. 20 kDa that were not visible in the resistant subline.
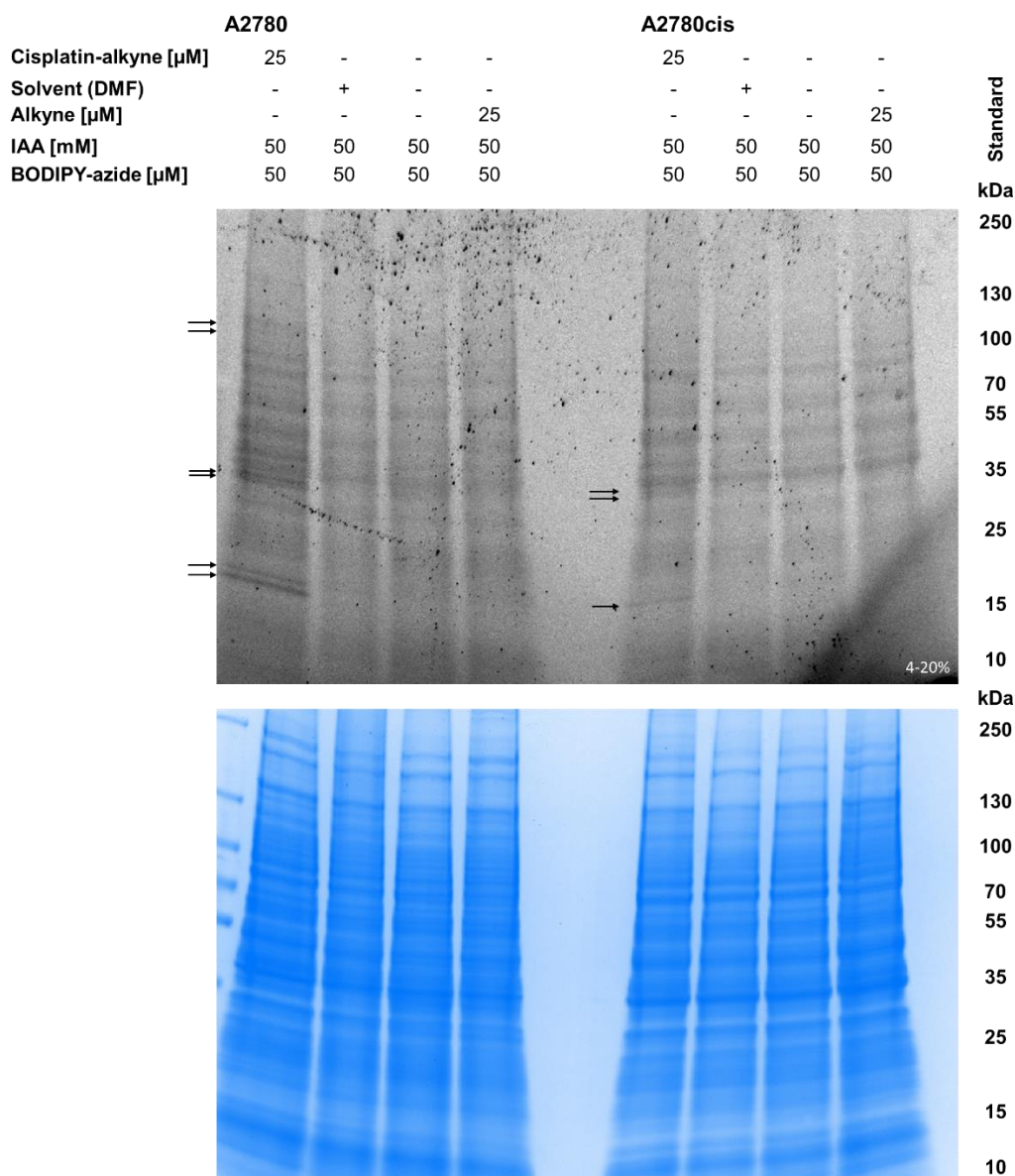
Figure 4.27 Representative fluorescence (upper panel) and Coomassie stained (lower panel) pictures after CuAAC whereby applying 50 mM IAA prior to treatment with either cisplatin-alkyne, DMF, alkyne tag or no treatment at all and 50 µM BODIPY-azide, 2 mM THPTA, 1 mM CuSO₄ and 1 mM sodium ascorbate to 100 µg of total protein of A2780 and A2780cis cancer cell samples.

However, in HCT-8 and HCT-8ox cancer cell samples no differences in binding patterns could be detected in samples that were handled according to the same

protocol (Figure 4.28). In comparison to samples of ovarian cancer cells, though, it can be stated that fluorescence intensity was even lower than recorded in A2780cis cancer cell samples.

	HCT-8				HCT-8ox				Standard
Cisplatin-alkyne [µM]	25	-	-	-	25	-	-	-	
Solvent (DMF)	-	+	-	-	-	+	-	-	
Alkyne [µM]	-	-	-	25	-	-	-	25	
IAA [mM]	50	50	50	50	50	50	50	50	
BODIPY-azide [µM]	50	50	50	50	50	50	50	50	

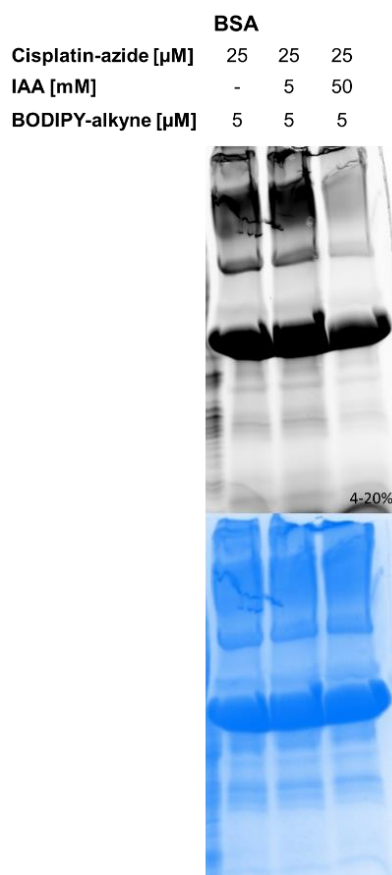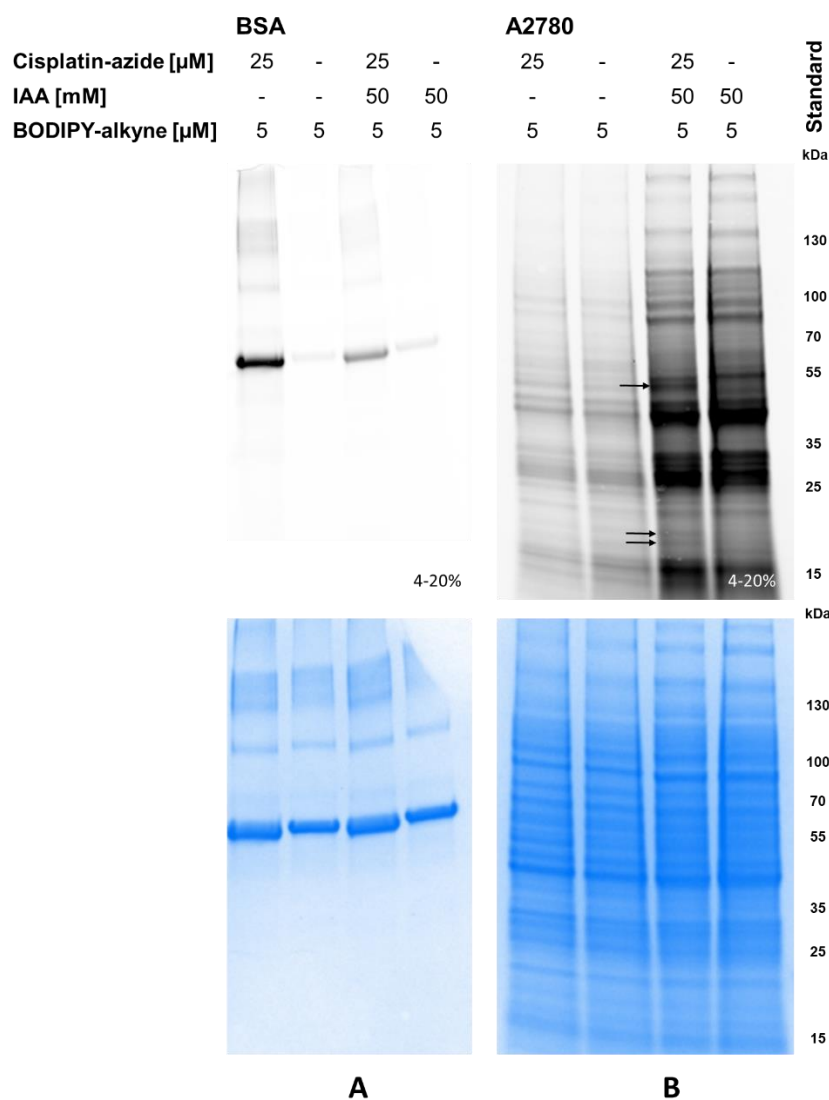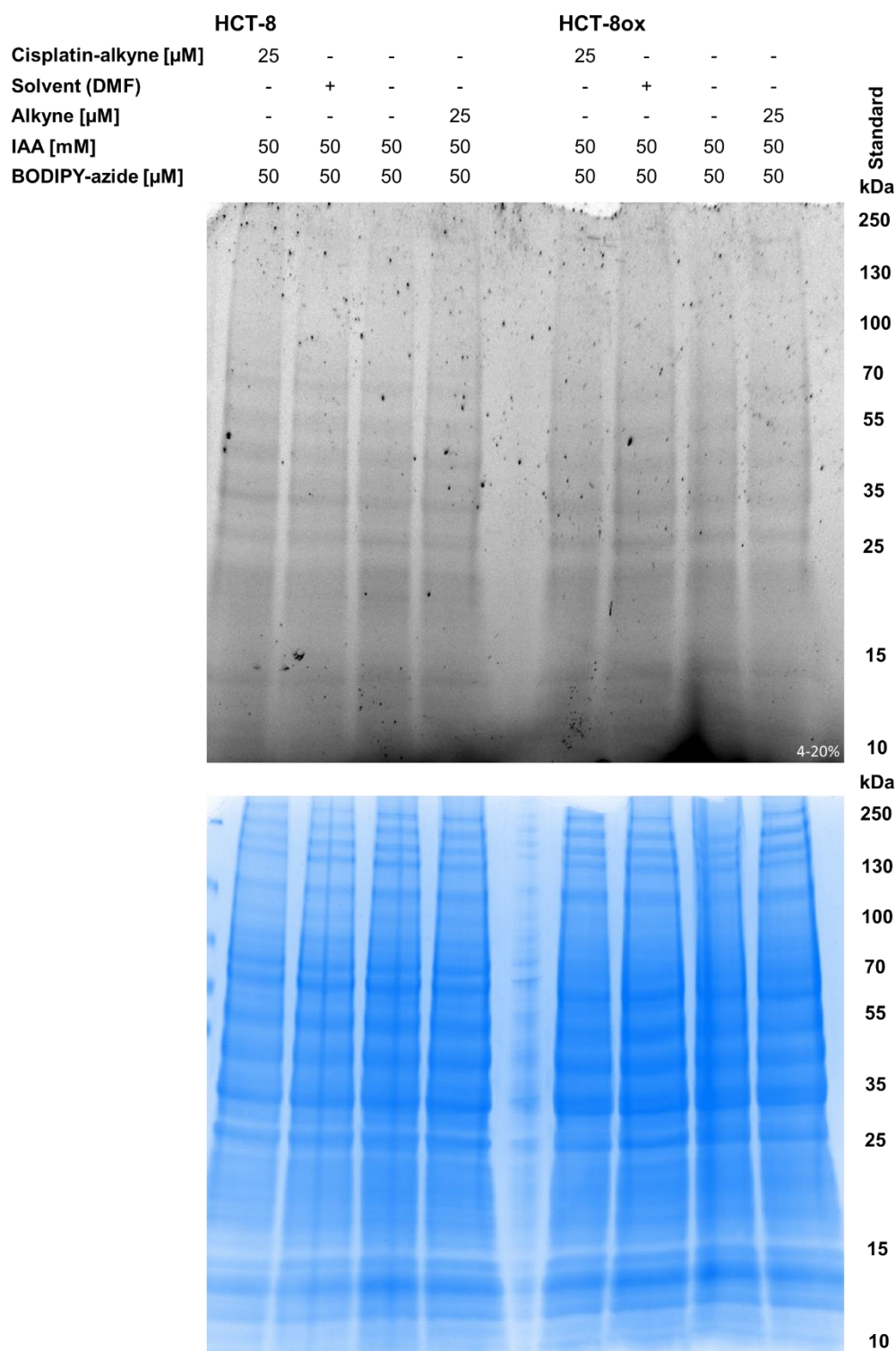**Figure 4.28 Representative fluorescence (upper panel) and Coomassie stained (lower panel) pictures after CuAAC whereby applying 50 mM IAA prior to treatment with either cisplatin-alkyne, DMF, alkyne tag or no treatment at all and 50 µM BODIPY-azide, 2 mM THPTA, 1 mM CuSO$_4$ and 1 mM sodium ascorbate to 100 µg of total protein of HCT-8 and HCT-8ox cancer cell samples.**

4.1.8   Comparison of Protein Detection Methods

When examining the three different approaches, it must be noted that the partially modified two-dimensional gel electrophoresis protein detection method originally based on the protocol of Kotz et al. yielded by far the most findings. Although the immunoprecipitation of cisplatin-protein complexes might be a target-oriented additional step and first promising results could be achieved by applying the copper-catalyzed azide-alkyne cycloaddition, only gels obtained through 2D gel electrophoresis could be processed further. This eventually led to the possibility to identify protein binding partners using fluorescence imaging and mass spectrometry (Chapter 4.2) and to modulate selective candidates of these by pharmacological inhibition or knockdown experiments (Chapter 4.3).

4.2   Identification of Protein Binding Partners

In general, even with help of software like Delta2D, overlay of two images of the same 2D gel can be performed only roughly if the gel has been moved due to recording at different times. Here, the fluorescence image of the gel visualizing BODIPY-cisplatin was taken approximately 24 hours before the Coomassie stained image that detected all proteins available in the sample. This in mind, there have been several attempts to optimize overlay, amongst others the incorporation of a reference protein grid [113,159]. While the sample was labeled with one fluorescence dye, the grid was labeled with another, thus, via visualization of both dyes separately but without any movement of the gels, enabling the identification of certain reference spots after subsequent staining of the total protein (e.g. with Coomassie). However, the application of such grids introduced into the gel by individually manufactured combs presented certain technical difficulties. Even more problematic, though, was the occurrence of fluorescence cross talk (also known as bleed-through). Despite the distinct differences of excitation/emission wavelengths of BODIPY-cisplatin and Sci5 (460-490/518-546 nm and 625-650/675-725 nm, respectively), Sci5-labeled protein grid could still be detected when exciting at 460-490 nm (Figure 4.29). This way, misleading results and overlap of proteins of interest with the protein grid could not be ruled out.
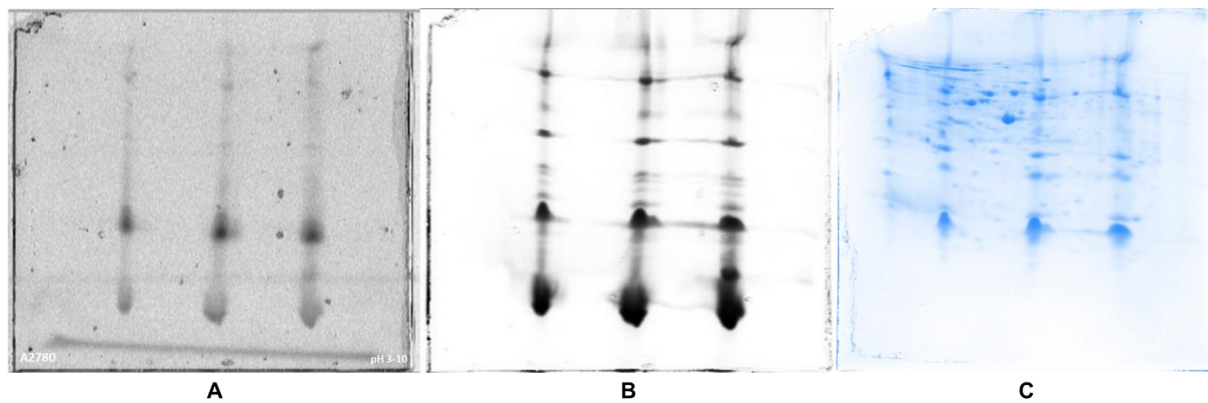
Figure 4.29 Representative fluorescence (A,B) and Coomassie stained (C) gel pictures of the reference protein grid. Fluorescence was detected at 460-490/518-546 nm (A) and 625-650/675-725 nm (B).

In order to ensure reliable overlay of fluorescence and Coomassie stained pictures, but without the risk of artefacts, the use of a reference protein grid on every gel was abandoned. As an alternative, all lysates were minimally labeled with Sci5 right before separation via two-dimensional gel electrophoresis as described in Chapter 3.9.2. By doing so, it was possible to detect both BODIPY-cisplatin and total protein in direct succession and to overlay the obtained images precisely hereinafter. Therefore, imaging reference gels, which presented particular protein patterns, could be generated via Delta2D (Figure 4.30). Overlay during subsequent experiments, where detection of the whole proteome of the sample was replaced by Coomassie staining, was simplified substantially by these imaging reference gels, as the characteristic protein patterns could be superimposed with absolute certainty. In addition to the protein marker that flanked the IPG strip in the second dimension, protein binding partner identification was even more facilitated.
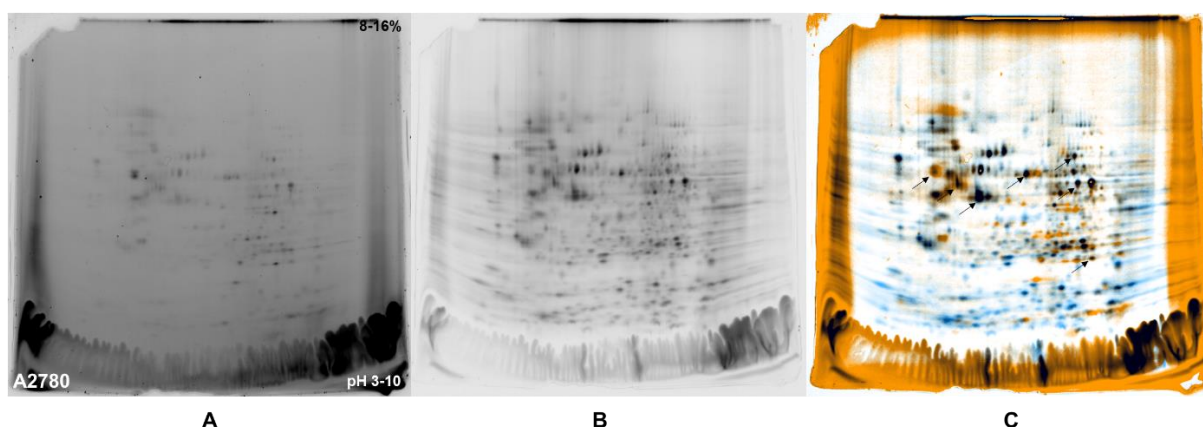
Figure 4.30 Representative fluorescence gel pictures of A2780 cancer cell samples after minimal labeling of the sample with Sci5. Fluorescence was detected at 460-490/518-546 nm (A) for BODIPY-cisplatin and 625-650/675-725 nm (B) for Sci5. Precise overlay of these two images via Delta2D allowed the identification of certain landmarking spots that could be superimposed with certainty later on (C, marked exemplarily with arrows).

With the optimization of the two-dimensional gel electrophoresis and the overlay procedure being successfully completed, the separation of cytosolic proteins via 2D gel electrophoresis and the combination of the fluorescence detection of BODIPY-cisplatin and colloidal Coomassie staining of proteins then led to the visualization of spots representing cytosolic cisplatin binding partners (Figure 4.31). It was obvious that the number differentiated between wildtype and resistant cell types on the one hand (Figure 4.31A vs. B and C vs. D) but also between cells with intrinsic and acquired cisplatin resistance (Figure 4.31B vs. C and B vs. D).
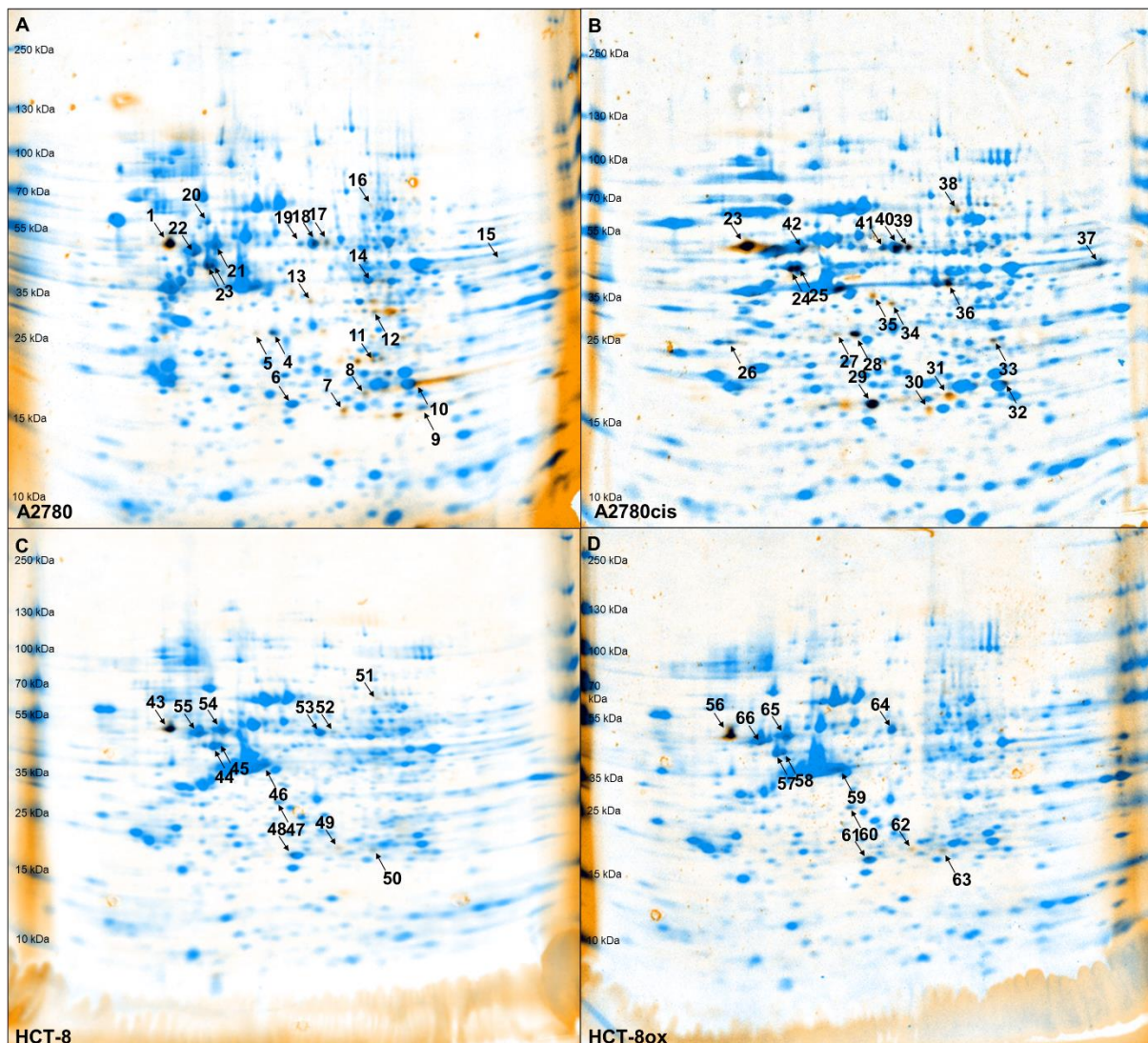
Figure 4.31 Overlay of fluorescence image and Coomassie staining in gels after two-dimensional gel electrophoresis of the cytosolic fractions of A2780 (A), A2780cis (B), HCT-8 (C) and HCT-8ox (D) cells treated with BODIPY-cisplatin.

While there were many fluorescent spots in both A2780 and A2780cis cells, BODIPY-cisplatin signals did not overlay to the same extent with the protein staining of HCT-8 and HCT-8ox cells. After identification of cytosolic proteins from picked spots via

LC-MS (Table 4.3), several proteins were chosen to be examined in more detail. The focus was primarily on proteins identified as binding partners either in ovarian or colorectal cancer cells. Thus, vimentin (identified only in A2780 and A2780cis cells, Figure 4.31, spots 21/22 and 42, respectively), glutathione-S-transferase π (identified in all investigated cell lines, Figure 4.31, spots 6, 29, 48 and 61 in A2780, A2780cis, HCT-8 and HCT-8ox cells, respectively), DJ-1 (identified only in A2780 and A2780cis cells, Figure 4.31, spots 7 and 30, respectively), and growth receptor factor bound protein 2 (identified only in HCT-8 and HCT-8ox cells, Figure 4.31, spots 49 and 62, respectively) were selected for further investigation. Noteworthy, fluorescence intensity of BODIPY-cisplatin was more pronounced in A2780cis and HCT-8ox cells in comparison to A2780 and HCT-8 cells, respectively. Especially in A2780cis cells, very high intensity of BODIPY-cisplatin in spots with vimentin and GSTP1 was observed (Figure 4.31B). This is particularly interesting, as neither in the case of vimentin nor in the case of GSTP1 significantly differential expressions of basal protein levels could be detected when examining A2780 vs. A2780cis and HCT-8 vs. HCT-8ox cell line pairs (Figure 4.32). Interestingly, vimentin expression in the HCT-8 cell lines was negligible, especially in comparison to the A2780 cell lines (Figure 4.32A).

Table 4.3 Cytosolic protein binding partners of BODIPY-cisplatin in cell lines investigated.

Cell line	Spot #	Protein	Accession #	M_r (kDa)	pI	Sequence coverage [%]
A2780	1	Protein disulfide-isomerase A1	P07237	57.1	4.87	31
	2	Protein disulfide-isomerase A6	Q15084	48.1	5.08	22
	3	Protein disulfide-isomerase A6	Q15084	48.1	5.08	37
	4	F-actin-capping protein subunit alpha-1	P52907	32.9	5.69	30
	5	Heme oxygenase 2	P30519	36	5.41	29
	6	Glutathione-S-transferase P1	P09211	23.3	5.64	16
	7	Protein/nucleic acid deglycase DJ-1	Q99497	19.9	6.79	24
	8	Proteasome subunit beta type-3	P49720	22.9	6.55	35
	9	Flavin reductase (NADPH)	P30043	22.1	7.65	34
	10	GTP-binding nuclear protein Ran	P62826	24.4	7.49	24
	11	Proteasome subunit alpha type 1	P25786	29.5	6.61	26
	12	Apolipoprotein L2	Q9BQE5	37.1	6.74	16
		Transaldolase	P37837	37.5	6.81	29
	13	L-lactate dehydrogenase B chain	P07195	36.6	6.05	32
	14	26S proteasome non-ATPase regulatory subunit 11	O00231	47.4	6.48	55
		Adenosylhomocysteinase	P23526	47.7	6.34	35
	15	Elongation factor 1-alpha 1	P68104	50.1	9.01	19
	16	Succinate dehydrogenase [ubiquinone] flavoprotein subunit, mitochondrial	P31040	72.6	7.39	16

Cell line	Spot #	Protein	Accession #	M_r (kDa)	pI	Sequence coverage [%]
A2780	17	Protein disulfide-isomerase A3	P30101	56.7	6.35	19
	18	Protein disulfide-isomerase A3	P30101	56.7	6.35	54
	19	Protein disulfide-isomerase A3	P30101	56.7	6.35	36
	20	Serine/threonine-protein phosphatase 2A 65 kDa regulatory subunit A alpha isoform	P30153	65.3	5.11	28
	21	Vimentin	P08670	53.6	5.12	63
		Nucleobindin-1	Q02818	53.8	5.25	58
	22	Vimentin	P08670	53.6	5.12	76
A2780cis	23	Protein disulfide-isomerase A1	P07237	57.1	4.87	49
	24	Protein disulfide-isomerase A6	Q15084	48.1	5.08	51
		Nucleobindin-2	P80303	50.2	5.12	64
		26S proteasome regulatory subunit 6B	P43686	47.3	5.21	46
	25	Protein disulfide-isomerase A6	Q15084	48.1	5.08	34
	26	Proliferating cell nuclear antigen	P12004	28.8	4.69	56
	27	Heme oxygenase 2	P30519	36	5.41	22
	28	F-actin-capping protein subunit alpha-1	P52907	32.9	5.69	15
	29	Glutathione S-transferase P1	P09211	23.3	5.64	71
	30	Protein/nucleic acid deglycase DJ-1	Q99497	19.9	6.79	25
	31	Heat shock protein beta-1	P04792	22.8	6.4	49
		Proteasome subunit beta type-3	P49720	22.9	6.55	21
	32	GTP-binding nuclear protein Ran	P62826	24.4	7.49	21
	33	Polyubiquitin-B	P0CG47	25.7	7.43	56
	34	L-lactate dehydrogenase B chain	P07195	36.6	6.05	32
	35	COP9 signalosome complex subunit 4	Q9BT78	46.2	5.83	15
	36	Adenosylhomocysteinase	P23526	47.7	6.34	36
		26S proteasome non-ATPase regulatory subunit 11	O00231	47.4	6.48	25
	37	Elongation factor 1-alpha 1	P68104	50.1	9.01	17
	38	Succinate dehydrogenase [ubiquinone] flavoprotein subunit, mitochondrial	P31040	72.6	7.39	25
	39	Protein disulfide-isomerase A3	P30101	56.7	6.35	24
	40	Protein disulfide-isomerase A3	P30101	56.7	6.35	69
	41	Protein disulfide-isomerase A3	P30101	56.7	6.35	41
	42	Nucleobindin-1	Q02818	53.8	5.25	25
		Vimentin	P08670	53.6	5.12	19
HCT-8	43	Protein disulfide-isomerase A1	P07237	57.1	4.87	53
	44	Protein disulfide-isomerase A6	Q15084	48.1	5.08	40
		Nucleobindin-2	P80303	50.2	5.12	54
		26S proteasome regulatory subunit 6B	P43686	47.3	5.21	41
	45	Protein disulfide-isomerase A6	Q15084	48.1	5.08	36
	46	Eukaryotic initiation factor 4A-I	P60842	46.1	5.48	19
	47	F-actin-capping protein subunit alpha-1	P52907	32.9	5.69	36
	48	Glutathione S-transferase P1	P09211	23.3	5.64	73
	49	Growth factor receptor-bound protein 2	P62993	25.2	6.32	28

Cell line	Spot #	Protein	Accession #	M_r (kDa)	pI	Sequence coverage [%]
HCT-8	50	Proteasome subunit beta type-3	P49720	22.9	6.55	47
	51	Phosphoglucomutase-2	Q96G03	68.2	6.73	21
	52	Protein disulfide-isomerase A3	P30101	56.7	6.35	40
	53	Protein disulfide-isomerase A3	P30101	56.7	6.35	65
	54	ATP synthase subunit beta, mitochondrial	P06576	56.5	5.4	41
		Nucleobindin-1	Q02818	53.8	5.25	39
	55	ATP-Synthase subunit beta, mitochondrial	P06576	56.5	5.4	25
HCT-8ox	56	Protein disulfide-isomerase A1	P07237	57.1	4.87	37
	57	Protein disulfide-isomerase A6	Q15084	48.1	5.08	26
	58	Protein disulfide-isomerase A6	Q15084	48.1	5.08	41
	59	Eukaryotic initiation factor 4A-I	P60842	46.1	5.48	33
	60	F-actin-capping protein subunit alpha-1	P52907	32.9	5.69	49
	61	Glutathione S-transferase P1	P09211	23.3	5.64	70
	62	Growth factor receptor-bound protein 2	P62993	25.2	6.32	45
	63	Proteasome subunit beta type-3	P49720	22.9	6.55	21
	64	Protein disulfide-isomerase A3	P30101	56.7	6.35	57
	65	ATP synthase subunit beta, mitochondrial	P06576	56.5	5.4	25
		Nucleobindin-1	Q02818	53.8	5.25	24
	66	ATP-Synthase subunit beta, mitochondrial	P06576	56.5	5.4	34
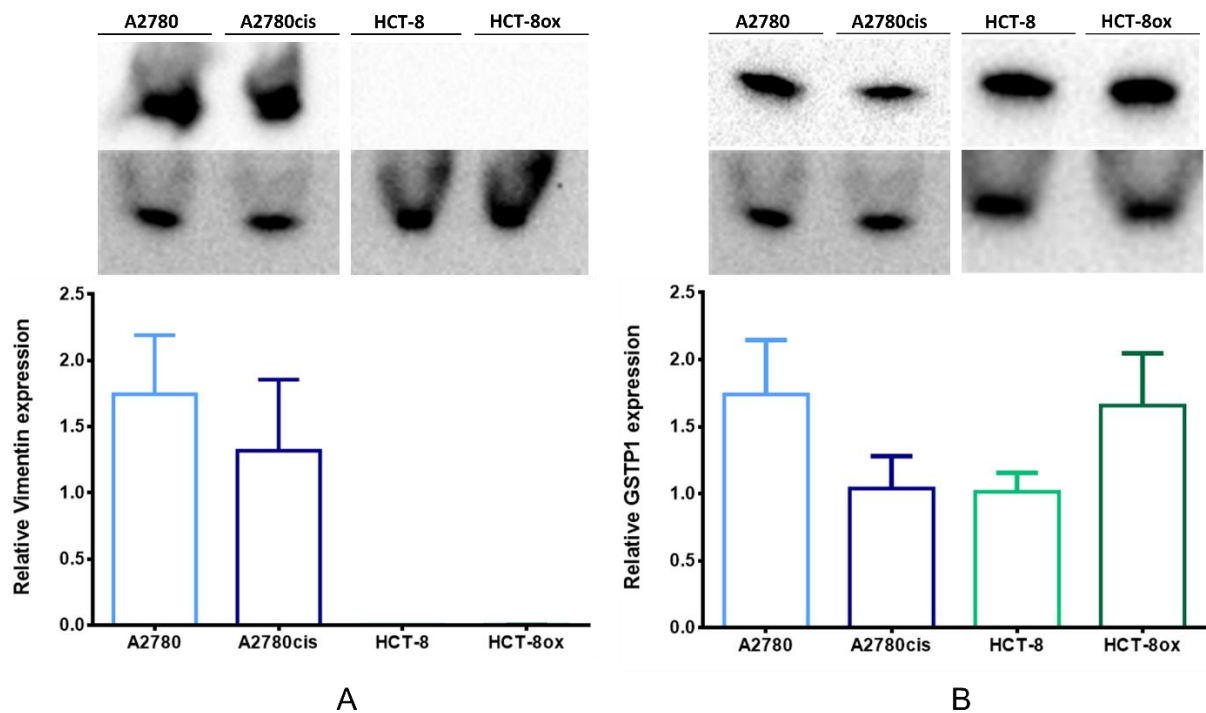
Figure 4.32 Representative Western Blots and densitometric quantification of basal vimentin (A) and GSTP1 (B) expression in A2780, A2780, HCT-8 and HCT-8ox cells (mean ± SEM, n = 3). GAPDH served as a loading control.

4.3 Modulation of Protein Binding Partners

To assess the impact of vimentin, GSTP1, DJ-1 and Grb2 on cisplatin sensitivity, these proteins were subjected to specific inhibitors on the one hand and specific small interfering RNA for gene silencing on the other hand (Chapter 3.1.1). Since the influence of the treatment should be evaluated not only in the cytosolic fraction of the cell lysate but in the entire cell, all treated cells were lysed with RIPA buffer to yield whole cell lysates as indicated in Chapter 3.3.1.4. In case of significant effects, further in-depth experiments, such as determination of the combination index and apoptosis assays, followed as described in detail below.

All experiments performed following protein binding partner identification were conducted with varying concentrations of cisplatin or oxaliplatin (Figure 1.5) to assess the protein's relevance for platinum sensitivity.

4.3.1 Vimentin

In order to assess the relevance of vimentin for cisplatin cytotoxicity, the recently developed vimentin inhibitor FiVe1 was employed (Chapter 3.1.1, [160]). After determination of the non-toxic concentration of FiVe1 (EC_{50} was 0.93 µM in A2780 cells and 0.80 µM in A2780cis cells, Figure 4.33A), cells were subjected to cisplatin in combination with FiVe1 at this non-toxic concentration of 0.2 µM over 72 hours. Both A2780 and A2780cis cells were significantly sensitized towards cisplatin (in A2780 cells EC_{50} changed from 1.17 µM to 0.78 µM and in A2780cis cells from 4.88 µM to 2.81 µM, Figure 4.33B). The RF of A2780cis cells was reduced from 4.2 to 3.6.
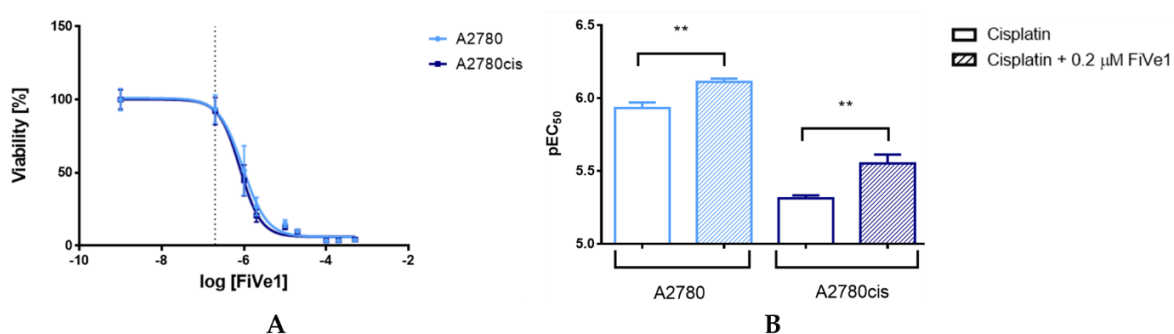
Figure 4.33 Cell viability of A2780 and A2780cis cells (mean ± SEM, n = 4) after treatment with vimentin inhibitor FiVe1 and determination of the non-toxic concentration (dotted line) (A). Cisplatin cytotoxicity in A2780 and A2780cis cells alone or upon incubation with non-toxic 0.2 µM FiVe1 (pEC$_{50}$, mean ± SEM, n = 4-6) (B). **, p < 0.01.

Furthermore, combination of cisplatin with 0.2 µM FiVe1 induced a more pronounced apoptosis compared to treatment with cisplatin alone measured by Annexin V/PI

apoptosis assay. The percentage of late apoptotic cells increased by 15.8% (p = 0.0071) in A2780 cells and by 20.4% (p < 0.0001) in A2780cis cells (Figure 4.34). The inhibitor of vimentin was used in the non-toxic concentration as mentioned above and itself showed no signs of increased apoptosis when applied alone in comparison to untreated cells (Figure 4.34).
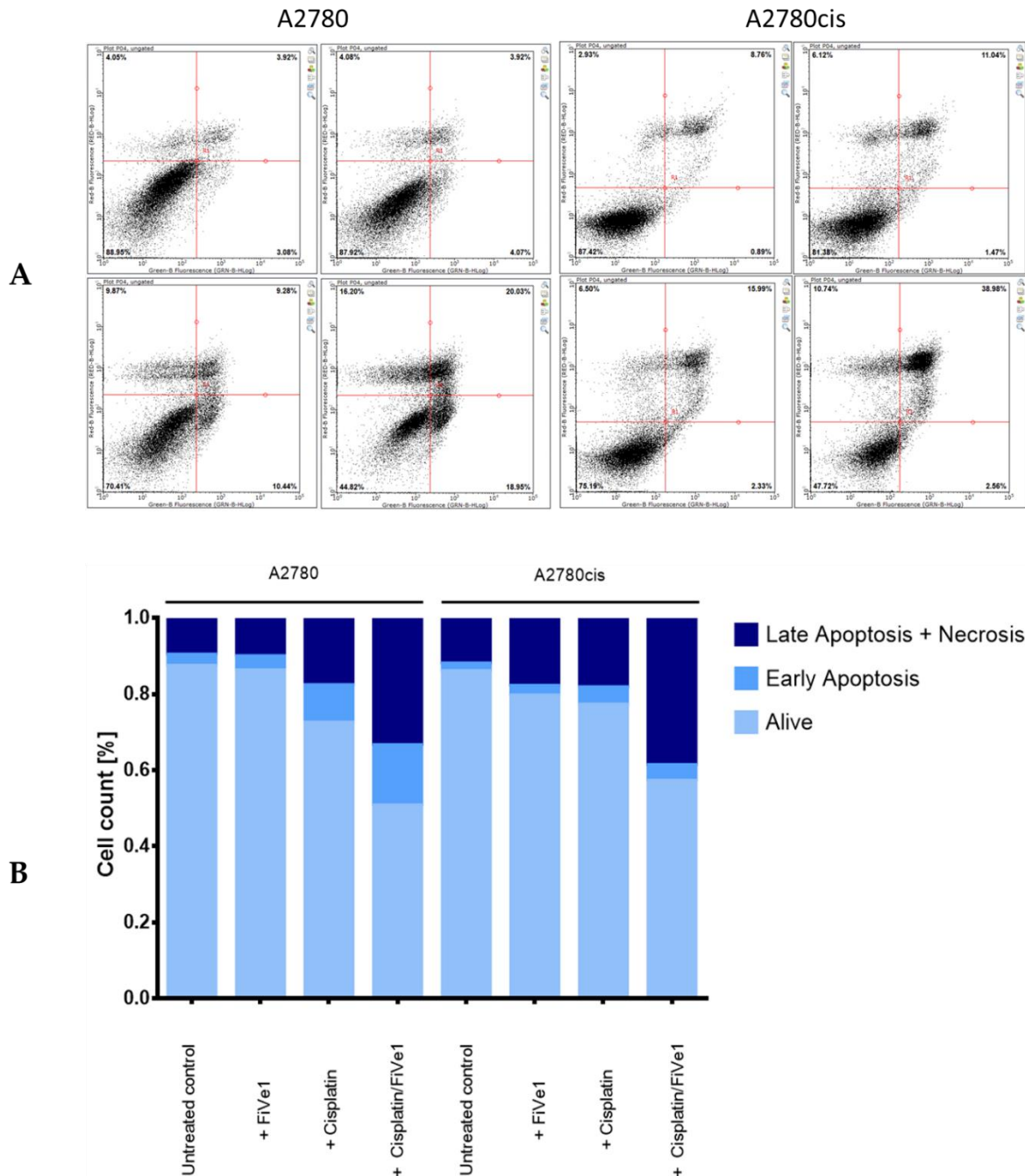
Figure 4.34 Flow cytometry analyses of Annexin V-FITC/PI double staining in A2780 and A2780cis cells after co-incubation of cisplatin with FiVe1 (lower right quadrant) in comparison to the treatment with the inhibitor (upper right quadrant) or cisplatin (lower left quadrant) alone and untreated cells (upper left quadrant) (A). The percentage of early apoptotic, late apoptotic and necrotic as well as alive cells (mean ± SEM, n = 4) in A2780 and A2780cis cells after co-incubation of cisplatin with FiVe1 in comparison to the treatment with each of the compounds alone and untreated cells (B).

In order to understand the pharmacological interaction between cisplatin and FiVe1, the CI was determined. It is especially interesting that the drug combination works synergistically (CI < 1) at effective concentration combinations of EC_{50} and higher, with better results in the resistant cell line (Figure 4.35).
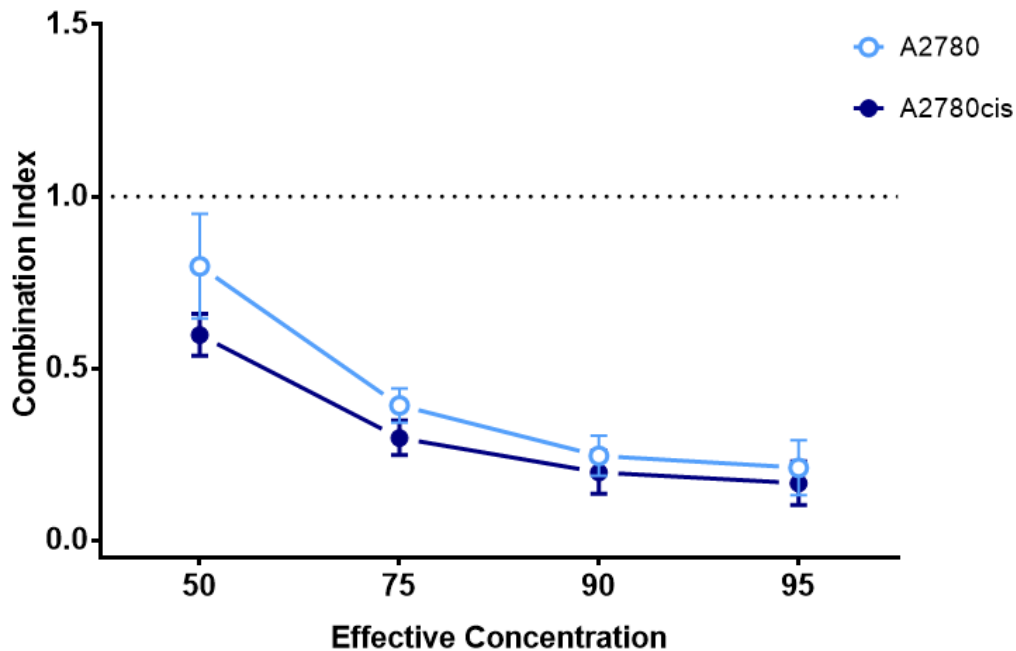
Figure 4.35 CI of cisplatin and FiVe1 as described by Chou et al. [140]. CI was determined at effective concentrations from EC_{50} to EC_{95} (mean ± SEM, n = 8).

In addition to pharmacological inhibition, knockdown experiments were conducted for all proteins chosen for further investigation, as mentioned before. All experiments started with siRNA-mediated transfection for 24 hours, followed by exposure to a platinum drug for 48 hours in case of cytotoxicity measurements. The expression of vimentin as detected by Western Blot 48 hours after transfection was decreased by 33% and 51% (p = 0.0149) in A2780 and A2780cis cells, respectively, in comparison to cells transfected with NC siRNA (Figure 4.36A). However, no significant effect of cisplatin cytotoxicity in the cells after vimentin knockdown could be detected (Figure 4.36B).

A

B

Figure 4.36 Representative Western Blot and densitometric quantification of protein expression after treatment with specific siRNA for vimentin and NC siRNA in A2780 and A2780cis cells. GAPDH served as a loading control (mean ± SEM, n = 3) (A). Cisplatin cytotoxicity in A2780 and A2780cis cells after vimentin knockdown, prior treatment with NC siRNA or no pre-treatment (pEC$_{50}$, mean ± SEM, n = 4) (B). *, p < 0.05.

4.3.2   Glutathione-S-Transferase π 1

GSTP1 was discovered to be a binding partner of BODIPY-cisplatin in all four cell lines used and since standard therapy of colorectal cancer is oxaliplatin, all experiments in HCT-8 and HCT-8ox cells were carried out with oxaliplatin additionally to cisplatin. The GSTP1 inhibitor Ezatiostat-HCl (Chapter 3.1.1, [161]) could be applied at the concentration up to 10 µM without harming the cells (EC$_{50}$ values were 33.69 µM and 31.97 µM in A2780 and A2780cis cells, respectively, and 67.79 µM and 61.60 µM in HCT-8 and HCT-8ox cells, respectively, Figure 4.37).

A

B
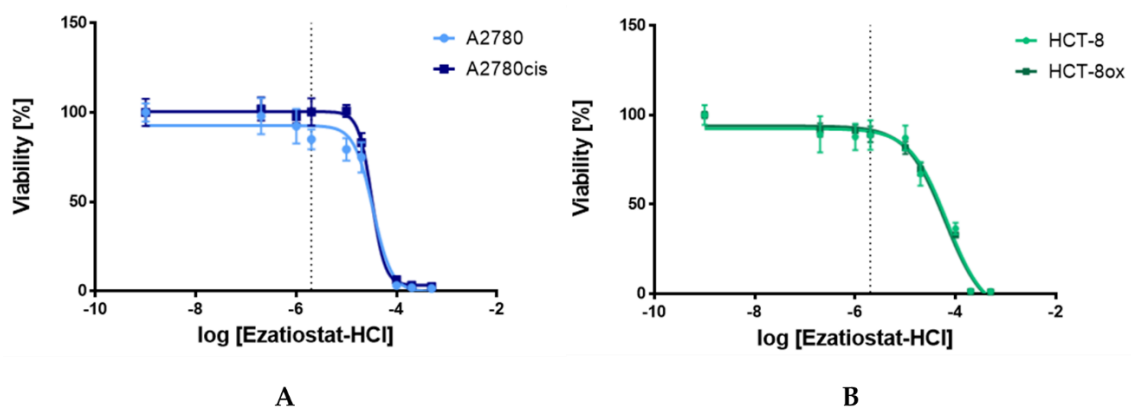
Figure 4.37 Cell viability of A2780 and A2780cis cells (A) and HCT-8 and HCT-8ox cells (B) (mean ± SEM, n = 4) after treatment with GSTP1 inhibitor Ezatiostat-HCl and determination of the non-toxic concentration (dotted lines).

Interestingly, no effect could be observed when combining either platinum drug with a non-toxic concentration of Ezatiostat-HCl (2 µM in co-incubation and 10 µM in pre-incubation experiments) in all cell lines used (Figure 4.38). The result was the same independent of the incubation scheme: either the tumor cells were exposed to the platinum drug and inhibitor simultaneously for 72 hours or there was a pre-incubation with the inhibitor over 48 hours before the cells were subjected to the platinum drug for the remaining time. Alternatively, pre-incubation over 24 hours was followed by the platinum drug exposure over 48 hours (Figure 4.38). Pre-incubation was considered since chemical interaction of cisplatin with Ezatiostat-HCl could not be ruled out.
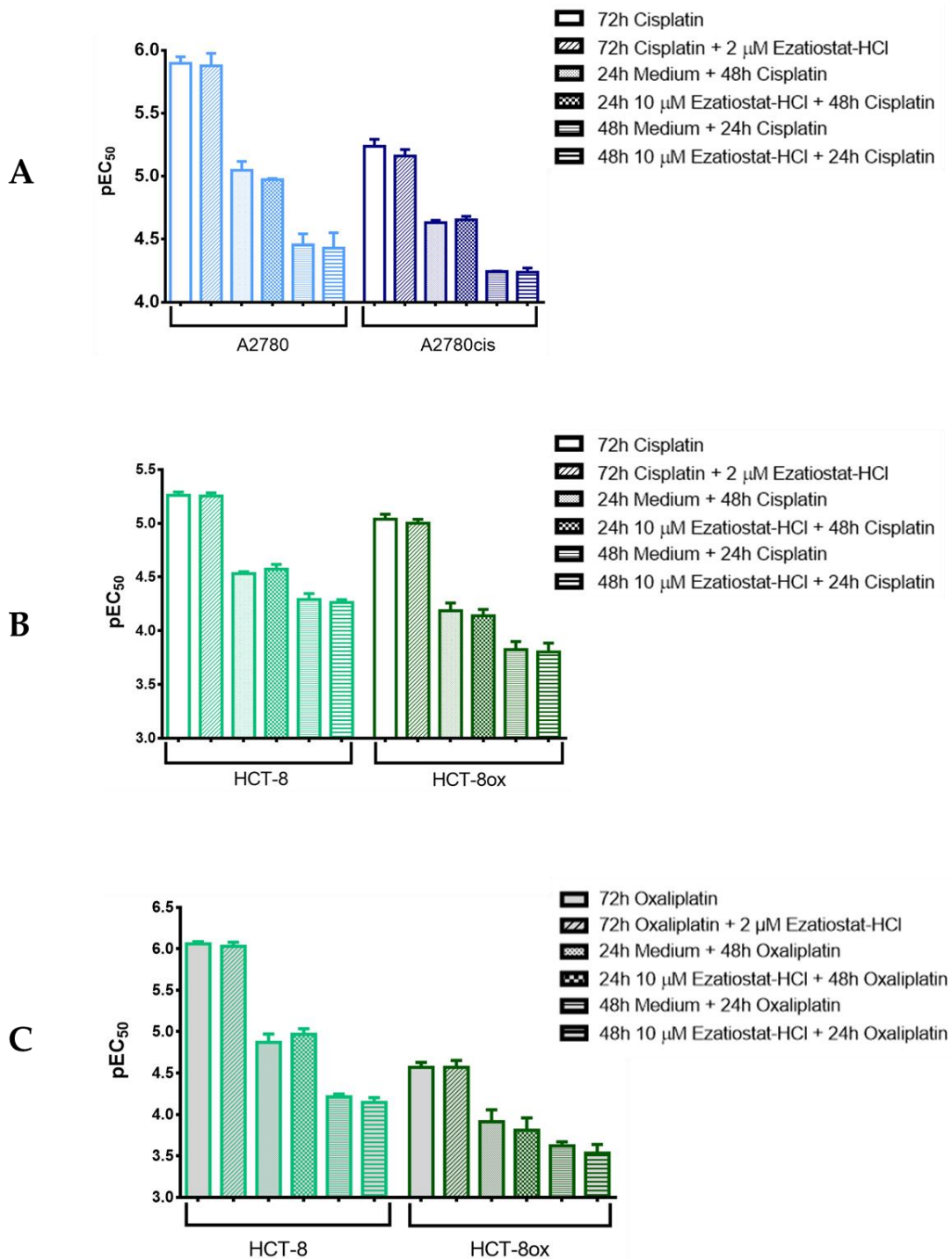
Figure 4.38 Cisplatin (A,B) or oxaliplatin (C) cytotoxicity in A2780, A2780cis, HCT-8 and HCT-8ox cells alone or upon co-incubation with Ezatiostat-HCl, either without or with 24 hours or 48 hours pre-incubation with the inhibitor before platinum drug treatment (pEC$_{50}$, mean ± SEM, n = 3-7).

While GSTP1 knockdown was nearly perfect in HCT-8 and HCT-8ox cells (decrease by 91% (p < 0.0001) and 95% (p < 0.0001), respectively), the expression of GSTP1 could only be reduced by 42% (p = 0.0032) in A2780 cells and by 8% in A2780cis cells (Figure 4.39A, Figure 4.40A). Due to the low transfection efficiency in the ovarian carcinoma cell line pair, no difference in cisplatin sensitivity was detected after transfection (Figure 4.39B). On the contrary, Figure 4.40B shows an obvious and

significant sensitization of both colorectal cancer cell lines to cisplatin after GSTP1 knockdown (EC_{50}: HCT-8 cells, 7.10 µM; HCT-8ox cells, 12.79 µM) compared to either NC (EC_{50}: HCT-8 cells, 19.10 µM, HCT-8ox cells, 34.28 µM) or cells without knockdown (EC_{50}: HCT-8 cells, 21.04 µM; HCT-8ox cells, 38.19 µM). As upon pharmacological inhibition, all knockdown experiments concerning the HCT-8 and HCT-8ox cells were carried out with both cisplatin and oxaliplatin. When treated with oxaliplatin (Figure 4.40C), only HCT-8 cells showed a significant change in susceptibility to the drug compared to negative knockdown control (EC_{50} decreased from 13.46 µM to 2.06 µM) or unmodified control (EC_{50} was reduced from 11.30 µM to 2.06 µM). The oxaliplatin-resistant HCT-8ox cell line showed a strong tendency to elevated sensitivity compared to both controls (EC_{50} decreased from 26.49 µM in the NC and from 27.80 µM in cells without knockdown to 6.34 µM). However, this difference was not statistically significant.
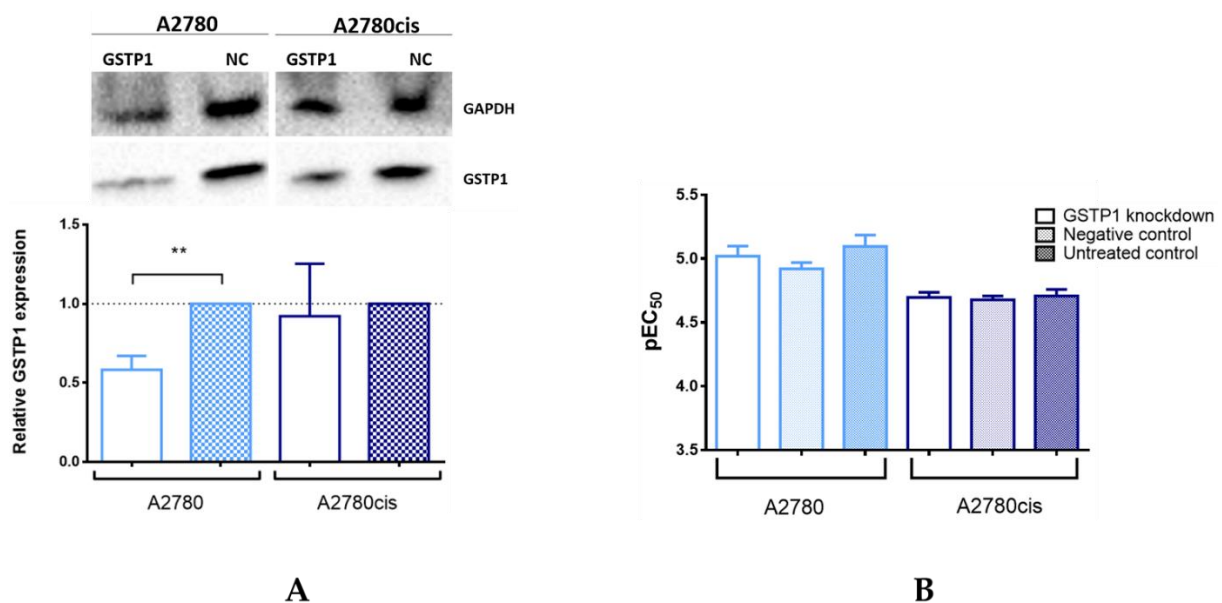
Figure 4.39 Representative Western Blot and densitometric quantification of protein expression after treatment with specific siRNA for GSTP1 and NC siRNA in A2780 and A2780cis cells. GAPDH served as a loading control (mean ± SEM, n = 3-4) (A). Cisplatin cytotoxicity in A2780 and A2780cis cells after GSTP1 knockdown, prior treatment with NC siRNA or no pre-treatment (pEC$_{50}$, mean ± SEM, n = 5) (B). **, p < 0.01.
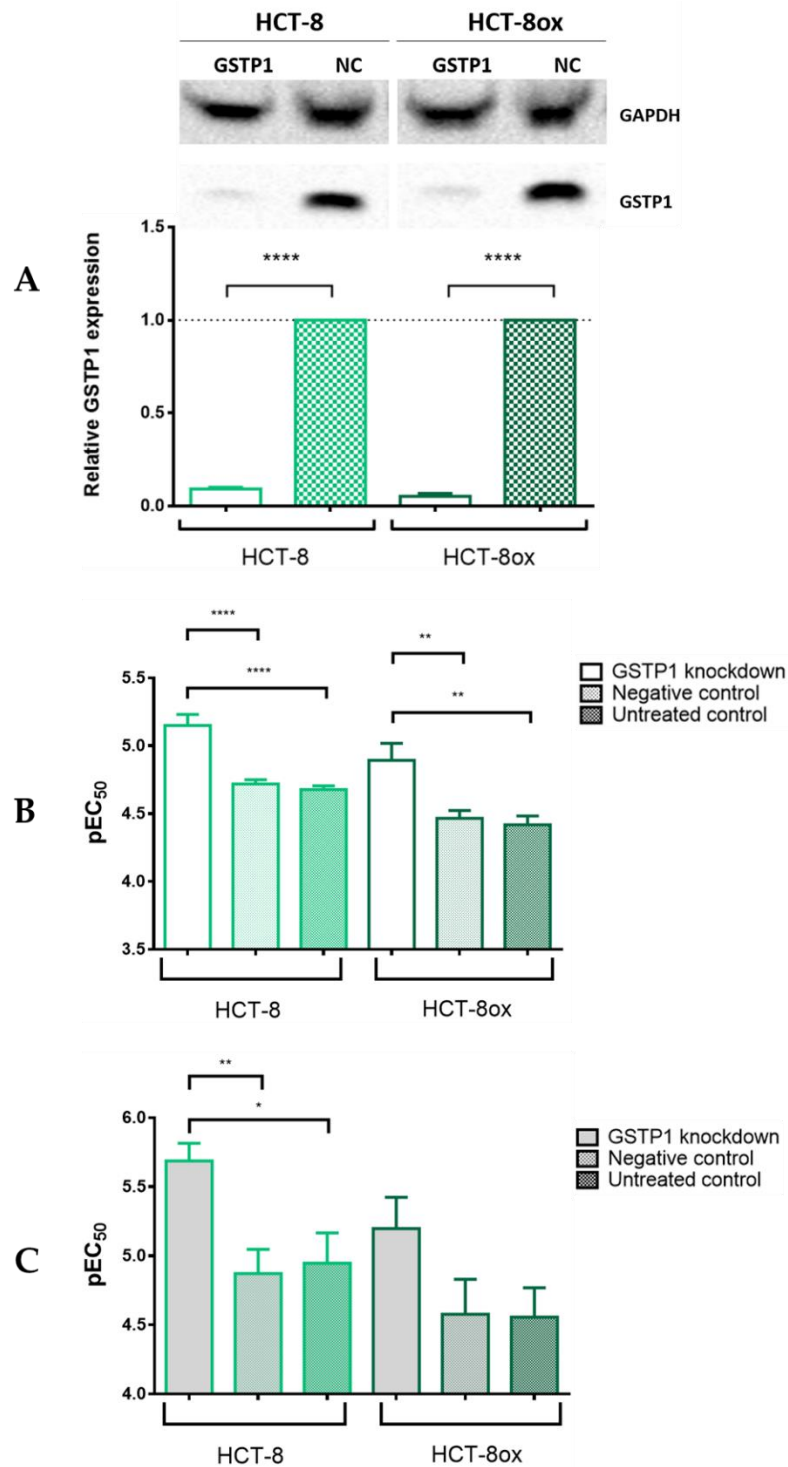
Figure 4.40 Representative Western Blots and densitometric quantification of protein expression after treatment with specific and NC siRNA for GSTP1 in HCT-8 and HCT-8ox cells. GAPDH served as a loading control (mean ± SEM, n = 3) (A). Cisplatin (B) and oxaliplatin (C) cytotoxicity in HCT-8 and HCT-8ox cells after GSTP1 knockdown, prior treatment with NC siRNA or no pre-treatment (pEC$_{50}$, mean ± SEM, n = 5-7). *, p < 0.05; **, p < 0.01; ****, p < 0.0001.

These results were further validated by an apoptosis assay, which revealed a significant increase in late apoptosis and necrosis in HCT-8 cells induced by cisplatin after knockdown of GSTP1 compared to either negative knockdown control (+34.5%, p = 0.0088) or cells without knockdown (+52.1%, p < 0.0001, Figure 4.41). In HCT-8ox

cells, we could detect significantly elevated levels of cisplatin-induced late apoptosis and necrosis after GSTP1 knockdown when compared to unmodified control (+36.8%, p = 0.0038), but not in comparison to negative knockdown controls (+26.3%, p = 0.1014, Figure 4.41).
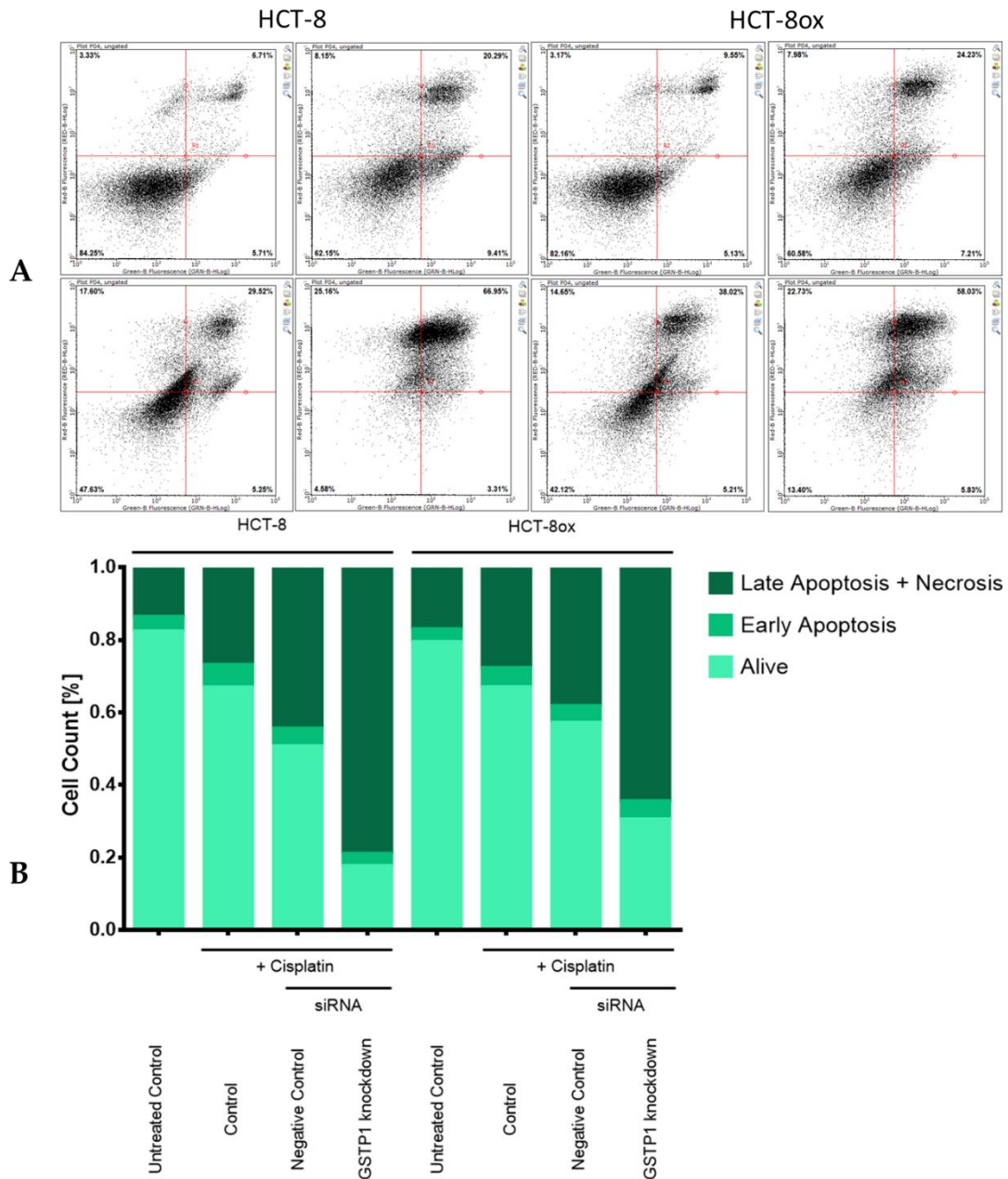
Figure 4.41 Flow cytometry analyses of Annexin V-FITC/PI double staining in HCT-8 and HCT-8ox cells after cisplatin treatment following GSTP1 knockdown (lower right quadrant) or NC siRNA treatment (lower left quadrant) or without knockdown (upper right quadrant) or untreated cells (upper left quadrant) (A). The percentage of early apoptotic, late apoptotic and necrotic as well as alive cells (mean ± SEM, n = 3-4) in HCT-8 and HCT-8ox cells after cisplatin treatment following GSTP1 knockdown or negative knockdown control or without knockdown (B).

With oxaliplatin, the results were quite similar: a significant increase in late apoptosis and necrosis after GSTP1 knockdown in both the HCT-8 (+38.9% with respect to NC, p < 0.0001, and +53.2% compared to unmodified control, p < 0.0001) and here also in

the HCT-8ox cell line (+25.8% with respect to NC, p = 0.0021, and +40.0% compared to unmodified control, p < 0.0001, Figure 4.42) could be detected.
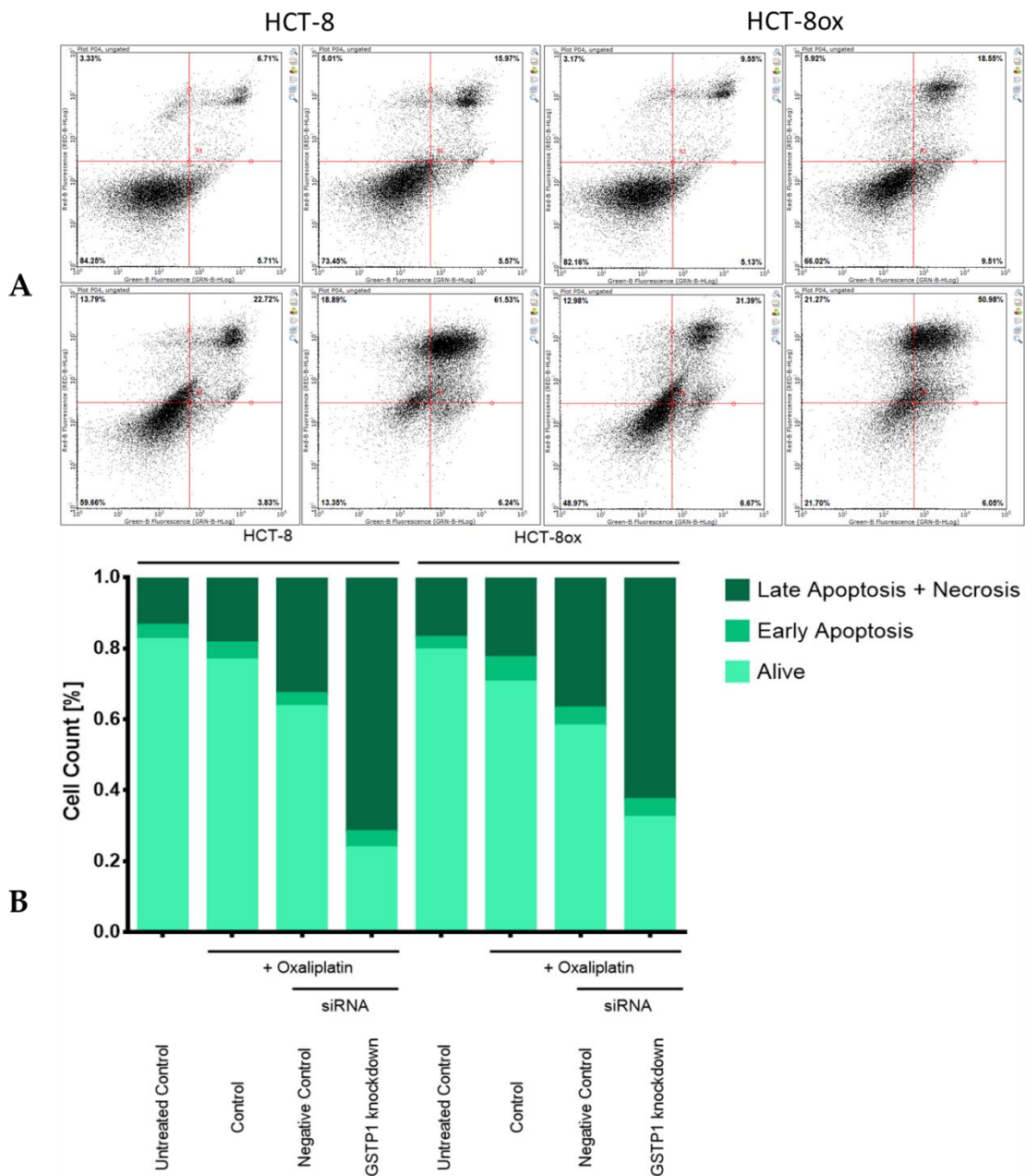
Figure 4.42 Flow cytometry analyses of Annexin V-FITC/PI double staining in HCT-8 and HCT-8ox cells after oxaliplatin treatment following GSTP1 knockdown (lower right quadrant) or NC siRNA treatment (lower left quadrant) or without knockdown (upper right quadrant) or untreated cells (upper left quadrant) (A). The percentage of early apoptotic, late apoptotic and necrotic as well as alive cells (mean ± SEM, n = 4) in HCT-8 and HCT-8ox cells after oxaliplatin treatment following GSTP1 knockdown or negative knockdown control or without knockdown (B).

4.3.3   Protein/Nucleic Acid Deglycase DJ-1

First, the concentration, at which DJ-1 inhibitor (Chapter 3.1.1, [162]) did not have any toxic effects, was established at 5 µM (EC_{50} was 82.74 µM in A2780 cells and 103.50 µM in A2780cis cells, Figure 4.43A). This concentration was then applied in all co-incubation experiments. While there was a slight trend towards increased sensitivity of A2780 cells upon combination of cisplatin and DJ-1 inhibitor (EC_{50} decreased from 1.50 µM to 0.67 µM, $p = 0.0602$), no such effect could be perceived in A2780cis cells (Figure 4.43B).
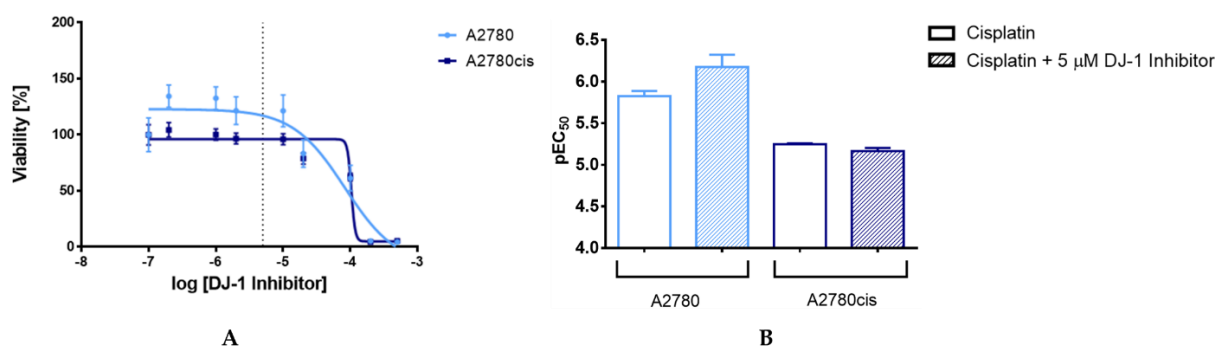
Figure 4.43 Cell viability of A2780 and A2780cis cells (mean ± SEM, n = 5) after treatment with DJ-1 inhibitor and determination of the non-toxic concentration (dotted line) (A). Cisplatin toxicity in A2780 and A2780cis cells alone or upon incubation with non-toxic 5 µM DJ-1 inhibitor (pEC_{50}, mean ± SEM, n = 5-6).

Considering that the knockdown of DJ-1 in both A2780 and A2780cis cells was successful (decrease in expression by 80% ($p < 0.0001$) and 65% ($p = 0.0005$), respectively, Figure 4.44A), the absence of any changes in sensitivity to cisplatin after knockdown was unexpected (Figure 4.44B).
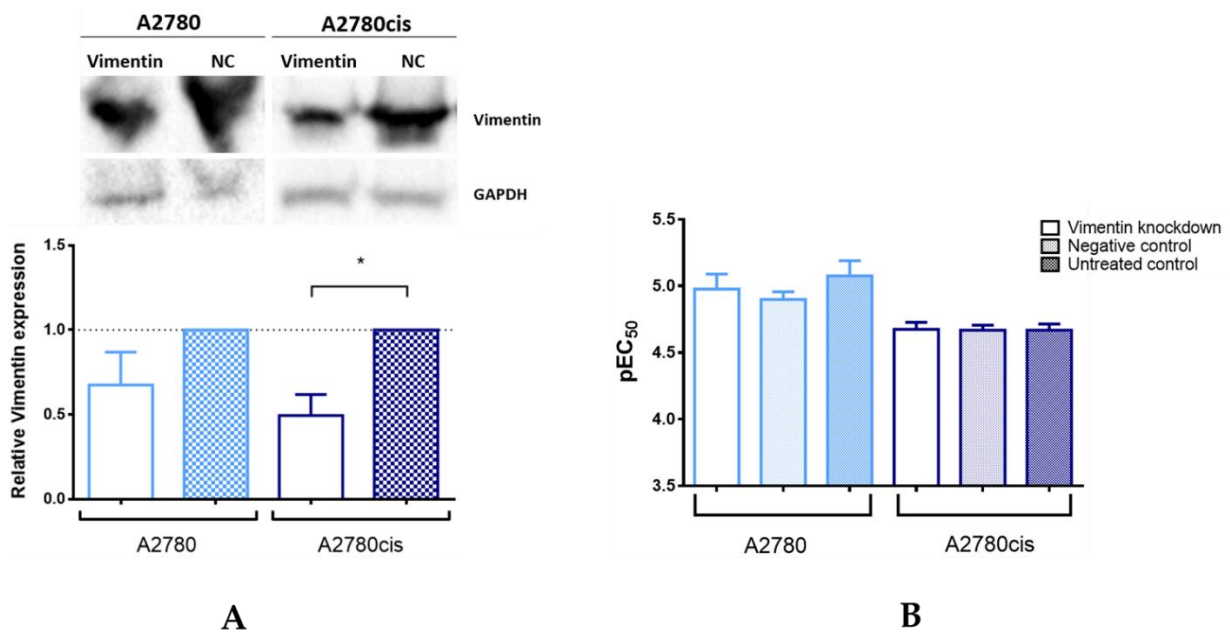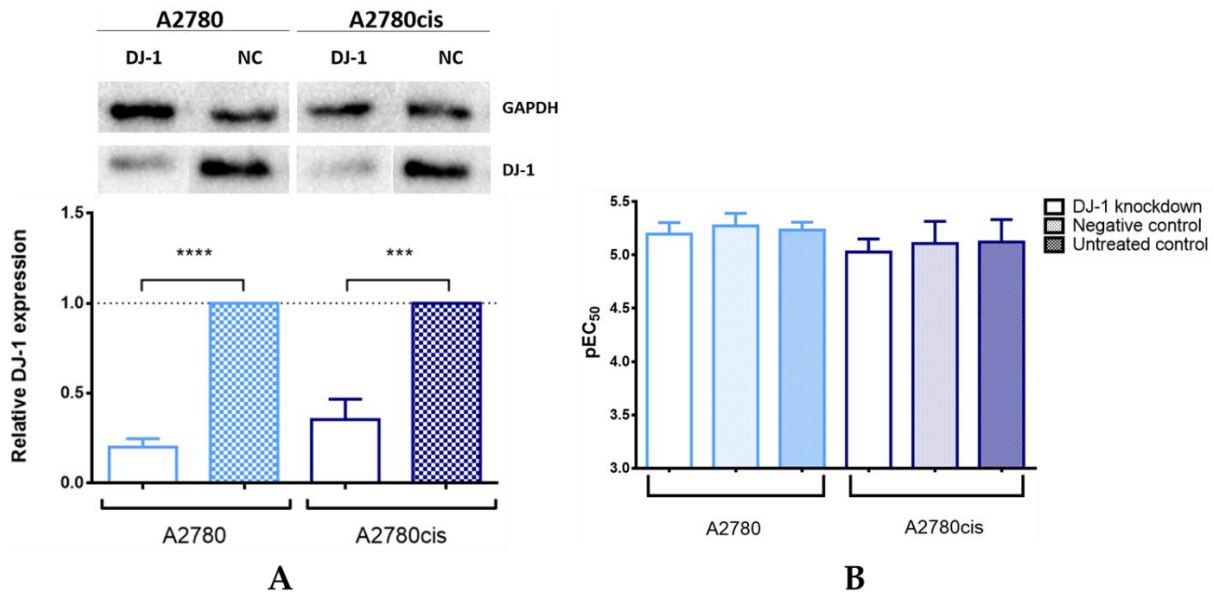
Figure 4.44 Representative Western Blots and densitometric quantification of protein expression after treatment with specific siRNA for DJ-1 and NC siRNA in A2780 and A2780cis cells. GAPDH served as a loading control (mean ± SEM, n = 4-5) (A). Cisplatin cytotoxicity in A2780 and A2780cis cells after DJ-1 knockdown, prior treatment with NC siRNA or no pre-treatment (pEC_{50}, mean ± SEM, n = 5-6) (B). ***, $p < 0.001$; ****, $p < 0.0001$.

4.3.4   Growth Factor Receptor-Bound Protein 2

Two inhibitors of Grb2 were evaluated, inhibitor A and inhibitor B, both developed by Simister at al. (Chapter 3.1.1, [163]). Non-toxic concentrations for further experiments were selected based on prior cytotoxicity testing of the inhibitors alone: 1 µM for inhibitor A (EC_{50}: HCT-8 cells, 9.15 µM; HCT-8ox cells, 2.88 µM) and 50 µM for inhibitor B (EC_{50}: HCT-8 cells, 169.60 µM; HCT-8ox cells, 86.66 µM, Figure 4.45).
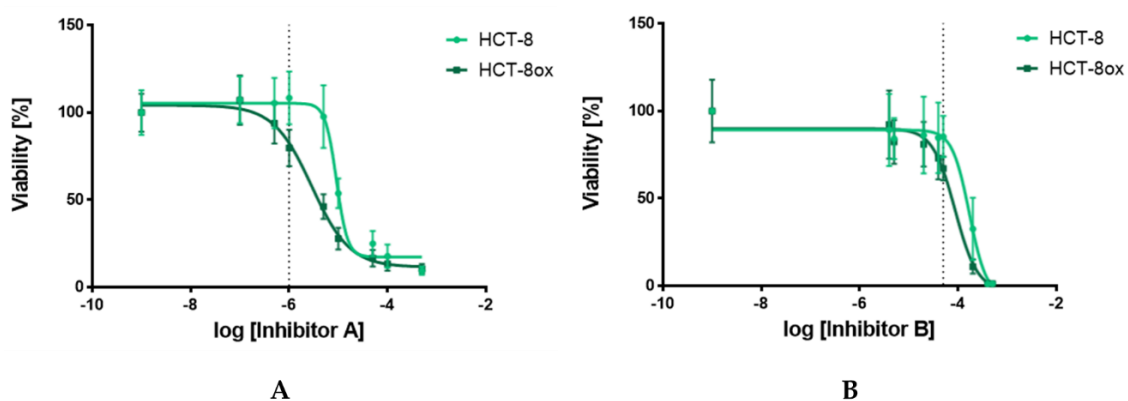
Figure 4.45 Cell viability of HCT-8 and HCT-8ox cells (mean ± SEM, n = 3) after treatment with Grb2 inhibitor A (A) or Grb2 inhibitor B (B) and determination of the non-toxic concentration (dotted lines).

There were no significant alterations in cell sensitivity to cisplatin upon co-incubation with any of the two inhibitors (Figure 4.46A). As oxaliplatin was concerned, inhibitor A did not affect cell sensitivity to the drug, whereas the combination with inhibitor B

resulted in loss of sensitivity in HCT-8 cells (EC_{50} increased from 2.17 µM to 5.43 µM, p = 0.0061) but not in the oxaliplatin-resistant HCT-8ox cell line (Figure 4.46B).
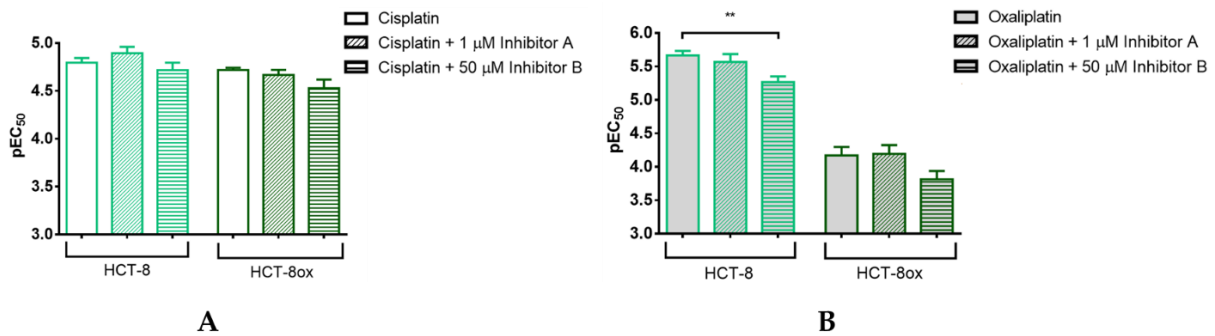
Figure 4.46 Cisplatin (A) and oxaliplatin (B) cytotoxicity in HCT-8 and HCT-8ox cells alone or upon co-incubation with either 1 µM inhibitor A or 50 µM inhibitor B (mean ± SEM, n = 5-6). **, p < 0.01.

The amount of Grb2 after knockdown decreased by 48% (p = 0.0005) in HCT-8 and by 13% in HCT-8ox cells (Figure 4.47A). This reduction of Grb2 levels had no effect on either cisplatin or oxaliplatin sensitivity in both cell lines after Grb2 knockdown (Figure 4.47B,C).
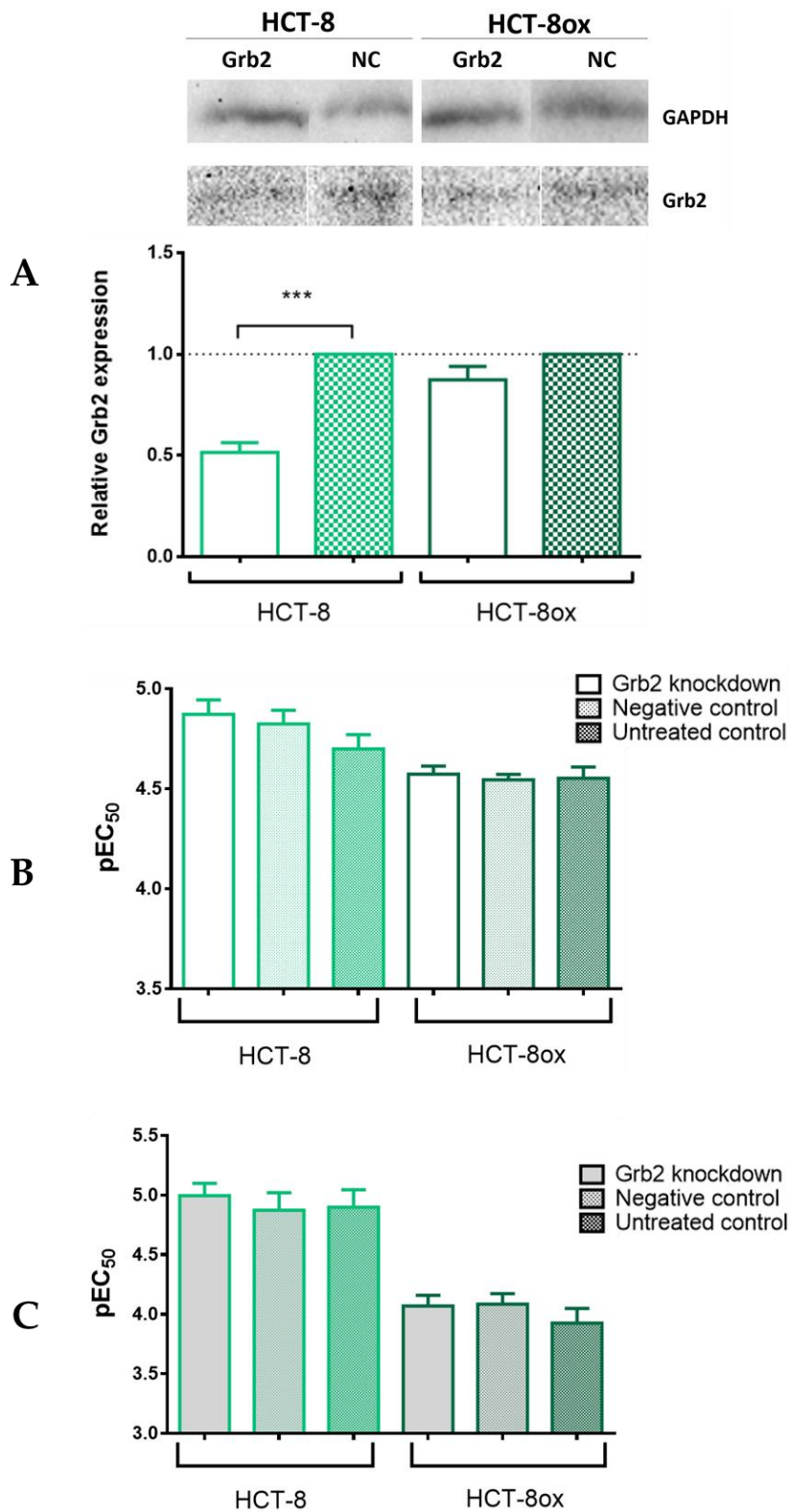
Figure 4.47 Representative Western Blots and densitometric quantification of protein expression after treatment with specific and NC siRNA for Grb2 in HCT-8 and HCT-8ox cells. GAPDH served as a loading control (mean ± SEM, n = 3) (A). Cisplatin (B) and oxaliplatin (C) cytotoxicity in HCT-8 and HCT-8ox cells after Grb2 knockdown, prior treatment with NC siRNA or no pre-treatment (pEC$_{50}$, mean ± SEM, n = 3-6). ***, p < 0.001.

5   Discussion

5.1   Approaches to Target Identification

With the aim of determining new biomarkers and novel targets of cancer chemotherapy in mind, several proteomic approaches have been employed to identify putative selective and non-selective protein binding partners of various drugs so far. Amongst others, (two-dimensional) gel electrophoresis and copper-catalyzed azide-alkyne cycloaddition, followed by protein identification via MS analysis have been used. Generally, the overall objective is to develop facile and rapid methods that enable non-targeted, i.e. without prior knowledge of potential targets, proteomic analysis and thereby allow a broad identification of cellular binding partners of drugs [164]. This way, specific, that are kinases such as EGFR, and unspecific intracellular protein targets of covalent kinase inhibitors could be detected [165]. Applying alkynylated variants of PF-6274484 and ibrutinib to human cancer cells with subsequent reaction with an azide-rhodamine reporter tag under CuAAC conditions, followed by SDS-PAGE and imaging of in-gel fluorescence allowed to determine a concentration-dependent specificity of the probes. Their high concentrations correlated with substantial proteome interaction, which in turn resulted in kinase inhibition-independent cytotoxicity. A similar approach was introduced by Chen et al., who proposed labeling of alkynylated analogs of kinase inhibitors with biotin-azo-azides in order to enrich binding partners of irreversible kinase inhibitors via subsequent reaction of biotin with streptavidin resins [166]. In another study, an alkyne-tagged analog of antitumor antibiotic duocarmycin was investigated, binding partners of which in lung cancer cells were purified from the sample by binding to rhodamine-biotin-azide and subsequent incubation with avidin beads. Identification was performed after gel electrophoretic separation via MS [167]. This procedure revealed aldehyde dehydrogenase 1 family, member A1 (ALDH1 A1) as a previously unknown binding partner.

Even though, platinum drugs are very commonly applied in many treatment schemes and have been approved for decades, a comprehensive understanding of cytoplasmic binding of Pt(II) complexes, such as cisplatin, is still lacking [168]. This is in part due to proportionately relatively few studies on the identification of intracellular platinum binding partners. Nevertheless, utilizing an azide-appended derivative of picoplatin, the working group of Prof. De Rose, University of Oregon, USA demonstrated binding to DNA and RNA oligonucleotides as well as feasibility of subsequent click reaction

with an alkyne fluorophore in vitro and in situ [168,169]. The same research group also tested a clickable alkyne-modified cis-diamine Pt(II) species and showed its binding to a DNA hairpin in vitro [118]. Interestingly, in this setting the Pt-bound DNA was revealed only upon click conjugation, as unreacted 'turn-on fluorophore' dansyl-azide is nonfluorescent. Furthermore, the modification of platinum-acridine compounds with an azide moiety was proven to be suitable for monitoring DNA binding in post-labeling experiments with Alexa Fluor 488-alkyne in vitro and also when applied to whole lung cancer cells [170]. Here, the fluorescence signal could be tracked during mitosis and interphase and it could be shown that the azide-appended compound accumulated in the nucleus and especially in the nucleolus. Accumulation in the nucleus was also shown by applying pre-tagged fluorescent platinum compounds to cancer cells. Tested in human osteosarcoma cells, CFDA-cisplatin accumulated in the nucleus 2-3 hours after treatment [171]. Considering platinum binding to intracellular proteins, Moghaddam et al. used BSA as a simple model protein for exploring the general ability of an azide-containing cisplatin analog to bind to proteins and participate in post-treatment labelling with an alkyne-tagged fluorophore [172]. In further studies, cisplatin binding was evaluated after separate incubation of standard proteins such as human serum albumin (HSA), myoglobin (MYO) and cytochrome c (CYT C) with the drug and in kidney tissue from a rat, which was previously treated with a monodose of cisplatin [173,174]. Here, approaches included separation by gel electrophoresis, by the unique method of OFFGEL-IEF, by size exclusion chromatography followed by laser ablation inductively coupled MS (LA-ICP-MS) and the final binding site identification by ESI-coupled Tandem Mass Spectrometry (ESI-MS/MS) in both cases [173,174]. The application of fluorescein-cisplatin (F-DDP) in ovarian cancer cells allowed detection of a substantial degree of colocalization between the compound and copper efflux transporter ATP7A [175]. As binding to this transporter was linked to platinum drug resistance, the result suggested a possibility of applying F-DDP for the detection of relevant intracellular binding partners [176,177]. While most of the above-mentioned conclusions were based on in vitro-experiments and/or only proved the general applicability of the analogs, Cunningham et al. made an effort to not only identify cisplatin protein binding partners in *Saccaromyces cerevisae*, but also to partly validate them by investigating how cisplatin affects the protein's function [178]. However, they only confirmed protein-platinum binding in vitro using recombinant protein, without further assessment of the protein's relevance on cytotoxicity. In general, labelling of an

isolated protein is likely to be biased as highly reactive probes bind to almost any protein in such an artificial environment [179]. Furthermore, the significance of investigation of anticancer drugs in yeast cells is questionable. In contrast, the combination of treatment of ovarian cancer cells with CFDA-cisplatin and protein separation by two-dimensional gel electrophoresis first enabled the identification of intracellular cisplatin-protein adducts via MS [113,114]. This was then followed by evaluation of relevance of several binding partners in the context of cisplatin resistance, amongst others PDIA1 and glucose-regulated protein 78 kDa (GRP78) [115,180].

Since conclusions on the effects of active substances and their analogs are the most reliable and informative if the results are obtained in biologically relevant settings, previously described, protocols of two-dimensional gel electrophoretic and CuAAC approaches appeared promising and were applied to living cancer cells to gain an idea of cisplatin binding to proteins in cellular context. These protocols were optimized to draw further conclusions about the influence of cisplatin and its protein binding patterns regarding intrinsic and acquired resistance. Where reasonable, protocols were adjusted to obtain even more easily applicable, faster and well reproducible strategies. All experiments were performed in the ovarian cancer cell line A2780 and the cisplatin-resistant subline A2780cis along with the colorectal cancer cell line HCT-8 and its oxaliplatin-resistant variant HCT-8ox. These two entities are of particular interest, since cisplatin is used in ovarian cancer treatment with good primary response rates, whereas colorectal cancer is intrinsically resistant to this drug [55,181]. As it is impossible to visually track unmodified cisplatin in the cell or determine its localization, cisplatin derivatives, modified according to the method, were used.

5.1.1 Protein Detection and Identification Based on Two-Dimensional Gel Electrophoresis

Ever since the first introduction of 2D gel electrophoresis by O'Farrell and colleagues in 1975 [182], up to now, it has mostly been used to analyze differences in protein expression of different tissues with or without exposure to certain treatments, e.g. pathological vs. normal or sensitive vs. resistant cells. In such experiments, the two-dimensional differential in-gel electrophoresis (2D-DIGE) approach usually is the method of choice. By minimally labeling up to three different samples with fluorescent dyes, it is possible to run and compare them simultaneously and therefore detect

biological variations. This way, the DIGE approach has proven to be a robust tool for biomarker discovery [183]. Unfortunately, this well-established procedure does not allow for the identification of binding partners of drugs. The aforementioned protocols of Kotz et al. were the first attempts to detect binding partners using a fluorophore-tagged drug (CFDA-cisplatin) and two-dimensional gel electrophoresis [113,114]. In contrast to the procedure presented in this thesis, A2780 cells treated with the cisplatin analog were examined for cytosolic protein binding partners in acidic and basic pH ranges in two independent projects. Even though the processing in a narrower pH range can generally increase the resolution of the separation and is definitely preferable for more specialized and detailed research [184], dealing with several separate IPG strips always means a considerable additional effort. With the aim of developing or applying universally applicable methods that can also be performed quickly, this was considered inconvenient in the present project. For this reason, IPG strips ranging from pH 3-10 were implemented. Since the higher concentrated acidic proteins require more space than the basic ones [125], the strips applied were nonlinear with an extended acid range. It has to be noted that a direct comparison of the protein binding partners detected did not show an increased yield of hits when dividing the identification process into two separate pH ranges (pH 4-7 and pH 6-10) vs. the broad range used in this project (pH 3-10 nonlinear) [113,114,185]. While the previous projects identified a total of 14 putative binding partners, the hits could be increased to 22 proteins in the same cell line (A2780, with an overlap of 5 proteins). However, this may also be due to the use of another tag instead of CFDA. The latter has in the meantime been shown to be an inferior model of the parent drug in comparison to the fluorescent derivative featuring the BODIPY dye (BODIPY-cisplatin) employed here, especially with regard to cytotoxicity, cellular accumulation but also to imaging properties [116,186,187]. Amongst others, BODIPY has the convenient properties of being extremely photostable, offering a high fluorescence yield and providing definite absorption and emission spectra [188,189]. Bulky fluorophores in general have the issue to influence the properties of the compound it is bound to, be it in terms of cellular uptake, organelle specificity or mechanism of action [170,190,191]. Even though BODIPY-cisplatin was less cytotoxic than the parent drug, cell lines with both intrinsic and acquired cisplatin resistance were cross-resistant to BODIPY-cisplatin, corresponding to the activity profile of cisplatin itself. These results, in combination with the findings regarding cellular distribution, suggested that BODIPY-

cisplatin mimics the biological behavior of the parent drug in the cell lines studied satisfactorily.

Also, the resolution and separation efficiency even in a 7 cm pH 3-10 range could be considerably improved by adapting the protocol as described in Chapter 4.1.5. The use of a gradient gel and the replacement of DTT by HED alone resulted in visible progress in spot discrimination. Notwithstanding, it is mandatory to fractionize the sample before applying it to 2D gel electrophoresis, especially when working with short IPG strips. Estimating that the human proteome comprises at least 20,000 proteins [192], reduction of complexity is essential if the feasibility of the method is to be ensured and any reliable conclusion is to be drawn from the analysis. Still, it must not result in an excessive number of fractions, as this would dramatically increase both effort and expenditure of time [193]. Moreover, the influence of DTT on the fluorescence yield when using fluorescently tagged cisplatin analogs could not be neglected. When using DTT in the solubilization buffer, apparent loss of fluorescence intensity was easily detected. The reason for this could be the high reactivity of platinum towards S-donor molecules, which under certain circumstances could destroy cisplatin-protein bonds [40,194]. This would mean that the loss of fluorescence could be explained not by extinction, but by reduced presence of the BODIPY-cisplatin-protein adducts. So even though a tendency towards poorer separation was seen when using HED instead of DTT in the solubilization of the sample, fluorescence could be detected. After consideration, a clearly visible detection BODIPY-cisplatin was conclusively preferred to the slightly poorer separation capacity. In the future experiments, the latter could be compensated by increasing the separation distance by using longer IPG strips and larger separation gels [195]. This would also help to cope with the negative aspects of wide pH ranges [196], but, of course, would also result in a loss of handling simplicity and rapidity of the method. Most desirable would be the application of horizontal, large gels, which would facilitate handling by far and does not require intricate merging of IPG strip and separation gel with subsequent sealing with stacking gel. Additionally, the amount of buffer volumes would be reduced and with a suitable apparatus, up to 4 gels could be run in parallel, thus increasing efficiency [197].

The superimposition of two or more 2D gel images is often difficult, mostly due to experimental variability, such as changes of gel size after Coomassie staining due to hydration, and usually requires the determination of so-called landmarking spots,

which are manually defined before the computer-aided image overlay [198]. This initially guided pairing of spots serves as a reference and makes warping of the gels much easier. Especially when the experimental setting results in a fluorescence image where only a small fraction of the whole protein load is visualized, the definition of protein spots that can be superimposed with certainty is indispensable. For this general purpose, Ackermann et al. introduced a simultaneous on-gel reference protein spot grid that was composed of proteins labeled fluorescently making it possible to image both reference proteins and sample proteins at the same time [159]. Yet, sequential imaging of BODIPY-cisplatin and a Sci5-labeled grid did not yield satisfactory results as there was a considerable bleed-through. Conversely, labelling of the total protein amount using Sci5 to identify reference spots and the subsequent elimination of additional labelling of the whole sample proved to be very feasible and allowed the detection of spots positive for both fluorescence and protein staining. These were then cut out and subsequently a total of 41 proteins were identified as potential binding partners via LC-MS analysis by Dr. Marc Sylvester and colleagues. Unfortunately, despite seemingly good separation and unambiguous superimposition of protein staining and fluorescence signals, identification did not yield single protein hits. This is actually a well-known problem, which is often neglected in practice and can mostly be attributed to narrow separation distances and/or pH gradients. Yet, even in 18x20 cm wide gels using a pH 3-10 gradient, only 32% of proteins identified were singlets [199]. Moreover, the fact that Pt-peptides could not be detected in the MS analysis also complicated a simple, direct identification of binding partners. One reason for this could be low relative abundance of Pt-bound peptides in comparison to unmodified peptides [113,194]. Apart from this, as already mentioned, the use of DTT, but also other thiol-containing reagents or ammonium bicarbonate buffer can negatively affect the binding of platinum to the proteins [40,173]. Nevertheless, due to the use of a parallelly running protein standard and a subdivision of the gel into different pH ranges, protein hits could very well be divided into plausible and implausible results, thus enabling definite protein identification in nearly every excised spot. Interestingly, previous works investigated other non-thiol-containing reducing agents in order to ensure good protein coverage in MS analysis without sacrificing preservation of Pt-protein bonds, since working under reducing conditions using DTT seems to cleave the platinum-protein binding to some extent and concluded that the detection of Pt-peptides probably

depends on the amount of platinum adducts present in the sample, but also on the strength of the binding [173].

In general, it must be taken into account that identification of highly expressed proteins is more likely given the detection limit of colloidal Coomassie and the potential loss of lower expressed proteins throughout the identification process [200]. Thus, the results have to be evaluated taking into account this limitation.

Needless to say, it is desirable to run a method and interpret results as objective as possible. Therefore, despite successful protein identification using the 2D protocol described above, it appeared beneficial to extend the method by an immunoprecipitation step. This way, exclusively binding partners of BODIPY-cisplatin would be screened and enriched prior to 2D gel electrophoresis by omitting fluorescence detection and consequently, this step would lead to simplification of downstream-analysis by MS. In doing so, the bias of the detection of mostly abundant proteins would also be eliminated, since immunoprecipitation, especially when applying magnetic beads, has been proven to be highly sensitive and capable of concentrating endogenous proteins from complex mixtures [145].

Incubation of both the BSA control and the lysate of cells treated with BODIPY-cisplatin with the anti-BODIPY antibody and subsequent exposure to magnetic beads initially revealed positive results by displaying minimally different protein elution patterns in treated and untreated samples. Nonetheless, the indirect immunoprecipitation approach proved unsuitable due to the co-elution of the antibody fragments, which obstructed parts of the protein stained images. Hence, a switch of the procedure to direct immunoprecipitation, where crosslinking of the beads with the antibody is done first, was required. After crosslinking with BS^3, leakage of antibody fragments could be prevented. Unfortunately, no difference between eluate and washing fraction could be detected in the lysates as well as the BSA control, which showed a very clearly visible band before and was now difficult to distinguish against the background. This can be attributed to crosslinking, since BS^3 is known to reduce the efficiency of binding of target proteins [145]. Replacing BS^3 with another crosslinker, such as DMP, was not an option, though, as this reagent was observed to produce significantly higher background binding [145], which would make subsequent 2D gel electrophoresis impracticable. In the future, however, other crosslinking agents could be taken into consideration and/or the amount of crosslinker used should be adjusted properly,

since, if used in excess, its reaction with too many primary amines of antibodies may lead to loss of antigen-binding capabilities of the same [143]. When using higher amounts of protein, extending the incubation time and lowering the temperature to 4 °C, different elution pattern of treated sample and negative control could be detected. This was the case for both the cell lysate sample as well as the BSA control. However, the results could not be reproduced in the second experiment. Here, changes in the quantity of the antibody could be considered. It would also be useful to clarify, whether the antibody acts too unspecifically or whether a general application in immunoprecipitation is possible. So far, the anti-BODIPY antibody has not been validated for this method, but, for lack of alternatives and similar objectives in published articles using this antibody, the application was still worth a try. Last but not least, there are many different elution buffers that all seem to result in variable, target protein-dependent and often poor elution [145]. When, as in this project, target proteins are unknown, optimizing an immunoprecipitation protocol to fit the purpose requires a lot of time and effort. Therefore, it must unfortunately be summarized that a great deal of adaptation would be needed for the immunoprecipitation method to efficiently facilitate protein identification.

5.1.2   Protein Identification Based on CuAAC

Bulky, massive fluorophores tagged to small molecules in order to visualize their localization and behavior in cells are known to affect the characteristic features of the parent molecules in one way or another, as mentioned before. Two-step protocols, where the compounds of interest are functionalized with very small reactive handles and actual labeling, with fluorophores for instance, takes place in an independent, second step are thus becoming increasingly popular [155,179]. In CuAAC approaches, terminal azides or alkynes are incorporated into the compound of interest with the aim of preserving as much of original properties as possible. This, of course, includes the reduction of perturbation of target binding and this way, application in whole cells is suggested to reflect the mode of action more appropriately in comparison to employing pre-tagged fluorescent drug analogs [179,190,201]. This applies to live cell imaging as well as to visualization after cell lysis [179,190]. For instance, comparing the subcellular localization of a platinum-azide with a pre-tethered fluorescent derivative, cisplatin-azide showed significantly higher fluorescence in the chromatin (relative to that observed in the nucleolus and cytosol) [201]. In line with this, the biological activity of

both the azide- and alkyne-cisplatin derivatives used in this project was also found to mimic the parent compound very well. Both displayed very similar cytotoxicity in cisplatin-sensitive ovarian cancer cells and were found cross-resistant in cisplatin-resistant A2780cis cells as well as in both intrinsically resistant colorectal cancer cell lines. Cisplatin-azide was more active than the alkyne-tagged complex, thus, being closer to the parent compound in biological behavior. This can be attributed to a significantly shorter tag.

In general, the application of azide and alkyne derivatives is considered not equally fruitful. By far the biggest problem with the use of cisplatin-alkynes is that this combination can lead to Pt(II)-catalyzed side reactions such as hydration or hydroamination [169,191]. Besides, alkynes are also prone to react with other alkynes, thus rendering the terminal moieties unavailable for CuAAC [202]. The possibility of such undesirable side reactions of Pt-alkynes, in combination with the somewhat higher cytotoxicity of the azide-functionalized analog, led to an initial focus on the latter. However, it turned out that CuAAC with the Pt-azide analog showed very high background binding and no differences in binding patterns in the cell sample and negative control could be detected. As this was attributed to unspecific binding of the alkyne-tagged fluorophore to cysteine-containing proteins in previous studies in HeLa and macrophage cells [155,156], lower concentrations of the alkyne reagent were likely to solve that issue. Indeed, background fluorescence was reduced, but labeling pattern of the sample and control were still indistinguishable. Therefore, the samples were pre-treated with IAA to alkylate free thiols and, thus, prevent any unspecific binding of BODIPY-alkyne to cysteine-containing proteins [155]. Unfortunately, this measure was only successful with the BSA control samples. Since the utilization of azide-tagged fluorophores was reported to give lower unspecific binding [157], cells were then treated with cisplatin-alkyne with subsequent visualization using BODIPY-azide.

Even though some alkynes were suspected to be involved in side reactions resulting in the blocking of the CuAAC, the Pt-alkyne employed in this project was used in a similar context and showed no disadvantageous effects [190]. In fact, it has previously been compared to its azide-bearing counterpart and proven to bind to DNA in similar yields [191]. In comparison to azide analogs, alkynes even possess the benefit of increased lipophilicity, which might positively influence its accumulation and reactivity in the cell [191]. Nonetheless, although slightly less unspecific binding may have

occurred after subsequent treatment with the BODIPY-azide, the reaction of azides with thiols also seemed to be of significance and was investigated before [158]. For this reason, a pre-treatment with IAA was carried out here as well, which in this case resulted in a considerably lower background binding and revealed a different binding pattern of the sample and control. However, the success achieved is of secondary importance, since an undisputed identification of the binding partners after one-dimensional electrophoretic separation is impossible. Admittedly, for a separation using two-dimensional gel electrophoresis the background binding is too prominent, even after pre-treatment with IAA, and although pre-treatment with the parent compound cisplatin would allow to discriminate between specific and unspecific binding, no real advantage in this case would be expected. This way, in addition to the treated sample, images of a negative control and subsequent overlay would be necessary. Considering the complexity of superimposing two 2D-gel images, the results of an overlay of 8 images (each treatment/control with corresponding Coomassie stained image) would certainly not be very reliable. Additionally, this preliminary result seemed to be rather cell line-specific, as it could be transferred well to A2780cis cells but not to HCT-8 cells.

Since both, azide as well as alkyne moieties, are obviously reactive towards thiols, however, the question of whether the compounds bind to the proteins exclusively through cisplatin or also through the azide/alkyne groups arises, as the binding partners are possibly the same. It is therefore feasible that the azides or alkynes bind to the proteins and thus block actual binding partners of cisplatin, which in turn cannot be detected, as CuAAC cannot take place (false negatives). Therefore, the application of CuAAC may not be suitable for the objective of identifying cisplatin binding partners, due to the similar binding behavior of the platinum core and tags and has to be investigated in more detail. To the very least, the method is probably hard to reproduce due to this problem, as in each run there is presumably no confidence whether cisplatin or the tag site binds to the protein. The reason why Cunningham et al., in contrast to in this project, were able to show quite good, clear results with little background binding may be due to the choice of an organism [178]. Proteins in yeast only have about half as many cysteines as proteins in mammalian cells [203], which could explain the absence of background binding in yeast. Still, it would not prevent the possibility of identification of false negative binding partners due to blocked CuAAC.

5.1.3   Comparison of Protein Detection Methods

Considering the advantages and disadvantages of the methods used here, but also the conclusion drawn from the results, it can be summarized that at this stage the identification of cisplatin binding partners can best be achieved by a combination of a fluorescently labeled cisplatin analog and 2D gel electrophoresis. This is true even though the azide- and alkyne-tagged analogs used for CuAAC are more similar to the parent compound than the fluorescent derivative and CuAAC also tends to be more suitable for high-throughput approaches [190]. Nevertheless, while the cytotoxicity caused by the catalyzing copper is not a problem in the treatment of cell lysates, it restricts the tracking of the sample in living cells and in such cases similar methods are needed, which quite likely have to be established first. Also, the high expectations, built up by previous literature results could not be fulfilled. While a high background binding may be negligible if the target protein is known, it is pretty much an exclusion criterion in an open approach. With the goal of a simple, rapid and highly sensitive identification of potential binding partners, a cell-specific outcome is also a negative aspect. Last but not least, other and yet unexamined questions have been raised such as potentially similar binding behavior of the platinum core and tags which call the general feasibility of the method in terms of its objectives into question and thus drastically reduce its value. In comparison, two-dimensional gel electrophoresis requires relatively much practice and dexterity and, with an average experimental time of almost 5 days, takes relatively long (as compared to CuAAC with approximately 2 days). However, once the method is established, the execution does not present any major difficulties and the results are well reproducible and easy to interpret. The novel idea to extend the 2D gel electrophoresis protocol by an immunoprecipitation of BODIPY-cisplatin labelled proteins, unfortunately turned out to be challenging and calls for extensive adaptation of the standard protocols for the purpose investigated here. Nevertheless, this approach is still very promising and could really improve identification of drug binding partners via 2D gel electrophoresis.

Finally, it should be pointed out that although results from in vitro experiments can provide important information about certain processes and structures within the cells, it is just as important to transfer them into corresponding in vivo models. Especially with regard to findings on drug delivery and pharmacokinetic characteristics, even more realistic information can be obtained from the latter.

5.2   Impact of Identified Binding Partners on Platinum Sensitivity

Interestingly, ovarian cancer cells appeared to be more prone to intracellular protein-cisplatin interactions than the colorectal cancer cell lines employed. Moreover, sensitive A2780 ovarian cancer cells revealed more binding partners than its resistant counterpart cell line A2780cis. Despite all open questions concerning the usefulness of the method, this was also the case after application of CuAAC. Defects in cellular uptake of cisplatin are likely to account for this difference. Reduced cisplatin accumulation in A2780cis cells compared to the parent sensitive cell line is well documented [204]. According to earlier results, HCT-8 colorectal cancer cells accumulated significantly less cisplatin than A2780 ovarian cancer cells after 2 hours incubation with 100 µM platinum drug (HCT-8 cells: 10.47 ± 0.88 ng Pt/10^6 cells, mean $\pm$ SEM, n = 6, [205]; A2780 cells: 17.68 ± 0.23 ng Pt/10^6 cells, mean $\pm$ SEM, n = 3, [206]; $p < 0.001$, unpaired t-test). Nevertheless, the fate of the drug in the cytosol is also of great importance. For the ovarian carcinoma cell line pair used in this study, it was previously shown that whereas cisplatin uptake is reduced approximately two-fold compared to the parent cell line, DNA platination is circa five times lower [186]. As mentioned at the beginning, cytosolic proteins probably play a greater role in this process. Here, the results clearly show that some binding partners are shared, both between sensitive and resistant, but also between cells with acquired and intrinsic resistance, while the others differ between cell lines. It should be noted that several of the identified proteins have already been reported as binding partners, e.g. vimentin, protein disulfide-isomerases PDIA1, PDIA3 and PDIA6, constitutive photomorphogenesis 9 (COP9) signalosome complex subunit 4, Elongation factor 1 alpha-1 (EF1A1) in different cell lines, which further substantiates the accuracy of the results obtained here [110,113,114,178].

In order to assess the relevance of BODIPY-cisplatin binding partners on cell sensitivity to cisplatin in ovarian cancer and colorectal cancer cells, vimentin, GSTP1, DJ-1 and Grb2 were chosen as the most interesting proteins for further characterization as they have been described earlier as differentially expressed and/or in connection with drug resistance in general [85,207–213], but evidence in the context of cisplatin activity in the cell lines used in this project is rather sparse. Although not pursued further in the course of this project, there are several more proteins that should be investigated in future studies. In particular, PCNA and COP9 signalosome complex subunit 4 should be mentioned with regard to a possible connection to an acquired resistance of ovarian

cancer cells and, amongst others, transaldolase and apolipoprotein L2, which might be essential for the mode of action of cisplatin as they have been identified in A2780, but not in A2780cis cells. With regard to the further characterization of intrinsic resistance mechanisms, the investigation of phoshoglucomutase-2 should be considered, since it was identified exclusively in the intrinsically resistant colorectal cancer cell lines. Additionally, an in vivo investigation should be carried out to assess the impact of the protein binding partners and, thus, the clinical significance of the interactions more realistically.

5.2.1 Vimentin

Vimentin is an interfilament protein that is associated with multiple roles in various illnesses, including Crohn's disease, rheumatoid arthritis and cancer [207]. In the latter, it is mainly involved in the epithelial-mesenchymal transition (EMT) process, which is a hallmark of metastatic tumor cells. Cells undergoing EMT express certain aggressive mesenchymal features, such as loss of cell-cell junctions and enhanced motility as well as invasiveness [214]. It has been shown that silencing of transforming growth factor ß1 (TGF-ß1), known to initiate EMT [215], led to the reversal of EMT to mesenchymal-epithelial transition (MET), which in turn resulted in restored sensitivity to cisplatin in lung cancer cells [216]. In cancer progression, vimentin's general role as a scaffolding protein of the cytoskeleton and canonical marker and regulator of EMT is just as important and extensively described as its ability to interfere with and mediate certain signaling pathways that are not directly linked to EMT processes, though partly intertwined [207,208,217–220]. Regarding its signaling properties, vimentin has largely been linked to the PI3K/Akt-pathway and associated with 14-3-3 protein leading to tumorigenesis, enhanced cellular migration and regulation of mitogenic signaling and apoptosis [208,218,221]. For example, it was postulated that the formation of an Akt-14-3-3-vimentin network increased multi drug resistance and invasiveness of Non-Hodgkin Lymphoma [221]. This was confirmed by experiments in cervical cancer cells and fibroblasts, where, though, aside from the interaction between Akt, 14-3-3 protein and vimentin, an additional involvement of beclin-1 was determined. Beclin-1 mediates autophagy and exerts its function as tumor suppressor protein, which is both inhibited through phosphorylation by Akt and subsequent association with 14-3-3 and vimentin. Interestingly, autophagy could be restored upon inhibition of vimentin [222]. Taken together, it can be assumed that after phosphorylation of both beclin-1 and vimentin

by Akt, a kind of complex between beclin-1, 14-3-3 and vimentin is formed, which then promotes tumorigenesis [208]. Furthermore, a connection between vimentin and ERK could be detected. It was observed that a direct interaction between vimentin and ERK first led to ERK activation and thereupon to increased transcription of vimentin in breast cancer cells [223]. Phosphorylated, thus activated, ERK kinases lead, amongst other things, to increased cell proliferation. Moreover, vimentin appears to mediate phosphorylation of EMT-inducing transcription factor Slug by ERK by protecting the latter from dephosphorylation. Phosphorylation of Slug then again results in increased expression of vimentin and Axl receptor tyrosine kinase (Axl), which appears to contribute to EMT-linked invasion [223]. Moreover, vimentin also seems to influence tumor angiogenesis. The silencing of vimentin in endothelial cells led to a decreased expression of the focal adhesion kinase (FAK), which normally complexes with vimentin and receptor for activated protein c kinase 1 (RACK1) during endothelial cell invasion for cell sprouting [220]. Vimentin also reportedly regulates the Notch signaling pathway and its angiogenetic activity by binding to the proangiogenic Jagged ligands [220]. Accordingly, vimentin appears to be upregulated in drug-resistant cancer cells of a great variety of entities and its expression generally correlates with poor survival rates [217,224,225] and metastatic spread [226]. The study of Lazarova et al. in CRC cells found that vimentin is differentially expressed depending on the metastatic state of the tumor and proposed the hypothesis that the expression of vimentin in colonic neoplastic cells may correlate with the stage of neoplastic progression and that vimentin therefore is the key factor in colonic neoplastic progression [227]. Interestingly, HCT-8 and HCT-8ox cells in this study showed negligible vimentin expression, which is in agreement with previous reports [228]. This probably explains why vimentin was not detected as a binding partner in HCT-8 and HCT-8ox cells. It therefore seems rather unlikely that vimentin expression correlates with intrinsic resistance to cisplatin in colorectal cancer.

Apart from repeated reports of an increased expression of vimentin associated with the development of resistance, the results of this work are an indication that vimentin additionally is a binding partner of cisplatin and could thus influence the sensitivity of cancer cells. As vimentin seems to be expressed in excess in resistant cancer cells, one possibility could be that most, if not all, of the applied platinum is scavenged by the protein, thus rendering the drug ineffective, while the remaining vimentin would still be able to exert its functions. There have been several attempts of pharmacological

inhibition of vimentin in cells before, yet application of Withaferin A has proved to be the most promising candidate thus far [229]. The inhibitor has demonstrated tumor- and metastasis-suppressing features and in combination with its own anti-tumor and anti-angiogenetic properties appears to be a suitable treatment also in combination with approved anti-cancer drugs [207]. However, the lack of specificity of the molecule is a drawback, which is why effects other than those triggered by vimentin inhibition cannot be ruled out [230]. Only recently discovered FiVe1, on the other hand, could be a potential improvement, as it is the inhibitor with the highest vimentin specificity so far [160,229]. Here, inhibition of vimentin by FiVe1 in ovarian cancer cells significantly sensitized both sensitive and resistant cells to cisplatin acting in a synergistic manner. Interestingly, the effect was more pronounced in the A2780cis cell line, although no differences in vimentin expression were detected between A2780 and A2780cis cells. Since fluorescence intensity was more pronounced in A2780cis cells, this suggests that BODIPY-cisplatin might bind to vimentin to a greater extent and therefore participates in the mediation of acquired resistance. After co-incubation with vimentin inhibitor FiVe1, the observed reversion of resistance could be due to the fact that vimentin was sufficiently occupied to allow the hence unbound cisplatin to bind to its target DNA. Of course, it has to be investigated further whether there really is more free platinum in the cell when combined with an inhibitor, as it is also imaginable that in this case platinum is prone to bind to other proteins. Then again, FiVe1 might even lead to an inhibition of vimentin's tumor-progressive properties. The compound has been shown to act through disorganizing and phosphorylating vimentin during metaphase leading to mitotic catastrophe [160]. Thus, it appears that FiVe1 sensitizes cells to cisplatin through interference with vimentin function. Interestingly, paclitaxel, a drug that also leads to mitotic disruption, is commonly combined with platinum drugs in clinical practice with higher overall survival and progression free survival in comparison to platinum treatment alone [231]. Overall, the results show that pharmacological inhibition of vimentin may be a valuable approach to specifically enhance sensitivity and tackle cisplatin resistance in ovarian cancer cells.

5.2.2   Glutathione-S-Transferase π 1

GSTP1 is one of the major phase II detoxification enzymes in the cytosol and is believed to play a significant role in the inactivation of drugs by conjugating them to glutathione with subsequent transportation out of the cells via e.g. membrane-bound

MRPs and P-gp efflux pumps [85,232,233]. Particularly problematic is that not only the enzyme itself but also the aforementioned efflux pumps have been found to be overexpressed in a variety of solid tumors [234]. Of note, though, is that strangely there is frequently no correlation of expression of MRPs, P-gp and GSTP1 when investigating the same sample [235,236]. Nevertheless, they have all been linked to a malignant potential and poor outcome [237,238]. In different entities, including neuroblastoma samples, high levels of GSTP1 and MRPs were suggested to correlate with reduced event-free and overall survival [239,240]. Similar results could be shown for the MDR1 gene coding for P-gp, which was described as an independent prognostic indicator of poor survival in e.g. uveal melanoma or renal clear cell carcinoma [241,242]. It should be noted that GSH itself could not be detected as a binding partner of cisplatin in this project. However, this may be due to a relatively slow reaction rate between cisplatin and GSH [243], which may have been outcompeted by more reactive thiol proteins within the two-hour incubation period. Also, the fact that GSH with a molecular weight of approximately 1 kDa is a very small peptide presents a challenge itself, as this low weight makes detection via gel electrophoresis of a sample, which is not fractionated by size, very difficult.

In addition to its function as an eliminator of exogenous substances, GSTP1 is also believed to be involved in intracellular signal transduction, which further promotes tumor survival. In this context, GSTP1 counteracts binding of apoptosis signal-regulating kinase 1 (ASK1) and TNF receptor-associated factor 2 (TRAF2) after exposure to ROS, which would ultimately lead to activation of mitogen-activated protein kinase kinase (MKK)3/4/6-p38 and MKK4/7-JNK pathways [85,234]. Their functions, in turn, are known to be manifold. Amongst others, they participate in the control of cell proliferation, differentiation and survival [244]. GSTP1 acts at multiple levels within the MAPK/JNK pathway. It is bound to JNK under normal conditions, preventing its phosphorylation and therefore inhibiting downstream signaling [85,161,234]. However, upon oxidative stress induced for instance by drug administration, GSTP1 molecules tend to dimerize and are hence unable to bind JNK. The dissociation of JNK from the complex then leads to phosphorylation of the downstream c-Jun protein and activation of pro-apoptotic, tumor-suppressive processes [85,161,234,244]. This mode of action is mimicked by GSTP1 inhibitor Ezatiostat-HCl (also referred to as TLK199), which inhibits interaction between JNK and GSTP1 through binding to the latter [161]. It is noteworthy that this inhibitor has

been granted orphan drug status by the FDA for the treatment of low- to intermediate-risk myelodysplastic syndrome in 2013 [161,245]. Oddly, the combination of the inhibitor with platinum drugs did not have any effect on sensitivity of both ovarian and colorectal cancer cells, in contrast to the results of Li et al. who could detect an enhanced sensitivity in a similar experimental setting in lung cancer cells. However, Li and colleagues used variable, partly very toxic, concentrations of Ezatiostat-HCl in a higher micromolar range [246]. Also, GSTP1 inhibition was more effective in cells where the protein was experimentally overexpressed prior to treatment with the inhibitor [246], which is a rather artificial setting and was therefore avoided in this study. Nevertheless, these results indicate that the use of Ezatiostat-HCl may be particularly promising in the case of entities that present overexpression of GSTP1. However, this effect might be cell-specific, since GSTP1 was proportionately overexpressed in HCT-8ox cells, yet no impact of co-incubation with the inhibitor could be detected.

Interestingly, a significant sensitization of both intrinsically cisplatin-resistant colorectal cancer cell lines to this drug after GSTP1-siRNA transfection was observed. This resulted in sensitivity levels comparable to those determined in the cisplatin-sensitive ovarian cancer cell line A2780. Sensitization to oxaliplatin was detected only in the HCT-8 cells and the effect was much less pronounced. On the one hand, this may be due to lower reactivity of oxaliplatin towards nucleophiles [247], therefore, compared to cisplatin, the loss of a binding partner would have less impact with respect to reaction rate and corresponding amount of free drug remaining in the cytosol. On the other hand, several working groups demonstrated that conjugation to glutathione plays only a minor role in the development of cisplatin resistance and that intracellular signaling is much more significant [100,248]. Chen et al. found that especially the JNK/p38 pathway mentioned above was involved in sensitization of mesothelioma cells to cisplatin upon GSTP1 knockdown, whereas the pathway seemed to be irrelevant for the effect of GSTP1 silencing on cell sensitivity to oxaliplatin [249]. However, no difference in cisplatin cytotoxicity after transfection of the ovarian cancer cells with GSTP1 siRNA could not observed, in contrast to previous reports [250]. This can be attributed to the relatively low transfection efficacy of the A2780 cell line pair, which appeared to be hard to transfect also in previous studies [251].

Intriguing and therefore worth highlighting is the recent finding that ERK signaling apparently leads to a transcriptional activation of GSTP1, which underlies cisplatin

resistance in lung cancer stem cells [246]. In addition, another study demonstrated sensitization of ovarian cancer cells against cisplatin by downregulation of ERK and upregulation of p38 [252]. Combined with the above-mentioned implications of GSTP1 in the p38 signaling pathway and the findings that vimentin is commonly abundant in resistant cells and can lead to ERK activation, this seems to be a very interesting starting point for future attempts to address the multifactorial mechanisms of resistance and combine vimentin inhibitor FiVe1 with a GSTP1 inhibitor.

5.2.3   Protein/Nucleic Acid Deglycase DJ-1

Originally identified as a putative oncogene, DJ-1 is involved in oxidative stress, proliferation and growth of various cancers [210]. In non-small cell lung cancer (NSCLC) cells and also in tissue samples of lung cancer patients an increased expression of the protein could be detected, which seemed to correlate with lymphatic metastases [253]. The functions of DJ-1 thereby are manifold [210]. The most commonly described are interactions with tumor suppressors phosphatase and tensin homolog (PTEN) and p53. The interaction with the tumor suppressor PTEN initiates an activation of the PI3K/Akt pathway, which results in increased cell proliferation and migration [254], as already mentioned before. Apart from this, DJ-1 binds to p53 and thus prevents its translocation into the nucleus and as a consequence the initiation of the pro-apoptotic p53/Bax/caspase pathway [255]. Moreover, DJ-1 is also involved in the oxidative stress response and, amongst other things, destabilizes the nuclear factor E2-related factor 2 (NRF2)/Kelch-like ECH-associated protein 1 (Keap1) complex, which in turn enables the transcription factor NRF2 to stimulate the expression of antioxidative proteins [256]. Thus, DJ-1 has been repeatedly associated with the development of resistance in tumor cells.

It was shown that DJ-1 was differentially expressed in resistant small-cell lung cancer (SCLC) cells on both mRNA and protein levels and that downregulation of DJ-1 led to sensitization to adriamycin, etoposide and cisplatin [257]. Also, in NSCLC cells DJ-1 could be identified as a cisplatin resistance marker using 2D gel electrophoresis, and silencing led to enhanced cisplatin cytotoxicity [258]. Another study showed that a knockdown of DJ-1 led to an increase in cisplatin-induced apoptosis in renal cell carcinoma [259]. While these studies reported increased sensitivity to cisplatin and other chemotherapeutics after DJ-1 knockdown, only few DJ-1 inhibitors have been discovered so far [162]. Even though enzymatic half maximal inhibitory concentration

(IC_{50}) of 0.28 µM of DJ-1 inhibitor as determined by Tashiro et al. [162] was exceeded in the co-incubation experiments in this project, the compound did not influence cisplatin sensitivity of A2780 and A2780cis cells. Only a tendency towards sensitization could be observed in the A2780 cells when treated with cisplatin and the inhibitor simultaneously. It is quite possible that IC_{50} values determined through measurements of enzymatic activity do not correspond to the inhibitory potency in cell-based assays [260]. Unexpectedly, the results of the knockdown experiments also differ from the from literature reports. Schumann et al. demonstrated that DJ-1 knockdown circumvented resistance of several ovarian cancer cells to cisplatin both in vitro and in vivo [261,262]. However, prior to silencing their resistant cells featured elevated DJ-1 protein levels [261,262], which was not the case in the cell line pair used here [261,262]. Apart from this, they also applied a self-constructed delivery system for DJ-1 siRNA to the cancer cells via a synthesized nanoplatform, which, on the one hand, can hardly be compared to simple transfection procedures like the one used in this project. On the other hand, this construct resulted in considerably decreased proliferation already itself and only marginally higher cytotoxicity was observed upon cisplatin addition, especially in the A2780cis cell line [261,262].

It can be concluded that DJ-1 might be a promising therapeutic target, especially in cancers overexpressing the protein, yet further investigation is needed, in particular with more thoroughly explored, specific, highly effective inhibitors. Interestingly, repression of both the beclin-1 mRNA and protein levels by DJ-1 led to a reduced autophagy of the cells in earlier studies [210]. Furthermore, it could be shown that DJ-1 exerted beclin-1 transcriptional regulation via the JNK-pathway [210]. These findings provide links to vimentin and GSTP1, further underlining the potential opportunities of a multi-inhibitory approach (Figure 5.1).

Figure 5.1 Simplified illustration of possible connections of signaling pathways of vimentin, GSTP1 and DJ-1 and their influences on tumor cell growth or repression without (A) or with (B) the application of specific pharmacological inhibitors. While cell proliferation and migration prevail when these proteins function properly, cell growth is suppressed under the influence of the deployed inhibitors.

5.2.4   Growth Factor Receptor-Bound Protein 2

Grb2, a small adaptor protein consisting of a single src homology 2 (SH2) domain flanked by two Src Homology 3 (SH3) domains [263], has been repeatedly investigated

in the context of cancer, however, with contradictory results. In several studies, overexpression of Grb2 led to elevated tumor growth, invasiveness and metastasis [264]. Among many other pathways, in which Grb2 may be involved, an interaction via its SH3 domains with Sos, a guanine-nucleotide exchange factor, which promotes the guanosine diphosphate (GDP)-guanosine triphosphate (GTP) exchange of Ras and thereby its activation, could be demonstrated [265,266]. As a consequence of growth factor receptor activation (e.g. of EGFR) and phosphorylation of the tyrosine kinase, Grb2 binds to the autophosphorylation site through its SH2 domain and brings Sos spatially close to the membrane-bound Ras, resulting in the activation of both Ras and subsequently initiation of the downstream MAPK cascade [265,266]. In line with this, overexpression of Grb2 and Sos was suggested as an important mechanism of oncogenesis in bladder cancer in another study [267]. Conversely, Timsah et al. show that Grb2 can play an opposite regulatory role. In the absence of growth-factor stimulation of the fibroblast growth factor receptor 2 (FGFR2), Grb2 seems to assume the role of a control protein by initiating dimerization of the receptor through binding to it via its SH3C-terminal domains without influencing downstream signaling, and thus the metastatic potential [268]. Grb2 competes thereby with another ligand of FGFR2, phospholipase c, gamma 1 (PLCγ1), which on the other hand stimulates cellular motility and metastasis. Timsah et al. found that depletion of Grb2 led to predominance of PLCγ1 activity and inhibition of PTEN, which then resulted in Akt activation and consequently in tumor progression [269]. In addition, the analysis of data from The Cancer Genome Atlas (TCGA) revealed that concurrent low levels of PLCγ1 and FGFR mRNA along with high Grb2 mRNA levels correlated with a favorable prognosis in patients [269]. Similarly, another study showed that the overexpression of Snail, an EMT trigger, is associated with both reduced expression of Grb2 as well as Grb2-mediated activation of P-gp. This in turn led to an increased viability of lung cancer cells when treated with paclitaxel [270].

However, the correlation between an EMT phenotype and the role of Grb2 in the cells used here can be ruled out fairly reliable due to the complete absence of vimentin expression. Nevertheless, given that the prevailing role of Grb2 in intracellular signaling could be cell type dependent, the effects of Grb2 inhibition and knockdown on cell sensitivity were evaluated in order to find out whether depletion of Grb2 could be favorable for antitumor activity of the platinum drugs in HCT-8 and HCT-8ox cells since less platinum would be scavenged by the protein and therefore more free

platinum would be available for the formation of cytotoxic crosslinks on DNA. In contrast to the case of DJ-1 inhibitor, the toxicity of both Grb2 SH3C-domain-inhibitors chosen in HCT-8 and HCT-8ox cells limited the concentration used in the experiments, and the IC_{50} of 5.7 mM (inhibitor A) and 320 µM (inhibitor B) as determined by Simister et al. could not be achieved [163]. There were no changes in cytotoxicity of both cisplatin and oxaliplatin upon combination with inhibitor A. Interestingly, a tendency towards lower sensitivity to cisplatin and a significant reduction in cytotoxicity in the case of oxaliplatin combination with inhibitor B was observed. On the one hand, the inhibitors used may have not been potent enough in the concentration range applied or have a different binding site than cisplatin. On the other hand, due to the inhibitor blocking the SH3C terminal, it is possible that the above-mentioned control function of Grb2 has been switched off and thus the survival signaling may have exceeded the effect expected from the increased amount of free platinum in the cytosol, thus resulting in tumor progressiveness. Grb2 knockdown did not induce any changes in susceptibility to the platinum drugs, which might be explained by rather moderate to low knockdown efficiency, especially in the resistant cell line. However, even with a more successful silencing of Grb2, similar results could be expected as with pharmacological inhibition due to the survival signaling activated by the loss of Grb2.

6   Conclusions and Outlook

The comparison of suitable methods for the identification of cisplatin binding partners after its uptake into the cell was clearly in favor of the two-dimensional gel electrophoresis. Both an extension by immunoprecipitation and the application of CuAAC did not lead to similarly acceptable results. Nevertheless, especially with regard to potential limitations of the common 2D, there is a high degree of optimization possibilities. In particular, the further establishment of the immunoprecipitation protocol should be pursued further in order to identify binding proteins more unambiguously and to avoid the problems related to different protein abundances within the cell. Also, a validation of the selected spots by LA-ICP-MS should be considered, which allows to locate platinum within the 2D gel and thus would allow to superimpose not only fluorophore and protein, but in parallel also a drug moiety. Especially considering that no Pt peptides were identified in the MS, this could ensure in even more confidence in the method.

By using 2D electrophoresis combined with MS some binding partners of cisplatin could be identified, of which vimentin, GSTP1, DJ-1 and Grb2 were then further investigated. However, future studies should also be conducted with other binding partners and in a broad range of ovarian and colorectal cancer cell lines. In this thesis, it could be shown that by pharmacological inhibition of vimentin a significant sensitization of ovarian cancer cells could be achieved and a knockdown of GSTP1 in intrinsically resistant colorectal cancer cells could sensitize them to cisplatin to a degree comparable to sensitive A2780 cells. Inhibition of Grb2, on the other hand, indicated that this protein may promote the cytotoxicity of cisplatin in HCT-8 cells and that inhibition of this interaction leads to enhanced resistance. With regard to the hypothesis that intracellular binding partners reduce the amount of free platinum, it is of interest to investigate the level of DNA platination after pharmacological inhibition or siRNA-mediated silencing of the binding partner. The use of inhibitors and knockdown should result in increased amounts of free cisplatin in the cytosol and thus lead to an increased proportion finding its way into the nucleus and to the DNA. Yet, resistance development through cytosolic interactions is often also closely related to the interference with normal functions of the proteins and thereby does not only result in deactivation of the chemotherapeutic agent. In this context, it is also interesting to what extent cellular signaling is altered by inhibition or knockdown of the protein/gene. Characterization of the involvement of certain signaling pathways may open new

possibilities to exploit them therapeutically. Likewise, it would be intriguing to monitor changes in protein functions after inhibition in order to assess to which degree a possible cell sensitization to the drug can actually be attributed to the obstruction of the protein. The specificity of the inhibitors used is not always sufficiently elucidated and could provide further information on the significance of the pharmacological intervention. Due to the multifactorial manifestation of resistance, it is additionally of interest to combine several inhibitors and, therefore, to engage on several levels simultaneously. On the basis of literature search, a high level of interaction between 3 of 4 identified binding partners of cisplatin, which were examined in detail, could be found. Hereby, vimentin, GSTP1 and DJ-1 seem to be linked via the Akt and JNK pathways, as well as via regulation of beclin-1, therefore, a parallel intervention might be beneficial. With regard to possible clinical relevance, it must of course also be kept in mind that the simultaneous application of different active compounds always entails an enhanced risk of adverse reactions. In line with this, a verification of the results obtained thus far in an in vivo setting should allow a better assessment as to what extent the substances and their combination hold potential of practical relevance.

7 Summary

Cisplatin is a widely used drug in treatment of various solid tumors, amongst others ovarian cancer. However, whereas acquired resistance significantly limits therapy success, some tumors such as colorectal cancer are intrinsically insensitive to cisplatin. Only a small amount of intracellular platinum binds to the target, genomic DNA. The fate of the remaining drug is still largely obscure. The aim of this thesis was to identify cytosolic binding partners of cisplatin in ovarian and colorectal cancer cells and to evaluate their relevance for cell sensitivity to cisplatin.

Three different approaches were examined for their performance to identify cisplatin binding partners. The application of copper-catalyzed azide-alkyne cycloaddition suffered from low specificity and high background binding. Immunoprecipitation was limited in terms of reproducibility and yield. By contrast, using the fluorescent cisplatin analog BODIPY-cisplatin, two-dimensional gel electrophoresis and MS, binding partners in the A2780 and cisplatin-resistant A2780cis ovarian carcinoma as well as in HCT-8 and oxaliplatin-resistant HCT-8ox ileocecal colorectal adenocarcinoma cell lines could successfully be identified.

Furthermore, the relevance of four of these proteins (vimentin, GSTP1, DJ-1 and Grb2) for the sensitivity of the cells to platinum drugs was assessed by means of pharmacological inhibition and siRNA-mediated knockdown. Interestingly, silencing of GSTP1 significantly sensitized intrinsically resistant HCT-8 and HCT-8ox cells to cisplatin. This finding implies the possible involvement of GSTP1 in the intrinsic resistance of colorectal cancer cells to cisplatin and may offer a great opportunity to further elucidate the distinct mechanisms of action of cisplatin vs. oxaliplatin in this tumor entity. It was also demonstrated that the inhibition of vimentin by the recently developed inhibitor FiVe1 led to a significant sensitization of ovarian cancer cells to cisplatin and to a reversal of resistance in the cisplatin-resistant cell line. These results warrant a further evaluation of vimentin as a target of antitumor therapy and FiVe1 as a possible combination partner of cisplatin.

8   References

1.   World Health Organization *World Health Statistics 2019*; **2019**; ISBN 9789241565707.

2.   International Agency for Research on Cancer. *World Cancer Report*; **2020**; ISBN 9789283204473.

3.   World Health Organization. *World Cancer Report*; **2014**; ISBN 9789283204299.

4.   International Agency for Research on Cancer. Cancer Today. Available online: https://gco.iarc.fr/today/home (accessed on Aug 21, 2020).

5.   Torre, L.A.; Bray, F.; Siegel, R.L.; Ferlay, J.; Lortet-Tieulent, J.; Jemal, A. Global Cancer Statistics, 2012. *CA Cancer J. Clin.* **2015**, *65*, 87–108.

6.   Bray, F.; Ferlay, J.; Soerjomataram, I.; Siegel, R.L.; Torre, L.A.; Jemal, A. Global Cancer Statistics 2018: GLOBOCAN Estimates of Incidence and Mortality Worldwide for 36 Cancers in 185 Countries. *CA Cancer J. Clin.* **2018**, *68*, 394–424.

7.   World Health Organization. *Global Action Plan for the Prevention and Control of Noncommunicable Diseases*; **2013**; ISBN 9789241506236.

8.   Sporn, M. The war on cancer. *Lancet Oncol.* **1996**, *347*, 1377–1381.

9.   Wang, S.; Liu, Y.; Feng, Y.; Zhang, J.; Swinnen, J.; Li, Y.; Ni, Y. A Review on Curability of Cancers: More Efforts for Novel Therapeutic Options Are Needed. *Cancers (Basel).* **2019**, *11*, 1782.

10.   Robert Koch Institut. *Krebs in Deutschland für 2015/2016*; **2016**; ISBN 9783896062987.

11.   American Cancer Society. *Cancer Facts & Figures 2019*; **2019**.

12.   Schwabe, U.; Paffrath, D.; Ludwig, W.-D.; Klauber, J. *Arzneiverordnungs-Report 2019*; Springer: Berlin, **2019**; ISBN 9783662590454.

13.   Cortez, A.J.; Tudrej, P.; Kujawa, K.A.; Lisowska, K.M. Advances in ovarian cancer therapy. *Cancer Chemother. Pharmacol.* **2018**, *81*, 17–38.

14.   Jayson, G.C.; Kohn, E.C.; Kitchener, H.C.; Ledermann, J.A. Ovarian cancer. *Lancet* **2014**, *384*, 1376–1388.

15.   Leilitinienprogramm Onkologie der AWMF; Deutsche Krebsgesellschaft e.V.; Deutsche Krebshilfe. S3-Leitlinie Diagnostik, Therapie und Nachsorge maligner Ovarialtumoren. Available online: www.awmf.org (accessed on Aug 23, 2020).

16.   Markman, M. Pharmaceutical Management of Ovarian Cancer: Current Status. *Drugs* **2019**, *79*, 1231–1239.

17.   Brenner, H.; Kloor, M.; Pox, C. Colorectal Cancer. *Lancet* **2014**, *383*, 1490–1502.

18.   Siegel, R.L.; Torre, L.A.; Soerjomataram, I.; Hayes, R.B.; Bray, F.; Weber, T.K.; Jemal, A. Global patterns and trends in colorectal cancer incidence in young

adults. *Gut* **2019**, *68*, 2179–2185.

19. Leitlinienprogramm Onkologie der AWMF; Deutsche Krebsgesellschaft e.V.; Deutsche Krebshilfe. S3-Leitlinie Kolorektales Karzinom. Available online: www.awmf.org (accessed on Aug 23, 2020).

20. Briffa, R.; Langdon, S.P.; Grech, G.; Harrison, D.J. Acquired and Intrinsic Resistance to Colorectal Cancer Treatment. In *Colorectal Cancer - Diagnosis, Screening and Management*; IntechOpen: London, **2018**; ISBN 9781789231014.

21. Hammond, W.A.; Swaika, A.; Mody, K. Pharmacologic resistance in colorectal cancer: A review. *Ther. Adv. Med. Oncol.* **2016**, *8*, 57–84.

22. Peyrone, M. Über die Einwirkung von Ammoniak auf Platinchlorür. *Justus Liebigs Ann. Chem.* **1845**, *55*, 205–213.

23. Rosenberg, B.; Van Camp, L.; Krigas, T. Inhibition of Cell Division in Escherichia Coli by Electrolysis Products from a Platinum Electrode. *Nature* **1965**, *205*, 698–699.

24. Rosenberg, B.; Van Camp, L.; Trosko, J.; Mansour, V. Platinum Compounds: A New Class of Potent Antitumour Agents. *Nature* **1969**, *222*, 385–386.

25. Rosenberg, B.; Van Camp, L. The Successful Regression of Large Solid Sarcoma 180 Tumors by Platinum Compounds. *Cancer Res.* **1970**, *30*, 1799–1802.

26. Harder, H.C.; Rosenberg, B. Inhibitory Effects of Anti-Tumor Platinum Compounds on DNA, RNA and Protein Synthesis in mammalian Cells in vitro. *Int. J. Cancer* **1970**, *6*, 207–216.

27. Howle, J.; Gale, G. Cis-Dichlorodiammineplatinum (II) - Persistent and Selective Inhibtion of Deoxyribonuceleic Acid Synthesis in vivo. *Biochem. Pharmacol.* **1970**, *19*, 2757–2762.

28. National Cancer Institute. The "Accidental" Cure - Platinum-based Treatment for Cancer: The Discovery of Cancer. Available online: https://www.cancer.gov/research/progress/discovery/cisplatin (accessed on Aug 23, 2020).

29. Galluzzi, L.; Senovilla, L.; Vitale, I.; Michels, J.; Martins, I.; Kepp, O.; Castedo, M.; Kroemer, G. Molecular mechanisms of cisplatin resistance. *Oncogene* **2012**, *31*, 1869–1883.

30. Adra, N.; Einhorn, L.H. Testicular Cancer Update. *Clin. Adv. Hematol. Oncol.* **2017**, *15*.

31. Wang, D.; Lippard, S.J. Cellular processing of platinum anticancer drugs. *Nat. Rev. Drug Discov.* **2005**, *4*, 307–320.

32. Mehmood, R.K. Review of cisplatin and oxaliplatin in current immunogenic and monoclonal antibody treatments. *Oncol. Rev.* **2014**, *8*, 36–43.

33. Kelland, L. The resurgence of platinum-based cancer chemotherapy. *Nat. Rev.*

Cancer **2007**, *7*, 573–584.

34. Rixe, O.; Ortuzar, W.; Alvarez, M.; Parker, R.; Reed, E.; Paull, K.; Fojo, T. Oxaliplatin, Tetraplatin, Cisplatin, and Carboplatin: Spectrum of Activity in Drug-Resistant Cell Lines and in the Cell Lines of the National Cancer Institute's Anticancer Drug Screen Panel. *Biochem. Pharmacol.* **1996**, *52*, 1855–1865.

35. Bruno, P.M.; Liu, Y.; Park, G.Y.; Murai, J.; Koch, C.E.; Eisen, T.J.; Pritchard, J.R.; Pommier, Y.; Lippard, S.J.; Hemann, M.T. A subset of platinum-containing chemotherapeutic agents kills cells by inducing ribosome biogenesis stress. *Nat. Med.* **2017**, *23*, 461–471.

36. Oun, R.; Moussa, Y.; Wheate, N. The side effects of platinum-based chemotherapy drugs: a review for chemists. *Dalt. Trans.* **2018**, *47*, 6645–6653.

37. Kenny, R.G.; Chuah, W.; Crawford, A.; Marmion, C.J. Platinum (IV) Prodrugs – A Step Closer to Ehrlich's Vision? *Eur. J. Inorg. Chem.* **2017**, *2017*, 1596–1612.

38. Wheate, N.; Walker, S.; Craig, G.; Oun, R. The status of platinum anticancer drugs in the clinic and in clinical trials. *Dalt. Trans.* **2010**, *39*, 8113–8127.

39. Hall, M.D.; Okabe, M.; Shen, D.; Liang, X.; Gottesman, M.M. The Role of Cellular Accumulation in Determining Sensitivity to Platinum-Based Chemotherapy. *Annu. Rev. Pharmacol. Toxicol.* **2008**, *48*, 495–535.

40. Pinato, O.; Musetti, C.; Sissi, C. Pt-based drugs: The spotlight will be on proteins. *Metallomics* **2014**, *6*, 380–395.

41. Brauckmann, C.; Wehe, C.A.; Kieshauer, M.; Lanvers-Kaminsky, C.; Sperling, M.; Karst, U. The interaction of platinum-based drugs with native biologically relevant proteins. *Anal. Bioanal. Chem.* **2013**, *405*, 1855–1864.

42. Riddell, I.A.; Lippard, S.J. Cisplatin and Oxaliplatin: Our Current Understanding of Their Actions. In *Metal Ions in Life Sciences*; Springer: Berlin, **2018**; Vol. 18, pp. 1-42; ISBN 9783110470734.

43. Planells-Cases, R.; Lutter, D.; Guyader, C.; Gerhards, N.M.; Ullrich, F.; Elger, D.A.; Kucukosmanoglu, A.; Xu, G.; Voss, F.K.; Reincke, S.M.; et al. Subunit composition of VRAC channels determines substrate specificity and cellular resistance to Pt-based anti-cancer drugs. *EMBO J.* **2015**, *34*, 2993–3008.

44. Ruprecht, N.; Hofmann, L.; Hungerbühler, M.N.; Kempf, C.; Heverhagen, J.T.; Tengg-Kobligk, H. Von Generation of Stable cisPt Resistant Lung Adenocarcinoma Cells. *Pharmaceuticals* **2020**, *13*.

45. Galluzzi, L.; Vitale, I.; Michels, J.; Brenner, C.; Szabadkai, G.; Harel-Bellan, A.; Castedo, M.; Kroemer, G. Systems biology of cisplatin resistance: Past, present and future. *Cell Death Dis.* **2014**, *5*, 1–18.

46. Siddik, Z.H. Cisplatin: Mode of cytotoxic action and molecular basis of resistance. *Oncogene* **2003**, *22*, 7265–7279.

47. Hagrman, D.; Goodisman, J.; Souid, A. Kinetic Study on the Reactions of

Platinum Drugs with Glutathione. *J. Pharmacol. Exp. Ther.* **2004**, *308*, 658–666.

48. Gonzalez, V.M.; Fuertes, M.A.; Alonso, C.; Perez, J.M. Is cisplatin-induced cell death always produced by apoptosis? *Mol. Pharmacol.* **2001**, *59*, 657–663.

49. Brouwers, E.E.M.; Huitema, A.; Beijnen, J.H.; Schellens, J.H.M. Long-term platinum retention after treatment with cisplatin and oxaliplatin. *BMC Clin. Pharmacol.* **2008**, *8*, 1–10.

50. Ott, I.; Gust, R. Medizinische Chemie der Platinkomplexe. *Pharm. Unserer Zeit* **2006**, *35*, 124–133.

51. Alcindor, T.; Beauger, N. Oxaliplatin: A review in the era of molecularly targeted therapy. *Curr. Oncol.* **2011**, *18*, 18–25.

52. Ip, V.; Mckeage, M.J.; Thompson, P.; Damianovich, D.; Findlay, M.; Liu, J.J. Platinum-specific detection and quantification of oxaliplatin and Pt(R,R-diaminocyclohexane)Cl2 in the blood plasma of colorectal cancer patients. *J. Anal. At. Spectrom.* **2008**, *23*, 881–884.

53. Perego, P.; Robert, J. Oxaliplatin in the era of personalized medicine: From mechanistic studies to clinical efficacy. *Cancer Chemother. Pharmacol.* **2016**, *77*, 5–18.

54. Buß, I.; Hamacher, A.; Sarin, N.; Kassack, M.U.; Kalayda, G.V. Relevance of copper transporter 1 and organic cation transporters 1-3 for oxaliplatin uptake and drug resistance in colorectal cancer cells. *Metallomics* **2018**, *10*, 414–425.

55. Misset, J.L.; Bleiberg, H.; Sutherland, W.; Bekradda, M.; Cvitkovic, E. Oxaliplatin clinical activity: A review. *Crit. Rev. Oncol. Hematol.* **2000**, *35*, 75–93.

56. Di Francesco, A.M.; Ruggiero, A.; Riccardi, R. Cellular and molecular aspects of drugs of the future: Oxaliplatin. *Cell. Mol. Life Sci.* **2002**, *59*, 1914–1927.

57. Rabik, C.A.; Dolan, M.E. Molecular Mechanisms of Resistance and Toxicity Associated with Platinating Agents. *Cancer Treat. Rev.* **2007**, *33*, 9–23.

58. Raymond, E.; Faivre, S.; Chaney, S.; Woynarowski, J.; Cvitkovic, E. Cellular and Molecular Pharmacology of Oxaliplatin. *Mol. Cancer Ther.* **2002**, *1*, 227–235.

59. Mezencev, R. Interactions of Cisplatin with non-DNA Targets and their Influence on Anticancer Activity and Drug Toxicity: The Complex World of the Platinum Complex. *Curr. Cancer Drug Targets* **2015**, *14*, 794–816.

60. Mandic, A.; Hansson, J.; Linder, S.; Shoshan, M.C. Cisplatin Induces Endoplasmic Reticulum Stress and Nucleus-independent Apoptotic Signaling. *J. Biol. Chem.* **2003**, *278*, 9100–9106.

61. Yu, F.; Megyesi, J.; Price, P.M. Cytoplasmic initiation of cisplatin cytotoxicity. *Am. J. Physiol. Ren. Physiol.* **2008**, *295*, 44–52.

62. More, S.S.; Akil, O.; Ianculescu, A.G.; Geier, E.G.; Lustig, L.R.; Giacomini,

K.M. Role of the Copper Transporter, CTR, in Platinum-Induced Ototoxicity. *J. Neurosci.* **2010**, *30*, 9500–9509.

63.   Vitale, I.; Galluzzi, L.; Castedo, M.; Kroemer, G. Mitotic Catastrophe: A Mechanism for Avoiding Genomic Instability. *Nat. Rev. Mol. Cell Biol.* **2011**, *12*, 385–392.

64.   Reardon, J.; Vaisman, A.; Chaney, S.; Sancar, A. Efficient Nucleotide Excision Repair of Cisplatin, Oxaliplatin, and Bis-aceto- ammine-dichloro-cyclohexylamine-platinum(IV) (JM216) Platinum Intrastrand DNA Diadducts. *Cancer Res.* **1999**, *59*, 3968–3971.

65.   Marteijn, J.A.; Lans, H.; Vermeulen, W.; Hoeijmakers, J.H.J. Understanding nucleotide excision repair and its roles in cancer and ageing. *Nat. Rev. Mol. Cell Biol.* **2014**, *15*, 465–481.

66.   Chaney, S.G.; Vaisman, A. Specificity of platinum-DNA adduct repair. *J. Inorg. Biochem.* **1999**, *77*, 71–81.

67.   Nehmé, A.; Baskaran, R.; Nebel, S.; Fink, D.; Howell, S.; Wang, J.; Christen, R. Induction of JNK and c-Abl signalling by cisplatin and oxalipaltin in mismatch repair-proficient and -deficient cells. *Br. J. Cancer* **1999**, *79*, 1104–1110.

68.   Köberle, B.; Tomicic, M.T.; Usanova, S.; Kaina, B. Cisplatin resistance: Preclinical findings and clinical implications. *Biochim. Biophys. Acta - Rev. Cancer* **2010**, *1806*, 172–182.

69.   Denicourt, C.; Dowdy, S.F. Targeting Apoptotic Pathways in Cancer Cells. *Science* **2004**, *305*, 1411–1413.

70.   Nguewa, P.A.; Fuertes, M.A.; Alonso, C.; Perez, J.M. Pharmacological Modulation of Poly(ADP-ribose)Polymerase-Mediated Cell Death: Exploitation in Cancer Chemotherapy. *Mol. Pharmacol.* **2003**, *64*, 1007–1014.

71.   Wu, G.S. The Functional Interactions Between the p53 and MAPK Signaling Pathways. *Cancer Biol. Ther.* **2004**, *3*, 156–161.

72.   Kim, S.; Lee, T.; Park, J.; Kwon, T.K. Overexpression of cFLIPs Inhibits Oxaliplatin-Mediated Apoptosis Through Enhanced XIAP Stability and Akt Activation in Human Renal Cancer Cells. *J. Cell. Biochem.* **2008**, *105*, 971–979.

73.   Housman, G.; Byler, S.; Heerboth, S.; Lapinska, K.; Longacre, M.; Snyder, N.; Sarkar, S. Drug resistance in cancer: An overview. *Cancers (Basel).* **2014**, *6*, 1769–1792.

74.   Klein, A. V.; Hambley, T.W. Platinum drug distribution in cancer cells and tumors. *Chem. Rev.* **2009**, *109*, 4911–4920.

75.   Stewart, D.J. Mechanisms of resistance to cisplatin and carboplatin. *Crit. Rev. Oncol. Hematol.* **2007**, *63*, 12–31.

76.   Holzer, A.K.; Howell, S.B. The Internalization and Degradation of Human Copper Transporter 1 following Cisplatin Exposure. *Cancer Res.* **2006**, *66*, 10944–10952.

77.   Plasencia, C.; Martínez-Balibrea, E.; Martinez-Cardús, A.; Quinn, D.; Abad, A.; Neamati, N. Expression analysis of genes involved in oxaliplatin response and development of oxaliplatin-resistant HT29 colon cancer cells. *Int. J. Oncol.* **2006**, *29*, 225–235.

78.   Martinez-Balibrea, E.; Martínez-Cardus, A.; Gines, A.; Ruiz De Porras, V.; Moutinho, C.; Layos, L.; Manzano, J.L.; Buges, C.; Bystrup, S.; Esteller, M.; et al. Tumor-related molecular mechanisms of oxaliplatin resistance. *Mol. Cancer Ther.* **2015**, *14*, 1767–1776.

79.   Safaei, R.; Holzer, A.K.; Katano, K.; Samimi, G.; Howell, S.B. The role of copper transporters in the development of resistance to Pt drugs. *J. Inorg. Biochem.* **2004**, *98*, 1607–1613.

80.   Lukanović, D.; Herzog, M.; Kobal, B.; Černe, K. The contribution of copper efflux transporters ATP7A and ATP7B to chemoresistance and personalized medicine in ovarian cancer. *Biomed. Pharmacother.* **2020**, *129*.

81.   Samimi, G.; Safaei, R.; Katano, K.; Holzer, A.K.; Rochdi, M.; Tomioka, M.; Goodman, M.; Howell, S.B. Increased Expression of the Copper Efflux Transporter ATP7A Mediates Resistance to Cisplatin, Carboplatin, and Oxaliplatin in Ovarian Cancer Cells. *Clin. Cancer Res.* **2004**, *10*, 4661–4669.

82.   Martinez-Balibrea, E.; Martínez-Cardús, A.; Musulén, E.; Ginés, A.; Manzano, J.L.; Aranda, E.; Plasencia, C.; Neamati, N.; Abad, A. Increased levels of copper efflux transporter ATP7B are associated with poor outcome in colorectal cancer patients receiving oxaliplatin-based chemotherapy. *Int. J. Cancer* **2009**, *124*, 2905–2910.

83.   Eastman, A. Cross-linking of Glutathione to DNA by Cancer Chemotherapeutic Platinum Coordination Complexes. *Chem. Biol. Interact.* **1987**, *61*, 241–248.

84.   Meijer, C.; Mulder, N.; Hospers, G.; Uges, D.; de Vries, E. The role of glutathione in resistance to cisplatin in a human small cell lung cancer cell line. *Br. J. Cancer* **1990**, *62*, 72–77.

85.   Allocati, N.; Masulli, M.; Di Ilio, C.; Federici, L. Glutathione transferases: Substrates, inihibitors and pro-drugs in cancer and neurodegenerative diseases. *Oncogenesis* **2018**, *7*.

86.   Liu, F. Mechanisms of Chemotherapeutic Drug Resistance in Cancer Therapy - A Quick Review. *Taiwan. J. Obstet. Gynecol.* **2009**, *48*, 239–244.

87.   Tazehkand, A.P.; Akbarzadeh, M.; Velaie, K.; Sadeghi, M.R.; Samadi, N. The role of Her2-Nrf2 axis in induction of oxaliplatin resistance in colon cancer cells. *Biomed. Pharmacother.* **2018**, *103*, 755–766.

88.   Bakka, A.; Endresen, L.; ABS, J.; PA, E.; Rugstad, H. Resistance against cis-Dichlorodiammineplatinum in Cultured Cells with a High Content of Metallothionein. *Toxicol. Appl. Pharmacol.* **1981**, *61*, 215–226.

89.   Sharma, R.P.; Edwards, I.R. cis-Platinum: Subcellular Distribution and Binding to Cytosolic Ligands. *Biochem. Pharmacol.* **1983**, *32*, 2665–2669.

90.   Brouwers, E.; Tibben, M.; Rosing, H.; Schellens, J.; Beijnen, J. The Application

of Inductively Coupled Plasma Mass Spectrometry in Clinical Pharmacological Oncology Research. *Mass Spectrom. Rev* **2008**, *27*, 67–100.

91. Pinato, O.; Musetti, C.; Farrell, N.P.; Sissi, C. Platinum-Based Drugs and Proteins: Reactivity and Relevance to DNA Adduct Formation. *J. Inorg. Biochem.* **2013**, *122*, 27–37.

92. Messori, L.; Merlino, A. Cisplatin binding to proteins: A structural perspective. *Coord. Chem. Rev.* **2016**, *315*, 67–89.

93. Reedijk, J. Why Does Cisplatin Reach Guanine-N7 with Competing S-Donor Ligands Available in the Cell? *Chem. Rev.* **1999**, *99*, 2499–2510.

94. Jakupec, M.A.; Galanski, M.; Keppler, B.K. Tumour-inhibiting platinum complexes – state of the art and future perspectives. *Rev. Physiol. Biochem. Pharmacol.* **2003**, 1–53.

95. Meister, A. Glutathione Metabolism and Its Selective Modification. *J. Biol. Chem.* **1988**, *263*, 17205–17208.

96. Kumar, G.N.; Surapaneni, S. Role of Drug Metabolism in Drug Discovery and Development. *Med. Res. Rev.* **2001**, *21*, 397–411.

97. Ishikawas, T. Glutathione-associated cis-Diamminedichloroplatinum(II) Metabolism and ATP-dependent Efflux from Leukemia Cells. *J. Biol. Chem.* **1993**, *268*, 20116–20125.

98. Kigawa, J.; Minagawa, Y.; Kanamori, Y.; Itamochi, H.; Cheng, X.; Okada, M.; Oishi, T.; Terakawa, N. Glutathione Concentration May Be a Useful Predictor of Response to Second-Line Chemotherapy in Patients with Ovarian Cancer. *Cancer* **1998**, *82*, 697–702.

99. Goto, S.; Morikawa, T.; Urata, Y.; Kondo, T.; Yoshida, K.; Suzuki, K. Augmentation of Transport for Cisplatin-Glutathione Adduct in Cisplatin-resistant Cancer Cells. *Cancer Res.* **1995**, *55*, 4297–4301.

100. Peklak-Scott, C.; Smitherman, P.K.; Townsend, A.J.; Morrow, C.S. Role of glutathione S-transferase P1-1 in the cellular detoxification of cisplatin. *Mol. Cancer Ther.* **2008**, *7*, 3247–3255.

101. Berners-Price, S.J.; Kuchel, P.W. Reaction of Cis- and Trans-[PtCl2(NH3)2] with Reduced Glutathione Inside Human Red Blood Cells, Studied by 1H and 15N-{1H} DEPT NMR. *J. Inorg. Biochem.* **1990**, *38*, 327–345.

102. Kasherman, Y.; Sturup, S.; Gibson, D. Is Glutathione the Major Cellular Target of Cisplatin? A Study of the Interactions of Cisplatin with Cancer Cell Extracts. *J. Med. Chem.* **2009**, *52*, 4319–4328.

103. Bernareggi, A.; Torti, L.; Maffei, R.; Carini, M.; Depta, G.; Casetta, B.; Farrell, N.; Spadacini, S.; Tognella, S. Characterization of cisplatin-glutathione adducts by liquid chromatography-mass spectrometry - Evidence for their formation in vitro but not in vivo after concomitant administration of cisplatin and glutathione to rats and cancer patients. *J Chromatogr B Biomed Appl* **1995**, *669*, 247–263.

104. Hagrman, D.; Goodisman, J.; Dabrowiak, J.C.; Souid, A.-K. Kinetic Study on

the Reaction of Cisplatin with Metallothionein. *Drug Metab. Dispos.* **2003**, *31*, 916–923.

105. Arnesano, F.; Natile, G. "Platinum on the road": Interactions of antitumoral cisplatin with proteins. *Pure Appl. Chem.* **2008**, *80*, 2715–2725.

106. Knipp, M.; Karotki, A. V; Chesnov, S.; Natile, G.; Sadler, P.J.; Brabec, V.; Vasák, M. Reaction of Zn7 Metallothionein with cis- and trans-[Pt(N-donor)2 Cl2] Anticancer Complexes: trans-PtII Complexes Retain Their N-Donor Ligands. *J. Med. Chem.* **2007**, *50*, 4075–4086.

107. Arnér, E.; Nakamura, H.; Sasada, T.; Yodoi, J.; Holmgren, A.; Spyrou, G. Analysis of the Inhibition of Mammalian Thioredoxin, Thioredoxin Reductase, and Glutaredoxin by cis-Diamminedichloroplatinum(II) and its Major Metabolite, the Glutathione-PLatinum Complex. *Free Radic. Biol. Med.* **2001**, *31*, 1170–1178.

108. Jungwirth, U.; Kowol, C.; Keppler, B.; Hartinger, C.; Berger, W.; Heffeter, P. Anticancer Activity of Metal Complexes: Involvement of Redox Processes. *Antioxidants Redox Signal.* **2011**, *15*, 1085–1127.

109. Wang, K.; Lu, J.; Li, R. The events that occur when cisplatin encounters cells. *Coord. Chem. Rev.* **1996**, *151*, 53–88.

110. Karasawa, T.; Sibrian-Vazquez, M.; Strongin, R.M.; Steyger, P.S. Identification of Cisplatin-Binding Proteins Using Agarose Conjugates of Platinum Compounds. *PLoS One* **2013**, *8*, 1–10.

111. Casini, A.; Reedijk, J. Interactions of anticancer Pt compounds with proteins: An overlooked topic in medicinal inorganic chemistry? *Chem. Sci.* **2012**, *3*, 3135–3144.

112. Wu, B.; Dröge, P.; Davey, C. Site selectivity of platinum anticancer therapeutics. *Nat. Chem. Biol.* **2008**, *4*, 110–112.

113. Kotz, S.; Kullmann, M.; Crone, B.; Kalayda, G.V.; Jaehde, U.; Metzger, S. Combination of two-dimensional gel electrophoresis and a fluorescent carboxyfluorescein-diacetate-labeled cisplatin analogue allows the identification of intracellular cisplatin-protein adducts. *Electrophoresis* **2015**, *36*, 2811–2819.

114. Kotz, S.; Kullmann, M.; Kalayda, G.V.; Dyballa-Rukes, N.; Jaehde, U.; Metzger, S. Optimized two-dimensional gel electrophoresis in an alkaline pH range improves the identification of intracellular CFDA-cisplatin-protein adducts in ovarian cancer cells. *Electrophoresis* **2018**, *39*, 1488–1496.

115. Kullmann, M.; Kalayda, G.V.; Hellwig, M.; Kotz, S.; Hilger, R.A.; Metzger, S.; Jaehde, U. Assessing the contribution of the two protein disulfide isomerases PDIA1 and PDIA3 to cisplatin resistance. *J. Inorg. Biochem.* **2015**, *153*, 247–252.

116. Jagodinsky, J.C.; Sulima, A.; Cao, Y.; Poprawski, J.E.; Blackman, B.N.; Lloyd, J.R.; Swenson, R.E.; Gottesman, M.M.; Hall, M.D. Evaluation of fluorophore-tethered platinum complexes to monitor the fate of cisplatin analogs. *J. Biol. Inorg. Chem.* **2015**, *20*, 1081–1095.

117. Urankar, D.; Košmrlj, J. Preparation of diazenecarboxamide-carboplatin conjugates by click chemistry. *Inorganica Chim. Acta* **2010**, *363*, 3817–3822.

118. White, J.D.; Guzman, L.E.; Zakharov, L.N.; Haley, M.M.; DeRose, V.J. An Alkyne-Appended, Click-Ready PtII Complex with an Unusual Arrangement in the Solid State. *Angew. Chemie - Int. Ed.* **2015**, *54*, 1032–1035.

119. Ramalingam, K.; Raju, N.; Nanjappan, P.; Nowotnik, D.P. Synthesis of Nitroimidazole Substituted 3,3,9,9-Tetramethyl-4,8-diazaundecane-2,10-dione Dioximes (Propylene Amine Oximes, PnAOs): Ligands for Technetium-99m Complexes with Potential for Imaging Hypoxic Tissue. *Tetrahedron Lett.* **1995**, *51*, 2875–2894.

120. Cambridge bioscience. CASY cell counter. Available online: https://www.bioscience.co.uk/cpl/casy-cell-counter (accessed on Jul 18, 2020).

121. Thermo Fisher Scientific. Overview of Cell Lysis and Protein Extraction. Available online: https://www.thermofisher.com/de/en/home/life-science/protein-biology/protein-biology-learning-center/protein-biology-resource-library/pierce-protein-methods/overview-cell-lysis-and-protein-extraction.html#extraction (accessed on May 27, 2020).

122. St. Michael's Hospital. Cell Viability/Apoptosis. Available online: http://stmichaelshospitalresearch.ca/staff-services/research-facilities/facilities/flow-cytometry-core/cell-viability-apoptosis/ (accessed on May 27, 2020).

123. Wessel, D.; Flügge, U.I. A method for the quantitative recovery of protein in dilute solution in the presence of detergents and lipids. *Anal. Biochem.* **1984**, *138*, 141–143.

124. Laemmli, U.K. Cleavage of Structural Proteins during the Assembly of the Head of Bacteriophage T4. *Nature* **1970**, *227*, 680–685.

125. Westermeier, R. *Electrophoresis in Practice*; 2nd ed.; Wiley-VCH: Weinheim, **2016**; ISBN 978-3-527-33892-4.

126. Sanchez, J.-C.; Rouge, V.; Pisteur, M.; Ravier, F.; Tonella, L.; Moosmayer, M.; Wilkins, M.R.; Hochstrasser, D.F. Improved and simplified in-gel sample application using reswelling of dry immobilized pH gradients. *Electrophoresis* **1997**, *18*, 324–327.

127. Olsson, I.; Larsson, K.; Palmgren, R.; Bjellqvist, B. Organic disulfides as a means to generate streak-free two-dimensional maps with narrow range basic immobilized ph gradient strips as first dimension. *Proteomics* **2002**, *2*, 1630–1632.

128. Bio-Rad Laboratories. 2-D Electrophoresis Workflow, How-To Guide. Available online: http://www.bio-rad.com/webroot/web/pdf/lsr/literature/Bulletin_2651.pdf (accessed on Aug 23, 2020).

129. Bio-Rad Laboratories. PROTEAN® IEF Cell Instruction Manual. Available online: https://www.imbb.forth.gr/imbb-people/images/Profi/pdf/protean_ief.pdf (accessed on Aug 23, 2020).

130. Diezel, W.; Kopperschläger, G.; Hofmann, E. An improved procedure for protein staining in polyacrylamide gels with a new type of Coomassie Brilliant Blue. *Anal. Biochem.* **1972**, *48*, 617–620.

131. Neuhoff, V.; Stamm, R.; Eibl, H. Clear background and highly sensitive protein staining with Coomassie Blue dyes in polyacrylamide gels: A systematic analysis. *Electrophoresis* **1985**, *6*, 427–448.

132. Neuhoff, V.; Arold, N.; Taube, D.; Ehrhardt, W. Improved staining of proteins in polyacrylamide gels including isoelectric focusing gels with clear background at nanogram sensitivity using Coomassie Brilliant Blue G-250 and R-250. *Electrophoresis* **1988**, 255–262.

133. Ünlü, M.; Morgan, M.E.; Minden, J.S. Difference gel electrophoresis: A single gel method for detecting changes in protein extracts. *Electrophoresis* **1997**, *18*, 2071–2077.

134. Westermeier, R.; Scheibe, B. Difference Gel Electrophoresis Based on Lys/Cys Tagging. In *2D PAGE: Sample Preparation and Fractionation*; Posch, A., Ed.; Humana Press, **2008**; Vol. 1, pp. 73-85; ISBN 978-1-58829-722-8.

135. Smejkal, G.B.; Robinson, M.H.; Lazarev, A. Comparison of fluorescent stains: Relative photostability and differential staining of proteins in two-dimensional gels. *Electrophoresis* **2004**, *25*, 2511–2519.

136. Miller, I.; Crawford, J.; Gianazza, E. Protein stains for proteomic applications: Which, when, why? *Proteomics* **2006**, *6*, 5385–5408.

137. Lopez, M.; Berggren, K.; Chernokalskaya, E.; Lazarev, A.; Robinson, M.; Patton, W. A comparison of silver stain and SYPRO Ruby Protein Gel Stain with respect to protein detection in two-dimensional gels and identification by peptide mass profiling. *Electrophoresis* **2000**, *21*, 3673–3683.

138. Nordic BioSite. RNAi - From Discovery to Nobel Prize in Record Time? Available online: https://nordicbiosite.com/blog/rnai-from-discovery-to-nobel-prize-in-record-time (accessed on May 22, 2020).

139. Covalab - R&D in Biotechnology. Covalight® Chemiluminescent Reagent. Available online: https://www.covalab.com/products-covalight (accessed on May 22, 2020).

140. Chou, T.; Talalay, P. Quantitative Dose-Effect Relationships: the Combined Effects of Multiple Drugs or Enzyme Inhibitors. *Adv. Enzyme Regul.* **1984**, 27–55.

141. Chou, T.C. Drug combination studies and their synergy quantification using the chou-talalay method. *Cancer Res.* **2010**, *70*, 440–446.

142. Chou, T.-C.; Martin, N. *CompuSyn software for drug combinations and for general dose-effect analysis, and user's guide*; ComboSyn, Inc.: Paramus, NJ, **2007**.

143. Thermo Fisher Scientific. Overview of the Immunoprecipitation (IP) Technique. Available online: https://www.thermofisher.com/de/en/home/life-science/protein-biology/protein-biology-learning-center/protein-biology-

resource-library/pierce-protein-methods/immunoprecipitation-ip.html#4
(accessed on May 28, 2020).

144. Thermo Fisher Scientific. Immunoprecipitation Crosslinking Protocol using
     Dynabeads. Available online: https://www.thermofisher.com/de/en/home/life-
     science/protein-biology/protein-assays-
     analysis/immunoprecipitation/dynabeads-immunoprecipitation-crosslinking-
     protocol.html (accessed on May 28, 2020).

145. Sousa, M.M.L.; Steen, K.W.; Hagen, L.; Slupphaug, G. Antibody cross-linking
     and target elution protocols used for immunoprecipitation significantly modulate
     signal-to noise ratio in downstream 2D-PAGE analysis. *Proteome Sci.* **2011**, *9*,
     1–8.

146. Hein, J.E.; Fokin, V. V. Copper-catalyzed azide–alkyne cycloaddition (CuAAC)
     and beyond: new reactivity of copper(I) acetylides. *Chem. Soc. Rev.* **2010**,
     1302–1315.

147. Kolb, H.C.; Finn, M.G.; Sharpless, K.B. Click Chemistry: Diverse Chemical
     Function from a Few Good Reactions. *Angew. Chem. Int. Ed.* **2001**, *40*, 2005–
     2021.

148. Banerjee, S.; Mazumdar, S. Electrospray Ionization Mass Spectrometry: A
     Technique to Access the Information beyond the Molecular Weight of the
     Analyte. *Int. J. Anal. Chem.* **2012**, *2012*, 1–40.

149. Rosenfeld, J.; Capdevielle, J.; Guillemot, J.C.; Ferrara, P. In-gel digestion of
     proteins for internal sequence analysis after one- or two-dimensional gel
     electrophoresis. *Anal. Biochem.* **1992**, *203*, 173–179.

150. Jenö, P.; Mini, T.; Moes, S.; Hintermann, E.; Horst, M. Internal sequences from
     proteins digested in polyacrylamide gels. *Anal. Biochem.* **1995**, *224*, 75–82.

151. The, M.; MacCoss, M.J.; Noble, W.S.; Käll, L. Fast and Accurate Protein False
     Discovery Rates on Large-Scale Proteomics Data Sets with Percolator 3.0. *J.
     Am. Soc. Mass Spectrom.* **2016**, *27*, 1719–1727.

152. Taus, T.; Köcher, T.; Pichler, P.; Paschke, C.; Schmidt, A.; Henrich, C.;
     Mechtler, K. Universal and confident phosphorylation site localization using
     phosphoRS. *J. Proteome Res.* **2011**, *10*, 5354–5362.

153. Kullmann, M. Identifying intracellular cisplatin interaction partners and
     assessing their contribution to cisplatin resistance. PhD Thesis, University of
     Bonn, Bonn, Germany, **2016**. URN: urn:nbn:de:hbz:5n-44624.

154. Dépagne, J.; Chevalier, F. Technical updates to basic proteins focalization
     using IPG strips. *Proteome Sci.* **2012**, *10*, 1–9.

155. Yang, Y.; Yang, X.; Verhelst, S.H.L. Comparative Analysis of Click Chemistry
     Mediated Activity-Based Protein Profiling in Cell Lysates. *Molecules* **2013**, *18*,
     12599–12608.

156. Van Geel, R.; Pruijn, G.J.M.; Van Delft, F.L.; Boelens, W.C. Preventing thiol-
     yne addition improves the specificity of strain-promoted azide-alkyne
     cycloaddition. *Bioconjug. Chem.* **2012**, *23*, 392–398.

157. Speers, A.E.; Cravatt, B.F.; Jolla, L. Profiling Enzyme Activities In Vivo Using Click Chemistry Methods. **2004**, *11*, 535–546.

158. Maricich, T.J.; Angeletakis, C.N. Reaction of Benzenesulfinyl Azide with Thiols and Amines. Preparation of Thiosulfinates and Sulfinamides. *J. Org. Chem.* **1983**, *49*, 1931–1934.

159. Ackermann, D.; Wang, W.; Streipert, B.; Geib, B.; Simone, K. Comparative fluorescence two-dimensional gel electrophoresis using a gel strip sandwich assembly for the simultaneous on-gel generation of a reference protein. **2012**, 1406–1410.

160. Bollong, M.J.; Pietilä, M.; Pearson, A.D.; Sarkar, T.R.; Ahmad, I.; Soundararajan, R.; Lyssiotis, C.A.; Mani, S.A.; Schultz, P.G.; Lairson, L.L. A vimentin binding small molecule leads to mitotic disruption in mesenchymal cancers. *Proc. Natl. Acad. Sci. U. S. A.* **2017**, *114*, E9903–E9912.

161. Mahadevan, D.; Sutton, G.R. Ezatiostat hydrochloride for the treatment of myelodysplastic syndromes. *Expert Opin. Investig. Drugs* **2015**, *24*, 725–733.

162. Tashiro, S.; Caaveiro, J.M.M.; Nakakido, M.; Tanabe, A.; Nagatoishi, S.; Tamura, Y.; Matsuda, N.; Liu, D.; Hoang, Q.Q.; Tsumoto, K. Discovery and Optimization of Inhibitors of the Parkinson's Disease Associated Protein DJ-1. *ACS Chem. Biol.* **2018**, *13*, 2783–2793.

163. Simister, P.C.; Luccarelli, J.; Thompson, S.; Appella, D.H.; Feller, S.M.; Hamilton, A.D. Novel inhibitors of a Grb2 SH3C domain interaction identified by a virtual screen. *Bioorganic Med. Chem.* **2013**, *21*, 4027–4033.

164. Ruebelt, M.C.; Leimgruber, N.K.; Lipp, M.; Reynolds, T.L.; Nemeth, M.A.; Astwood, J.D.; Engel, K.H.; Jany, K.D. Application of Two-Dimensional Gel Electrophoresis To Interrogate Alterations in the Proteome of Genetically Modified Crops. 1. Assessing Analytical Validation. *J. Agric. Food Chem.* **2006**, *54*, 2154–2161.

165. Lanning, B.R.; Whitby, L.R.; Dix, M.M.; Douhan, J.; Gilbert, A.M.; Hett, E.C.; Johnson, T.O.; Joslyn, C.; Kath, J.C.; Niessen, S.; et al. A road map to evaluate the proteome-wide selectivity of covalent kinase inhibitors. *Nat. Chem. Biol.* **2014**, *10*, 760–769.

166. Chen, Y.C.; Zhang, C. A chemoproteomic method for identifying cellular targets of covalent kinase inhibitors. *Genes and Cancer* **2016**, *7*, 148–153.

167. Wirth, T.; Schmuck, K.; Tietze, L.F.; Sieber, S.A. Duocarmycin Analogues Target Aldehyde Dehydrogenase 1 in Lung Cancer Cells. *Angew. Chemie - Int. Ed.* **2012**, *51*, 2874–2877.

168. Osborn, M.F.; White, J.D.; Haley, M.M.; DeRose, V.J. Platinum-RNA Modifications Following Drug Treatment in S. cerevisiae Identified by Click Chemistry and Enzymatic Mapping. *ACS Chem. Biol.* **2014**, *9*, 2404–2411.

169. White, J.D.; Osborn, M.F.; Moghaddam, A.D.; Guzman, L.E.; Haley, M.M.; DeRose, V.J. Picazoplatin, an Azide-Containing Platinum(II) Derivative for Target Analysis by Click Chemistry. *J. Am. Chem. Soc.* **2013**, *135*, 11680–11683.

170. Ding, S.; Qiao, X.; Suryadi, J.; Marrs, G.S.; Kucera, G.L.; Bierbach, U. Using Fluorescent Post-Labeling To Probe the Subcellular Localization of DNA-Targeted Platinum Anticancer Agents. *Angew. Chemie - Int. Ed.* **2013**, *52*, 3350–3354.

171. Molenaar, C.; Teuben, J.; Heetebrij, R.; Tanke, H.; Reedijk, J. New insights in the cellular processing of platinum antitumor compounds, using fluorophore-labeled platinum complexes and digital fluorescence microscopy. *J. Biol. Inorg. Chem.* **2000**, *5*, 655–665.

172. Moghaddam, A.D.; White, J.D.; Cunningham, R.M.; Loes, A.N.; Haley, M.M.; DeRose, V.J. Convenient detection of metal-DNA, metal-RNA, and metal-protein adducts with a click-modified Pt(II) complex. *Dalt. Trans.* **2015**, *44*, 3536–3539.

173. Moreno-Gordaliza, E.; Caňas, B.; Palacios, M.A.; Gómez-Gómez, M.M. Characterization of Pt-protein complexes by nHPLC–ESI-LTQ MS/MS using a gel-based bottom-up approach. *Talanta* **2012**, *88*, 599–608.

174. Moraleja, I.; Moreno-Gordaliza, E.; Mena, M.L.; Gómez-Gómez, M.M. Combining TBP-based rOFFGEL-IEF with FASP and nLC-ESI-LTQ-MS/MS for the analysis of cisplatin-binding proteins in rat kidney. *Talanta* **2014**, *120*, 433–442.

175. Safaei, R.; Katano, K.; Larson, B.J.; Samimi, G.; Holzer, A.K.; Naerdemann, W.; Tomioka, M.; Goodman, M.; Howell, S.B. Intracellular Localization and Trafficking of Fluorescein-Labeled Cisplatin in Human Ovarian Carcinoma Cells. *Clin. Cancer Res.* **2005**, *11*, 756–767.

176. Samimi, G.; Katano, K.; Holzer, A.K.; Safaei, R.; Howell, S.B. Modulation of the Cellular Pharmacology of Cisplatin and Its Analogs by the Copper Exporters ATP7A and ATP7B. *Mol. Pharmacol.* **2004**, *66*, 25–32.

177. Calandrini, V.; Arnesano, F.; Galliani, A.; Nguyen, T.H.; Ippoliti, E.; Carloni, P.; Natile, G. Platination of the copper transporter ATP7A involved in anticancer drug resistance. *Dalt. Trans.* **2014**, *43*, 12085–12094.

178. Cunningham, R.M.; DeRose, V.J. Platinum Binds Proteins in the Endoplasmic Reticulum of S. cerevisiae and Induces Endoplasmic Reticulum Stress. *ACS Chem. Biol.* **2017**, *12*, 2737–2745.

179. Wright, M.H.; Sieber, S.A. Chemical proteomics approaches for identifying the cellular targets of natural products. *Nat. Prod. Rep.* **2016**, *33*, 681–708.

180. Kullmann, M.; Kotz, S.; Hellwig, M.; Kalayda, G.V.; Metzger, S.; Jaehde, U. GRP78 knockdown does not affect cytotoxicity of cisplatin in ovarian cancer cells. *Int. J. Clin. Pharmacol. Ther.* **2015**, *53*, 1038–1040.

181. Graham, J.; Muhsin, M.; Kirkpatrick, P. Oxaliplatin. *Nat. Rev. Drug Discov.* **2004**, *3*, 11–12.

182. O'Farrell, P.H. High Resolution Two-Dimensional Electrophoresis of Proteins. *J. Biol. Chem.* **1975**, *250*, 4007–4021.

183. Kondo, T. Cancer biomarker development and two-dimensional difference gel

electrophoresis (2D-DIGE). *Biochim. Biophys. Acta - Proteins Proteomics* **2019**, *1867*, 2–8.

184. Wildgruber, R.; Harder, A.; Obermaier, C.; Boguth, G.; Weiss, W.; Fey, S.; Larsen, P.; Görg, A. Towards higher resolution: Two-dimensional Electrophoresis of Saccharomyces cerevisiae proteins using overlapping narrow immobilized pH gradients. *Electrophoresis* **2000**, *21*, 2610–2616.

185. Möltgen, S.; Piumatti, E.; Massafra, G.M.; Metzger, S.; Jaehde, U.; Kalayda, G.V. Cisplatin Protein Binding Partners and Their Relevance for Platinum Drug Sensitivity. *Cells* **2020**, *9*, E1322.

186. Kalayda, G.V.; Wagner, C.H.; Buß, I.; Reedijk, J.; Jaehde, U. Altered localisation of the copper efflux transporters ATP7A and ATP7B associated with cisplatin resistance in human ovarian carcinoma cells. *BMC Cancer* **2008**, *8*, 1–12.

187. Miller, M.A.; Askevold, B.; Yang, K.S.; Kohler, R.H.; Weissleder, R. Platinum Compounds for High-Resolution In Vivo Cancer Imaging. *ChemMedChem* **2014**, *9*, 1131–1135.

188. Ulrich, G.; Ziessel, R.; Harriman, A. The Chemistry of Fluorescent Bodipy Dyes: Versatility Unsurpassed. *Angew. Chemie - Int. Ed.* **2008**, *47*, 1184–1201.

189. Boens, N.; Leen, V.; Dehaen, W. Fluorescent indicators based on BODIPY. *Chem. Soc. Rev.* **2012**, *41*, 1130–1172.

190. White, J.D.; Haley, M.M.; DeRose, V.J. Multifunctional Pt(II) Reagents: Covalent Modifications of Pt Complexes Enable Diverse Structural Variation and In-Cell Detection. *Acc. Chem. Res.* **2016**, *49*, 56–66.

191. Wirth, R.; White, J.D.; Moghaddam, A.D.; Ginzburg, A.L.; Zakharov, L.N.; Haley, M.M.; DeRose, V.J. Azide vs Alkyne Functionalization in Pt(II) Complexes for Post-treatment Click Modification: Solid-State Structure, Fluorescent Labeling, and Cellular Fate. *J. Am. Chem. Soc.* **2015**, *137*, 15169–15175.

192. Kim, M.-S.; Pinto, S.M.; Getnet, D.; Nirujogi, R.S.; Manda, S.S.; Chaerkady, R.; Madugundu, A.K.; Kelkar, D.S.; Isserlin, R.; Jain, S.; et al. A draft map of the human proteome. *Nature* **2014**, *509*, 575–581.

193. Zuo, X.; Speicher, D.W. A Method for Global Analysis of Complex Proteomes Using Sample Prefractionation by Solution Isoelectrofocusing Prior to Two-Dimensional Electrophoresis. *Anal. Biochem.* **2000**, *284*, 266–278.

194. Moraleja, I.; Moreno-Gordaliza, E.; Esteban-Fernández, D.; Mena, M.L.; Linscheid, M.W.; Gómez-Gómez, M.M. A shotgun approach for the identification of platinum-protein complexes. *Anal. Bioanal. Chem.* **2015**, *407*, 2393–2403.

195. Görg, A.; Obermaier, C.; Boguth, G.; Weiss, W. Recent developments in two-dimensional gel electrophoresis with immobilized pH gradients: Wide pH gradients up to pH 12, longer separation distances and simplified procedures. *Electrophoresis* **1999**, *20*, 712–717.

196. Görg, A.; Obermaier, C.; Boguth, G.; Harder, A.; Scheibe, B.; Wildgruber, R.; Weiss, W. The current state of two-dimensional electrophoresis with immobilized pH gradients. *Electrophoresis* **2000**, *21*, 1037–1053.

197. Hanneken, M.; König, S. Horizontal comparative fluorescence two-dimensional gel electrophoresis for improved spot coordinate detection. *Electrophoresis* **2014**, *35*, 1118–1121.

198. Görg, A.; Weiss, W.; Dunn, M.J. Current two-dimensional electrophoresis technology for proteomics. *Proteomics* **2004**, *4*, 3665–3685.

199. Campostrini, N.; Areces, L.B.; Rappsilber, J.; Pietrogrande, M.C.; Dondi, F.; Pastorino, F.; Ponzoni, M.; Righetti, P.G. Spot overlapping in two-dimensional maps: A serious problem ignored for much too long. *Proteomics* **2005**, *5*, 2385–2395.

200. Zhou, S.; Bailey, M.J.; Dunn, M.J.; Preedy, V.R.; Emery, P.W. A quantitative investigation into the losses of proteins at different stages of a two-dimensional gel electrophoresis procedure. *Proteomics* **2005**, *5*, 2739–2747.

201. Qiao, X.; Ding, S.; Liu, F.; Kucera, G.L.; Bierbach, U. Investigating the cellular fate of a DNA-targeted platinum-based anticancer agent by orthogonal double-click chemistry. *J. Biol. Inorg. Chem.* **2014**, *19*, 415–426.

202. Nwe, K.; Brechbiel, M.W. Growing Applications of '"Click Chemistry"' for Bioconjugation in Contemporary Biomedical Research. *Cancer Biother. Radiopharm.* **2009**, *24*, 289–302.

203. Miseta, A.; Csutora, P. Relationship Between the Occurrence of Cysteine in Proteins and the Complexity of Organisms. *Mol. Biol. Evol.* **2000**, *17*, 1232–1239.

204. Zisowsky, J.; Koegel, S.; Leyers, S.; Devarakonda, K.; Kassack, M.U.; Osmak, M.; Jaehde, U. Relevance of drug uptake and efflux for cisplatin sensitivity of tumor cells. *Biochem. Pharmacol.* **2007**, *73*, 298–307.

205. Buß, I. Cellular Influx and Cytotoxicity of Oxaliplatin Analogues. PhD Thesis, University of Bonn, Bonn, Germany, **2010**. URN: urn:nbn:de:hbz:5N-22889.

206. Garmann, D. Reaktivität und zelluläre Aufnahme albuminbindender Platinkomplexe und neuer Oxaliplatin-Analoga. PhD Thesis, University of Bonn, Bonn, Germany, **2007**. URN: urn:nbn:de:hbz:5N-10733.

207. Danielsson, F.; Peterson, M.; Caldeira Araújo, H.; Lautenschläger, F.; Gad, A. Vimentin Diversity in Health and Disease. *Cells* **2018**, *7*, 147.

208. Kidd, M.E.; Shumaker, D.K.; Ridge, K.M. The role of Vimentin intermediate filaments in the progression of lung cancer. *Am. J. Respir. Cell Mol. Biol.* **2014**, *50*, 1–6.

209. Goto, S.; Iida, T.; Cho, S.; Oka, M.; Kohno, S.; Kondo, T. Overexpression of glutathione S-transferase π enhances the adduct formation of cisplatin with glutathione in human cancer cells. *Free Radic. Res.* **1999**, *31*, 549–558.

210. Cao, J.; Lou, S.; Ying, M.; Yang, B. DJ-1 as a human oncogene and potential

therapeutic target. *Biochem. Pharmacol.* **2015**, *93*, 241–250.

211. Chen, Y.; Kang, M.; Lu, W.; Guo, Q.; Zhang, B.; Xie, Q.; Wu, Y. DJ-1, a novel biomarker and a selected target gene for overcoming chemoresistance in pancreatic cancer. *J. Cancer Res. Clin. Oncol.* **2012**, *138*, 1463–1474.

212. Xu, Z. hong; Yao, T. zhu; Liu, W. miR-378a-3p sensitizes ovarian cancer cells to cisplatin through targeting MAPK1/GRB2. *Biomed. Pharmacother.* **2018**, *107*, 1410–1417.

213. Yu, G.Z.; Chen, Y.; Long, Y.Q.; Dong, D.; Mu, X.L.; Wang, J.J. New insight into the key proteins and pathways involved in the metastasis of colorectal carcinoma. *Oncol. Rep.* **2008**, *19*, 1191–1204.

214. Shibue, T.; Weinberg, R.A. EMT, CSCs, and drug resistance: the mechanistic link and clinical implications. *Nat. Rev. Clin. Oncol.* **2017**, *14*, 611–629.

215. Cervantes-Arias, A.; Pang, L.Y.; Argyle, D.J. Epithelial-mesenchymal transition as a fundamental mechanism underlying the cancer phenotype. *Vet. Comp. Oncol.* **2013**, *11*, 169–184.

216. Wang, J.; Chen, Y.; Xiang, F.; Li, M.; Li, H.; Chi, J.; Ren, K. Suppression of TGF-β1 enhances chemosensitivity of cisplatin-resistant lung cancer cells through the inhibition of drug-resistant proteins. *Artif. Cells, Nanomedicine Biotechnol.* **2018**, *46*, 1505–1512.

217. Satelli, A.; Li, S. Vimentin as a potential molecular target in cancer therapy Or Vimentin, an overview and its potential as a molecular target for cancer therapy. *Cell Mol Life Sci.* **2011**, *68*, 3033–3046.

218. Ivaska, J.; Pallari, H.M.; Nevo, J.; Eriksson, J.E. Novel functions of vimentin in cell adhesion, migration, and signaling. *Exp. Cell Res.* **2007**, *313*, 2050–2062.

219. Qiu, L.; Zhang, G.F.; Yu, L.; Wang, H.Y.; Jia, X.J.; Wang, T.J. Novel oncogenic and chemoresistance-inducing functions of resistin in ovarian cancer cells require miRNAs-mediated induction of epithelial-to-mesenchymal transition. *Sci. Rep.* **2018**, *8*, 1–10.

220. Sharma, P.; Alsharif, S.; Fallatah, A.; Chung, B.M. Intermediate Filaments as Effectors of Cancer Development and Metastasis: A Focus on Keratins, Vimentin, and Nestin. *Cells* **2019**, *8*, 1–21.

221. Maxwell, S.A.; Cherry, E.M.; Bayless, K.J. Akt, 14-3-3ζ, and vimentin mediate a drug-resistant invasive phenotype in diffuse large B-cell lymphoma. *Leuk. Lymphoma* **2011**, *52*, 849–864.

222. Wang, R.C.; Wei, Y.; An, Z.; Zou, Z.; Xiao, G.; Bhagat, G.; White, M.; Reichelt, J.; Levine, B. Akt-Mediated Regulation of Autophagy and Tumorigenesis Through Beclin 1 Phosphorylation. *Science* **2012**, *338*, 956–959.

223. Virtakoivu, R.; Mai, A.; Mattila, E.; Franceschi, N. De; Imanishi, S.Y.; Corthals, G.; Kaukonen, R.; Saari, M.; Cheng, F.; Torvaldson, E.; et al. Vimentin-ERK Signaling Uncouples Slug Gene Regulatory Function. *Cancer Res.* **2015**, *75*, 2349–2362.

224. Galazis, N.; Pang, Y.L.; Galazi, M.; Haoula, Z.; Layfield, R.; Atiomo, W. Proteomic biomarkers of endometrial cancer risk in women with polycystic ovary syndrome: A systematic review and biomarker database integration. *Gynecol. Endocrinol.* **2013**, *29*, 638–644.

225. Yin, S.; Chen, F.; Yang, G. Vimentin immunohistochemical expression as a prognostic factor in gastric cancer: A meta-analysis. *Pathol. Res. Pract.* **2018**, *214*, 1376–1380.

226. Battaglia, R.A.; Delic, S.; Herrmann, H.; Snider, N.T. Vimentin on the move: new developments in cell migration. *F1000Research* **2018**, *7*, 1–10.

227. Lazarova, D.L.; Bordonaro, M. Vimentin, colon cancer progression and resistance to butyrate and other HDACis. *J. Cell. Mol. Med.* **2016**, *20*, 989–993.

228. Liu, Y.; Du, F.; Zhao, Q.; Jin, J.; Ma, X.; Li, H. Acquisition of 5-fluorouracil resistance induces epithelial-mesenchymal transitions through the Hedgehog signaling pathway in HCT-8 colon cancer cells. *Oncol. Lett.* **2015**, *9*, 2675–2679.

229. Strouhalova, K.; Prechová, M.; Gandalovicova, A.; Brábek, J.; Gregor, M.; Rosel, D. Vimentin Intermediate Filaments as Potential Target for Cancer Treatment. *Cancers (Basel).* **2020**, *12*, 184–204.

230. Nagalingam, A.; Kuppusamy, P.; Singh, S. V; Sharma, D. Mechanistic Elucidation of the Antitumor Properties of Withaferin A in Breast Cancer. *Cancer Res.* **2014**, *74*, 2617–2629.

231. Yunos, N.M.; Beale, P.; Yu, J.Q.; Strain, D.; Huq, F. Studies on Combinations of Platinum with Paclitaxel and Colchicine in Ovarian Cancer Cell Lines. *Anticancer Res.* **2010**, *30*, 4025–4038.

232. Sheehan, D.; Meade, G.; Foley, V.M.; Dowd, C.A. Structure, function and evolution of glutathione transferases: implications for classification of non-mammalian members of an ancient enzyme superfamily. *Biochem. J.* **2001**, *16*, 1–16.

233. Board, P.G.; Menon, D. Glutathione transferases, regulators of cellular metabolism and physiology. *Biochim. Biophys. Acta* **2013**, *1830*, 3267–3288.

234. Dong, S.C.; Sha, H.H.; Xu, X.Y.; Hu, T.M.; Lou, R.; Li, H.; Wu, J.Z.; Dan, C.; Feng, J. Glutathione S-transferase π: A potential role in antitumor therapy. *Drug Des. Devel. Ther.* **2018**, *12*, 3535–3547.

235. Calatozzolo, C.; Gelati, M.; Ciusani, E.; Sciacca, F.L.; Pollo, B.; Cajola, L.; Marras, C.; Silvani, A.; Vitellaro-Zuccarello, L.; Croci, D.; et al. Expression of drug resistance proteins Pgp, MRP1, MRP3, MRP5 AND GST-π in human glioma. *J. Neurooncol.* **2005**, *74*, 113–121.

236. Wang, J.; Zhang, J.; Zhang, L.; Zhao, L.; Fan, S.; Yang, Z.; Gao, F.; Kong, Y.; Xiao, G.G.; Wang, Q. Expression of P-gp, MRP, LRP, GST-π and TopoIIα and intrinsic resistance in human lung cancer cell lines. *Oncol. Rep.* **2011**, *26*, 1081–1089.

237. Ogino, S.; Konishi, H.; Ichikawa, D.; Matsubara, D.; Shoda, K.; Arita, T.;

Kosuga, T.; Komatsu, S.; Shiozaki, A.; Okamoto, K.; et al. Glutathione S-transferase Pi 1 is a valuable predictor for cancer drug resistance in esophageal squamous cell carcinoma. *Cancer Sci.* **2019**, *110*, 795–804.

238. Pasello, M.; Michelacci, F.; Scionti, I.; Hattinger, C.M.; Zuntini, M.; Caccuri, A.M.; Scotlandi, K.; Picci, P.; Serra, M. Overcoming Glutathione S-Transferase P1–Related Cisplatin Resistance in Osteosarcoma. *Cancer Res.* **2008**, *68*, 6661–6668.

239. Norris, M.; Bordow, S.; Marshall, G.; Haber, P.; Cohn, S.; Haber, M. Expression of the Gene for Multidrug-Resistance-Associated Protein and Outcome in Patients With Neuroblastoma. *N. Engl. J. Med.* **1996**, *334*, 231–238.

240. Fletcher, J.I.; Gherardi, S.; Murray, J.; Burkhart, C.A.; Russell, A.; Ashton, L.J.; London, W.B.; Valli, E.; Smith, J.; Marshall, G.M.; et al. N-Myc Regulates Expression of the Detoxifying Enzyme Glutathione Transferase GSTP1, a Marker of Poor Outcome in Neuroblastoma. *Cancer Res.* **2012**, *72*, 845–853.

241. Dunne, B.M.; McNamara, M.; Clynes, M.; Shering, S.G.; Larkin, A.M.; Moran, E.; Barnes, C.; Kennedy, S.M. MDR1 Expression is Associated With Adverse Survival in Melanoma of the Uveal Tract. *Hum. Pathol.* **1998**, *29*, 594–598.

242. Mignogna, C.; Staibano, S.; Altieri, V.; Rosa, G. De; Pannone, G.; Santoro, A.; Zamparese, R.; Armiento, M.D.; Rocchetti, R.; Mezza, E.; et al. Prognostic significance of multidrug-resistance protein (MDR-1) in renal clear cell carcinomas: A five year follow-up analysis. *BMC Cancer* **2006**, *6*, 293–303.

243. Hagrman, D.; Goodisman, J.; Souid, A.K. Kinetic Study on the Reactions of Platinum Drugs with Glutathione. *J. Pharmacol. Exp. Ther.* **2004**, *308*, 658–666.

244. Wagner, E.F.; Nebreda, Á.R. Signal integration by JNK and p38 MAPK pathways in cancer development. *Nat. Rev. Cancer* **2009**, *9*, 537–549.

245. U.S. Food & Drug Adminsitration. Orphan Drug Designations and Approvals Available online: https://www.accessdata.fda.gov/scripts/opdlisting/oopd/detailedIndex.cfm?cfgridkey=20123823 (accessed on Aug 23, 2020).

246. Li, J.; Ye, T.; Liu, Y.; Kong, L.; Sun, Z.; Liu, D.; Wang, J.; Rosie Xing, H. Transcriptional Activation of Gstp1 by MEK/ERK Signaling Confers Chemo-Resistance to Cisplatin in Lung Cancer Stem Cells. *Front. Oncol.* **2019**, *9*, 1–14.

247. Küng, A.; Strickmann, D.B.; Galanski, M.; Keppler, B.K. Comparison of the binding behavior of oxaliplatin, cisplatin and analogues to 5′-GMP in the presence of sulfur-containing molecules by means of capillary electrophoresis and electrospray mass spectrometry. *J. Inorg. Biochem.* **2001**, *86*, 691–698.

248. De Luca, A.; Parker, L.J.; Ang, W.H.; Rodolfo, C.; Gabbarini, V.; Hancock, N.C.; Palone, F.; Mazzetti, A.P.; Menin, L.; Morton, C.J.; et al. A structure-based mechanism of cisplatin resistance mediated by glutathione transferase P1-1. *Proc. Natl. Acad. Sci. U. S. A.* **2019**, *116*, 13943–13951.

249. Chen, J.; Solomides, C.; Simpkins, H. Sensitization of mesothelioma cells to

platinum-based chemotherapy by GSTπ knockdown. *Biochem. Biophys. Res. Commun.* **2014**, *447*, 77–82.

250. Sawers, L.; Ferguson, M.J.; Ihrig, B.R.; Young, H.C.; Chakravarty, P.; Wolf, C.R.; Smith, G. Glutathione S-transferase P1 (GSTP1) directly influences platinum drug chemosensitivity in ovarian tumour cell lines. *Br. J. Cancer* **2014**, *111*, 1150–1158.

251. Tanyi, J.L.; Morris, A.J.; Wolf, J.K.; Fang, X.; Hasegawa, Y.; Lapushin, R.; Auersperg, N.; Sigal, Y.J.; Newman, R.A.; Felix, E.A.; et al. The Human Lipid Phosphate Phosphatase-3 Decreases the Growth, Survival, and Tumorigenesis of Ovarian Cancer Cells: Validation of the Lysophosphatidic Acid Signaling Cascade as a Target for Therapy in Ovarian Cancer. *Cancer Res.* **2003**, *63*, 1073–1082.

252. Liu, H.; Yu, C.; Yang, Z.H.U.; He, J.; Chen, W.; Yin, J.; Li, W.; Liu, H.; Wang, Y. Tubeimoside I sensitizes cisplatin in cisplatin-resistant human ovarian cancer cells (A2780/DDP) through down-regulation of ERK and up-regulation of p38 signaling pathways. *Mol. Med. Rep.* **2011**, *4*, 985–992.

253. Bai, J.; Guo, C.; Sun, W.; Li, M.; Meng, X.; Yu, Y.; Jin, Y.; Tong, D.; Geng, J.; Huang, Q.; et al. DJ-1 may contribute to metastasis of non-small cell lung cancer. *Mol. Biol. Rep.* **2012**, *39*, 2697–2703.

254. Kim, R.H.; Peters, M.; Jang, Y.; Shi, W.; Pintilie, M.; Fletcher, G.C.; DeLuca, C.; Liepa, J.; Zhou, L.; Snow, B.; et al. DJ-1, a novel regulator of the tumor suppressor PTEN. *Cancer Cell* **2005**, *7*, 263–273.

255. Fan, J.; Ren, H.; Jia, N.; Fei, E.; Zhou, T.; Jiang, P.; Wu, M.; Wang, G. DJ-1 Decreases Bax Expression through Repressing p53 Transcriptional Activity. *J. Biol. Chem.* **2008**, *283*, 4022–4030.

256. Liu, C.; Chen, Y.; Kochevar, I.E.; Jurkunas, U. V Decreased DJ-1 Leads to Impaired Nrf2-Regulated Antioxidant Defense and Increased UV-A-Induced Apoptosis in Corneal Endothelial Cells. *Invest. Ophthalmol. Vis. Sci.* **2014**, *55*, 5551–5560.

257. Gao, H.; Niu, Y.; Li, M.; Fang, S.; Guo, L. Identification of DJ-1 as a contributor to multidrug resistance in human small-cell lung cancer using proteomic analysis. *Int. J. Exp. Pathol.* **2017**, *98*, 67–74.

258. Zeng, H.Z.; Qu, Y.Q.; Zhang, W.J.; Xiu, B.; Deng, A.M.; Liang, A. Bin Proteomic Analysis Identified DJ-1 as a Cisplatin Resistant Marker in Non-Small Cell Lung Cancer. *Int. J. Mol. Sci.* **2011**, *12*, 3489–3499.

259. Trivedi, R.; Dihazi, G.H.; Eltoweissy, M.; Mishra, D.P.; Mueller, G.A.; Dihazi, H. The antioxidant protein PARK7 plays an important role in cell resistance to Cisplatin-induced apoptosis in case of clear cell renal cell carcinoma. *Eur. J. Pharmacol.* **2016**, *784*, 99–110.

260. Postnikova, E.; Cong, Y.; DeWald, L.E.; Dyall, J.; Yu, S.; Hart, B.J.; Zhou, H.; Gross, R.; Logue, J.; Cai, Y.; et al. Testing therapeutics in cell-based assays: Factors that influence the apparent potency of drugs. *PLoS One* **2018**, *13*, 1–18.

261. Schumann, C.; Chan, S.; Khalimonchuk, O.; Khal, S.; Moskal, V.; Shah, V.; Alani, A.W.G.; Taratula, O.; Taratula, O. Mechanistic Nanotherapeutic Approach Based on siRNA-Mediated DJ-1 Protein Suppression for Platinum-Resistant Ovarian Cancer. *Mol. Pharm.* **2016**, *13*, 2070–2083.

262. Schumann, C.; Chan, S.; Millar, J.A.; Bortnyak, Y.; Carey, K.; Fedchyk, A.; Wong, L.; Korzun, T.; Moses, A.S.; Lorenz, A.; et al. Intraperitoneal nanotherapy for metastatic ovarian cancer based on siRNA-mediated suppression of DJ-1 protein combined with a low dose of cisplatin. *Nanomedicine* **2018**, *14*, 1395–1405.

263. Lowenstein, E.J.; Daly, R.; Batzer, A.; Li, W.; Margolis, B.; Lammers, R.; Ullrich, A.; Skolnik, E.; Bar-Sagi, D.; Schlessinger, J. The SH2 and SH3 Domain-Containing Protein GRB2 Links Receptor Tyrosine Kinases to ras Signaling. *Cell* **1992**, *70*, 431–442.

264. Giubellino, A.; Burke, T.R.; Bottaro, D.P. Grb2 signaling in cell motility and cancer. *Expert Opin. Ther. Targets* **2008**, *12*, 1021–1033.

265. Tari, A.M.; Hung, M.-C.; Li, K.; Lopez-Berestein, G. Growth inhibition of breast cancer cells by Grb2 downregulation is correlated with inactivation of mitogen-activated protein kinase in EGFR, but not in ErbB2, cells. *Oncogene* **1999**, *18*, 1325–1332.

266. Ijaz, M.; Shahbaz, M.; Jiang, W.; Fathy, A.H.; Nesa, E.U.; Wang, D. Oncogenic Role of Grb2 in Breast Cancer and Grb2 Antagonists as Therapeutic Drugs. *Cancer Ther. Oncol.* **2017**, *3*.

267. Watanabe, T.; Shinohara, N.; Moriya, K.; Sazawa, A.; Kobayashi, Y.; Ogiso, Y.; Takiguchi, M.; Yasuda, J.; Koyanagi, T.; Kuzumaki, N.; et al. Significance of the Grb2 and Son of Sevenless (Sos) Proteins in Human Bladder Cancer Cell Lines. *IUBMB Life* **2000**, *49*, 317–320.

268. Timsah, Z.; Ahmed, Z.; Lin, C.C.; Melo, F.A.; Stagg, L.J.; Leonard, P.G.; Jeyabal, P.; Berrout, J.; O'Neil, R.G.; Bogdanov, M.; et al. Competition between Grb2 and Plcγ1 for FGFR2 regulates basal phospholipase activity and invasion. *Nat. Struct. Mol. Biol.* **2014**, *21*, 180–188.

269. Timsah, Z.; Ahmed, Z.; Ivan, C.; Berrout, J.; Gagea, M.; Zhou, Y.; Pena, G.N.A.; Hu, X.; Vallien, C.; Kingsley, C. V.; et al. Grb2 depletion under non-stimulated conditions inhibits PTEN, promotes Akt-induced tumor formation and contributes to poor prognosis in ovarian cancer. *Oncogene* **2016**, *35*, 2186–2196.

270. Tomono, T.; Yano, K.; Ogihara, T. Snail-Induced Epithelial-to-Mesenchymal Transition Enhances P-gp-Mediated Multidrug Resistance in HCC827 Cells. *J. Pharm. Sci.* **2017**, *106*, 2642–2649.

Appendix A

Cytotoxicity Assays

Cytotoxicity of Cisplatin

Individual pEC_{50} values for cisplatin cytotoxicity in A2780 and A2780cis cells (results of individual testing).

pEC_{50}	A2780	A2780cis
	6.043	5.223
	5.892	5.300
	5.988	5.371
	5.938	5.361
	5.954	5.315
	5.776	5.289
Mean	5.932	5.312
SEM	0.037	0.021

Individual pEC_{50} values for cisplatin cytotoxicity in HCT-8 and HCT-8ox cells (results of individual testing).

pEC_{50}	HCT-8	HCT-8ox
	5.332	5.076
	5.263	4.904
	5.253	5.135
	5.139	4.942
	5.347	5.190
	5.222	4.976
Mean	5.259	5.037
SEM	0.031	0.047

Cytotoxicity of Oxaliplatin

Individual pEC_{50} values for oxaliplatin cytotoxicity in A2780 and A2780cis cells (results of individual testing).

pEC_{50}	A2780	A2780cis
	6.385	5.888
	6.884	5.635
	6.406	5.842
	6.577	5.591
	6.126	5.970
	6.104	5.915
	6.184	5.848
	6.295	6.376
Mean	6.370	5.883
SEM	0.093	0.085

Individual pEC$_{50}$ values for oxaliplatin cytotoxicity in HCT-8 and HCT-8ox cells (results of individual testing).

pEC$_{50}$	HCT-8	HCT-8ox
	6.013	4.874
	6.063	4.469
	6.077	4.521
	6.169	4.475
	6.039	4.600
	5.945	4.643
	6.105	4.399
Mean	6.059	4.569
SEM	0.027	0.060

Cytotoxicity of BODIPY-cisplatin

Individual pEC$_{50}$ values for BODIPY-cisplatin cytotoxicity in A2780 and A2780cis cells (results of individual testing).

pEC$_{50}$	A2780	A2780cis
	4.789	4.006
	4.660	4.004
	4.814	4.013
	4.789	4.006
	4.660	4.004
Mean	4.742	4.007
SEM	0.034	0.002

Individual pEC$_{50}$ values for BODIPY-cisplatin cytotoxicity in HCT-8 and HCT-8ox cells (results of individual testing).

pEC$_{50}$	HCT-8	HCT-8ox
	3.978	3.788
	4.178	3.841
	3.948	3.788
	4.006	3.707
Mean	4.028	3.781
SEM	0.052	0.028

Cytotoxicity of FiVe1

Individual pEC_{50} values for FiVe1 cytotoxicity in A2780 and A2780cis cells (results of individual testing).

pEC_{50}	A2780	A2780cis
	6.256	6.214
	6.162	6.195
	6.133	6.180
	5.796	5.925
Mean	6.087	6.129
SEM	0.100	0.068

Cytotoxicity of Cisplatin/FiVe1

Individual pEC_{50} values for cisplatin cytotoxicity in A2780 and A2780cis cells without and with co-treatment with FiVe1 (results of individual testing).

pEC_{50}	A2780		A2780cis	
	Cisplatin	Cisplatin + FiVe1	Cisplatin	Cisplatin + FiVe1
	6.043	6.164	5.233	5.471
	5.892	6.055	5.300	5.684
	5.988	6.128	5.371	5.424
	5.938	6.096	5.361	5.625
	5.954		5.315	
	5.776		5.289	
Mean	5.932	6.111	5.312	5.551
SEM	0.037	0.023	0.021	0.062

Cytotoxicity of Ezatiostat-HCl

Individual pEC_{50} values for Ezatiostat-HCl cytotoxicity in A2780 and A2780cis cells (results of individual testing).

pEC_{50}	A2780	A2780cis
	4.566	4.578
	4.530	4.662
	4.448	4.463
	4.333	4.306
Mean	4.469	4.502
SEM	0.052	0.077

Individual pEC$_{50}$ values for Ezatiostat-HCl cytotoxicity in HCT-8 and HCT-8ox cells (results of individual testing).

pEC$_{50}$	HCT-8	HCT-8ox
	4.207	4.198
	4.159	4.217
	4.181	4.174
	4.102	4.134
Mean	4.162	4.181
SEM	0.022	0.018

Cytotoxicity of Cisplatin/Ezatiostat-HCl

Individual pEC$_{50}$ values for cisplatin cytotoxicity in A2780 cells without and with co-treatment with Ezatiostat-HCl, either without or with 24 hours or 48 hours pre-incubation with the inhibitor before platinum drug treatment (results of individual testing).

pEC$_{50}$	A2780					
	72h Cisplatin	72h Cisplatin + Ezatiostat-HCl	24h Medium + 48h Cisplatin	24h Ezatiostat-HCl + 48h Cisplatin	48h Medium + 24h Cisplatin	48h Ezatiostat-HCl + 24h Cisplatin
	5.834	5.783	4.907	4.947	4.580	4.673
	5.625	5.505	4.973	4.985	4.499	4.323
	6.043	5.896	5.312	4.951	4.289	4.292
	5.892	6.361	5.057	4.988		
	5.988	5.933	4.989	4.992		
	5.938	5.937				
	5.954	5.722				
Mean	5.896	5.877	5.048	4.973	4.456	4.429
SEM	0.052	0.099	0.070	0.010	0.087	0.122

Individual pEC$_{50}$ values for cisplatin cytotoxicity in A2780cis cells without and with co-treatment with Ezatiostat-HCl, either without or with 24 hours or 48 hours pre-incubation with the inhibitor before platinum drug treatment (results of individual testing).

pEC$_{50}$	A2780cis					
	72h Cisplatin	72h Cisplatin + Ezatiostat-HCl	24h Medium + 48h Cisplatin	24h Ezatiostat-HCl + 48h Cisplatin	48h Medium + 24h Cisplatin	48h Ezatiostat-HCl + 24h Cisplatin
	4.973	5.168	4.581	4.642	4.238	4.291
	5.114	4.941	4.631	4.560	4.248	4.248
	5.233	5.112	4.598	4.700	4.246	4.176
	5.300	5.372	4.691	4.710		
	5.371	5.137	4.656	4.663		
	5.361	5.138				
	5.315	5.262				
Mean	5.238	5.161	4.631	4.655	4.244	4.238
SEM	0.055	0.050	0.020	0.027	0.003	0.034

Individual pEC$_{50}$ values for cisplatin cytotoxicity in HCT-8 cells without and with co-treatment with Ezatiostat-HCl, either without or with 24 hours or 48 hours pre-incubation with the inhibitor before platinum drug treatment (results of individual testing).

pEC$_{50}$	HCT-8					
	72h Cisplatin	72h Cisplatin + Ezatiostat-HCl	24h Medium + 48h Cisplatin	24h Ezatiostat-HCl + 48h Cisplatin	48h Medium + 24h Cisplatin	48h Ezatiostat-HCl + 24h Cisplatin
	5.332	5.192	4.547	4.491	4.283	4.247
	5.263	5.265	4.547	4.660	4.199	4.227
	5.253	5.232	4.555	4.700	4.388	4.314
	5.139	5.368	4.543	4.474		
	5.347	5.339	4.463	4.532		
	5.222	5.155				
		5.216				
Mean	5.259	5.252	4.531	4.571	4.290	4.263
SEM	0.031	0.029	0.017	0.046	0.055	0.026

Individual pEC$_{50}$ values for cisplatin cytotoxicity in HCT-8ox cells without and with co-treatment with Ezatiostat-HCl, either without or with 24 hours or 48 hours pre-incubation with the inhibitor before platinum drug treatment (results of individual testing).

pEC$_{50}$	HCT-8ox					
	72h Cisplatin	72h Cisplatin + Ezatiostat-HCl	24h Medium + 48h Cisplatin	24h Ezatiostat-HCl + 48h Cisplatin	48h Medium + 24h Cisplatin	48h Ezatiostat-HCl + 24h Cisplatin
	5.076	4.947	4.268	4.146	3.678	3.677
	4.904	4.877	4.075	4.146	3.883	3.770
	5.135	4.982	4.429	4.345	3.912	3.958
	4.942	5.148	4.052	4.070		
	5.190	5.088	4.105	3.985		
	4.976	5.042				
		4.910				
Mean	5.037	4.999	4.186	4.138	3.824	3.802
SEM	0.047	0.037	0.072	0.060	0.074	0.083

Cytotoxicity of Oxaliplatin/Ezatiostat-HCl

Individual pEC$_{50}$ values for oxaliplatin cytotoxicity in HCT-8 cells without and with co-treatment with Ezatiostat-HCl, either without or with 24 hours or 48 hours pre-incubation with the inhibitor before platinum drug treatment (results of individual testing).

pEC$_{50}$	HCT-8					
	72h Oxaliplatin	72h Oxaliplatin + Ezatiostat-HCl	24h Medium + 48h Oxaliplatin	24h Ezatiostat-HCl + 48h Oxaliplatin	48h Medium + 24h Oxaliplatin	48h Ezatiostat-HCl + 24h Oxaliplatin
	6.013	5.993	4.763	4.791	4.293	4.220
	6.063	5.884	4.762	4.847	4.208	4.189
	6.077	6.079	4.658	5.010	4.125	4.200
	6.169	6.186	4.938	5.010	4.224	3.976
	6.039	5.906	5.228	5.179		
	5.945	6.130				
	6.105					
Mean	6.059	6.030	4.870	4.967	4.213	4.146
SEM	0.027	0.050	0.100	0.069	0.035	0.057

Individual pEC_{50} values for oxaliplatin cytotoxicity in HCT-8ox cells without and with co-treatment with Ezatiostat-HCl, either without or with 24 hours or 48 hours pre-incubation with the inhibitor before platinum drug treatment (results of individual testing).

pEC_{50}	HCT-8ox					
	72h Oxaliplatin	72h Oxaliplatin + Ezatiostat-HCl	24h Medium + 48h Oxaliplatin	24h Ezatiostat-HCl + 48h Oxaliplatin	48h Medium + 24h Oxaliplatin	48h Ezatiostat-HCl + 24h Oxaliplatin
	4.874	4.343	3.819	3.669	3.528	3.326
	4.469	4.300	3.716	3.585	3.686	3.646
	4.521	4.732	3.537	3.457	3.650	3.628
	4.475	4.749	4.277	4.138		
	4.600	4.572	4.216	4.196		
	4.643	4.717				
	4.399					
Mean	4.569	4.569	3.913	3.809	3.621	3.533
SEM	0.060	0.083	0.144	0.150	0.048	0.104

Cytotoxicity of DJ-1 Inhibitor

Individual pEC_{50} values for DJ-1 inhibitor cytotoxicity in A2780 and A2780cis cells (results of individual testing).

pEC_{50}	A2780	A2780cis
	4.793	4.589
	4.696	4.538
	4.500	4.659
	4.924	4.502
	4.941	4.606
Mean	4.771	4.579
SEM	0.081	0.027

Cytotoxicity of Cisplatin/DJ-1 Inhibitor

Individual pEC_{50} values for cisplatin cytotoxicity in A2780 and A2780cis cells without and with co-treatment with DJ-1 inhibitor (results of individual testing).

pEC_{50}	A2780		A2780cis	
	Cisplatin	Cisplatin + DJ-1 Inhibitor	Cisplatin	Cisplatin + DJ-1 Inhibitor
	5.693	5.716	5.283	5.029
	6.023	6.123	5.232	5.215
	5.806	6.094	5.269	5.193
	5.897	6.616	5.225	5.232
	5.702	6.326	5.255	5.246
			5.219	5.074
Mean	5.824	6.175	5.247	5.165
SEM	0.062	0.148	0.011	0.037

Cytotoxicity of Grb2 Inhibitors A and B

Individual pEC_{50} values for Grb2 inhibitor A cytotoxicity in HCT-8 and HCT-8ox cells (results of individual testing).

pEC_{50}	HCT-8	HCT-8ox
	4.973	5.485
	5.064	5.608
	5.066	5.531
Mean	5.034	5.541
SEM	0.031	0.036

Individual pEC_{50} values for Grb2 inhibitor B cytotoxicity in HCT-8 and HCT-8ox cells (results of individual testing).

pEC_{50}	HCT-8	HCT-8ox
	3.347	4.053
	3.864	4.051
	3.703	
Mean	3.638	4.052
SEM	0.153	0.001

Cytotoxicity of Cisplatin/Grb2 Inhibitor A

Individual pEC_{50} values for cisplatin cytotoxicity in HCT-8 and HCT-8ox cells without and with co-treatment with Grb2 inhibitor A (results of individual testing).

pEC_{50}	HCT-8		HCT-8ox	
	Cisplatin	Cisplatin + Grb2 Inhibitor A	Cisplatin	Cisplatin + Grb2 Inhibitor A
	4.854	5.124	4.807	4.642
	4.775	5.005	4.702	4.798
	4.673	4.710	4.716	4.456
	4.724	4.751	4.711	4.684
	4.951	4.825	4.656	4.807
		4.953		4.614
Mean	4.795	4.895	4.718	4.667
SEM	0.049	0.065	0.025	0.053

Cytotoxicity of Cisplatin/ Grb2 Inhibitor B

Individual pEC_{50} values for cisplatin cytotoxicity in HCT-8 and HCT-8ox cells without and with co-treatment with Grb2 inhibitor B (results of individual testing).

pEC_{50}	HCT-8		HCT-8ox	
	Cisplatin	Cisplatin + Grb2 Inhibitor B	Cisplatin	Cisplatin + Grb2 Inhibitor B
	4.854	4.948	4.807	4.580
	4.775	4.746	4.702	4.595
	4.673	4.521	4.716	4.169
	4.724	4.549	4.711	4.389
	4.951	4.606	4.656	4.659
		4.934		4.785
Mean	4.795	4.717	4.718	4.530
SEM	0.049	0.078	0.025	0.089

Cytotoxicity of Oxaliplatin/Grb2 Inhibitor A

Individual pEC_{50} values for oxaliplatin cytotoxicity in HCT-8 and HCT-8ox cells without and with co-treatment with Grb2 inhibitor A (results of individual testing).

pEC_{50}	HCT-8		HCT-8ox	
	Oxaliplatin	Oxaliplatin + Grb2 Inhibitor A	Oxaliplatin	Oxaliplatin + Grb2 Inhibitor A
	5.855	5.890	4.579	4.640
	5.587	5.642	3.948	4.057
	5.456	5.145	3.866	3.854
	5.727	5.583	4.221	4.282
	5.695	5.570	4.236	4.128
Mean	5.664	5.566	4.170	4.192
SEM	0.067	0.120	0.126	0.131

Cytotoxicity of Oxaliplatin/Grb2 Inhibitor B

Individual pEC_{50} values for oxaliplatin cytotoxicity in HCT-8 and HCT-8ox cells without and with co-treatment with Grb2 inhibitor B (results of individual testing).

pEC_{50}	HCT-8		HCT-8ox	
	Oxaliplatin	Oxaliplatin + Grb2 Inhibitor B	Oxaliplatin	Oxaliplatin + Grb2 Inhibitor B
	5.855	5.434	4.579	4.124
	5.587	5.216	3.948	3.510
	5.456	4.961	3.866	3.532
	5.727	5.386	4.221	3.894
	5.695	5.330	4.236	4.004
Mean	5.664	5.265	4.170	3.813
SEM	0.067	0.084	0.126	0.125

Cytotoxicity of Cisplatin-azide

Individual pEC_{50} values for cisplatin-azide cytotoxicity in A2780 and A2780cis cells (results of individual testing).

pEC_{50}	A2780	A2780cis
	5.353	4.703
	5.234	4.691
	5.392	4.673
Mean	5.326	5.689
SEM	0.048	0.009

Individual pEC_{50} values for cisplatin-azide cytotoxicity in HCT-8 and HCT-8ox cells (results of individual testing).

pEC_{50}	HCT-8	HCT-8ox
	4.631	4.932
	4.548	4.812
	4.979	4.772
Mean	4.719	4.839
SEM	0.132	0.048

Cytotoxicity of Cisplatin-alkyne

Individual pEC_{50} values for cisplatin-alkyne cytotoxicity in A2780 and A2780cis cells (results of individual testing).

pEC_{50}	A2780	A2780cis
	4.904	4.273
	5.067	4.448
	5.253	4.118
Mean	5.075	4.280
SEM	0.101	0.095

Individual pEC_{50} values for cisplatin-alkyne cytotoxicity in HCT-8 and HCT-8ox cells (results of individual testing).

pEC_{50}	HCT-8	HCT-8ox
	3.715	3.980
	4.164	4.090
	4.195	3.995
	4.053	
Mean	4.032	4.022
SEM	0.110	0.034

Appendix B

Knockdown Experiments

Vimentin Knockdown

Vimentin expression in A2780 and A2780cis cells with vimentin knockdown in relation to cells with negative knockdown (results of individual testing).

	A2780	A2780cis
	Vimentin knockdown	**Negative knockdown**
	0.950	0.417
	0.777	0.736
	0.299	0.330
Mean	0.676	0.494
SEM	0.195	0.124

Individual pEC_{50} values for cisplatin cytotoxicity in A2780 and A2780cis cells without knockdown, with negative knockdown and with vimentin knockdown (results of individual testing).

	A2780			A2780cis		
	Vimentin knockdown	**Negative knockdown**	**Untreated control**	**Vimentin knockdown**	**Negative knockdown**	**Untreated control**
	4.817	4.817	4.948	4.663	4.670	4.691
	5.071	4.960	5.334	4.649	4.707	4.683
	4.768	4.787	4.834	4.570	4.564	4.542
	5.252	5.031	5.189	4.818	4.733	4.759
Mean	4.977	4.899	5.076	4.675	4.669	4.669
SEM	0.113	0.058	0.113	0.052	0.037	0.046

GSTP1 Knockdown

GSTP1 expression in A2780 and A2780cis cells with GSTP1 knockdown in relation to cells with negative knockdown (results of individual testing).

	A2780	A2780cis
	GSTP1 knockdown	**GSTP1 knockdown**
	0.376	0.418
	0.632	0.798
	0.796	1.547
	0.525	
Mean	0.582	0.921
SEM	0.089	0.332

Individual pEC$_{50}$ values for cisplatin cytotoxicity in A2780 and A2780cis cells without knockdown, with negative knockdown and with GSTP1 knockdown (results of individual testing).

	A2780			A2780cis		
	GSTP1 knockdown	Negative knockdown	Untreated control	GSTP1 knockdown	Negative knockdown	Untreated control
	5.046	5.005	5.172	4.676	4.713	4.860
	4.860	4.817	4.948	4.695	4.670	4.691
	5.226	4.960	5.334	4.733	4.707	4.683
	4.819	4.787	4.834	4.566	4.564	4.542
	5.145	5.031	5.189	4.813	4.733	4.759
Mean	5.019	4.920	5.095	4.697	4.677	4.707
SEM	0.079	0.050	0.090	0.040	0.030	0.052

GSTP1 expression in HCT-8 and HCT-8ox cells with GSTP1 knockdown in relation to cells with negative knockdown (results of individual testing).

	HCT-8	HCT-8ox
	GSTP1 knockdown	GSTP1 knockdown
	0.092	0.056
	0.076	0.078
	0.108	0.023
Mean	0.092	0.052
SEM	0.009	0.016

Individual pEC$_{50}$ values for cisplatin cytotoxicity in HCT-8 and HCT-8ox cells without knockdown, with negative knockdown and with GSTP1 knockdown (results of individual testing).

	HCT-8			HCT-8ox		
	GSTP1 knockdown	Negative knockdown	Untreated control	GSTP1 knockdown	Negative knockdown	Untreated control
	4.961	4.799	4.664	4.748	4.510	4.207
	5.196	4.811	4.793	4.868	4.509	4.561
	5.195	4.660	4.553	4.558	4.538	4.563
	4.855	4.717	4.709	5.305	4.651	4.602
	5.317	4.594	4.678	4.986	4.429	4.172
	5.371	4.782	4.699		4.154	4.428
		4.670	4.645		4.465	4.390
Mean	5.149	4.719	4.677	4.893	4.465	4.418
SEM	0.082	0.031	0.082	0.125	0.058	0.066

Individual pEC$_{50}$ values for oxaliplatin cytotoxicity in HCT-8 and HCT-8ox cells without knockdown, with negative knockdown and with GSTP1 knockdown (results of individual testing).

	HCT-8			HCT-8ox		
	GSTP1 knockdown	**Negative knockdown**	**Untreated control**	**GSTP1 knockdown**	**Negative knockdown**	**Untreated control**
	5.702	5.005	4.846	5.754	4.161	4.062
	5.942	5.141	5.490	4.569	3.811	4.049
	6.092	5.043	4.877	4.642	4.891	4.766
	5.467	4.710	5.451	5.283	5.165	5.099
	5.987	5.090	5.008	5.035	4.857	4.804
	5.438	5.228	4.007	5.902		
	5.182	3.880				
Mean	5.687	4.871	4.947	5.198	4.577	4.556
SEM	0.128	0.176	0.220	0.227	0.253	0.212

DJ-1 Knockdown

DJ-1 expression in A2780 and A2780cis cells with DJ-1 knockdown in relation to cells with negative knockdown (results of individual testing).

	A2780	A2780cis
	DJ-1 knockdown	**DJ-1 knockdown**
	0.321	0.777
	0.148	0.186
	0.177	0.335
	0.289	0.340
	0.070	0.127
Mean	0.201	0.353
SEM	0.046	0.114

Individual pEC$_{50}$ values for cisplatin cytotoxicity in A2780 and A2780cis cells without knockdown, with negative knockdown and with DJ-1 knockdown (results of individual testing).

	A2780			A2780cis		
	DJ-1 knockdown	**Negative knockdown**	**Untreated control**	**DJ-1 knockdown**	**Negative knockdown**	**Untreated control**
	5.513	5.024	4.942	4.578	4.685	4.674
	4.900	5.783	5.307	4.970	5.014	5.101
	5.481	5.369	5.316	5.261	5.091	4.900
	5.143	5.118	5.271	5.405	4.856	5.906
	5.212	5.312	5.328	4.841	5.890	5.027
	4.925	5.025		5.110		
Mean	5.196	5.272	5.223	5.028	5.107	5.122
SEM	0.107	0.118	0.073	0.122	0.208	0.209

Grb2 Knockdown

Grb2 expression in HCT-8 and HCT-8ox cells with Grb2 knockdown in relation to cells with negative knockdown (results of individual testing).

	HCT-8	HCT-8ox
	Grb2 knockdown	Grb2 knockdown
	0.608	0.826
	0.453	1.005
	0.486	0.786
Mean	0.516	0.872
SEM	0.047	0.067

Individual pEC_{50} values for cisplatin cytotoxicity in HCT-8 and HCT-8ox cells without knockdown, with negative knockdown and with Grb2 knockdown (results of individual testing).

	HCT-8			HCT-8ox		
	Grb2 knockdown	Negative knockdown	Untreated control	Grb2 knockdown	Negative knockdown	Untreated control
	4.970	4.842	4.578	4.524	4.600	4.655
	4.915	4.933	4.825	4.540	4.517	4.540
	4.730	4.695	4.693	4.654	4.516	4.461
Mean	4.872	4.823	4.699	4.573	4.544	4.552
SEM	0.073	0.069	0.071	0.041	0.028	0.056

Individual pEC_{50} values for oxaliplatin cytotoxicity in HCT-8 and HCT-8ox cells without knockdown, with negative knockdown and with Grb2 knockdown (results of individual testing).

	HCT-8			HCT-8ox		
	Grb2 knockdown	Negative knockdown	Untreated control	Grb2 knockdown	Negative knockdown	Untreated control
	4.720	4.460	4.534	3.700	3.853	3.663
	5.447	5.047	5.254	4.157	4.228	4.165
	4.938	5.114	4.922	4.063	4.045	3.764
	4.818	4.868	4.880	3.961	4.211	4.105
	4.986			4.334		
	5.059			4.196		
Mean	4.995	4.872	4.898	4.069	4.084	3.924
SEM	0.103	0.147	0.147	0.090	0.087	0.124

Appendix C

Apoptosis Assays

Percentage of late apoptotic/necrotic, early apoptotic and alive A2780 cells after co-incubation of cisplatin with FiVe1 in comparison to the treatment with each of the compounds alone and untreated cells.

	A2780			
	Untreated control	**FiVe1**	**Cisplatin**	**Cisplatin/FiVe1**
Late Apoptosis + Necrosis	0.080	0.080	0.192	0.362
	0.093	0.119	0.116	0.244
	0.089	0.064	0.085	0.270
	0.131	0.147	0.321	0.469
Mean	0.098	0.103	0.178	0.336
SEM	0.011	0.019	0.053	0.051
Early Apoptosis	0.031	0.041	0.104	0.190
	0.035	0.026	0.096	0.189
	0.023	0.041	0.082	0.229
	0.030	0.041	0.113	0.027
Mean	0.030	0.037	0.099	0.158
SEM	0.003	0.004	0.007	0.045
Alive	0.890	0.879	0.704	0.448
	0.872	0.855	0.789	0.567
	0.889	0.896	0.834	0.502
	0.839	0.812	0.567	0.505
Mean	0.872	0.861	0.723	0.506
SEM	0.012	0.018	0.059	0.024

Percentage of late apoptotic/necrotic, early apoptotic and alive A2780cis cells after co-incubation of cisplatin with FiVe1 in comparison to the treatment with each of the compounds alone and untreated cells.

	A2780cis			
	Untreated control	**FiVe1**	**Cisplatin**	**Cisplatin/FiVe1**
Late Apoptosis + Necrosis	0118	0.170	0.177	0.372
	0.147	0.201	0.194	0.312
	0.103	0.179	0.139	0.370
	0.117	0.172	0.225	0.497
Mean	0.121	0.180	0.184	0.388
SEM	0.009	0.007	0.018	0.039
Early Apoptosis	0.026	0.035	0.061	0.026
	0.031	0.028	0.074	0.074
	0.014	0.021	0.025	0.041
	0.009	0.015	0.023	0.026
Mean	0.020	0.025	0.046	0.042
SEM	0.005	0.004	0.013	0.011
Alive	0.856	0.795	0.763	0.601
	0.822	0.771	0.732	0.614
	0.883	0.800	0.836	0.589
	0.874	0.814	0.752	0.477
Mean	0.859	0.795	0.771	0.570
SEM	0.014	0.009	0.023	0.032

Percentage of late apoptotic/necrotic, early apoptotic and alive HCT-8 cells after cisplatin treatment following GSTP1 knockdown, negative knockdown control or without knockdown in addition to an untreated control.

	HCT-8		
	Control	Negative Control	GSTP1 knockdown
Late Apoptosis + Necrosis	0.196	0.170	0.721
	0.284	0.471	0.921
	0.416	0.312	0.578
	0.184	0.830	0.943
Mean	0.270	0.446	0.791
SEM	0.054	0.142	0.087
Early Apoptosis	0.054	0.057	0.038
	0.094	0.053	0.033
	0.067	0.074	0.049
	0.033	0.010	0.015
Mean	0.062	0.048	0.034
SEM	0.013	0.014	0.007
Alive	0.750	0.773	0.242
	0.622	0.476	0.046
	0.517	0.614	0.374
	0.783	0.160	0.041
Mean	0.668	0.506	0.176
SEM	0.061	0.130	0.081

Percentage of late apoptotic/necrotic, early apoptotic and alive HCT-8ox cells after cisplatin treatment following GSTP1 knockdown, negative knockdown control or without knockdown in addition to an untreated control.

	HCT-8ox		
	Control	**Negative Control**	**GSTP1 knockdown**
Late Apoptosis + Necrosis	0.179	0.235	0.479
	0.322	0.527	0.808
	0.381	0.389	0.436
	0.231		0.863
Mean	0.279	0.384	0.646
SEM	0.045	0.084	0.110
Early Apoptosis	0.063	0.077	0.080
	0.072	0.052	0.058
	0.009	0.008	0.009
	0.070		0.052
Mean	0.054	0.046	0.050
SEM	0.015	0.020	0.015
Alive	0.758	0.688	0.442
	0.606	0.421	0.134
	0.610	0.603	0.556
	0.699		0.085
Mean	0.668	0.571	0.304
SEM	0.037	0.079	0.115

Percentage of late apoptotic/necrotic, early apoptotic and alive HCT-8 cells after oxaliplatin treatment following GSTP1 knockdown or negative knockdown control or without knockdown in addition to an untreated control.

	HCT-8		
	Control	**Negative Control**	**GSTP1 knockdown**
Late Apoptosis + Necrosis	0.129	0.1664	0.707
	0.210	0.3651	0.804
	0.283	0.2946	0.570
	0.127	0.4929	0.795
Mean	0.187	0.330	0.719
SEM	0.037	0.068	0.054
Early Apoptosis	0.033	0.032	0.032
	0.056	0.038	0.062
	0.075	0.063	0.056
	0.030	0.015	0.032
Mean	0.048	0.037	0.045
SEM	0.011	0.010	0.008
Alive	0.838	0.802	0.261
	0.735	0.597	0.134
	0.642	0.642	0.375
	0.843	0.493	0.173
Mean	0.764	0.633	0.236
SEM	0.048	0.064	0.054

Percentage of late apoptotic/necrotic, early apoptotic and alive HCT-8ox cells after oxaliplatin treatment following GSTP1 knockdown or negative knockdown control or without knockdown in addition to an untreated control.

	HCT-8ox		
	Control	**Negative Control**	**GSTP1 knockdown**
Late Apoptosis + Necrosis	0.095	0.149	0.493
	0.245	0.444	0.723
	0.382	0.358	0.579
	0.194	0.534	0.720
Mean	0.229	0.371	0.629
SEM	0.060	0.082	0.056
Early Apoptosis	0.094	0.085	0.090
	0.095	0.067	0.061
	0.010	0.016	0.011
	0.075	0.031	0.041
Mean	0.067	0.050	0.051
SEM	0.020	0.016	0.017
Alive	0.811	0.766	0.416
	0.660	0.490	0.217
	0.608	0.626	0.410
	0.731	0.435	0.240
Mean	0.703	0.579	0.321
SEM	0.044	0.074	0.054

Appendix D

Combination Index Experiments

CI values determined at effective concentrations of EC_{50}, EC_{75}, EC_{90} and EC_{95} of the combination of cisplatin and FiVe1 in A2780 cells.

	A2780			
	EC_{50}	EC_{75}	EC_{90}	EC_{95}
	0.289	0.199	0.179	0.186
	0.395	0.227	0.171	0.157
	0.913	0.305	0.102	0.049
	0.931	0.392	0.165	0.092
	0.684	0.400	0.242	0.175
	0.410	0.502	0.636	0.760
	1.345	0.539	0.227	0.128
	1.411	0.571	0.242	0.138
Mean	0.797	0.392	0.246	0.211
SEM	0.152	0.050	0.058	0.080

CI values determined at effective concentrations of EC_{50}, EC_{75}, EC_{90} and EC_{95} of the combination of cisplatin and FiVe1 in A2780cis cells.

	A2780cis			
	EC_{50}	EC_{75}	EC_{90}	EC_{95}
	0.593	0.150	0.043	0.019
	0.611	0.154	0.043	0.019
	0.769	0.214	0.060	0.025
	0.885	0.288	0.094	0.044
	0.417	0.235	0.133	0.090
	0.358	0.344	0.332	0.324
	0.519	0.444	0.383	0.347
	0.626	0.552	0.490	0.454
Mean	0597	0297	0.197	0.166
SEM	0.061	0.050	0.063	0.063